



HAL
open science

Porous PEGDA/PEG hydrogel membranes : Permeability, Filtration and Structure

Malak Alaa Eddine

► **To cite this version:**

Malak Alaa Eddine. Porous PEGDA/PEG hydrogel membranes : Permeability, Filtration and Structure. Condensed Matter [cond-mat]. Sorbonne Université, 2023. English. NNT : 2023SORUS031 . tel-04056846

HAL Id: tel-04056846

<https://theses.hal.science/tel-04056846v1>

Submitted on 3 Apr 2023

HAL is a multi-disciplinary open access archive for the deposit and dissemination of scientific research documents, whether they are published or not. The documents may come from teaching and research institutions in France or abroad, or from public or private research centers.

L'archive ouverte pluridisciplinaire **HAL**, est destinée au dépôt et à la diffusion de documents scientifiques de niveau recherche, publiés ou non, émanant des établissements d'enseignement et de recherche français ou étrangers, des laboratoires publics ou privés.

THÈSE DE DOCTORAT
DE L'UNIVERSITÉ PSL

Préparée à l'École Supérieure de Physique
et de Chimie Industrielles de la ville de Paris

**Porous PEGDA/PEG hydrogel membranes :
Permeability, Filtration and Structure**

*Membranes d'hydrogel poreuses de PEGDA/PEG :
Perméabilité, filtration et structure*

Soutenue par

Malak ALAA EDDINE

Le 31 Janvier 2023

Ecole doctorale n° ED 397

Physique et Chimie des Matériaux

Spécialité

Chimie des matériaux

Composition du jury :

Jean-Baptiste SALMON

Directeur de recherche, LOF Bordeaux

Président du Jury

Fouzia BOULMEDAIS

Directrice de recherche, ICS Strasbourg

Rapporteur

Patrice BACCHIN

Professeur d'Université, LGC Toulouse

Rapporteur

Mark TIBBITT

Associate Professor, ETH Zurich

Examineur

Cécile MONTEUX

Directrice de recherche, ESPCI Paris

Directrice de thèse

Sabrina BELBEKHOUCHE

Maitresse de conférence, ICMPE Thiais

Co-Directrice de thèse

Bruno BRESSON

Ingénieur de recherche, ESPCI Paris

Co-encadrant de thèse

Thomas SALEZ

Chercheur CNRS, LOMA Bordeaux

Invité

RÉSUMÉ

Les hydrogels, qui sont des réseaux de chaînes de polymères dans l'eau, sont caractérisés par des structures poreuses et hydrophiles qui en font en principe des matériaux avantageux utilisés dans le domaine de la filtration. Le contrôle du transport des solutés et des particules dans ces réseaux de polymères peut être réalisé en contrôlant leur morphologie microscopique et leur porosité. Dans cette thèse, nous concevons des membranes d'hydrogel composites autoportantes basées sur la polymérisation du poly (éthylène glycol) diacrylate PEGDA en présence de chaînes de poly (éthylène glycol) PEG. Nous étudions l'effet de la concentration et de la masse molaire du PEG sur les propriétés de perméabilité à l'eau ainsi que sur la sélectivité des membranes composites PEGDA/PEG et leur lien avec leurs propriétés structurales. Nous montrons que les chaînes de PEG restent irréversiblement piégées dans la matrice du PEGDA, même après plusieurs cycles de filtration, ce qui contredit la littérature existante rapportant l'utilisation de chaînes de PEG comme agents de porogènes pour induire la porosité dans les matrices réticulées. Nous observons que l'ajout de chaînes de PEG, avec des concentrations et des masses molaires différentes, permet de régler la perméabilité à l'eau des systèmes d'hydrogel PEGDA/PEG sur plusieurs ordres de grandeur. Nous montrons que la perméabilité présente un maximum avec la concentration de recouvrement des chaînes de PEG, ce qui est un phénomène robuste observé pour les différentes masses molaires de PEG étudiées. En plus, nous étudions la sélectivité de membranes de PEGDA/PEG en filtrant des particules de polystyrène de différentes tailles. Nos résultats suggèrent que la présence de chaînes de PEG dans la matrice du PEGDA crée des défauts locaux à l'échelle nanométrique dans la densité de réticulation qui peuvent contrôler la perméation des particules et de l'eau à travers les échantillons.

MOTS CLÉS

Hydrogel, PEGDA, PEG, perméabilité, sélectivité, structure

ABSTRACT

Hydrogels, which are networks of polymer chains in water, are characterized by porous and hydrophilic structures that make them in principle advantageous materials used in the field of filtration. Controlling the transport of solute and particle in such polymer networks can be achieved by controlling their microscopic morphology and porosity. In this thesis, we design free-standing composite hydrogel membranes based on the polymerization of poly (ethylene glycol) diacrylate PEGDA in the presence of poly (ethylene glycol) PEG chains. We investigate the effect of PEG concentration and molar mass on the water permeability properties as well as the selectivity of PEGDA/PEG composite membranes and their link with their structural properties. We show that the PEG chains remain irreversibly trapped in the PEGDA matrix even after several filtration cycles which contradicts existing literature reporting the use of PEG chains as templating agents to induce porosity in cross-linked matrices. We observe that the addition of PEG chains, with different concentrations and molar masses, allows to tune the water permeability of the PEGDA/PEG hydrogel systems over several orders of magnitude. We show that the permeability presents a maximum with the overlap concentration of PEG chains, which is a robust phenomenon observed for several molar masses. In addition, we investigate the selectivity of the PEGDA/PEG membranes by filtering polystyrene particles of different sizes. Our results suggest that the presence of PEG chains in the PEGDA matrix provides some local nanoscale defects in the cross-linking density that may control the permeation of particles and water across the samples.

KEYWORDS

Hydrogel, PEGDA, PEG, permeability, selectivity, structure

CONTENTS:

Résumé en Français	i
General introduction	1
1 Literature review	5
1.1 HYDROGELS	5
1.1.1 History and generalities.....	5
1.1.2 Classification.....	6
1.1.3 Structure of hydrogels	9
A) Polymer coils and solutions	9
B) Morphology controlled by phase separation	13
1.1.4 Properties of hydrogels.....	14
A) Swelling behavior	14
B) Mechanical properties	16
1.2 FILTRATION PROCESS	19
1.2.1 Definition and generalities	19
1.2.2 Flow, permeation and retention through porous medium	22
1.2.3 Clogging and concentration polarization	25
1.3 HYDROGELS FOR FILTRATION.....	27
1.3.1 Hydrogels as diffusion barriers	27
1.3.2 Hydrogels as coating films for filtration processes	30
1.3.3 Hydrogels as free-standing membranes for filtration processes	32
1.3.4 PEGDA based hydrogel membranes for filtration	34
1.3.4.1 Generalities of PEGDA hydrogel.....	35
A) PEGDA hydrogel synthesis and application	35
B) Structural and mechanical properties of PEGDA hydrogel	36
C) Controlling PEGDA hydrogel porosity	43
1.3.4.2 Water permeability properties of free-standing PEGDA membrane	45
1.3.4.3 Water permeability properties of PEGDA/PEG membrane.....	48
1.4 POSITIONNING OF THE PhD WORK WITH RESPECT TO THE LITERATURE STUDY	51
References	52
2 Large and non-linear permeability amplification with polymeric additives in hydrogel membranes	69
2.1 ABSTRACT	69
2.2 KEYWORDS.....	69

2.3	INTRODUCTION	70
2.4	EXPERIMENTAL SECTION.....	71
2.4.1	Materials.....	71
2.4.2	PEGDA hydrogels preparation.....	71
2.4.3	Chemical composition of hydrogels.....	72
2.4.4	Atomic Force Microscopy (AFM) measurements	72
2.4.5	Mechanical measurements	72
2.4.6	Filtration experiments	73
2.5	RESULTS.....	75
2.5.1	Hydrogel membranes characterization.....	75
2.5.2	Mechanical characterization.....	78
2.5.3	Roles of pressure and PEG concentration on water intrinsic permeability	79
2.6	DISCUSSION.....	83
2.6.1	Permeability variation with the PEG concentration.....	83
2.6.2	Non-linear variation of the flow rate-pressure curve	84
2.7	CONCLUSION	87
References	88
3	Sieving and clogging in PEG-PEGDA hydrogel membranes.....	93
3.1	ABSTRACT	93
3.2	KEYWORDS.....	93
3.3	INTRODUCTION	94
3.4	EXPERIMENTAL SECTION.....	95
3.4.1	Materials.....	95
3.4.2	PEGDA hydrogels preparation.....	95
3.4.3	Particles characterization.....	96
3.4.4	AFM characterization.....	96
3.4.5	CryoSEM characterization	96
3.4.6	Particles filtration experiments.....	97
3.5	RESULTS AND DISCUSSION.....	98
3.5.1	Sieving of nanometric and micrometric particles by PEG/PEGDA hydrogels and relation to the hydrogels structure.....	98
3.5.1.1	Filtration experiments	98
3.5.1.2	Link between particles filtration and the structure of PEG/PEGDA hydrogels	100
3.5.2	Clogging of the PEG/PEGDA hydrogels by nano and microparticles.....	104
3.6	CONCLUSION	110

References	111
4 Effect of PEG content and molar mass on the morphological structure and water permeability properties of PEGDA/PEG composite hydrogel membranes	117
4.1 ABSTRACT	117
4.2 KEYWORDS.....	118
4.3 INTRODUCTION.....	118
4.4 EXPERIMENTAL.....	119
4.4.1 Materials.....	119
4.4.2 PEGDA hydrogels preparation.....	119
4.4.3 Morphological characterization of hydrogel membranes.....	120
4.4.4 Permeability experiments	120
4.5 RESULTS.....	121
4.5.1 Permeability variations around C^* for varying PEG molar masses.....	121
4.5.2 Fraction of the PEG chains trapped in the PEGDA matrix	124
4.5.3 Role of PEG concentration and molar mass on hydrogel's structure	126
4.6 DISCUSSION.....	129
4.7 CONCLUSION	133
References	134
Conclusion & Perspectives	139
Supporting Information of Chapter 2	145
Supporting Information of Chapter 3	149
Supporting Information of Chapter 4	151

Résumé en Français

Les hydrogels, qui sont des réseaux de chaînes de polymères dans l'eau, présentent des structures poreuses et hydrophiles. Ces caractéristiques ont récemment été exploitées dans le domaine de la filtration et du traitement des eaux usées. En effet, leur structure en réseau, leur morphologie et leur porosité permettent de contrôler la diffusion et le transport de différentes espèces (e.g. composé chimique, particules...). Dans ce contexte, les études rapportées dans la littérature ont principalement décrit l'utilisation d'hydrogels comme couches de revêtement sur des surfaces hydrophobes de membranes dites classiques de filtration et permettent notamment d'améliorer leur résistance à l'encrassement. Cependant, le contrôle de la structure de porosité et des propriétés de perméabilité des membranes d'hydrogel en tant que tel est rarement étudié pour les applications de filtration.

Dans ce travail de thèse, nous nous sommes intéressés à développer un système d'hydrogel, avec des propriétés de perméabilité bien contrôlées, préparé en une seule étape en milieu aqueux et capable de résister à de forte pression appliquée pendant la filtration (~ 1 Bar). Pour ce faire, nous avons préparé différentes séries de membranes d'hydrogel par photopolymérisation d'un mélange de poly (éthylène glycol) diacrylate (PEGDA) et de poly (éthylène glycol) (PEG). Nous avons étudié l'effet de la concentration et de la masse molaire du PEG (masses molaires entre 600 et 600 000 g.mol⁻¹) sur la perméabilité à l'eau, les propriétés mécaniques et la filtration sélective de particules de tailles différentes. De plus, nous avons étudié l'évolution de la structure de l'hydrogel par des études de microscopie à force atomique (AFM) et de cryo-microscopie électronique à balayage (cryoMEB). Nous avons enfin proposé une organisation des chaînes de PEG dans la matrice du PEGDA qui pourrait expliquer la plupart de nos mesures structurelles et de perméabilité.

Les principales conclusions obtenues sont mises en évidence ci-dessous :

Effet de la concentration et de la masse molaire du PEG sur la perméabilité intrinsèque à l'eau à une faible pression appliquée (100 mBar)

Afin de mesurer la perméabilité des systèmes d'hydrogel de PEG/PEGDA, nous avons utilisé un système de filtration frontale utilisant une cellule d'ultra-filtration où la pression appliquée est contrôlable (Figure 0.1). Les perméats liquides sont récupérés et pesés au cours du temps afin de mesurer le débit Q (m³.s⁻¹).

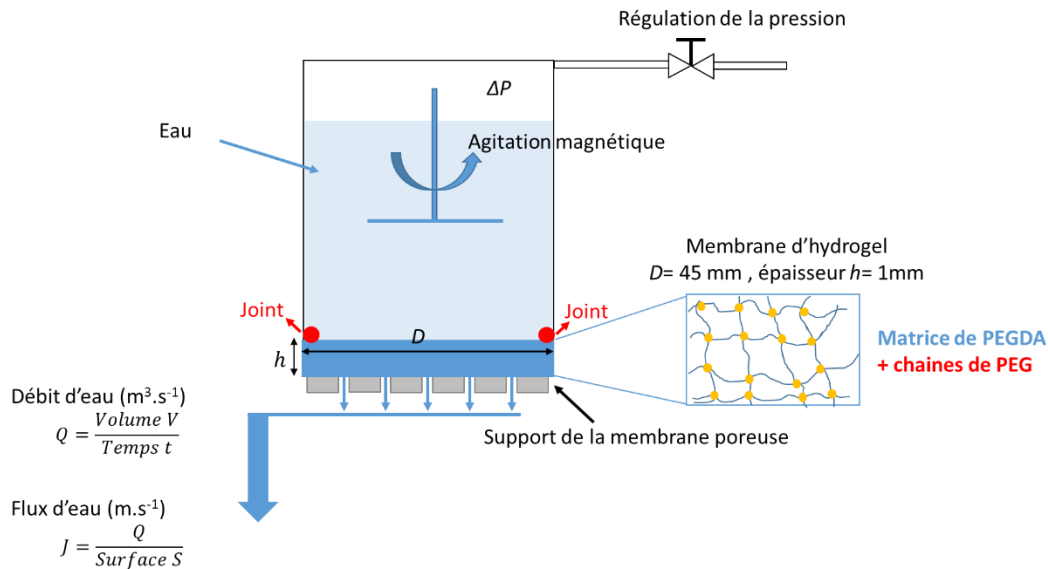


Figure 0.1. Schéma représentatif des expériences de la filtration frontale en utilisant les matrices d'hydrogels développées.

La perméabilité à l'eau, notée K , est calculée à partir de la loi de Darcy selon l'équation 0.1:

$$K = \frac{Q\mu h}{\Delta P S} \quad (0.1)$$

où Q est le débit d'eau ($\text{m}^3 \cdot \text{s}^{-1}$) calculé à partir de la pente de la variation du volume de perméat accumulé (m^3) en fonction du temps t (s), μ est la viscosité de l'eau (Pa.s), h est l'épaisseur de l'hydrogel (m), S est la surface de la membrane d'hydrogel (m^2) et ΔP est la différence de pression à travers la membrane (Pa).

Par rapport à la membrane d'hydrogel de PEGDA pur, nous avons remarqué que la teneur en PEG, pour les différentes masses molaires utilisées, permet de moduler la perméabilité à l'eau K sur plusieurs ordres de grandeur (Figure 0.2). Pour les PEG de faibles masses molaires (600 et 3000 $\text{g} \cdot \text{mol}^{-1}$), une augmentation continue de la perméabilité à l'eau avec l'augmentation de la teneur en PEG a été observée. Par exemple, pour le PEGDA/PEG-600 $\text{g} \cdot \text{mol}^{-1}$ (Figure 0.2 a), la perméabilité à l'eau passe d'environ $3,6 \times 10^{-18} \text{ m}^2$ à $\sim 0,8 \times 10^{-16} \text{ m}^2$ lorsque la teneur en PEG passe de 7,7 à 29,5 % en masse. En comparaison, la perméabilité à l'eau des hydrogels PEGDA/PEG-3000 $\text{g} \cdot \text{mol}^{-1}$ varie d'environ trois ordres de grandeur ($4 \times 10^{-18} \text{ m}^2$ à $\sim 10 \times 10^{-16} \text{ m}^2$) avec la teneur en PEG (Figure 0.2 b). En revanche, pour les fortes masses molaires de PEG ($\geq 10\,000 \text{ g} \cdot \text{mol}^{-1}$), la perméabilité à l'eau augmente avec la teneur en PEG jusqu'à atteindre un optimum avec une concentration critique en PEG (Figure 0.2 c à f). Au-dessus de cette concentration critique, la perméabilité à l'eau diminue lorsque la teneur en PEG augmente. Il est intéressant de noter que cette concentration correspond à la concentration de recouvrement critique des chaînes de PEG, notée C^* . Par conséquent, la concentration en PEG est un paramètre clé pour moduler la perméabilité à l'eau de l'hydrogel final.

De plus, nous avons observé que le maximum de la perméabilité obtenu à C^* est un phénomène robuste quel que soit la masse molaire en PEG étudiée.

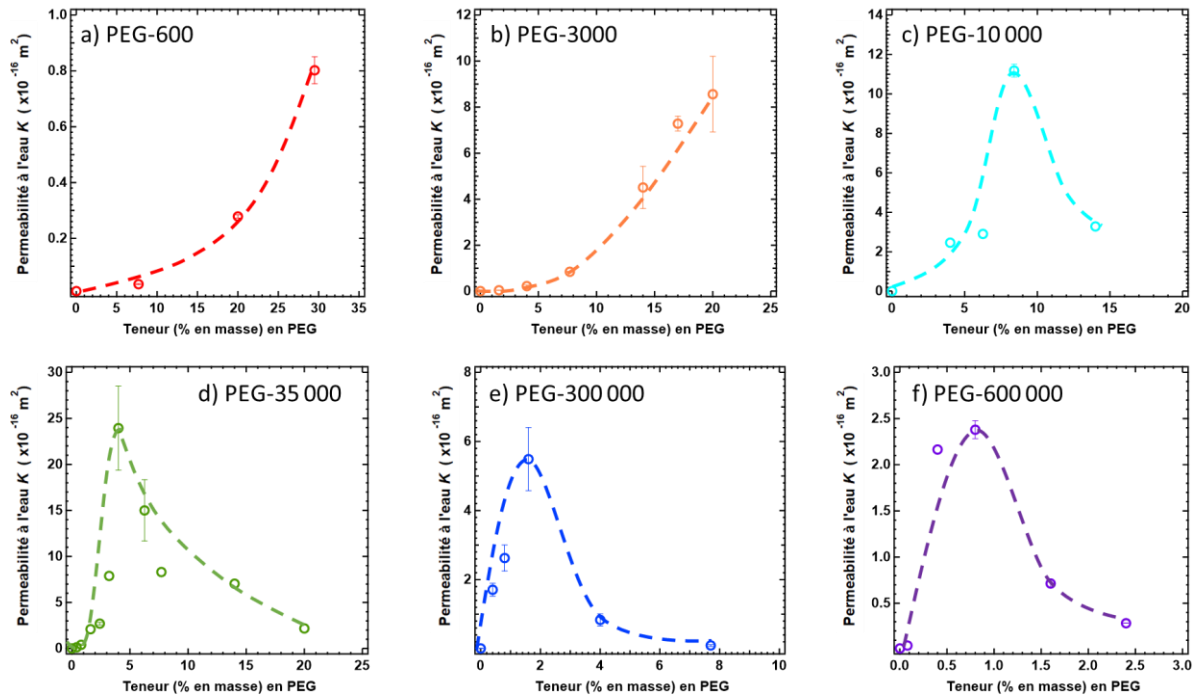


Figure 0.2. Variation de la perméabilité à l'eau obtenue à $P=10000$ Pa en fonction de la teneur en a) PEG-600 g.mol^{-1} ; b) PEG-3000 g.mol^{-1} ; c) PEG-10 000 g.mol^{-1} ; d) PEG-35 000 g.mol^{-1} ; e) PEG-300 000 g.mol^{-1} et f) PEG-600 000 g.mol^{-1} dans le mélange de prépolymérisation du PEGDA/PEG.

Variation non-linéaire de la perméabilité intrinsèque avec la pression

En présence de chaînes de PEG, nous avons obtenu une variation non linéaire du flux d'eau en fonction de la pression appliquée (entre 400 et 800 mBar) contrairement à l'échantillon de PEGDA pur (Figure 0.3). Nous avons observé que les flux d'eau atteignent un plateau au-dessus de pressions de l'ordre de 500 mBar, en fonction des teneurs et des masses molaires en PEG (Figure 0.3 b). De plus, nous avons trouvé que la perte de perméabilité, noté $\left(\frac{K_{max}-K}{K_{max}}\right)$, où K_{max} est la perméabilité obtenue à une pression de 20 mBar, augmente avec la concentration en PEG (Figure 0.4 b). Nous avons montré que cette perte de perméabilité est due à la compression des hydrogels sous l'effet de la pression.

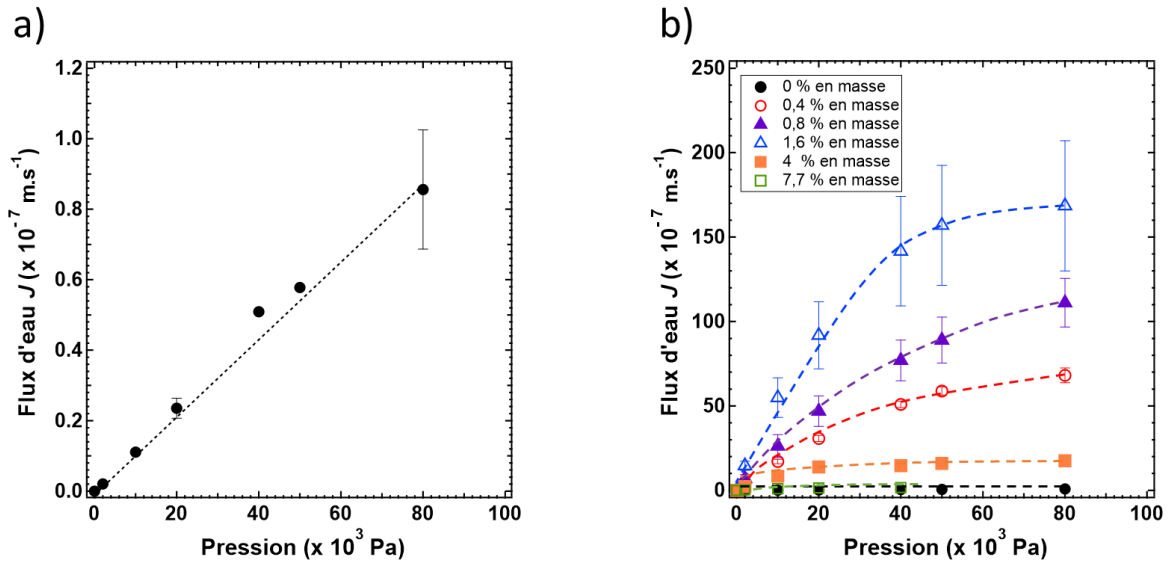


Figure 0.3. Variation du flux d'eau en fonction de la pression appliquée pour des membranes d'hydrogel de PEGDA a) sans PEG et b) avec différentes teneurs en PEG 300 000 g.mol^{-1} .

Nous avons en effet étudié les propriétés mécaniques des hydrogels en utilisant des expériences de compression. Nous avons d'abord constaté que la forte déformation imposée (par exemple $\sim 30\%$), conduit à l'expulsion de l'eau de la membrane de l'hydrogel contenant différents teneurs en PEG, contrairement à l'hydrogel de PEGDA pur. Ce résultat montre que l'ajout de PEG permet de rendre les membranes plus déformables ce conduit à un changement de la porosité de l'hydrogel. De plus, nous avons remarqué que les échantillons contenant du PEG avaient un module effectif plus faible que les hydrogels de PEGDA pur. La valeur des modules de Young calculée pour de faibles déformations diminue lorsque la teneur en PEG augmente (Figure 0.4 b). Cette diminution du module des hydrogels avec la teneur en PEG est en corrélation avec le fait que la perte de perméabilité augmente. Par conséquent, nous avons suggéré que la variation non linéaire de la perméabilité avec la pression était due à la compression des hydrogels et à la diminution de la taille des pores sous l'action d'une pression importante.

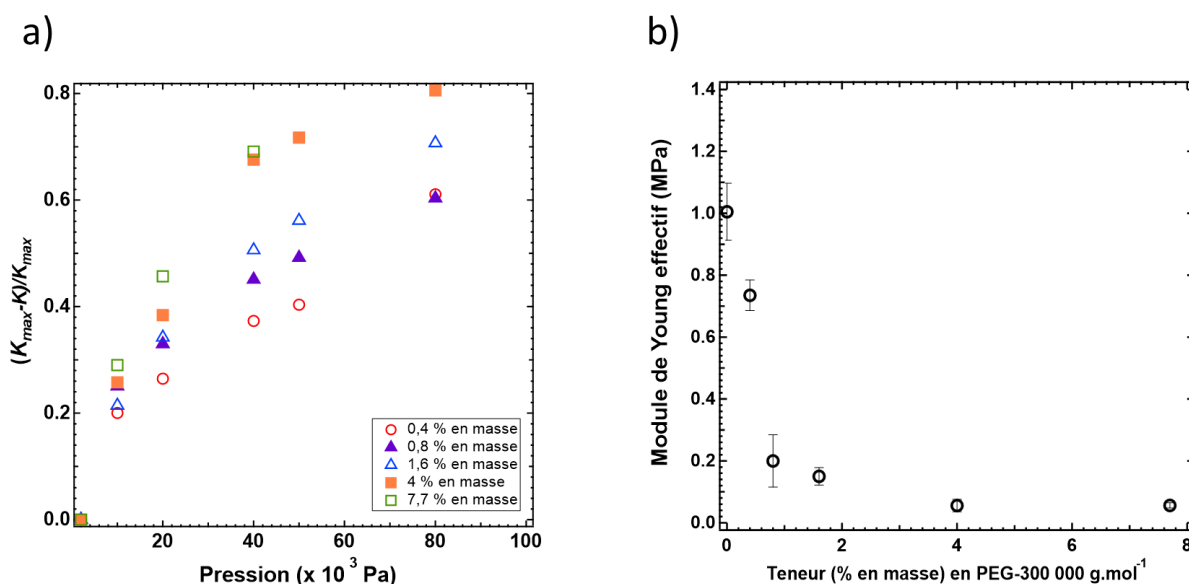


Figure 0.4. a) Variation de la perte de la perméabilité en fonction de la pression appliquée pour les hydrogels de PEGDA préparés avec différentes teneurs en PEG- 300 000 $g.mol^{-1}$. b) Variation du module de Young effectif en fonction de la teneur en PEG-300 000 $g.mol^{-1}$.

Influence de la teneur en PEG sur la structure morphologique de l'hydrogel PEGDA/PEG

Le deuxième objectif de ce travail était de comprendre l'effet de l'ajout des chaînes de PEG (à différentes concentrations et masses molaires) sur la structuration de la matrice de PEGDA. Tout d'abord, nous avons montré que cet ajout de chaînes de PEG n'affectait pas la polymérisation du PEGDA. Nous avons ensuite analysé la fraction du PEG libérée de l'hydrogel que ce soit dans le surnageant d'eau ou dans le perméat après des expériences de filtration cycliques (Figure 0.5). Nous avons obtenu que 80 % des petites chaînes du PEG (i.e. 600 et 3000 $g.mol^{-1}$) restent irréversiblement piégées dans la matrice. Pour le PEG à forte masse molaire (i.e. 300 000 $g.mol^{-1}$), 96 % des chaînes restent piégées dans la matrice. Par conséquent, nous avons supposé que les chaînes de PEG peuvent être greffées chimiquement à la matrice PEGDA par un mécanisme de transfert de chaîne.

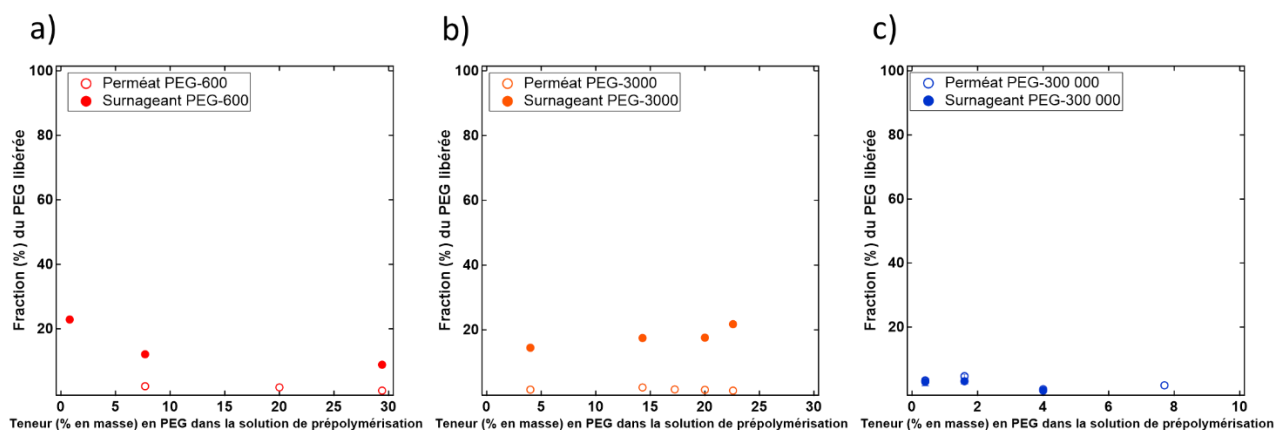


Figure 0.5. Variation de la fraction du PEG calculée dans le liquide surnageant (symbole plein) et dans le perméat après une filtration cyclique (symbole vide) en fonction de la teneur en PEG dans la solution de prépolymérisation pour a) PEG-600, b) PEG-3000 et c) PEG-300 000 $\text{g}\cdot\text{mol}^{-1}$.

Afin de mieux comprendre la structure des hydrogels PEG/PEGDA, nous avons utilisé la microscopie à force atomique (AFM) en phase liquide et la cryo-microscopie électronique à balayage (cryoMEB). La Figure 0.6 montre la structure obtenue pour un gel préparé avec différents teneurs en PEG-300 000 $\text{g}\cdot\text{mol}^{-1}$. En ce qui concerne l'hydrogel de PEGDA, nous avons remarqué qu'il se structure en cavités de 200 nm, remplies d'eau en raison d'une séparation de phase entre le PEGDA ($700 \text{ g}\cdot\text{mol}^{-1}$) et l'eau. Ce résultat est en accord avec ce qui est décrit dans la littérature. Lors de l'ajout de PEG, nous avons observé un changement dans la structure de l'hydrogel de PEGDA avec l'apparition de cavités plus grandes de $\sim 1 \mu\text{m}$, mises en évidence par les images cryoMEB. En AFM, nous avons observé la présence d'hétérogénéités de quelques dizaines de nanomètres dans les parois riches en PEGDA entre les cavités de taille micrométrique.

En corrélant ces observations avec nos résultats de perméabilité, nous avons suggéré que les cavités de 200 nm pour l'échantillon de PEGDA pur sont fermées (i.e. porosité fermée). De plus, pour les membranes d'hydrogel PEGDA/PEG, nous avons supposé que les cavités de taille micrométrique observées ne forment probablement pas un réseau percolant et que la présence de chaînes de PEG piégée dans la matrice de PEGDA crée des défauts de réticulation. Par conséquent, la perméation de l'eau est plutôt contrôlée par la structure des parois, séparant les cavités micrométriques, riches en PEGDA.

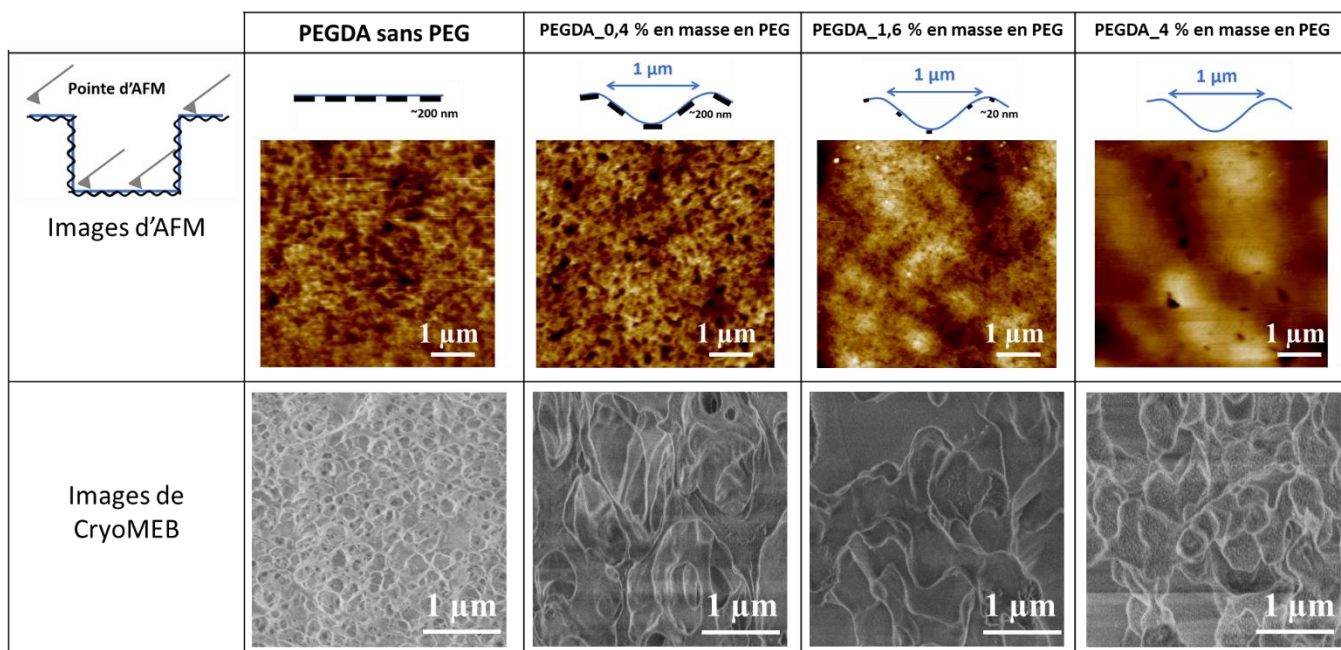


Figure 0.6. Images AFM et images cryoMEB de la membrane d'hydrogel préparée avec du PEGDA et différentes teneurs en PEG-300 000 g.mol^{-1} .

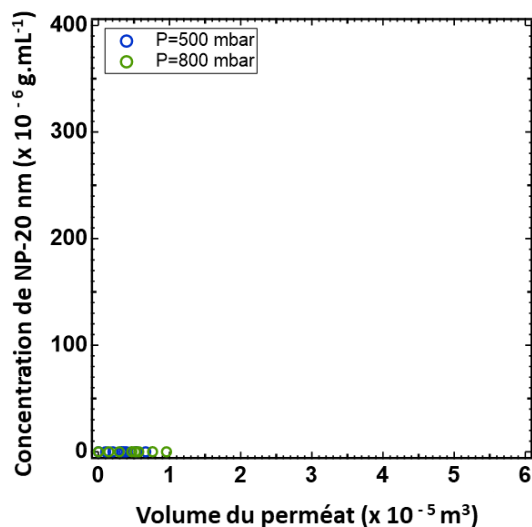
L'échelle moyenne en Z dans les images AFM est de ± 50 nm.

Filtration de particules à travers les membranes PEGDA/PEG hydrogel

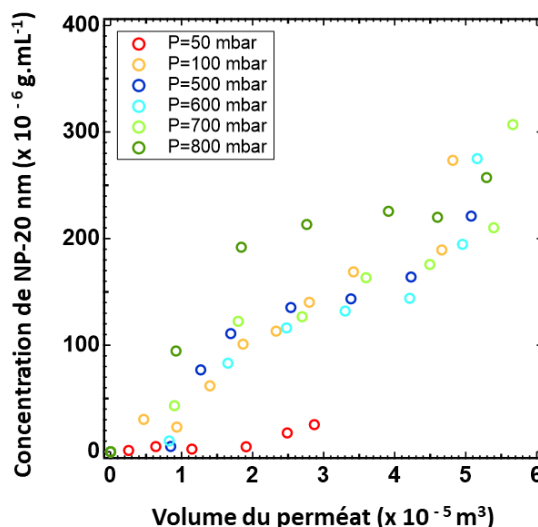
Par la suite, nous avons étudié la filtration de particules de polystyrène de différentes tailles (modifiées par des fonctions carboxylates et ainsi chargées négativement ($\zeta = -43,4$ mV)), à travers une membrane de PEGDA/PEG (différentes teneurs en PEG-300 000 g.mol^{-1}).

Tout d'abord, nous avons remarqué que la perméation des nanoparticules de 20 nm (NP-20 nm) dépend à la fois de la composition du PEGDA/PEG et de la pression appliquée pendant la filtration. Pour les hydrogels préparés avec du PEGDA pur (Figure 0.7 a) et du PEGDA avec une forte teneur en PEG (par exemple à une concentration $C = 4$ % en masse supérieure à C^* , Figure 0.7 d), nous avons remarqué que les NP-20 nm ne traversent pas les hydrogels même sous l'effet d'une forte pression (i.e. 800 mBar). Cependant, pour les membranes composées de 0,4 % et 1,6 % en masse de PEG (Figure 0.7 b et c), la concentration de NP-20 nm dans le perméat augmente avec le volume du perméat et dépend de la pression appliquée. Par exemple, cette concentration est presque nulle à une pression de 50 mBar pour le PEGDA/PEG_0,4 % en masse alors qu'elle devient non nulle au-dessus de 50 mBar pour le PEGDA/PEG_1,6 % en masse. Il semble donc qu'il existe une pression critique au-dessus de laquelle les NP-20 nm peuvent pénétrer et traverser ces hydrogels.

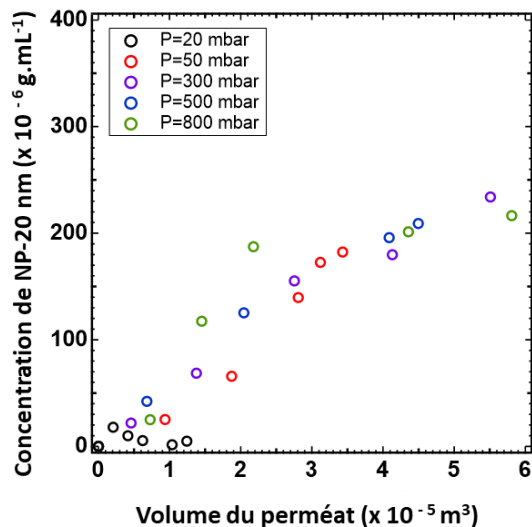
a) 0 % en poids de PEG



b) 0,4 % en poids de PEG



c) 1,6 % en poids de PEG



d) 4 % en poids de PEG

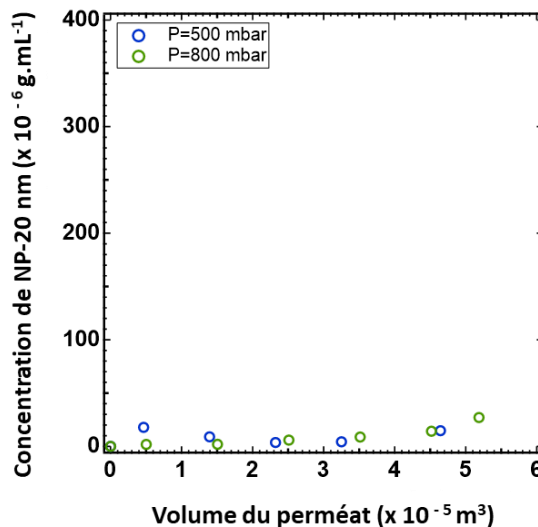


Figure 0.7. Variation de la concentration de nanoparticules NP-20 nm calculée dans le perméat en fonction du volume du perméat sous différentes pressions appliquées pour une membrane d'hydrogel préparée avec du PEGDA et a) 0 % en masse, b) 0,4 % en masse, c) 1,6 % en masse et d) 4% en masse de PEG-300 000 g.mol⁻¹.

Pour l'hydrogel le plus perméable (contenant 1,6 % en masse de PEG), nous avons également filtré des particules de polystyrène, de même nature que précédemment, mais ayant des diamètres plus grands, i.e. de 100 nm (NP-100 nm) et de 1 μ m (MP-1 μ m). Comme le démontre la Figure 0.8, ni les particules de 100 nm ni celles de 1 μ m ne traversent la membrane du PEGDA/PEG. Par conséquent, ces résultats suggèrent que la perméation de l'eau et des particules est contrôlée par les défauts nanométriques créés par les chaînes de PEG piégées dans les parois du PEGDA entre les cavités de taille micrométrique.

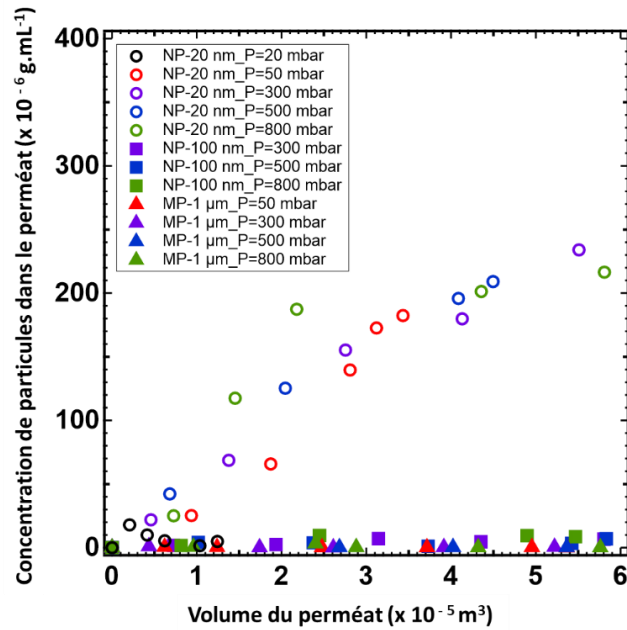


Figure 0.8. Variation de la concentration en nanoparticules NP-100 nm et microparticules MP-1 μ m calculée dans le perméat en fonction du volume du perméat sous différentes pressions appliquées pour une membrane d'hydrogel préparée avec du PEGDA et 1,6 % en masse de PEG-300 000 g.mol⁻¹. Les symboles vides correspondent à la concentration de nanoparticules NP-20 nm de latex.

Au final, sur la base de tous les résultats obtenus (AFM, CryoMEB, perméabilité et filtration des particules), nous avons proposé l'évolution de la structure de l'hydrogel en fonction de la concentration en PEG représentée par le schéma de la Figure 0.9.

A faible concentration en PEG, les chaînes de PEG piégées dans les parois séparant les cavités de taille micrométrique contrôlent la perméation des particules et de l'eau à travers les hydrogels (Figure 0.9 a). Par contre, à concentration plus élevée en PEG (Figure 0.9 b), la formation des brosses due aux présences de chaînes de PEG dans la surface interne des cavités de taille micrométrique ralentit la perméation de l'eau et des particules.

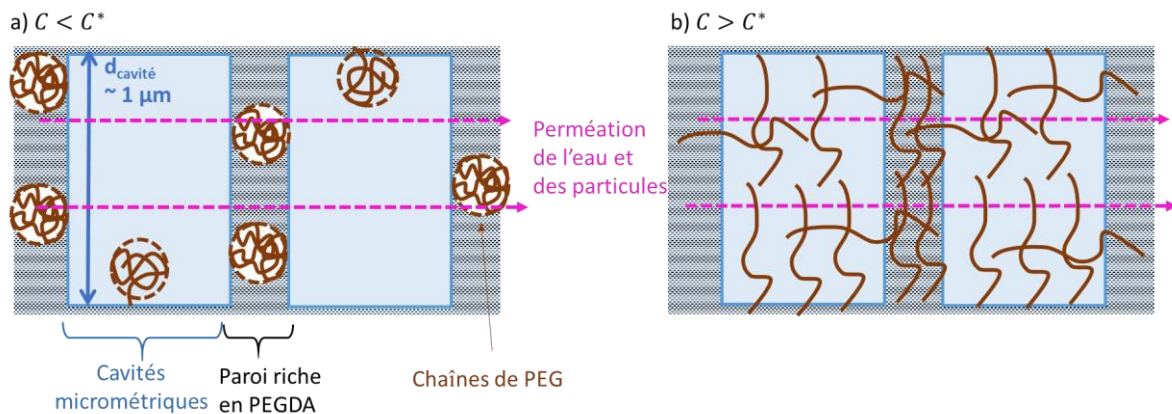


Figure 0.9. Schéma représentatif de l'organisation de l'hydrogel PEGDA/PEG pour une concentration en PEG a) $C < C^*$ et b) $C > C^*$.

En perspective, d'autres études structurales peuvent être réalisées pour compléter celle que nous avons menés sur le système d'hydrogel de PEGDA/PEG en utilisant des mesures de diffusions de neutrons aux petits angles (SANS). En utilisant du PEG deutéré, cette technique permettra de sonder uniquement la structure du PEGDA et de voir l'effet direct de l'ajout de PEG sur la structure de la matrice du PEGDA. En plus, les propriétés de sélectivité de ces hydrogels composites peuvent être aussi étudiées en remplaçant les chaînes de PEG neutres par des autres chaînes de polymères pouvant établir des interactions (électrostatiques, liaisons d'hydrogène,) avec le soluté à filtrer.

General introduction

Hydrogels, which are cross-linked three dimensional hydrophilic networks, are characterized by an inherent capacity to absorb large amounts of water, tunable biodegradability, controllable mechanical and chemical properties, and porous 3D structure. Owing to these unique properties, hydrogels are promising materials in various biomedical fields, including tissue engineering scaffold design, biosensing and drug delivery. In addition, they have attracted research's attention in the context of filtration and separation process, as coating used to improve the fouling resistance of conventional filtration membranes. In all these applications, it is crucial to find robust and simple methods to obtain hydrogels with a good control of their porous structure, permeability to water, nutrients or particles as well as mechanical properties.

We have chosen to design poly (ethylene glycol) diacrylate PEGDA hydrogels containing various amounts of poly (ethylene glycol) PEG chains of varying molar masses because this system can be easily synthesized using a radical polymerization under UV light. Moreover, PEGDA-based hydrogels combine many advantages such as mechanical resistance, biocompatibility and hydrophilic structure.

In this work, we study the effect of the PEG concentration and molar mass on the permeability and filtration properties of the hydrogels and relate these to their structure. The novelty with respect to the literature is that we use large PEG chains that remain trapped in the PEGDA matrix. In fact, the existing literature previously used short PEG chains as templating agents to promote porosity, that are removed by an additional rinsing step after polymerization. In our case the addition of large PEG chains allows to develop a new PEGDA/PEG composite membrane in a simple and one-step method, with a control of the hydrogel permeability over several orders of magnitude.

The manuscript will be structured as follows:

Chapter 1 is a literature review composed of three parts. First, we will recall the hydrogel networks, their classification and their key properties. Then we will describe briefly the different characteristics of filtration process, including their types and modes and the materials of the classical filtration membranes. The last part of this chapter consists in combining the use of hydrogel systems for different filtration applications. We will be interested to review the filtration through thin hydrogel films coated on classical membranes as well as the filtration

through free-standing hydrogel systems. A particular interest is given to PEGDA-based membranes for filtration process.

Afterwards, the experimental results of this work will be presented as a compendium of three Chapters that each contain a short state of the art and experimental part.

Chapter 2 is a copy of an article which was recently published in *Macromolecules* (Eddine, M. A.; Belbekhouche, S.; de Chateauneuf-Randon, S.; Salez, T.; Kovalenko, A.; Bresson, B.; Monteux, C., Large and Nonlinear Permeability Amplification with Polymeric Additives in Hydrogel Membranes. *Macromolecules* **2022**, *55* (21), 9841-9850, DOI 10.1021/acs.macromol.2c01462). This Chapter is devoted to the experimental study of the effect of large PEG chains of 300 000 g.mol⁻¹ on the PEGDA hydrogel properties. We investigate first the effect of PEG-300 000 g.mol⁻¹ contents on the polymerization reaction of PEGDA oligomer. We report the dependence of the PEGDA/PEG hydrogel permeability on the PEG concentration and applied pressure and correlate these permeability measurements with the mechanical properties of the hydrogels as well as their structure. Another key point of this Chapter is the quantification of the amount of PEG chains remaining trapped in the matrix, which is surprisingly high.

In Chapter 3 the filtration of latex particles suspensions with different sizes through composite PEGDA/PEG-300 000 g.mol⁻¹ hydrogel membranes is studied. We investigate the effect of applied pressure and PEG contents on the filtration of nano and microparticles through the PEGDA/PEG hydrogel membranes. The results are discussed with respect to atomic force microscopy (AFM) and cryoscanning electron microscopy (cryoSEM) measurements and enable us to deduce important information about the structure of the hydrogels. Furthermore, we study the effect of the clogging of the hydrogels with the particles on the permeation flux.

Chapter 4 deals the effect of PEG molar mass on the permeability and structure properties of the PEG/PEGDA hydrogels. We investigate, in a systematic manner, if the dependence of the water permeability measurement on the PEG contents is a robust phenomenon for a wide range of PEG molar masses. Moreover, we determine whether the PEG molar mass influences the removal of the PEG chains from the hydrogel matrix. Similarly, to the previous study of Chapter 2 and 3, we investigate the evolution of the hydrogel structure as a function of PEG content and molar mass by performing AFM and cryoSEM measurements.

Chapter 1

Literature review

This first chapter is devoted to the description of concepts underlying this work and previous literature studies. It is composed of three parts. First, we will describe hydrogel systems, their classification and their main properties. Secondly, we will be interested in studying the different processes of filtration. We will describe briefly the different types, mode, materials and properties of filtration membranes used in the studied context. In the last part of this chapter, we will make an overview of the use of hydrogel membranes in the field of filtration. A specific interest is given to the structural, mechanical and permeability properties of PEGDA-based hydrogel membranes, used in this work.

1.1 HYDROGELS

1.1.1 History and generalities

A hydrogel is a three-dimensional network of polymer swollen, as represented in (Figure 1.1), with a large amount of water. This current definition of a hydrogel with its specific properties, mainly its high affinity to water, was established in 1960 by Wichterle and Lim after their synthesis of polyhydroxyethylmethacrylate (pHEMA)-based hydrogel ¹. This first synthetic hydrogel was used in many applications that require permanent contact with human tissues, such as the contact lenses, an invention patented in 1968 ². It was at this period that hydrogel technology has progressed in a wide range of applications ³, such as the food ⁴, the pharmaceuticals and the biomedical fields ⁵. In addition, they have gained a significant interest in tissue engineering ^{6,7}, drug delivery ⁸⁻¹² and scaffolds regeneration ¹³. Hydrogels are also used for water/wastewater treatment and for separation processes ¹⁴⁻¹⁸. These different applications have motivated researchers to study the relationship between the structure of hydrogels and their biocompatibility ¹⁹.

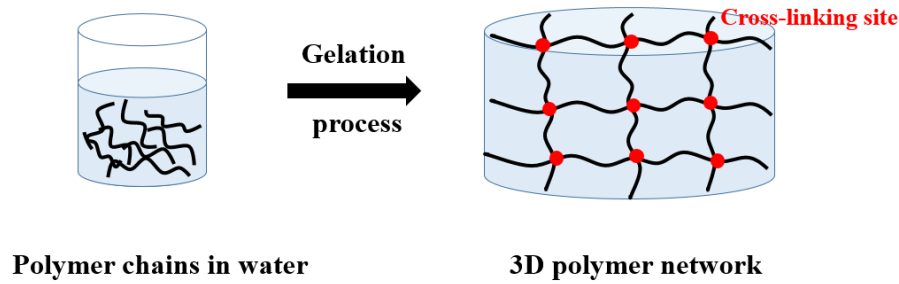


Figure 1.1. Schematic illustration of a hydrogel network.

1.1.2 Classification

The large variety of matrices (origin, structure, functionality, etc.) from which hydrogels can be formed and the various possible ways of gelation process have given rise to several types of hydrogels with different chemical and physical properties. As a result, several classifications of these materials have emerged in recent years²⁰⁻²².

Hydrogels are classified according to different criteria²³, such as the source of the polymer (natural or synthetic), the charge of the hydrogel (non-ionic, cationic or anionic), the type of cross-linking based on physical or chemical cross-linking junctions, their biodegradability and their physical and mechanical properties (stiffness, elasticity,...).

The classification of hydrogels based on their different characteristics is important for their further use and application. However, the two main criteria often used to distinguish the gels are the polymer source and the type of cross-linking.

For example, based on the source of polymer, natural hydrogels are generally formed from polysaccharides (hyaluronic acid, alginate, chitosan...) or from proteins (collagen, gelatin...). They constitute the most physiological hydrogels because some of them are constituents of the extracellular matrix (ECM) *in vivo*. The main disadvantage of natural hydrogels is the possible variability of properties from one batch to another due to their natural origin which can induce a variation of their composition. However, the synthetic hydrogels such as poly (vinyl alcohol) (PVA), poly (ethylene glycol) (PEG), or polyacrylic acid (PAAc) are characterized by a more controlled and reproducible structure. The hydrolysis or biodegradation of these materials can also be programmed over variable and well-defined periods (ranging between several days to months), depending on the final applications. This is one of the reasons why we have chosen the PEG-based hydrogels in our studies.

Hydrogels are also classified according to the type of cross-linking, into two groups: physical hydrogels and chemical hydrogels ²⁴. The characteristics of each hydrogel are detailed below.

Physical gels:

Physical hydrogels, also called reversible hydrogels, have a very significant place in a wide field of applications (e.g. wound dressing ²⁵, drug delivery,...), because of their ease of processing without the need for a chemical cross-linking agent. This transient character is due to the low energy of the connections between the macromolecular chains (hydrogen bond, ionic bond, hydrophobic interaction....) ²⁶⁻²⁹. The number and strength of these cross-linking points depend directly on the thermodynamic and mechanical states of the gel, thus inducing a reversibility of the gelation process. This means that associations can be broken and reformed continuously under the effect of a variation of physico-chemical conditions during gelation process (temperature, pH, polymer concentration, ionic strength...) ³⁰.

Chemical gels:

In contrast to the previous gels, chemical gels are made of polymer chains linked together by covalent bonds. The cross-linking points of the network have a permanent character which gives it a great stability and is globally less dependent on external factors (pH, temperature, mechanical deformation...). This stability makes the formed network insoluble in any solvent and their swelling properties depend on their affinity to water. Generally speaking, chemically cross-linked gels often have much higher mechanical properties than their physically cross-linked counterparts ³¹.

The main methods of preparation of chemical hydrogels reported in the literature are the chemical cross-linking and the radical polymerization detailed below.

1. **Chemical cross-linking:** This technique is based on chemical reaction of bi-functional cross-linking agent with a hydrophilic polymer holding appropriate functional group such as carboxylic acid (-COOH), hydroxyl (-OH) and amino (-NH₂). The most common cross-linking agents used for the formation of chemical hydrogels are the epichlorohydrin, glutaraldehyde, adipic acid dihydrazide (DHA) or polyaldehydes,... For example, gelatin and albumin based hydrogels were prepared using dialdehyde or formaldehyde as cross-linking agents ³². On the other hand, PEG-based hydrogels can be also prepared by chemical cross-linking, using PEG-derivatives as cross-linking agents ³³.

2. **Radical polymerization:** Radical polymerization is considered as the most commonly used method to obtain chemical hydrogels with the advantages of high reactivity, high conversion and mild reaction conditions. The radical polymerization process follows up the subsequent steps: initiation, propagation and termination. To initiate the polymerization, initiators must be added to the system containing monomers and cross-linking agents to generate free radicals ³⁴.

One can distinguish three types of initiators used in this technique:

- a) Thermal initiators, generating radicals by thermal decomposition. Azobisisobutyronitrile (AIBN) and benzoyl peroxide (BPO) are well-known thermal radical initiators.
- b) Redox initiators, for which the production of radicals results from a redox reaction. Ammonium persulfate (APS) and potassium persulfate (KPS) both are commonly used as redox initiator in radical polymerization reaction ³⁵. For example, the polyacrylamide hydrogels are synthesized using acrylamide monomer and bis-acrylamide as cross-linking agent. This polymerization technique requires the use of APS and N, N, N', N' Tetramethylethylenediamine (TEMED) to induce and initiate the polymerization reaction of polyacrylamide.
- c) Photochemical initiators, generating radicals under the effect of light or UV radiation. These are in general aromatic ketones which undergo homolytic cleavage of C-C upon UV exposure, with formation of two radical fragments, as shown in (Figure 1.2).

The benzoyl radical is known to be highly reactive toward vinyl and acrylic monomers. In some cases, the second radical fragment can also participate to initiate the polymerization. Benzylic ketals, benzoin, α -amino aromatic ketones and acylphosphine oxides are the most effective photoinitiators belong to this category.

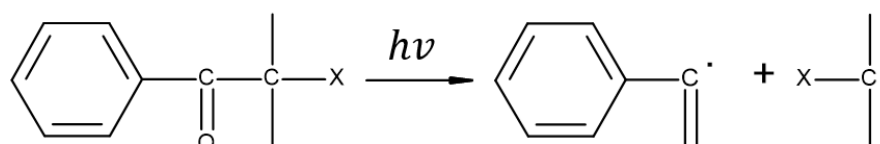


Figure 1.2. Formation of radical fragments under UV light.

The photoinitiated polymerization process is considered as an efficient method for hydrogels synthesis. This technique provides many advantages during the hydrogels preparation such as no need to use catalysts or additives to initiate the polymerization. As the free radicals are generated under the effect of UV light, the cross-linking density of the polymer network chain can be controlled by changing the irradiation dose. Due to these benefits, the chemical hydrogels prepared by the photopolymerization method have been widely used for many biomedical applications. As example, due to their biocompatibility and water solubility, PEG-based polymer (such as poly (ethylene glycol) diacrylate (PEGDA) and poly (ethylene glycol) monomethacrylate (PEGMA)) have been widely used in photoradical polymerization to contribute to the development of PEG-based hydrogels used as a scaffold for cells delivery involved in tissue regeneration^{36, 37}. In addition, they have gained an interest in the industrial and filtration process. Consequently, PEGDA-based hydrogels employed as a membrane for filtration experiments have been chosen in this work.

1.1.3 Structure of hydrogels

Hydrogels are a porous structure characterized by an inherent pore size directly related to the length of the polymer chain, the concentration of polymer in the pre-gel solution, as well as the cross-linking density³⁸. An important structural parameter of the hydrogel is the mesh size (ξ) defined as the distance between two effective cross-links points²². Generally, the typical hydrogel mesh size is in the nanometer range. In order to understand the structural properties of hydrogels, different behaviors such as the conformation of an ideal polymer chain as well as the behavior of a polymer in solution must first be defined.

A) Polymer coils and solutions

Conformation of an ideal chain:

First, we will report the main results on the conformations of an ideal chain, i.e. without interactions between monomers or between solvent molecules.

Considering a flexible chain of $n+1$ backbone atoms A_i ($0 \leq i \leq n$), the bond vector \vec{r}_i connects to A_{i-1} to A_i .

The polymer is in its ideal state if there are no net interactions between atoms A_i and A_j that are separated by a sufficient number of bonds along the chain so that $|i - j| \geq 1$.

The end-to-end distance vector is the sum of all n bond vectors in the chains (Equation 1.1):

$$\vec{R}_n = \sum_{i=1}^n \vec{r}_i \quad (1.1)$$

Different individual chains will have different bond vectors and hence different end-to-end vectors. The conformation of a flexible polymer is represented in (Figure 1.3).

The average end-to-end vector of an isotropic collection of chains n backbone atoms is zero, $\langle \vec{R}_n \rangle = 0$.

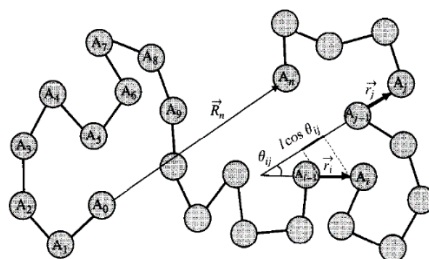


Figure 1.3. One conformation of a flexible polymer.

One of the simplest model of an ideal polymer is the freely jointed chain model with a constant bond length $l = |\vec{r}_i|$ and no correlation between the directions of different bond vectors.

The mean-square end-to-end distance of a freely jointed chain is (Equation 1.2):

$$\langle R^2 \rangle = nl^2 \quad (1.2)$$

where l is the length of the C-C bond ($\sim 1.54 \text{ \AA}$).

In a flexible polymer chain, there are in fact correlations between \vec{r}_i , these correlations disappearing when the \vec{r}_i are very far from each other: it is therefore necessary to correct equation by a corrective term C_n called the Flory's characteristic ratio. The characteristic ratio is larger than unity for all polymers ($C_n > 1$). In the case of an ideal chain with large number of main-chains bonds ($n \rightarrow \infty$), this term will be noted C_∞ . The variation of the Flory's characteristic ratio as a function of the chain length is represented in (Figure 1.4). Its numerical value depends on the local stiffness of the polymer chain with typical numbers of 7-9 for many flexible polymers. Polymers with bulkier side groups may have a highest C_∞ , owing to the side groups sterically hindering bond rotation (as in polystyrene with $C_\infty = 9.5$). In contrast poly(ethylene glycol) has a C_∞ of about 5.

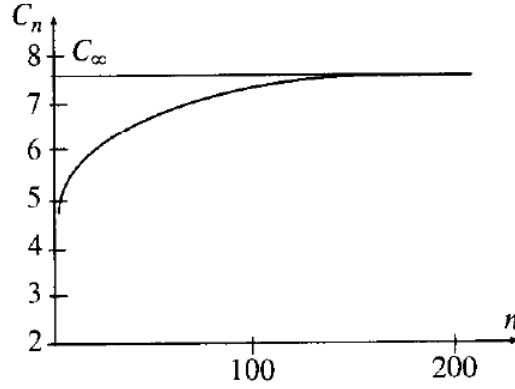


Figure 1.4. Flory's characteristic ratio C_n saturates at C_∞ for long chains.

Consequently, the mean-square end-to-end distance can be approximated for long chains (Equation 1.3):

$$\langle R^2 \rangle \approx C_\infty n l^2 \quad (1.3)$$

This mean-square end-to-end distance can be a characteristic of the size of linear chains. However, for branched or ring polymers, this quantity is not well defined, because they either have too many ends or no ends at all. Since all objects possess a radius of gyration, it can characterize the size of polymers of any architecture.

The radius of gyration is defined as the average distance between monomers in a given conformation and the polymer's center of mass as represented in (Figure 1.5).

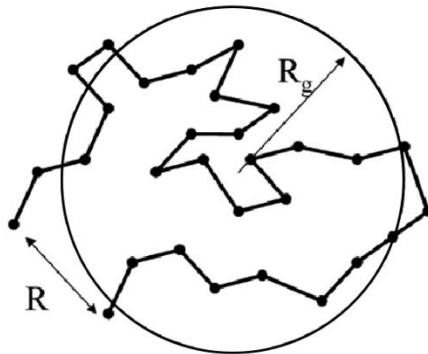


Figure 1.5. Schematic representation of a statistical coil with R the end-to-end distance and R_g the radius of gyration.

In the case of a linear ideal chain, we have (Equation 1.4):

$$\langle R_g^2 \rangle = \frac{\langle R^2 \rangle}{6} = \frac{C_\infty n l^2}{6} \quad (1.4)$$

Polymer in solutions:

Depending on the concentration and mass of the polymer in solution, different regimes can describe their behavior. For entropic reasons, the polymer chains are not unfolded but contract on themselves to form coils. The behavior of a polymer in solution has been described in particular by De Gennes³⁹, as represented in (Figure 1.6). At low polymer concentration, in the diluted regime, the polymer chains (coils) are distributed in an isolated manner throughout the solvent volume. When the concentration of polymer (or its volume fraction ϕ) is increased, the distance between coils decreases. At some point, the polymer chains start to contact and overlap between them and the concentration associated with this is called the critical overlap concentration C^* . This concentration marks the first transition between the diluted and the semi-diluted regime. The second transition is reached when the polymer concentration is above C^* (concentrated regime). In this later case, the coils are fully interpenetrated with $C = C^{**} > C^*$ and the chains are totally entangled in a 3D network.

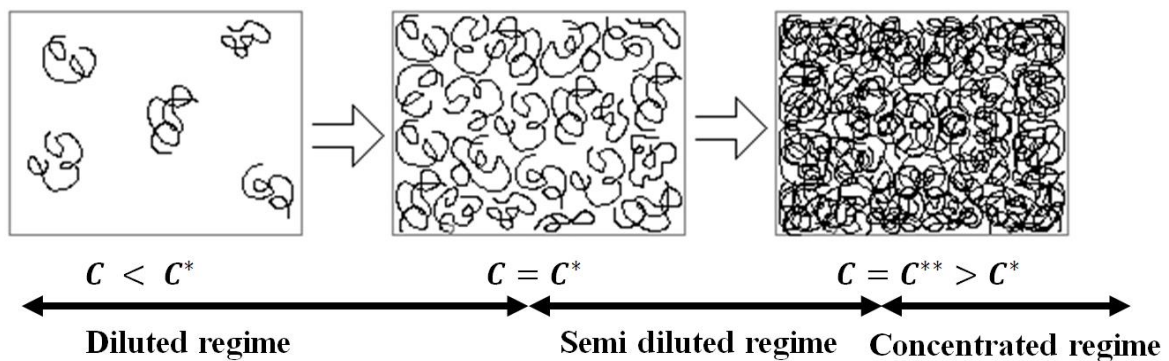


Figure 1.6. Schematic representation of the behavior of a polymer in solution.

In addition, the critical overlap concentration C^* of polymer chains, beyond the semi-diluted regime, can be calculated by Equation 1.5⁴⁰:

$$C^* = \frac{\overline{Mw}}{\frac{4}{3}\pi R_g^3 N_A} \quad (1.5)$$

where \overline{Mw} is the average molar mass of the polymer, N_A is Avogadro number: $N_A = 6.023 \times 10^{23} \text{ mol}^{-1}$.

Furthermore, the rheological study of polymer solutions allows to determine their critical recovery concentration C^* . When C^* is reached, polymer chains start to interact with each other in the solution. This results in an increase in the viscosity of the solution. The C^* of a polymer

is obtained by plotting the viscosity measured at zero shear as a function of the polymer concentration. The break in the slope of this variation gives access to C^* .

B) Morphology controlled by phase separation

One way to control the structure of hydrogel network is to trigger a phase separation. This technique was widely used for the preparation of polymeric membrane with tailored separation performance. Phase separation can be induced by a variety of stimuli, including temperature, polymerization reaction (continuous increase in the fraction of molecules with high molecular weight) or unfavorable interactions between mixture polymer species^{41, 42}.

In homogeneous mixtures of fluids, phase separation takes place via nucleation and growth (Figure 1.7 A (i)) or via spinodal decomposition to form a bicontinuous network formed by interconnected channels (Figure 1.7 A (ii)). Because the interface between these biphasic structures costs energy, their microscopic features tend to vanish over time, with interfacial forces driving their coarsening into two macroscopic domains (Figure 1.7 A (iii)). These demixing pathways entail very different morphologies.

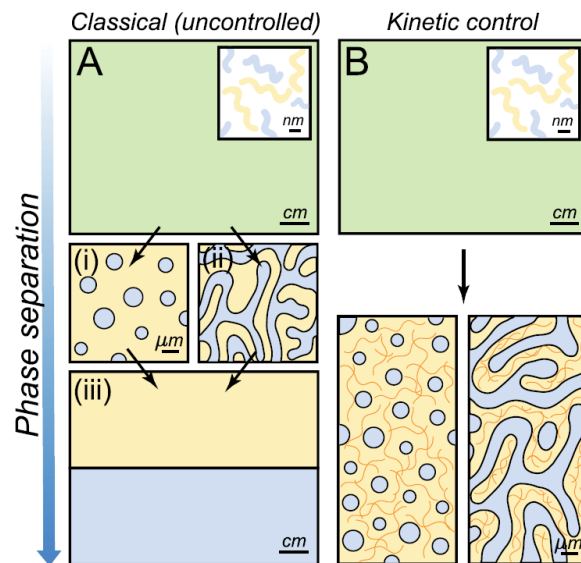


Figure 1.7. Liquid–liquid phase separation and some established methods to control it. (A) Classical (uncontrolled) phase separation of a homogeneous mixture where the two immiscible components (blue and yellow) demix by either (i) nucleation and growth or (ii) spinodal decomposition until they form (iii) two distinct macroscopic phases. (B) Kinetic control of phase separation⁴³.

Vitrification or gelation of one phase is a powerful approach to arrest liquid–liquid phase separation at the microscale (Figure 1.7 B). For example, porous polymer membranes for filtration (with pore diameters in the range of nm to several μm), are made from a polymer solution where phase separation is triggered by a rapid thermal or solvent-composition quench⁴⁴. Phase separation arrests microscopically when the polymer-rich phase vitrifies, i.e. when it reaches a glassy state, due to the reduced mobility of the polymer chains. Using this kinetic approach, the final structure of the material can be tuned over multiple length nano or macro-scales, as it depends on the competition between the coarsening rate of the phase-separated domains and the quenching rate of the system.

Consequently, phase separation method became a ubiquitous process and found applications in a variety system to fabricate advanced functional materials with engineered microstructures⁴³. Some examples include the fabrication of metal alloys⁴⁵, colloidal particles^{46, 47} and porous materials^{48, 49} for filtration process.

1.1.4 Properties of hydrogels

The use of hydrogels in different fields of application such as tissue engineering, drug delivery and filtration process require the understanding and the control of their main properties, in particular their swelling and mechanical properties.

A) Swelling behavior

The swelling property of hydrogels is their ability to absorb and retain a large amount of water due to the presence of hydrophilic groups within the polymer network chains such as $-\text{OH}$ and $-\text{COOH}$ ^{50, 51}. They are influenced by many factors such as the concentration of the polymer and its molar mass, the neutral or charged nature of the polymer, the cross-linking density, the nature of the cross-linking agent, the cross-linking method, the drying techniques and other environmental factors such as pH, temperature and ionic strength.

The swelling of the network can be expressed by the weight swelling ratio Q (Equation 1.6):

$$Q = \frac{W_s}{W_0} \quad (1.6)$$

where W_s is the weight of the swollen hydrogel, and W_0 is the weight of the hydrogel right after preparation.

When hydrogels are immersed in water (Figure 1.8), the polymer chains tend to expand to their fully solvated state, while the cross-linked structure applies an oppositely oriented force that pulls back until the expanding and retracting forces counterbalance each other and the swelling equilibrium is achieved.

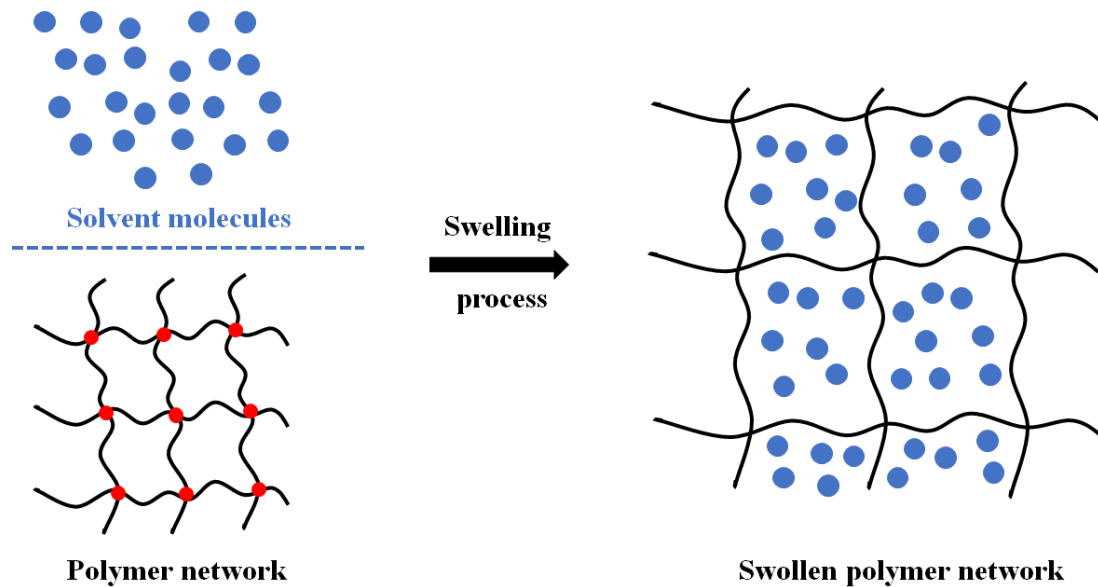


Figure 1.8. Schematic illustration of polymer network swelling.

The swelling of hydrogels is described most commonly by the Flory-Huggins equation of state. The free energy change associated with mixing the polymer chains with the solvent, ΔG_{mix} , is given by Equation 1.7³⁰ :

$$\Delta G_{mix} = \Delta H_{mix} - T\Delta S_{mix} \quad (1.7)$$

where ΔG_{mix} is the total free energy change of mixing, ΔH_{mix} is the change of enthalpy of mixing, ΔS_{mix} is the entropy change of mixing, and T is the temperature.

Enthalpy changes occur due to the interactions between the polymer and solvent molecules. ΔG_{mix} must be negative for the producing of the mixture and the swelling of the gel.

In regards to the enthalpy, swelling is favorable when ΔH_{mix} is negative. This will occur if specific interactions form between the polymer and solvent molecules, to produce a mixed state of lower energy. However, if it is more preferable (a lower energy state) for the polymer and solvent molecules to interact only with themselves, then ΔH_{mix} will be positive and mixing of the two phases will not be favorable.

In addition to the enthalpy changes associated with mixing, there will also be entropy variation ΔS_{mix} . Mixing has an entropic advantage since the homogenization of the solvent and polymer molecules creates a more random system. However, in a hydrogel, upon swelling of the polymer chains with the solvent, the chains elongate resulting in an entropic penalty.

The total free energy of the neutral gels system is characterized by change of the Gibbs energy ΔG_{total} considered as additive contributions due to mixing of the cross-linked polymer with the solvent, ΔG_{mix} , and due to deformation of elastically active network chains, ΔG_{el} .

ΔG_{total} is given by Equation 1.8:

$$\Delta G_{total} = \Delta G_{mix} + \Delta G_{el} \quad (1.8)$$

For mixing and swelling to occur, ΔG_{total} , should be negative, so that the process will be spontaneous³⁰.

B) Mechanical properties

The mechanical behavior of hydrogels is generally described using rubber elasticity and viscoelasticity theories, and studied experimentally by the temporal response of the gel under stress. Hydrogels mechanical parameters, such as Young's modulus E , failure strength, viscoelasticity, shear modulus G' and others can be evaluated through mechanical tests, including compression, indentation, tensile and shear testing⁵². The tensile, the compression and shear tests are usually used to characterize the hydrogel mechanical properties (Figure 1.9). Tensile testing consists of hydrogel tensile deformation at a constant rate of elongation and recording the force required to maintain that rate of elongation. The force and elongation of the material are used to obtain a graph of stress versus strain, from which mechanical parameters can be derived⁵³. On the other hand, the compression test involves compressing of the hydrogel between two plates. The force required to compress the hydrogel and the amount of deformation are used to derive a stress versus strain graph from which the compressive modulus and compressive strength can be determined.

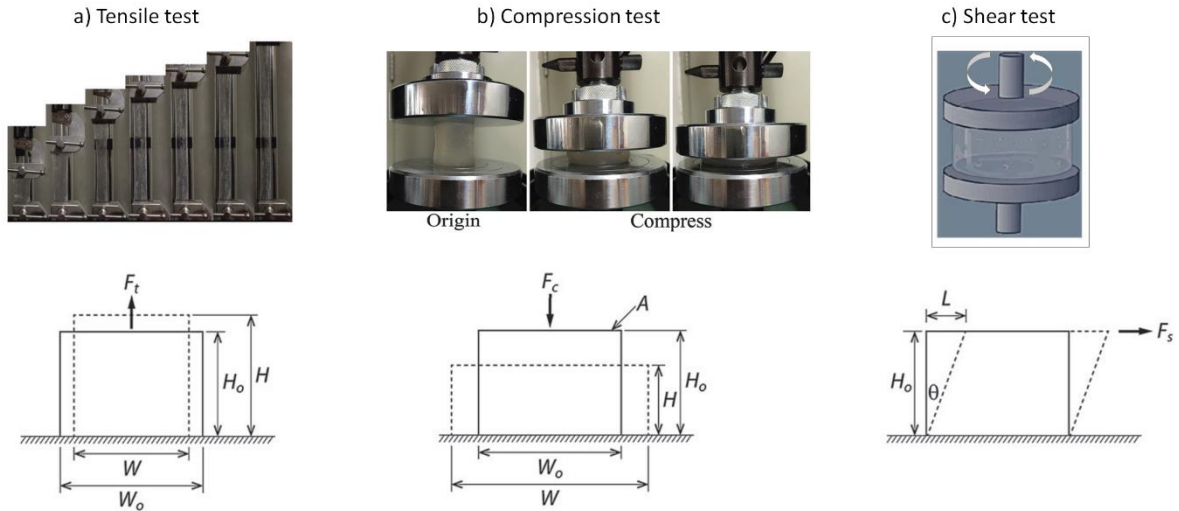


Figure 1.9. Photographs of the poly (vinyl alcohol) (PVA)/poly (vinyl pyrrolidone) (PVP) hydrogels during a) the uniaxial tensile test, b) the unconfined compressive test and c) the shear test⁵⁴.

In order to obtain the mechanical parameters of the hydrogels, the engineering stress and strain are calculated, respectively, using the following equation:

- 1) The engineering stress is obtained by the applied force over the original cross-sectional area (Equation 1.9):

$$\sigma = \frac{F}{A_0} \quad (1.9)$$

where, σ is the engineering stress (Pa); F is the applied force (N) and A_0 is the original cross-sectional area (m²).

- 2) The engineering strain, on the other hand, is measured as the ratio of the elongation to the initial hydrogel length (Equation 1.10):

$$\varepsilon = \frac{\delta}{H_0} \quad (1.10)$$

where, ε is the engineering strain (unitless); δ is the elongation at any point during uniform elongation stage (mm) : $\delta = H - H_0$; H is the height at any point during uniform elongation (mm) and H_0 is the initial hydrogel height (mm).

- 3) And finally, the Young's modulus E or elastic modulus which is the constant that relates the engineering stress and the strain of an elastic material, is given by Hooks' law (Equation 1.11):

$$\sigma = E \cdot \varepsilon \quad (1.11)$$

In addition, hydrogels are also characterized by the shear modulus G' which is measured using a rheometer with parallel plates. Shear modulus is related to the Young's modulus E by the Poisson's ratio, ν , which measures the contraction of the hydrogel perpendicular to the direction of the applied force. In general, the values of ν are between -1 and 0.5 depending on the materials properties. It is 0.5 for incompressible materials.

G' is given by Equation 1.12:

$$G' = \frac{E}{2(1+\nu)} \quad (1.12)$$

For a hydrogel, the physical origin of the elastic modulus is the stretching of the chains and the loss of the entropy when the material is sheared or stretched.

For a model of chain networks, the constant coefficient relating the stress to the strain is equivalent to the shear modulus defined before, and it is given by Equation 1.13:

$$G' = \frac{nK_bT}{V} = \nu K_bT = \frac{\rho RT}{M_s} \quad (1.13)$$

where $\nu = n/V$ is the number of elastic segments per unit volume; ρ is the network density (mass per unit volume); M_s is the average molar mass of an elastic segment and R is the constant of perfect gases. In general, the modulus increases with temperature (entropic origin) and linearly with the density of elastic segments.

Based on their Young's and shear moduli, hydrogels can be classified into two categories: soft and rigid gels. Soft hydrogels have a Young's moduli ranging from tens of Pa to hundreds of KPa, such as alginates gels⁵⁵. Whereas, the rigid gels have higher modulus, in the range of MPa to GPa. They are less deformable and can break when the stress exceeds a threshold value.

As for the swelling behavior of the hydrogels, their mechanical parameters may be affected mainly by the polymer concentration, the cross-linking density, the energy of the chemical bonds as well as the physical entanglements between polymer chains. For example, a chemically cross-linked network has a higher elastic modulus than the physically cross-linked one, because the energy of a covalent bond is higher than that of a physical bond.

In general, the hydrogel stiffness can be improved by increasing the stiffness of the polymer backbone (e.g. by replacing acrylates with methacrylates). As well, increasing the cross-linking density of a gel by increasing the content of cross-linking agent or the polymer concentration⁵⁶ makes the hydrogels stiffer as their elastic modulus is proportional to the cross-linking density.

In addition to the parameters mentioned above, the mechanical properties of the gel can be affected by the experimental parameters of hydrogel synthesis such as reaction time, temperature, amount and type of solvent used. Thus, the choice of the polymer constituting the matrix of the gel and the control of processing conditions during polymerization are key parameters to be considered in order to obtain a final biomaterial with desired mechanical characteristics.

As discussed before, the objectives of this work is to study the use of hydrogels membranes in the context of filtration. Then, the aim of the following section is to discuss the different types, mode, materials and properties of filtration membranes used in the filtration process.

1.2 FILTRATION PROCESS

1.2.1 Definition and generalities

a) Definition

Filtration is a physical separation process that separates two different phases of a mixture through a filter medium allowing the fluid to pass but retains solid matters. The driving force for this transport can be a gradient of pressure, chemical potential, electrical potential or temperature across the medium⁵⁷. There are three different groups of filters⁵⁸⁻⁶⁰:

- 1) Surface filters which are thin barriers, illustrated by a common filter cloth or laboratory filter paper involving the retention of solid matters mainly on the surface of the medium.
- 2) Depth filters which allow to retain different matter throughout the porous medium and not just on its surface. These filters have the advantage of retaining a large mass of solutes before clogging. Sands and anthracite are usually used as filter media.
- 3) Membranes which are used as selective barriers allowing the passage of certain components and the retention of others. Pressure driven membrane filtrations are the most used membranes in separation industry, in particular in water and wastewater treatment. There are used to separate various-sized particles, organisms and chemical species ranging from few nanometers to microns^{61, 62}.

b) Types of membranes: MF, UF, NF, RO:

Based on the solutes sizes and the molecules molecular weights, the applied pressure and the type of membrane, there are four different membrane processes classified in (Table 1.1) ^{63, 64}.

Table 1.1. Size of solutes, applied pressure and type of membrane.

Process	Size of solutes	Applied pressure (bar)	Type of membrane
Microfiltration	0.025 -10 μm microparticles	0.1 – 5	Porous
Ultrafiltration	5 - 100 nm macromolecules	0.5 – 9	Porous
Nanofiltration	0.5 - 5 nm molecules	4 – 20	Porous
Reverse Osmosis	< 1 nm salts	20 – 80	Nonporous

The microfiltration (MF), ultrafiltration (UF) and nanofiltration (NF) processes use porous membranes with pore diameters of several microns, tens of nanometers and less than 10 nm, respectively. However, the reverse osmosis (RO) process uses dense membranes that do not have distinct pores. Each membrane is able to withstand to an applied pressure, depending on its characteristics. In general, these processes are used in different applications, such as dairy and food industries as well as pharmaceutical industry.

c) Filtration mode:

There are two main modes filtration for pressure driven membrane processes: dead-end and cross-flow filtrations, as presented in (Figure 1.10) ⁶⁵. The mechanism of each mode is described below.

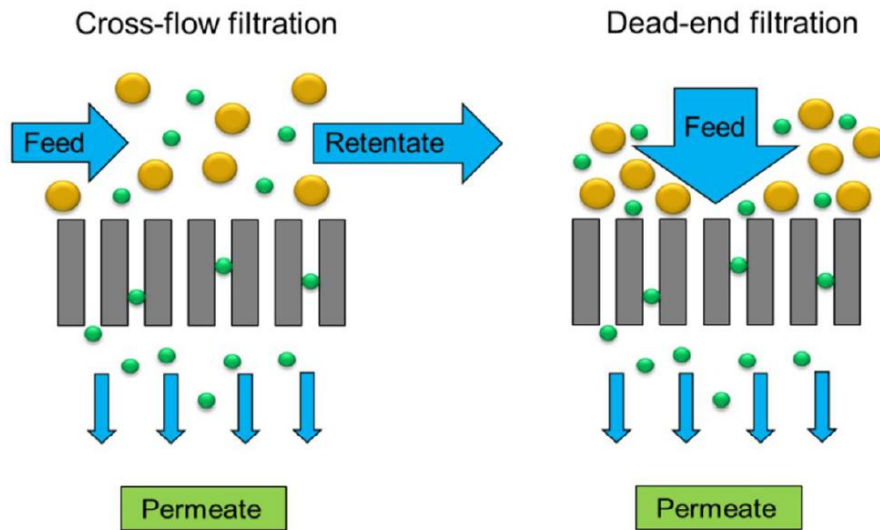


Figure 1.10. Configurations of cross-flow filtration and dead-end filtration.

Dead-end filtration:

In the dead-end process, the fluid flow (liquid or gaseous) is perpendicular to the membrane surface. In this mode, the retained matters are more probable to accumulate on the surface of the membrane as a result of the no recirculation of the retentate (the solution that does not permeate through the surface of the membrane). In addition, the system operation is based on total recovery of the feed water ⁶⁶. The main advantages of this process are that the fabrication of dead-end membranes is relatively less expensive and the process is easy to implement, thus it is mainly used on a small scale in laboratories. On the other hand, dead-end membranes are easily fouled which requires periodic interruption of the process to clean or replace the filter, or the use of conventional pre-filters (cartridge, bag filters) to remove the larger particles.

Cross-flow filtration:

In the cross-flow filtration mode, the feed flow is tangential to the membrane surface. Unlike the previous mode, the retentate is recirculated and blended with the feed water, whereas the permeate (the solution that passes through the membrane) is recovered on the other side ⁶⁶. Tangential flow membranes are less susceptible to fouling due to the high shear rates of the fluid flow. They are also characterized by low energy consumption, increased product yield, selective and consistent separation, reduced maintenance and no additives, flocculants or chemicals needed.

d) Materials groups:

According to the materials used in the preparation of the membrane, pressure driven membranes are generally classified into two main groups: polymeric⁶⁷ and inorganic membranes⁶⁸.

Polymeric membranes are currently dominant in drinking water treatment and desalination due to their low cost and simplicity of implementation. The most polymers used in this field are polysulfone (PS), polyethersulfone (PES), polyacrylonitrile (PAN) and poly(vinyl fluoride) (PVDF). They are characterized by their resistance to oxidation (e.g. by chlorine), to temperature and to extreme pH. However, their disadvantages, such as hydrophobicity, low long-term stability, easy fouling and short lifetime, can limit their applications⁶⁹.

On the other hand, membranes made of inorganic materials (such as ceramic, glass and carbon membranes) are generally more resistant to extreme pH and temperature conditions and also possess mechanical resistance. Generally, metallic (carbon) and glass membranes (silicon oxide or silica, SiO₂) have not gained much popularity due to their high cost and complex manufacturing⁷⁰. Whereas the ceramic membranes have attracted interest to their potential use in industries such as the treatment of waste streams⁷¹, as they can withstand high experimental conditions (temperatures, pH, pressure)⁷², and characterized by they longer lifetimes, higher hydrophilicity and lower fouling⁷³.

1.2.2 Flow, permeation and retention through porous medium

The performance of membranes is usually evaluated by water permeability in the filtration process, as well as rejection or selectivity of solutes. As a definition, the permeability is the ability of a porous medium to allow the passage of a fluid. The permeability depends on the size and density of the pores, the thickness of the membrane and its tortuosity.

The filtration through porous membrane is defined by three important terms. The feed solution which is the initial solution sent to the membrane (it is characterized by an initial concentration and volume, noted C_0 and V_0 , respectively). The retentate which is the solution retained by the membrane (with C_R and V_R), and the permeate which is the solution that passes through the membrane (C_P and V_P).

Permeate flow Q is the volume of the fluid (V_P) that passes through a given section per unit of time (t). Permeate flow Q is expressed in $\text{m}^3 \cdot \text{s}^{-1}$. Q is written in Equation 1.14:

$$Q = \frac{\text{Volume of fluid } (V_P)}{\text{time}(t)} \quad (1.14)$$

Permeate flux J is the permeate flow through the membrane per unit of area. It is expressed in $\text{m}\cdot\text{s}^{-1}$, in Equation 1.15:

$$J = \frac{\text{Permeate flow } (Q)}{\text{membrane area } (S)} \quad (1.15)$$

According to Darcy's law, the permeate flux can be expressed as a function of the transmembrane applied pressure (Equation 1.16):

$$J = \frac{Q}{S} = \frac{K\Delta P}{\mu h} \quad (1.16)$$

where J is the permeate flux ($\text{m}\cdot\text{s}^{-1}$); Q is the permeate flow ($\text{m}^3\cdot\text{s}^{-1}$); S is the membrane section (m^2); K is the membrane permeability (m^2); ΔP is the transmembrane pressure (Pa); μ is the liquid viscosity (Pa.s) and h is the membrane thickness (m).

Membrane permeability describes its resistance to the infiltration by a fluid. It can be calculated from the slope of the line of the variation of the flux versus the applied pressure $J = f(\Delta P)$, as shown in (Figure 1.11). This variation can be linear or non-linear depending on the properties of the filtration membrane used or the type of solute to be filtered. This non linearity can be caused either by the compression of the filtration membrane at high pressure or by the changing of the feed solution viscosity, temperature, ... In the case of solute filtration, the non-linearity is due to the pores clogging resulting in a decrease of the permeate flux J , as explained later.

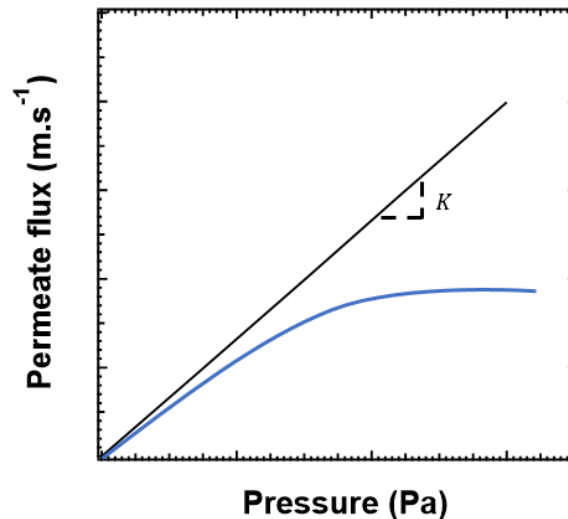


Figure 1.11. Different variation of the flux as a function of the transmembrane pressure applied.

In general, this permeability is defined by the properties of porous membrane, e.g. porosity. In contrast to Darcy's law, several models have been used in the literature for relating the permeability to pore size distribution in a porous medium. Among these models, we will describe the capillary bundles and Carman-Kozeny models.

a) The capillary bundles model:

The capillary bundles model considers that the porous medium behaves hydrodynamically as a set of conduits through a matrix. They can be straight or curved, parallel or randomly oriented, with constant or variable cross-section.

For approximation, it is possible to consider that the whole porous network is made up of a bundle of straight capillaries with identical diameter d . The fluid flux in a capillary of diameter d under a pressure gradient ΔP is given by Poiseuille in Equation 1.17:

$$J = \frac{1}{\mu} \frac{\Delta P}{h} \frac{d^2}{32} \quad (1.17)$$

As a result, the permeability K of a porous membrane reads in Equation 1.18:

$$K = \frac{\varepsilon d^2}{32\tau} \quad (1.18)$$

where ε is the membrane porosity (defined as the fraction of pores in the medium) and τ the membrane tortuosity.

b) Carman Kozeny (C-K) model:

Based on the parallel capillaries model, C-K model links the permeability to the properties of porous medium considered as a packed bed of solids of diameter d . This model expresses permeability as a function of the specific surface area S_V (m^{-1}). In this condition, $S_V = 6/d$.

The C-K formula for permeability can be derived is Equation 1.19:

$$K = C_{CK} \frac{\varepsilon^3}{S_V^2 (1-\varepsilon)^2} \quad (1.19)$$

Where C_{CK} is an empirical Carman–Kozeny constant. The value of C_{CK} depends on the type of the microstructure, e.g. for model granular microstructures is equal ~ 0.2 .

Other than permeability feature, the porous membrane is characterized by its selectivity property. Membrane selectivity is defined by the retention rate R , which is the ability of the membrane to retain a solute during the filtration. R is written in Equation 1.20:

$$R = 1 - \frac{C_P}{C_R} \quad (1.20)$$

where C_P and C_R are the solute concentration in the permeate and in the retentate, respectively. If the compound studied is totally retained by the membrane (i.e. $C_P = 0$) thus $R=1$. In contrast, if the compound is not retained at all ($C_P = C_0 = C_R$) thus $R=0$.

1.2.3 Clogging and concentration polarization

As described before, the performance of the filtration membrane depends on both the water permeability and the selectivity of the membrane. These two features are primarily affected by two phenomena: the fouling and the concentration polarization^{74, 75}.

Membrane fouling is defined by the deposit of suspended or dissolved substances from the feed solution on the membrane surface at its pore openings, or within its pores (Figure 1.12)^{76, 77}. Membrane fouling leads to a decrease in the membrane performance: it causes a decrease in membrane pore size or even a pore clogging⁷⁸, a decrease in permeate flux and the retention of smaller solutes⁷⁹. This fouling can be reversible if it can be removed by several washing steps or by varying the filtration conditions (decreasing of the driving pressure for example). Whereas it is irreversible if the filtration membrane has definitively lost its initial characteristics⁸⁰.

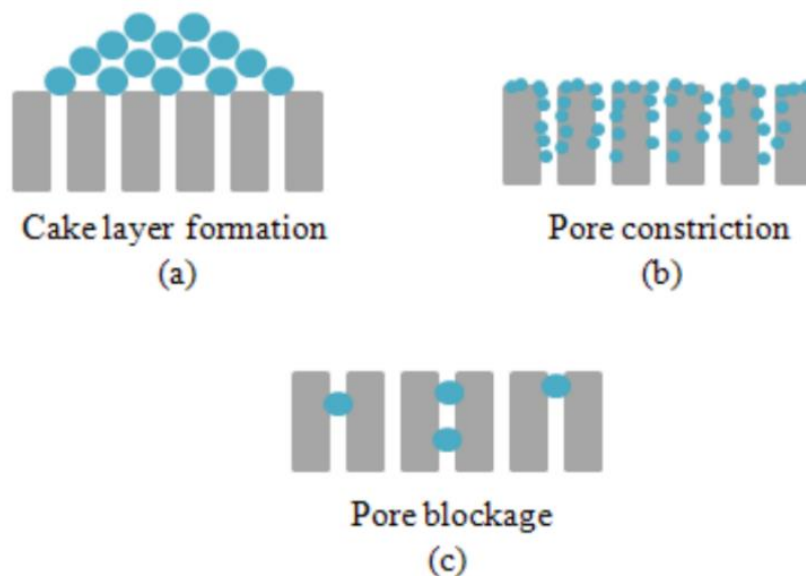


Figure 1.12. Mechanisms of fouling in membrane filtration: (a) cake layer, (b) pore constriction and (c) pore blockage⁸¹.

The concentration polarization (CP) results from the accumulation of retained solutes A in a thin layer adjacent to the membrane surface⁸². This will generate a concentration gradient, meaning that the concentration of solute near the membrane surface $C_{A,m}$ is much higher than that of the overall feed solution $C_{A,f}$ ⁸³. As a result, this concentration builds up produce a diffusive flux of solute back to the feed bulk as shown in (Figure 1.13). This phenomenon results in water flux decline. It might also change the membrane separation properties, due to surface charge variations. CP is considered as an example of reversible fouling⁸⁴.

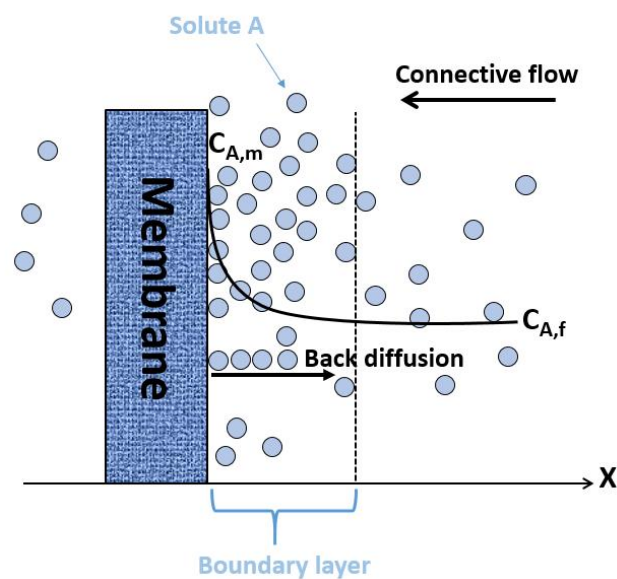


Figure 1.13. Mechanism of concentration polarization.

The two phenomena of fouling and CP are related, which means that operation under severe CP conditions may lead to the formation of membrane fouling. They are major obstacles to the use of membrane technology because of their effects on water flux, membrane separation properties and permeate quality. For these reasons, different measures are necessary to limit fouling and concentration polarization^{85, 86}.

Proper choice of membranes materials and properties (e.g. hydrophilicity, roughness, and electrical charge), choice of operating conditions and membrane cleaning may prevent biofilm build-up on membranes or pores clogging⁸⁷. The first strategy to minimize membrane fouling is to use the appropriate membrane for a specific operation. The choice of operating conditions during membrane filtration is also essential, as it can affect fouling. As mentioned above, cross-flow filtration is more advantageous than dead-end filtration for reducing fouling problems.

The applied pressure and the water flux play also an important role in the fouling and CP phenomena.

Finally, even with the correct choice of membrane and operating conditions, the membranes must be cleaned regularly, either by physical ways (such as sponges, water jets or back flushing)⁸⁸, or chemical ways including the use of acids and bases to remove foulants and impurities⁸⁹.

As mentioned in the first section, the filtration process can also be performed using hydrogel membranes. In this context, we will be interested in the following section to report the different hydrogels systems used in this sense in the literature. A special description will be given to PEGDA-based hydrogels in the last part of this section, as it is the targeted hydrogel herein.

1.3 HYDROGELS FOR FILTRATION

Due to their porous network structure, hydrogels can be used as diffusion medium for the transport of different particles and substances. As the diffusion of solutes in hydrogels has application in a wide variety of biomedical applications (such as drug delivery), it is therefore important to have an understanding of the parameters governing solute diffusion within hydrogels, as well as the means by which they affect diffusion. As well, hydrogels are also used as filtration media for the controlled permeability or rejection properties of solutes under applied pressure. In this section, we will describe first the effects that may impact the solute diffusion properties, and then the filtration process through hydrogel membranes in the form of thin coated films on classical support or as free-standing membranes.

1.3.1 Hydrogels as diffusion barriers

Hydrogels are open systems where substances can diffuse into and out. However, as a result of their structures, solute movement in hydrogels is restricted to a much greater extent than in an aqueous medium⁹⁰. In this case, hydrogels may serve as a selective barrier. For this reason, many researchers have sought to understand the factors that affect solute movement through hydrogel membranes. Consequently, various models have been established to describe the diffusion behaviors. These models include those based on obstruction^{91, 92}, hydrodynamic⁹³ and free volume theories^{94, 95}, as illustrated in (Figure 1.14).

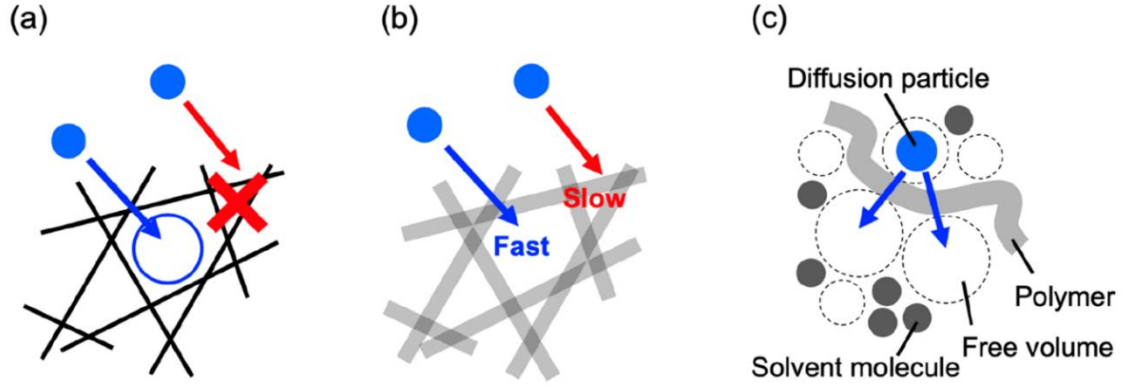


Figure 1.14. Schematic illustrations of three major theories ((a) obstruction, (b) hydrodynamic, and (c) free volume theories) describing the diffusion behavior of hard sphere particles in polymer networks ⁹⁶.

In the obstruction theory, the polymer network is considered to behave as an obstacle preventing the diffusion of particles (Figure 1.14 a). Based on this theory, Ogston model has assumed that the polymers are randomly oriented in straight rigid fibers, and the diffusion coefficient of a particle (D) is given by the possibility of a particle penetrating through the suspension as (Equation 1.21):

$$\frac{D}{D_0} = e^{-K\phi} \quad (1.21)$$

where D_0 is the diffusion coefficient of a particle in the absence of polymers, K is the retardation coefficient depending on the shape of a particle, and ϕ is the polymer volume fraction.

In the hydrodynamic theory, the existence of polymer causes the hydrodynamic friction and decreases the diffusion rate of particles, as illustrated in (Figure 1.14 b). Cukier model which is the representative model for this theory, gives D/D_0 as a function of the screening constant (κ) related to the friction caused by the network, as written in Equation 1.22:

$$\frac{D}{D_0} = e^{-\kappa R} \quad (1.22)$$

where R is the radius of the particle.

The third theory is the free volume theory, in which particles diffuse passing through free volumes of solvent and polymer (Figure 1.14 c). Yasuda applied this concept to the particle diffusion in gels. In Yasuda's model, D/D_0 is given by the possibility of a particle finding a proper free volume as (Equation 1.23):

$$\frac{D}{D_0} = \exp\left(-\frac{xR}{V_{fs}}\left(\frac{\phi}{1-\phi}\right)\right) \quad (1.23)$$

where x is a constant and V_{fs} is the free volume of a solvent.

Models based on this theory contain more parameters than those on other theories, described before. However, they are limited to describe the diffusion of small particles in hydrogels with high water content.

The review of Witten *et al.* describes the effect of steric hindrance and chemical interaction on the particle transport through hydrogel network⁹⁷. In general, the transport of a solute through a gel is controlled by the solute's size, its interactions with the components of the gel, or a combination of the two, as shown in (Figure 1.15). As described in the previous models, hydrogels with a polymeric mesh size constrains the diffusion of large particles, with a size above the mesh size of the gels (Figure 1.15 a). Moreover, depending on their chemistry, the gel components interact with solutes through electrostatic or hydrophobic interaction thereby differentially affecting diffusion. A lack of interactions enables unhindered diffusion while binding to hydrogels, reduces the effective solute diffusivity and hinders penetration^{98,99}.

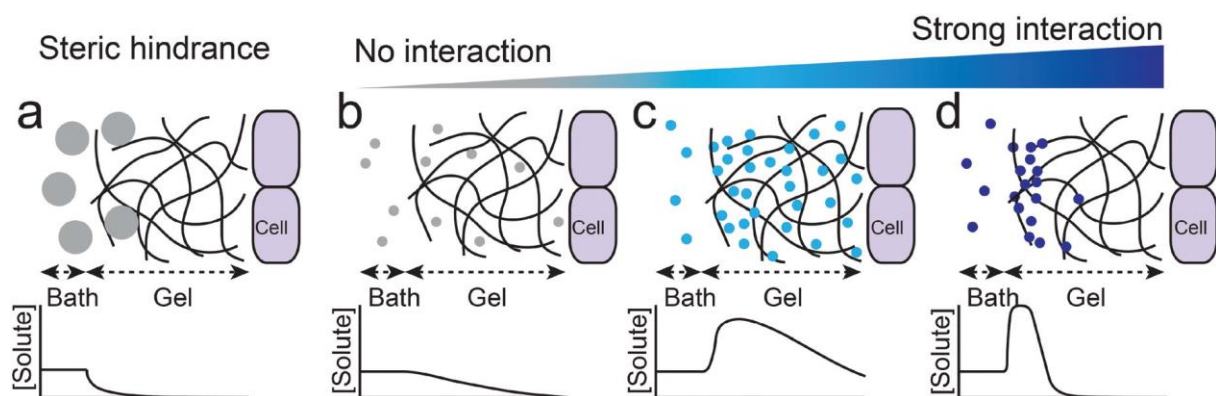


Figure 1.15. Effects of steric hindrance and chemical interactions on gel penetration. (a) Particles above the mesh size are unable to penetrate the gel, even if they do not interact with the gel (b) small inert particles penetrate gels (c) weak interactions with gel polymers can enhance partitioning into the gel and subsequent penetration (d) binding to the gel causes enrichment of solute at the bath-gel interface but slowed gel penetration⁹⁷.

For example, Hansing *et al.* have described numerically and experimentally, how repulsive electrostatic interactions may influence the diffusion of particles in the extracellular matrix, without the presence of hydrodynamic interaction HI¹⁰⁰.

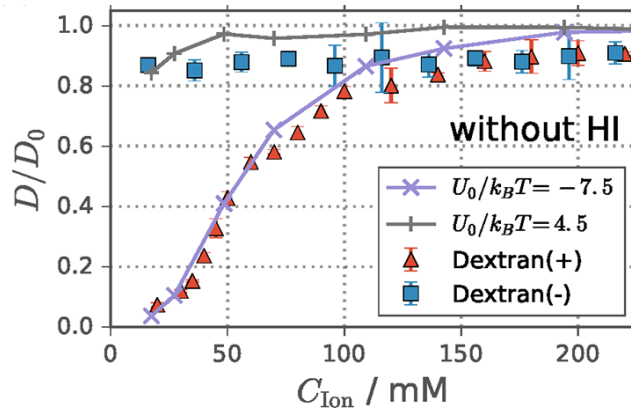


Figure 1.16. Diffusivity of negatively charged Alexa 488 fluorophores in positive dextran (+) and negative dextran (-) hydrogels as a function of the salt concentration C_{ion} including the counter ions without HI. The experimental data are presented as full symbols, and the simulation data are presented as line connected crosses¹⁰⁰.

The obtained results are represented in (Figure 1.16). The diffusion of negatively charged fluorophore Alexa 488 in similarly charged dextran gel (-), is almost unhindered for most salt concentrations. On the other hand, the diffusivity of Alexa 488 molecules in oppositely charged dextran (+) gels basically goes to zero for small C_{ion} , due to the forte attraction between the opposite charges. Increasing the concentration of salts will increase the screening of the electrostatic attraction between Alexa 488 and the cationic dextran polymers. Consequently, D strongly increases until it reaches the diffusivity of a neutral gel with completely screened electrostatic interactions, which is $D/D_0 \approx 1$.

Other than a diffusion barrier, hydrogel network is used as a filtration membrane in the presence of applied pressure. Thus, in the next sections, we will describe how the hydrogel membranes can be used for such kind of application, either as a coating layer on classical filtration membranes or used as a free-standing membranes.

1.3.2 Hydrogels as coating films for filtration processes

In general, polymeric UF membranes, composed of PS, PES, PAN and PVDF, are widely applied in many separation fields and water treatment for their good thermal, chemical and mechanical stability. However, the hydrophobicity of these membranes is one of their main issues in separation techniques, such as for protein purification, biological wastewater treatment

to name but a few. This causes significant membrane fouling, resulting in increased operating costs and more frequent cleaning and replacement of the membrane. Therefore, typical membrane surface modification methods, using hydrophilic polymeric substances, have been introduced recently to improve the inherent anti-fouling properties of membranes¹⁰¹⁻¹¹⁶. Owing to their superior hydrophilicity, hydrogels, cross-linked three-dimensional network structures, have attracted researchers' attention to form more stable hydration layers to prevent proteins fouling on membrane surfaces.

The recent studies showed modification of filtration membrane with hydrogel layers are gathered in Table 1.2.

Table 1.2. Comparison of several newly published work of hydrogel modified membranes.

Hydrogel material	Matrix membrane	Preparation method	Film thickness (μm)	Contact angle ($^\circ$)	Permeability ($\text{L}\cdot\text{m}^{-2}\cdot\text{h}^{-1}\cdot\text{bar}^{-1}$)	Rejection rate of BSA (%)	References
PNAGA	PVDF	UV-initiated radical graft polymerization	0.2	0	191	99	[101]
Calcium alginate	PVDF	Impregnating and cross-linking	0.2 ± 0.1	18.9 ± 5.6	63.8	98.5	[102]
Calcium alginate	PVDF	Dip-coating and cross-linking	2-10	39.7	30	99	[103]
PEGMA	PVDF	Plasma- initiated radical graft polymerization	-	50	60	90.8	[104]
Copolymerized Polyampholyte hydrogel (AMPS-co-DMC)	PVDF	Alkali treatment and radical graft polymerization	-	35	45	96.7	[105]
VSA	PES	UV-initiated radical polymerization	-	11	24.1	-	[106]
Copolymerized Polyampholyte hydrogel (VSA-co-METMAC)	PES	UV-initiated radical graft polymerization	0.09	61	50	90	[107]
POSS-PEGM	PES	Coating and cross linking	3.4 ± 1.1	46	48.3	97	[108]
PVA/Glutaraldehyde	GO-PES	Coating and cross-linking	0.1	18	21.7	92	[109]
PVA/Succinic acid	PS	Coating and cross-linking	$0.1-0.6$	25.5 ± 3.5	6.3	-	[110]
PEGDA	PS	Interfacially initiated free radical polymerization	< 0.1	-	5.9 ± 0.4	99	[111]
PEGDA	PS	UV-initiated radical graft polymerization	≤ 0.1	38.9 ± 1.5	20.46	97	[112]
PEGDA	PS	UV-initiated radical graft polymerization	3	52	36 ± 2	-	[113]

The different methods used to modify hydrophobic filtration membranes allow the formation of a hydrogel layer with a thickness ranging between several hundreds of nanometer to about ten of micrometer. The thickness of the hydrogel films depends largely on the grafting degree of the polymer on the support membrane, the polymer concentration constituting the matrix, the duration of the cross-linking reaction as well as the UV-irradiation dose and exposure time. Surface modification of hydrophobic membranes has significantly enhanced the membrane hydrophilicity, the water permeability as well as the anti-fouling properties. For example, the water contact angle (WCA) of the PVDF membrane have largely decreased from 118° to 0° , after their modification with poly(N-acryloyl glycinamide) PNAGA hydrogels layers, illustrating the superior membranes hydrophilicity¹⁰¹. Furthermore, the modified membranes coated with these water-absorbing networks exhibit extremely high anti-fouling efficiency in bovine serum albumin (BSA, 66 kDa), used as a protein model, for filtration tests. In most of

these studies, the high rejection rate of BSA (> 97%), by hydrogel-modified membranes, provides new insights for anti-fouling membrane design and application in protein purification, bio-separation and so on.

Despite these enhanced properties, coating and grafting methods of hydrogels still have some drawbacks, mainly the adsorption of part of the pollutants that pass through the hydrogel layer by the hydrophobic support during filtration. Consequently, the resistance to the protein and pollutant fouling of the modified membrane is not well controlled.

1.3.3 Hydrogels as free-standing membranes for filtration processes

To avoid the problem of filtration membranes fouling, free-standing membranes prepared with hydrogel materials are used without the need for a hydrophobic substrate. However, few researchers have used the hydrogels as free-standing materials for filtration due to the poor mechanical properties of the most common hydrogels. Therefore, recent studies have focused on the development of tough hydrogel systems that may be used directly as filtration membranes.

Among these studies, Zhang *et al.* have synthesized a free-standing calcium alginate/polyacrylamide (CA/PAM) hydrogel filtration membrane via UV radiation-reduced polymerization ¹¹⁷. This hybrid gel system was characterized by its strong extensibility and pressure-resistance properties ¹¹⁸. The mechanical behavior of this system is strongly affected by the densities of ionic and covalent cross-links. The highest elastic modulus value is 100 KPa, depending on the fraction of acrylamide. Thanks to these properties, CA/PAM hydrogel with a thickness of 0.244 mm, presents a higher water flux recovery after the alternating filtration flux between the pure water and BSA solution, as represented in (Figure 1.17). This result indicates that CA/PAM filtration membrane exhibited excellent anti-fouling properties for BSA.

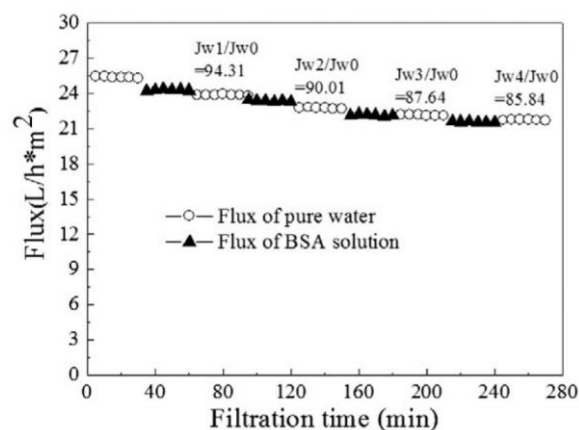


Figure 1.17. The alternating filtration flux between pure water and BSA solution of CA/PAM membrane ¹¹⁷.

The interesting features of this filtration membrane provide it promising application prospects in the fields of protein separation, microorganism filtration, and removal of dye (99.75 % rejection for Brilliant Blue G250).

In the same context on dye separation, a recent study developed a free-standing carboxylated titanium dioxide/calcium alginate (TiO₂-COOH/CaAlg) hydrogel filtration membrane ¹¹⁹. TiO₂-COOH nanoparticles were used as the reinforcing agent to improve the mechanical performance of the hydrogel system. Consequently, these membranes have shown a high efficiency to reject dyes of different sizes. The results presented in (Figure 1.18) show the rejection ratios of 20 wt% TiO₂-COOH/CaAlg membrane for dyes with different molar mass. Interestingly, the rejections of dye are not entirely consistent with the size of dye molecules. The rejection sequence is: 98.4% (Mw Brilliant blue G250 = 858.1 Da) > 96.8% (Mw Direct black 38 = 781.7 Da) > 95.9% (Mw Congo red = 696.7 Da) > 89.2% (Mw Acid red 66 = 556.5 Da) > 87.7% (Mw Brilliant yellow = 624.6 Da) > 83.0% (Mw New cocchine = 604.5 Da) > 73.9% (Mw Phloxine B = 829.6 Da). This difference is mainly explained by the electrostatic repulsion effect, in addition to the steric hindrance effect of the dye.

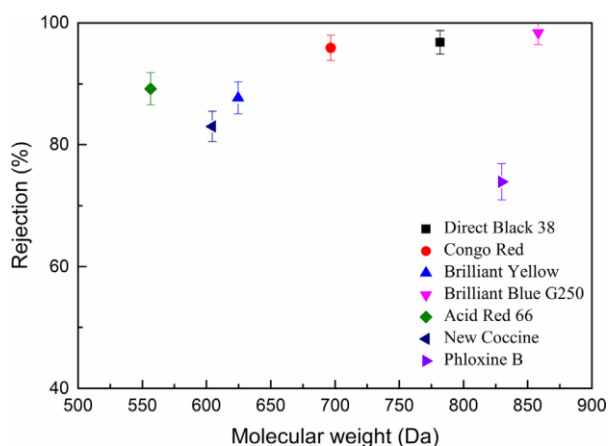


Figure 1.18. The rejection ratio for dye vs. molecular weight of dye ¹¹⁹.

Recently, PEG-based hydrogels have attracted researchers' attention as free-standing membranes for filtration process. PEG is characterized by its highly hydrophilic nature, its non-toxicity and its anti-fouling properties. It is able to coordinate with surrounding water molecules by hydrogen bonding and repel organic or biofouling agents. These properties provide it to be suggested for use in a wide range of biomedical application ^{120, 121}. Substituting PEG terminal hydroxyl groups with acrylates, forming PEGDA, allows the polymer to be cross-linked to form a three-dimensional polymer network. One of the reported mechanism of PEGDA polymerization under UV light is described in the next section.

PEGDA-hydrogel has proven its efficiency as a free-standing membrane to tune water permeability, solute rejection and protein fouling resistance in filtration process ^{33, 113, 114, 122-124}. In addition, it is characterized by highly tunable properties such as mechanical and structural properties, depending on the molar mass or concentration of the polymer ¹²⁵. The use of PEGDA free-standing hydrogels for filtration process and the resulting properties are detailed in the next section.

1.3.4 PEGDA based hydrogel membranes for filtration

Due to its tunable and well-characterized mechanical and structural properties, PEGDA is used as a promising material to develop a free-standing membrane for filtration. In this section, we will first describe the mechanism of the PEGDA photopolymerization and the significant properties of PEGDA hydrogels, then their uses as membranes for filtration.

1.3.4.1 Generalities of PEGDA hydrogel

A) PEGDA hydrogel synthesis and application

Poly (ethylene glycol) diacrylate (PEGDA) is a derivative of poly (ethylene glycol) (PEG) which is a charge neutral polymer available in a wide range of molar masses. The chemical structure of PEGDA is shown in (Figure 1.19 A).

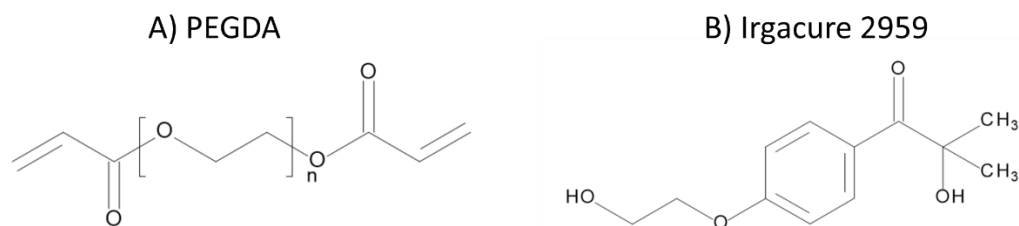


Figure 1.19. Chemical structure of A) poly (ethylene glycol) diacrylate and B) Irgacure 2959 photoinitiator.

Due to its biocompatibility and water solubility, PEGDA is widely used in many biomedical applications such as scaffolds for tissue engineering, drug delivery for therapeutic applications, contact lens and biosensing¹²⁶⁻¹²⁹. PEGDA polymer can be cross-linked under an ultraviolet light source in the presence of a photoinitiator in order to obtain insoluble three-dimensional polymer networks.

Typical photoinitiators used for the polymerization of PEGDA are aromatic ketones such as 1-Hydroxycyclohexyl phenyl ketone (HCPK), 2,2-Dimethoxy-2-phenylacetophenone or 2-Hydroxy-4'-(2-hydroxyethoxy)-2-methylpropiophenone commonly named Irgacure 2959.

In this work, we have used the Irgacure 2959 as a photoinitiator in the photopolymerization of PEGDA. Its chemical structure is also shown in (Figure 1.19 B).

The general process of free radical polymerization of PEGDA is schematically represented in Figure 1.20. In the initiation step, the photoinitiator molecule, is cleaved via UV light and produces a radical species, R^* . The most reactive radical species then attacks a PEGDA chain, producing a new radical center on the vinyl carbon of the PEGDA chain. This radical center is then free to attack another PEGDA chain, creating a cross-link between the chains. Consequently, a new radical center is created on the second PEGDA chain in the propagation reaction. The termination step occurs when two radical centers combine together.

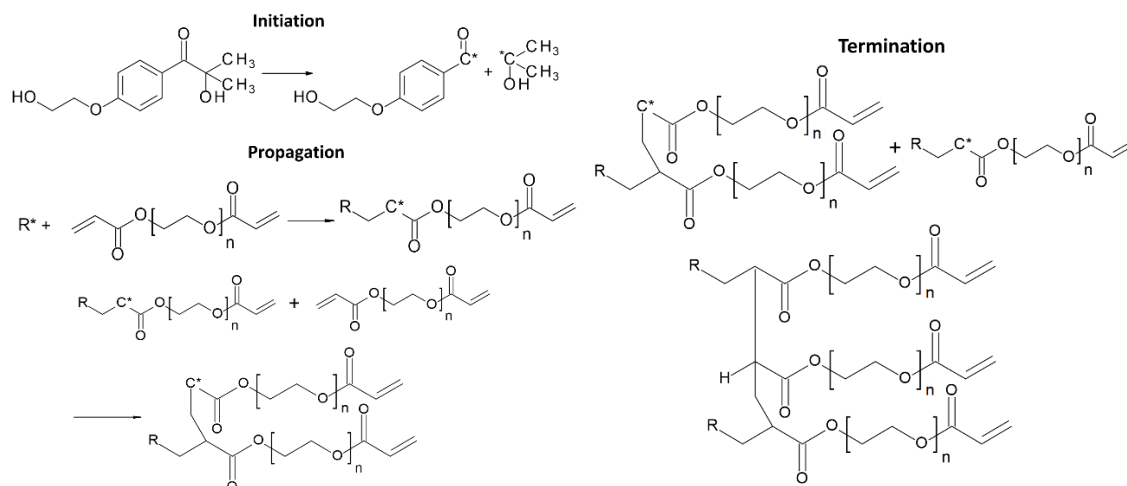


Figure 1.20. Process of free radical polymerization of PEGDA polymer: initiation, propagation, and termination.

In general, the polymerization of PEGDA in the presence of a solvent (water) results on hydrogels with different degree of polymer network heterogeneity, depending mainly on the water composition in the prepolymerization solution. By analyzing the structure of PEGDA hydrogels, we will see in the next section that hydrogels prepared with large content of water are porous and heterogeneous gels, in contrast to gels prepared with low water content.

B) Structural and mechanical properties of PEGDA hydrogel

The structure and properties of PEG-based hydrogels depend mainly on PEGDA polymer chain length and PEGDA:water content in the prepolymerization mixture.

In order to investigate the hydrogel structure, conventional (SEM) and cryoscanning electron microscopy (cryoSEM) are the most used techniques.

For example, Kang *et al.*¹¹⁴ have studied the surface morphology and interior structure of PEGDA membranes with a molar mass of $302 \text{ g}\cdot\text{mol}^{-1}$ and different water content (from 0 to 55 wt%) by SEM. They have found that the interior and surface morphologies of these

membranes were similar. For brevity, they have shown only the images of the cross-sectional morphologies of two membranes prepared with pure and 45 wt% PEGDA/55 wt% water, as represented in (Figure 1.21).

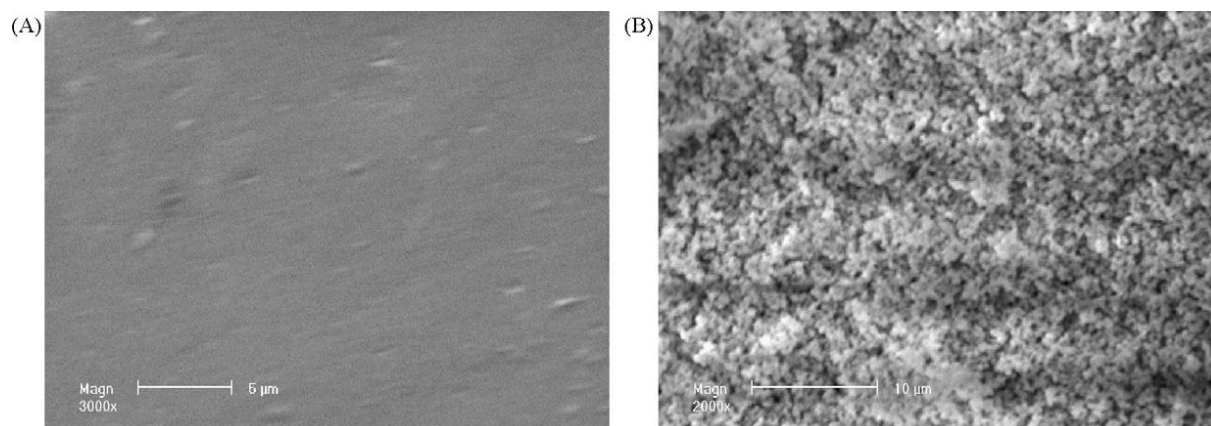


Figure 1.21. Cross-sectional SEM images of membranes prepared with various PEGDA in prepolymerization mixture. (A) 100 wt% PEGDA and (B) 45 wt% PEGDA/55 wt% water¹¹⁴.

As shown in (Figure 1.21 A), the membrane prepared with 100 wt % of PEGDA exhibited an essentially uniform, smooth and nonporous structure. However, the hydrogel prepared with 45 wt% of PEGDA and 55 wt% of water presented a rough and porous structure (Figure 1.21 B). In addition, different other studies have been interested in the structure of cross-linked PEGDA membranes by using cryoSEM. Indeed, this technique has shown its advantage to observe the frozen, hydrated polymer samples without critical point dehydration, as required by conventional SEM¹³⁰.

We reported here the study of Wu *et al.*¹²⁴ who have investigated the structure of PEGDA-700 g.mol⁻¹ hydrogels with different water content using cryoSEM. The resulting cryoSEM images are represented in (Figure 1.22). PEGDA hydrogel with large content of water (80 wt% of water) (Figure 1.22 a) reveals lacy morphology with a fairly small regular pore size of 150-250 nm, consistent in appearance throughout. As the water content in the prepolymerization mixture decreases to 50 wt% (Figure 1.22 b) or 0 wt% (Figure 1.22 c), films exhibit essentially a uniform and nonporous structure. These results were also obtained in the studies of Ju *et al.*¹¹³.

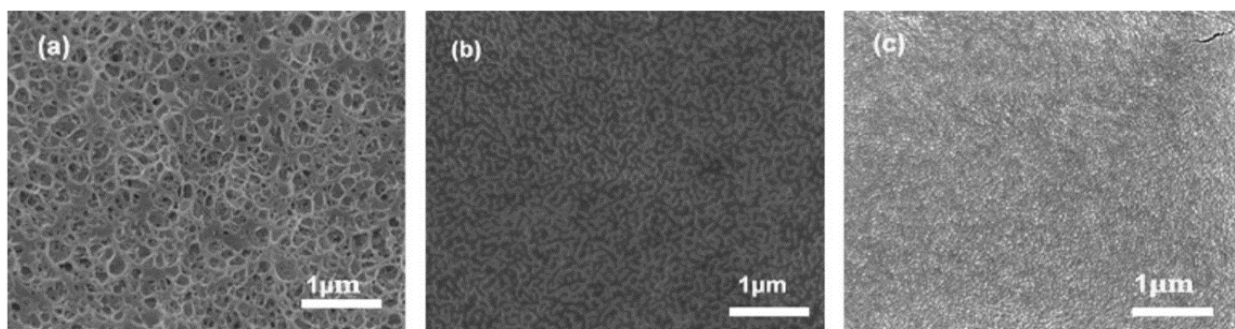


Figure 1.22. CryoSEM micrographs of PEGDA hydrogels membranes with (a) 20 wt%, (b) 50 wt% and c) 100 wt% of PEGDA content ¹²⁴.

This difference in hydrogels structure is expected because the appearance of PEGDA-700 $\text{g}\cdot\text{mol}^{-1}$ free-standing films right after polymerization turned gradually from transparent to translucent as prepolymerization water content increased from 50 to 80 wt%, as reported in the study of Ju *et al.* ¹²². This behavior is explained by the polymerization induced phase separation (PIPS) process which occurs during cross-linking. This phase separation will occur if the water content in the prepolymerization mixture exceeds the maximum equilibrium water content of the cross-linked polymer during polymerization. Consequently, the extra water is rejected out of the network, forming a water-rich phase, separated from the polymer-rich one ^{131, 132}. In some cases, the water-rich domains are dispersed in the film in regions with sizes ranging from 100 nm to $1\mu\text{m}$ ¹³²⁻¹³⁴. These regions (i.e. pores) scatter light, resulting in a loss of transparency.

The variation of the equilibrium water content in hydrated PEGDA cross-linked films as a function of the prepolymerization water content for various PEGDA chain length have been studied by Ju *et al.* ¹²². To obtain this data, the membranes were first immersed in and equilibrated with deionized water to calculate their swollen weights, W_s , after blotting the free water on the surface; and then dried in a vacuum oven at $\sim 80^\circ\text{C}$ for 24 h, prior to determine their dry weights, W_d .

The equilibrium water content of the hydrogel membrane is calculated as follows in Equation 1.24:

$$X(\%) = \frac{W_s - W_d}{W_s} \quad (1.24)$$

The results are presented in (Figure 1.23).

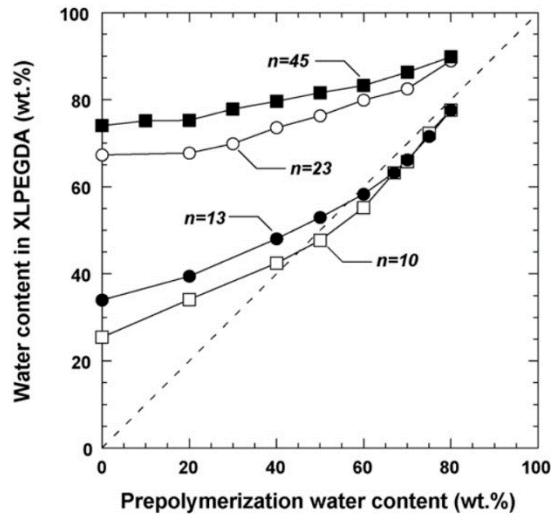


Figure 1.23. Equilibrium water content in hydrated PEGDA free-standing hydrogels prepared with various chain lengths PEGDA of various chain lengths as a function of the prepolymerization water content ¹²².

In this figure, the dashed line is the parity line, representing the case where the equilibrium water content in cross-linked PEGDA membrane (XLPEGDA) equals the water content in the prepolymerization mixture. First, for the films prepared with the same PEGDA chain length, the equilibrium water content increases as prepolymerization water content increases. For example, for PEGDA chains with $n=13$, the equilibrium water content increases from 33 to 78 wt%, when the prepolymerization water content increases from 0 to 80 wt%, respectively. As well, films prepared using longer PEGDA chains generally have higher equilibrium water content when the prepolymerization water content is held constant. When the PEGDA films can absorb additional water (i.e., beyond that present in the prepolymerization mixture) after cross-linking, the water content values are above the parity line. While the points below the parity line correspond to the situation where the film cannot absorb, at equilibrium, as much water as was present in the initial prepolymerization mixture. The additional water forming voids during the cross-linking process, as explained by the PIPS process.

In addition to these works, researchers have been interested to study the molecular origin of the nanostructured heterogeneities of PEGDA hydrogels, by small angle X-ray (SAXS) and neutron scattering (SANS) techniques^{135, 136}. These techniques are able to probe length scales relevant to the polymer network.

For example, Molina *et al.*¹³⁷ has explained the heterogeneous structure of PEGDA gels resulting from polymerization-induced microphase separation, by using SANS technique. In this study, the gels were prepared in D₂O to enhance contrast between polymer and solvent. In this context, they have proposed structural model of PEGDA hydrogels based on self-excluding, highly branched star-like polymers arranged in a fractal network. The porous network is represented as a two-phase medium composed of a high-density network phase (composed of PEGDA stars) coexisting with water voids of sizes of the order of hundreds of nanometers, as represented in Figure 1.24.

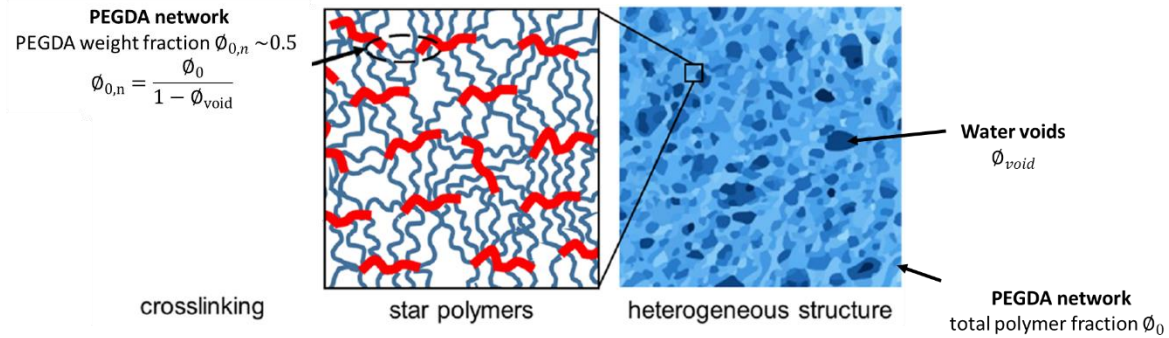


Figure 1.24. Schematic representation of a hydrogel of stars arranged into a fractal structure. Red lines represent acrylic backbones and blue lines represent PEG macromers¹³⁷.

In order to elucidate the mechanism of heterogeneity in PEGDA hydrogels, they have measured the void volume fraction ϕ_{void} , as well as the polymer network volume fraction, $\phi_{0,n}$, which is the volume fraction of polymer in the PEGDA dense phase. They have studied how ϕ_{void} and $\phi_{0,n}$ depend on the total PEGDA concentration, ϕ_0 , and PEGDA molar mass.

The polymer content in the PEGDA rich phase is defined as follows (Equation 1.25):

$$\phi_{0,n} = \frac{\phi_0}{1 - \phi_{void}} \quad (1.25)$$

The results are represented in (Figure 1.25). The polymer concentration in the dense phase is $\phi_{0,n} \sim 0.5$, nearly independent on both polymer molar mass and the total PEGDA concentration ϕ_0 (Figure 1.25 a). This result is surprising as this value should be fixed by a competition between the enthalpy changes due to the interaction between the polymer and solvent

molecules, and the entropic components of free energy change of mixing, as described in section 1.1.4. Hence, we would expect that $\phi_{0,n}$ decreases with increasing PEG molar mass. This value of $\phi_{0,n}$ being almost constant, it follows that decreasing the total water volume fraction, or increasing the total polymer fraction, ϕ_0 , leads to a decrease in volume fraction of voids ϕ_{void} (Figure 1.25 b).

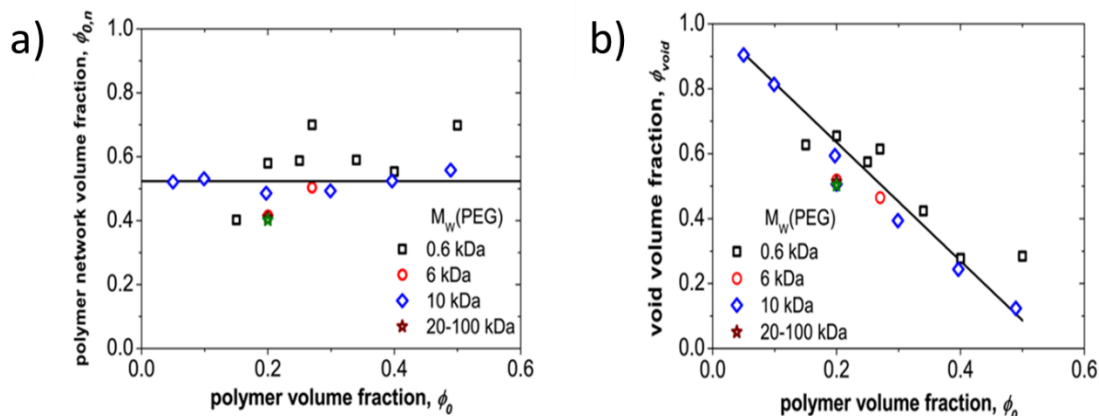


Figure 1.25. Variation of a) polymer volume fraction and b) void volume fraction in the network phase as a function of the total polymer volume fraction for different PEGDA molar mass¹³⁷.

Furthermore, based on the SANS fitting parameters of hydrogels, formed from varying molar mass and volume fraction of PEGDA, they found characteristic void sizes in the range of tens to hundreds of nanometers. These values are much larger than the average distance between cross-links in the hydrogel systems. Thus, they suggest that the formation of these voids is due to a polymerization-induced phase separation process, as observed before with the microscopic images.

Among the several proposed mechanisms to explain the nanoscale heterogeneities in hydrogels, the results obtained are based on the mechanism explained in Reference¹³⁸. When the polymerization reaction starts and the molar mass of the newly formed branched polymers increases, there can be an entropically driven phase separation between polymer-rich and polymer-poor phases which leads to networks with heterogeneities of different morphologies depending on the phase behavior and the competition between the reaction rate and the phase separation rate¹³⁸.

In conclusion, studying the heterogeneity and the porous structure of PEGDA hydrogels is critical in determining their different macroscopic properties for the majority of their application.

Beyond that, PEGDA hydrogels have sufficient mechanical properties, making them the most hydrogels used in the separation and wastewater treatment processes^{33, 113, 114, 122-124}. The mechanical properties of the PEGDA hydrogels can be controlled by varying the molar mass or concentration of the polymer. For example, the increase in elastic modulus is due to increasing polymer concentration or decreasing polymer molar mass^{125, 139-141}. For example, Kang *et al.*¹¹⁴ compared the mechanical performance of membranes prepared with various content of PEGDA-302 g.mol⁻¹ in prepolymerization mixture. As represented in (Table 1.3), the decrease of PEGDA content in prepolymerization solution from 100 to 45 wt%, decreases the tensile strength (σ_b) from 2.84 to 0.42 MPa, and Young's modulus (E) from 87.35 to 2.43 MPa of the prepared membranes, respectively. In contrast, it increases the breaking elongation (ϵ_b) slightly from 6.84 % to 9.87 %, respectively. This difference in properties is related to the decrease of cross-link density, and therefore the enlarge of pore size of the membrane, as the PEGDA content decreases in prepolymerization solution.

Table 1.3. Comparison of the mechanical performance of membranes prepared with various PEGDA-302 g.mol⁻¹ in prepolymerization mixture¹¹⁴.

PEGDA content (wt%)	Tensile strength σ_b (MPa)	Breaking elongation ϵ_b (%)	Young's module E' (MPa)
100	2.82	6.84	87.35
60	1.66	7.45	14.21
55	0.87	7.94	8.25
50	0.53	8.56	4.74
45	0.42	9.87	2.43

As well, the effect of various content of PEGDA-258 g.mol⁻¹ on the elastic modulus of PEGDA-based hydrogels samples measured in tensile tests and the corresponding strains at break is also studied by Gabler *et al.*¹⁴². As shown in (Figure 1.26), when the PEGDA content increases from 20 to 50 wt%, the elastic modulus increases up to 12 MPa. However, the strain at break (Z) decreases from about 40% down to 10% for high PEGDA contents.

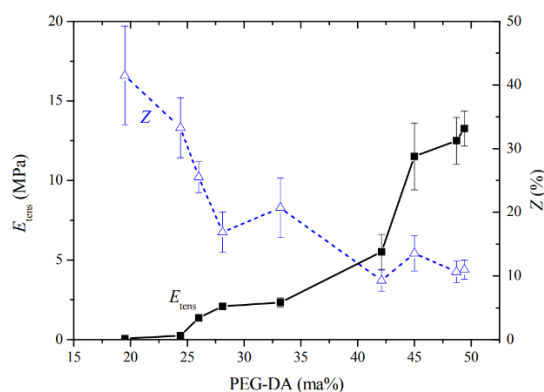


Figure 1.26. Effect of PEGDA content on the elastic modulus and the strain at break for PEGDA based hydrogels ¹⁴².

PEG molar mass can also be an effect on the mechanical properties of PEGDA hydrogels. For example, the elastic modulus of PEGDA hydrogels with PEG chains of 2000 g.mol⁻¹ is about 60 KPa. This value decreases to ~ 35 and 5 KPa when the PEG molar mass increases to 10 000 and 20 000 g.mol⁻¹, respectively ¹⁴³.

Collectively, these properties make PEGDA hydrogels one of the most widely used materials for biomedical application ¹⁴⁴ as well as for filtration and microfluidic devices.

C) Controlling PEGDA hydrogel porosity

As mentioned before, the hydrogel porosity, which is related to the mesh size between the cross-links points, is about several nm. This nanoporosity may affect the diffusion properties of the resulting gel as well as the control transport of large molecules and solute. To increase the transport properties and hydrogel porosity, several methods, such as the use of porogens, phase separation, and foaming have been reported in the literature ¹⁴⁵⁻¹⁴⁷. These methods allow to introduce porosity in hydrogel network for significant diffusion of large solutes and proteins within the network or for filtration process. Among these techniques, the use of porogens is the most facile method, which provides superior control and tunability of the porous structure of the cross-linked hydrogels. It involves the photo-crosslinking of the prepolymerization solution containing porogen, followed by dissolution of the incorporated porogen.

For example, in order to create porous hydrogel with pore sizes ranging between 20 to 80 μm , salts crystals (sodium chloride) of a defined size are added to the precursors polymer solution, before polymerization ¹⁴⁸. The salt crystals are then leached out, by incubation the gels in large volume of water, resulting in porous hydrogels for applications in tissue engineering. The structures of porous hydrogels obtained by salt-leaching are represented in (Figure 1.27).

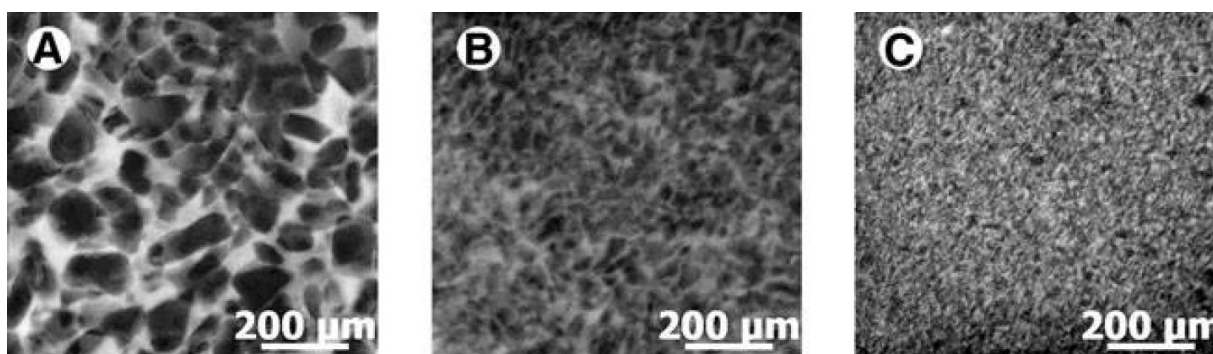


Figure 1.27. Confocal images of middle regions of porous PEGDA hydrogels generated with salt crystals in size ranges of 50–100 μm (A), 25–50 μm (B), and 5–20 μm (C)¹⁴⁸.

Calcium carbonate (CaCO_3) particles are also used as a sacrificial solid to generate porosity in the PEGDA based hydrogel after dissolution¹⁴⁹. By using an acid treatment, the carbonates dissolve homogeneously throughout the matrix, resulting in a porous structure as shown in (Figure 1.28). The SEM images provide evidence of non-connected porosity most likely due to the well dispersed of calcite. In addition, the porosity of the samples increases with the amount of calcite.

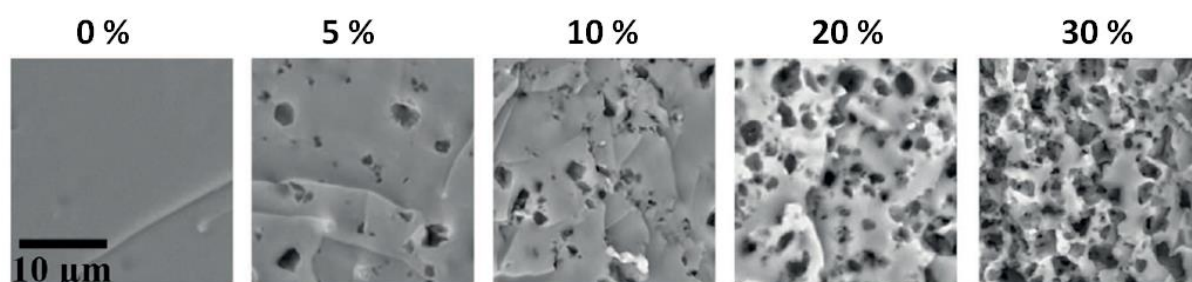


Figure 1.28. SEM views of cut samples of the porous PEGDA-monoliths prepared with volume fractions of calcite between 0 and 0.3¹⁴⁹.

Polymer chains such as small PEG chains with a molar mass $< 35\,000\text{ g}\cdot\text{mol}^{-1}$, are often used as a water-soluble porogen, and previous studies have shown that incorporation of the PEG produces a porous morphology in PEGDA hydrogels¹⁵⁰. This porous structure, of the order of tens of nanometer, depending on the PEG chains length, permitted significant diffusion of 250 kDa dextran compared to the non-porous structure.

PEG is successfully used as a porogen, as it forms large pores with a "protein-friendly" surface, such as bovine serum albumin protein (BSA). It has been found that PEG $600\text{ g}\cdot\text{mol}^{-1}$ serves as an effective porogen to allow for the capture of large ($\sim 1000\text{--}3700\text{ nt}$ long) mRNAs¹⁵¹. As

PEG 600 porogens do not participate in the photo-cross-linking reaction, they are supposed to be removed from the hydrogel by simple rinsed, although this has not been proven. Other studies imply the use of large PEG chains with molar mass such as 4000, 6000 and 10 000 g.mol⁻¹ as the pore-forming agent¹⁵². The high average diameter of PEG macromolecules (i.e. coil formation) in aqueous media attributed to the high PEG molar mass, results in large pores within the hydrogel structure. The difficulties of removing the PEG porogen with high molar mass from the structure limited the use of porogen¹⁵³.

In conclusion, regardless the method used to create pore in hydrogel structure, the overall structure of the porous network is greatly influenced by the type, molar mass and concentration of the porogen used¹⁵⁴. Furthermore, the control of the hydrogel porosity is of great interest for the control of these membranes permeability in the context of filtration applications. However, the formation of porous hydrogel network using these templating approaches is achieved in two steps. One of them consists on the removal of the template (or porogen) either by rinsing the membrane or by specific chemical treatment which limit their use for different applications.

In the next section, we will detail the use of free-standing PEGDA membrane for filtration applications. In particular, we will report the water permeability and the protein rejection of PEGDA free-standing membranes.

1.3.4.2 Water permeability properties of free-standing PEGDA membrane

PEGDA membranes have attracted the researchers' attention for filtration applications due to their hydrophilic nature, biocompatibility, and excellent fouling resistance^{155, 156}.

In these cross-linked polymers, great attention was given to the influence of water content and PEGDA chains length on the physico-chemical, solute transport and water permeability properties of the hydrogel^{33, 114, 122, 124}.

For example, Ju *et al.*¹¹³ have studied the effect of water content (0-80 wt%) on the water permeability for cross-linked PEGDA-700 g.mol⁻¹ materials synthesized by UV-photopolymerization. Water permeability was measured during dead-end filtration at ambient temperature using stirred ultrafiltration cells and MilliQ water as the feed solution. As shown in (Table 1.4), it increases significantly as prepolymerization water content increases. For example, the water permeability for PEGDA films with 80 wt% water is 30 times higher than those prepared with 50 wt% water in the prepolymerization mixture.

Table 1.4. Water permeability of XLPEGDA free-standing films prepared with different amounts of water in the prepolymerization mixture.

Water content (wt.%)	Water permeability (L.μm/(h.m ² .bar)
50	5.3 ± 0.4
60	10 ± 0.7
67	19 ± 1
70	29 ± 5.2
75	61 ± 2.5
80	150 ± 14

Varying the PEGDA chain length results also in changing the cross-link density, the chemistry and structure of the PEGDA network¹²². Figure 1.29 presents the influence of PEGDA chain length and prepolymerization water content on hydrogel water permeability. As shown before, water permeability increases as prepolymerization water content increases, for films prepared at the same PEGDA chain length. For short-chain PEGDA ($n = 10$ and 13) samples, PIPS occurs when prepolymerization water content increases. This creates a separate water phase in these samples that may contribute to increasing their water permeability.

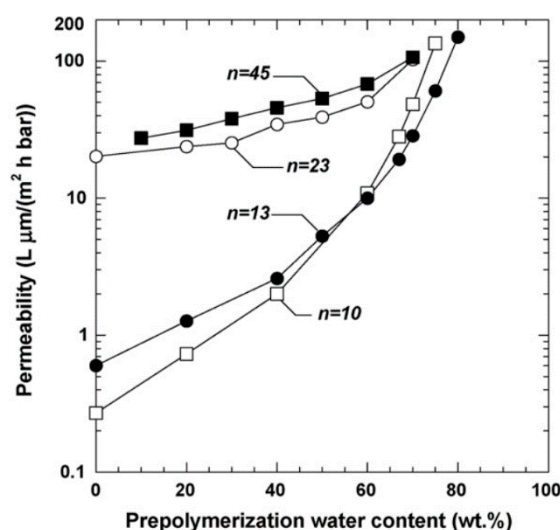


Figure 1.29. Variation of water permeability of PEGDA free-standing films prepared with PEGDA of various chain lengths as a function of water content in the prepolymerization solution¹²².

Moreover, longer PEGDA chain networks ($n = 23$ and 45) exhibit higher water permeability than short-chain networks when both are prepared at the same prepolymerization water content. This trend is reasonable because increases in PEGDA chain length should reduce cross-link density, thereby increasing network mesh size, as well as the water transport and permeability. In addition, PEGDA free-standing hydrogels exhibit excellent anti-fouling BSA protein and solvent resistant properties. BSA accumulation on the hydrogel surface during water purification processes is also influenced by the PEGDA chain length and prepolymerization water content. Films prepared by higher prepolymerization water content and longer PEGDA chain length are more hydrophilic, thus their surfaces generally exhibit less BSA adhesion, as represented in (Figure 1.30).

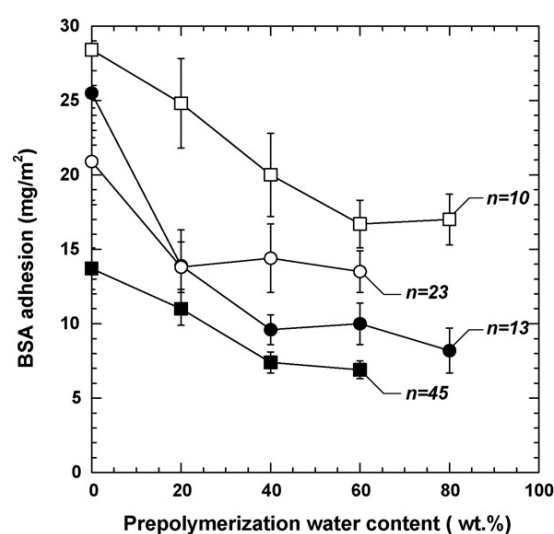


Figure 1.30. BSA adhesion to the surface of XLPEGDA free-standing films prepared with PEGDA films of various chain lengths and various prepolymerization water contents ¹²².

In another word, the good protein anti-fouling properties is represented by the effect of BSA filtration on the water flux of PEGDA membrane. As Figure 1.31 shows, water permeability of PEGDA ($n = 13$) with 80 wt% water, is almost constant after treatment with BSA solution and is not affected by BSA at a concentration of 1 g.L^{-1} ¹²⁴. The BSA rejection is around 96%.

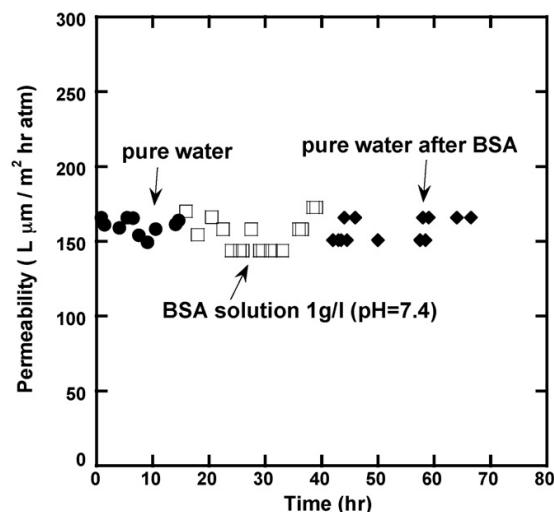


Figure 1.31. Permeability variation as a function of time for PEGDA film with 80 wt% of water during filtration with BSA solution ¹²⁴.

1.3.4.3 Water permeability properties of PEGDA/PEG membrane

As mentioned above, the transport properties and porous structure of PEGDA hydrogel can be enhanced and controlled by the use of polymer porogen such as PEG chains of low molar mass. In this context, Salmon *et al.* ¹⁵⁷ have reported the fabrication of PEGDA-700 g.mol⁻¹ hydrogels, with controlled permeability to water flow, and tunable nano-porosity, in the presence of PEG-1000 g.mol⁻¹ in the prepolymerization solution. They have synthesized these thin permeable hydrogels within microfluidic channels, due to their great advantages in many applications such as membrane based separation processes ^{158, 159}, pre-concentration or purification of biological samples ^{160, 161}, and in situ investigations of fouling mechanisms and flow control ^{162, 163}. They have measured the trans-membrane flux v for PEGDA membrane under different applied pressure. As the water flux varies linearly with the applied pressure, they can determine the membrane permeability K from a linear fit using the Darcy's law, as shown in Figure 1.32 a. The permeability obtained was about $K \approx 4 \times 10^{-17} \text{ m}^2$, depending on the membrane formulation and exposure conditions.

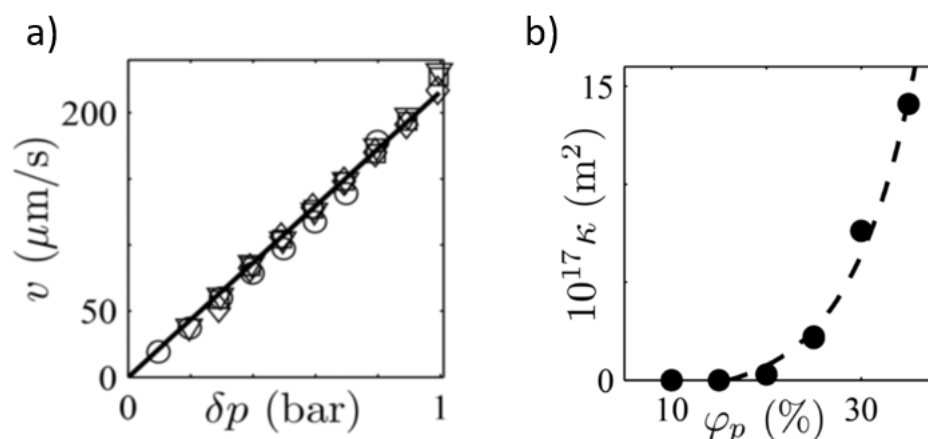


Figure 1.32. a) Variation of the trans-membrane flux as a function of the trans-membrane pressure, b) Variation of water permeability as a function of PEG-1000 $\text{g}\cdot\text{mol}^{-1}$ porogen content ¹⁵⁷.

In order to increase this permeability, they have screened the role of PEG-1000 porogen content on the measured water permeability. The results are presented in Figure 1.32 b. As expected, the membrane permeability increases up to $15 \times 10^{-17} \text{ m}^2$, when the porogen concentration increases from 10 to 30 %, due to a decrease in the cross-linking density.

Furthermore, other studies have demonstrated the ability to control the solute effective diffusivity within a multilayer microfluidic PEGDA hydrogels as a function of solute molecular weight and hydrogel concentration ¹⁶⁴, as shown in Figure 1.33.

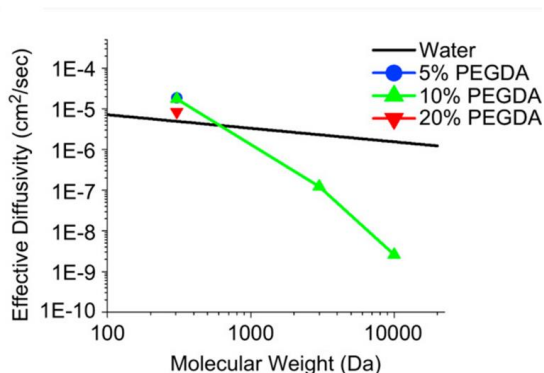


Figure 1.33. Variation of the measured effective diffusivity as a function of solute molecular weight and PEGDA hydrogel concentration ¹⁶⁴.

The diffusional transport of higher molecular weight solutes with larger hydrodynamic radii occurred at a slower rate when compared to that of lower molecular weight solutes. In addition,

PEGDA hydrogel concentration has shown also an effect on transport properties. Increases in hydrogel concentration from 5 to 20% (w/v) were shown to be inversely related to solute diffusion rate and the effective diffusivity of the hydrogel-solute system. At the low hydrogel concentration (5%), toluidine blue ($M_w = 305$ Da) had the highest effective diffusivity ($1.86 \times 10^{-5} \text{ cm}^2 \cdot \text{s}^{-1}$). However, when increasing the hydrogel concentration to 10 and 20%, the effective diffusivity of toluidine blue decreased to 1.75×10^{-5} and $8.45 \times 10^{-6} \text{ cm}^2 \cdot \text{s}^{-1}$, respectively. As already mentioned above, this trend was attributed to the decrease in average hydrogel pore size as a function of increasing PEGDA concentration.

1.4 POSITIONNING OF THE PhD WORK WITH RESPECT TO THE LITERATURE STUDY

In conclusion, we have reported in this chapter the different structural, mechanical and swelling properties of hydrogel networks in general. In addition, we have described studies concerning various filtration processes and classical porous membranes. Finally, we have made an overview of the hydrogel systems used in the context of filtration and separation, either as a thin coating films on the hydrophobic membranes or as free-standing hydrogels membranes. We have seen that PEGDA based hydrogels present several advantages with respect to filtration experiments i.e simple synthesis method, good mechanical properties and hydrophilic nature. The main originality of our approach with respect to the existing literature is that we add large PEG chains into the prepolymerization solution, that -we will show later- are trapped in the PEGDA matrix. This enables us to control the nanometric and micrometric porous structure of the hydrogels as well as their permeability over several orders of magnitude. Another advantage of our PEGDA/PEG membranes with respect to the literature is that they are prepared in a one-step process. Finally, we provide a systematic study of the effect of PEG concentrations and molar masses on the evolution of permeability and structural properties of PEGDA/PEG hydrogel membrane.

References

1. Wichterle, O.; Lim, D., Hydrophilic gels for biological use. *Nature* **1960**, *185* (4706), 117-118, DOI 10.1038/185117a0.
2. Wichterle, O., Reshaping a xerogel by mechanical removal and swelling to form a hydrogel contact lens. Google Patents: 1968.
3. Wichterle, O., *The beginning of the soft lens. Soft Contact Lenses: Clinical and Applied Technology*. 1978.
4. Chen, X.; Martin, B.; Neubauer, T.; Linhardt, R.; Dordick, J.; Rethwisch, D., Enzymatic and chemoenzymatic approaches to synthesis of sugar-based polymer and hydrogels. *Carbohydrate polymers* **1995**, *28* (1), 15-21, DOI 10.1016/0144-8617(95)00082-8.
5. Kashyap, N.; Kumar, N.; Kumar, M. R., Hydrogels for pharmaceutical and biomedical applications. *Critical Reviews™ in Therapeutic Drug Carrier Systems* **2005**, *22* (2), 107-150, DOI 10.1615/CritRevTherDrugCarrierSyst.v22.i2.10.
6. Lee, K. Y.; Mooney, D. J., Hydrogels for tissue engineering. *Chemical reviews* **2001**, *101* (7), 1869-1880, DOI 10.1021/cr000108x.
7. Tang, J. D.; Mura, C.; Lampe, K. J., Stimuli-Responsive, Pentapeptide, Nanofiber Hydrogel for Tissue Engineering. *J. Am. Chem. Soc.* **2019**, *141* (12), 4886-4899, DOI 10.1021/jacs.8b13363.
8. Peppas, N. A.; Bures, P.; Leobandung, W.; Ichikawa, H., Hydrogels in pharmaceutical formulations. *European journal of pharmaceuticals and biopharmaceutics* **2000**, *50* (1), 27-46, DOI 10.1016/S0939-6411(00)00090-4.
9. Liu, W.; Lee, B. S.; Mieler, W. F.; Kang-Mieler, J. J., Biodegradable Microsphere-Hydrogel Ocular Drug Delivery System for Controlled and Extended Release of Bioactive Aflibercept In Vitro. *Curr. Eye Res.* **2019**, *44* (3), 264-274, DOI 10.1080/02713683.2018.1533983.
10. Karimi, A. R.; Tarighatjoo, M.; Nikraves, G., 1,3,5-Triazine-2,4,6-tribenzaldehyde derivative as a new crosslinking agent for synthesis of pH-thermo dual responsive chitosan hydrogels and their nanocomposites: Swelling properties and drug release behavior. *Int. J. Biol. Macromol.* **2017**, *105* (Pt 1), 1088-1095, DOI 10.1016/j.ijbiomac.2017.07.128.
11. Mara Luz Peralta, R.; Joaquin Antonio, G.; Lucas, E. F.; Claudio Javier, P.; Mara Emilia, V.; Guillermo Javier, C., Sustainable and smart keratin hydrogel with pH-sensitive

swelling and enhanced mechanical properties. *Materials science & engineering. C, Materials for biological applications* **2017**, *78*, 619-626, DOI 10.1016/j.msec.2017.04.120.

12. Debele, T. A.; Mekuria, S. L.; Tsai, H. C., Polysaccharide based nanogels in the drug delivery system: Application as the carrier of pharmaceutical agents. *Mater. Sci. Eng. C Mater. Biol. Appl.* **2016**, *68*, 964-981, DOI 10.1016/j.msec.2016.05.121.

13. Li, J.; Chen, G.; Xu, X.; Abdou, P.; Jiang, Q.; Shi, D.; Gu, Z., Advances of injectable hydrogel-based scaffolds for cartilage regeneration. *Regen. Biomater.* **2019**, *6* (3), 129-140, DOI 10.1093/rb/rbz022.

14. Mohammadzadeh Pakdel, P.; Peighambardoust, S. J., Review on recent progress in chitosan-based hydrogels for wastewater treatment application. *Carbohydr. Polym.* **2018**, *201*, 264-279, DOI 10.1016/j.carbpol.2018.08.070.

15. Zhao, Y.-F.; Zhu, L.-P.; Yi, Z.; Zhu, B.-K.; Xu, Y.-Y., Zwitterionic hydrogel thin films as antifouling surface layers of polyethersulfone ultrafiltration membranes anchored via reactive copolymer additive. *J. Membr. Sci.* **2014**, *470*, 148-158, DOI 10.1016/j.memsci.2014.07.023.

16. Zhao, K.; Zhang, X.; Wei, J.; Li, J.; Zhou, X.; Liu, D.; Liu, Z.; Li, J., Calcium alginate hydrogel filtration membrane with excellent anti-fouling property and controlled separation performance. *J. Membr. Sci.* **2015**, *492*, 536-546, DOI 10.1016/j.memsci.2015.05.075.

17. Lu, R.; Zhang, C.; Piatkovsky, M.; Ulbricht, M.; Herzberg, M.; Nguyen, T. H., Improvement of virus removal using ultrafiltration membranes modified with grafted zwitterionic polymer hydrogels. *Water Res.* **2017**, *116*, 86-94, DOI 10.1016/j.watres.2017.03.023.

18. Gao, S.; Zhu, Y.; Wang, J.; Zhang, F.; Li, J.; Jin, J., Layer-by-Layer Construction of Cu²⁺/Alginate Multilayer Modified Ultrafiltration Membrane with Bioinspired Superwetting Property for High-Efficient Crude-Oil-in-Water Emulsion Separation. *Adv. Funct. Mater.* **2018**, *28* (49), 1801944, DOI 10.1002/adfm.201801944.

19. Kopeček, J.; Yang, J., Hydrogels as smart biomaterials. *Polymer international* **2007**, *56* (9), 1078-1098, DOI 10.1002/pi.2253.

20. Zheng, Y.; Wang, A., Superadsorbent with three-dimensional networks: From bulk hydrogel to granular hydrogel. *European Polymer Journal* **2015**, *72*, 661-686, DOI 10.1016/j.eurpolymj.2015.02.031.

21. Wang, Y., Programmable hydrogels. *Biomaterials* **2018**, *178*, 663-680, DOI 10.1016/j.biomaterials.2018.03.008.

22. Chai, Q.; Jiao, Y.; Yu, X., Hydrogels for Biomedical Applications: Their Characteristics and the Mechanisms behind Them. *Gels* **2017**, *3* (1), 6, DOI 10.3390/gels3010006.
23. Patel, A.; Mequanint, K., Hydrogel Biomaterials. 2011.
24. Akhtar, M. F.; Hanif, M.; Ranjha, N. M., Methods of synthesis of hydrogels ... A review. *Saudi Pharmaceutical Journal : SPJ* **2016**, *24*, 554 - 559, DOI 10.1016/j.jsps.2015.03.022.
25. Yang, J.; Chen, Y.; Zhao, L.; Feng, Z.; Peng, K.; Wei, A.; Wang, Y.; Tong, Z.; Cheng, B., Preparation of a chitosan/carboxymethyl chitosan/AgNPs polyelectrolyte composite physical hydrogel with self-healing ability, antibacterial properties, and good biosafety simultaneously, and its application as a wound dressing. *Composites Part B: Engineering* **2020**, *197*, 108139, DOI 10.1016/j.compositesb.2020.108139.
26. Zhao, F.; Yao, D.; Guo, R.; Deng, L.; Dong, A.; Zhang, J., Composites of polymer hydrogels and nanoparticulate systems for biomedical and pharmaceutical applications. *Nanomaterials* **2015**, *5* (4), 2054-2130, DOI 10.3390/nano5042054.
27. Abdurrahmanoglu, S.; Cilingir, M.; Okay, O., Dodecyl methacrylate as a crosslinker in the preparation of tough polyacrylamide hydrogels. *Polymer* **2011**, *52* (3), 694-699, DOI 10.1016/j.polymer.2010.12.044.
28. Voo, W.-P.; Ooi, C.-W.; Islam, A.; Tey, B.-T.; Chan, E.-S., Calcium alginate hydrogel beads with high stiffness and extended dissolution behaviour. *European Polymer Journal* **2016**, *75*, 343-353, DOI 10.1016/j.eurpolymj.2015.12.029.
29. Dankers, P. Y.; Hermans, T. M.; Baughman, T. W.; Kamikawa, Y.; Kieltyka, R. E.; Bastings, M. M.; Janssen, H. M.; Sommerdijk, N. A.; Larsen, A.; Van Luyn, M. J., Hierarchical formation of supramolecular transient networks in water: a modular injectable delivery system. *Advanced materials* **2012**, *24* (20), 2703-2709, DOI 10.1002/adma.201104072.
30. Flory, P. J., *Principles of polymer chemistry*. Cornell university press: 1953.
31. Thakur, V. K.; Thakur, M. K., *Hydrogels: recent advances*. Springer: 2018.
32. Zhang, L.; Liu, J.; Zheng, X.; Zhang, A.; Zhang, X.; Tang, K., Pullulan dialdehyde crosslinked gelatin hydrogels with high strength for biomedical applications. *Carbohydrate Polymers* **2019**, *216*, 45-53, DOI 10.1016/j.carbpol.2019.04.004.
33. Sagle, A. C.; Ju, H.; Freeman, B. D.; Sharma, M. M., PEG-based hydrogel membrane coatings. *Polymer* **2009**, *50* (3), 756-766, DOI 10.1016/j.polymer.2008.12.019.

34. Matyjaszewski, K.; Davis, T. P., *Handbook of radical polymerization*. Wiley Online Library: 2002; Vol. 922.
35. Jayaramudu, T.; Raghavendra, G. M.; Varaprasad, K.; Sadiku, R.; Raju, K. M., Development of novel biodegradable Au nanocomposite hydrogels based on wheat: for inactivation of bacteria. *Carbohydrate polymers* **2013**, *92* (2), 2193-2200, DOI 10.1016/j.carbpol.2012.12.006.
36. Burdick, J. A.; Anseth, K. S., Photoencapsulation of osteoblasts in injectable RGD-modified PEG hydrogels for bone tissue engineering. *Biomaterials* **2002**, *23* (22), 4315-4523, DOI 10.1016/s0142-9612(02)00176-x.
37. Elisseeff, J.; Anseth, K.; Sims, D.; McIntosh, W.; Randolph, M.; Yaremchuk, M.; Langer, R., Transdermal photopolymerization of poly(ethylene oxide)-based injectable hydrogels for tissue-engineered cartilage. *Plast. Reconstr. Surg* **1999**, *104* (4), 1014-1022, DOI 10.1097/00006534-199909040-00017.
38. Gulrez, S. K.; Al-Assaf, S.; Phillips, G. O., *Hydrogels: methods of preparation, characterisation and applications*. 2011; Vol. 117150.
39. De Gennes, P.-G.; Gennes, P.-G., *Scaling concepts in polymer physics*. Cornell university press: 1979.
40. Elias, H. G., *Chemical Structure*. 2008; p 7-40.
41. Guillen, G. R.; Pan, Y.; Li, M.; Hoek, E. M., Preparation and characterization of membranes formed by nonsolvent induced phase separation: a review. *Industrial & Engineering Chemistry Research* **2011**, *50* (7), 3798-3817, DOI 10.1021/ie101928r.
42. Fily, Y.; Marchetti, M. C., Athermal phase separation of self-propelled particles with no alignment. *Physical review letters* **2012**, *108* (23), 235702, DOI 10.1103/PhysRevLett.108.235702.
43. Fernández-Rico, C.; Sai, T.; Sicher, A.; Style, R. W.; Dufresne, E. R., Putting the Squeeze on Phase Separation. *JACS Au*. **2022**, *2* (1), 66-73, DOI 10.1021/jacsau.1c00443.
44. Ingrid, M. W.; Remko, B.; Beerlage, M. J. M.; Astrid, M. W. B.; Marco Leonardus Huber, S.; Heiner, S., Recent advances in the formation of phase inversion membranes made from amorphous or semi-crystalline polymers. *Journal of Membrane Science* **1996**, *113*, 361-371, DOI 10.1016/0376-7388(95)00256-1.
45. Smith, T.; Esser, B.; Antolin, N.; Carlsson, A.; Williams, R.; Wessman, A.; Hanlon, T.; Fraser, H.; Windl, W.; McComb, D., Phase transformation strengthening of high-temperature superalloys. *Nature communications* **2016**, *7* (1), 1-7, DOI 10.1038/ncomms13434.

46. van Ravensteijn, B. G.; Kegel, W. K., Tuning particle geometry of chemically anisotropic dumbbell-shaped colloids. *Journal of colloid and interface science* **2017**, *490*, 462-477, DOI 10.1016/j.jcis.2016.11.045.
47. Moerman, P. G.; Hohenberg, P. C.; Vanden-Eijnden, E.; Brujic, J., Emulsion patterns in the wake of a liquid–liquid phase separation front. *Proceedings of the National Academy of Sciences* **2018**, *115* (14), 3599-3604, DOI 10.1073/pnas.1716330115.
48. Xue, L.; Zhang, J.; Han, Y., Phase separation induced ordered patterns in thin polymer blend films. *Prog. Polym. Sci.* **2012**, *37*, 564-594, DOI 10.1016/j.progpolymsci.2011.09.001.
49. Wang, D.-M.; Lai, J.-Y., Recent advances in preparation and morphology control of polymeric membranes formed by nonsolvent induced phase separation. *Curr. Opin. Chem. Eng.* **2013**, *2*, 229–237, DOI 10.1016/j.coche.2013.04.003.
50. Bhadani, R.; Mitra, U. K. In *Synthesis and studies on water swelling behaviour of polyacrylamide hydrogels*, Macromolecular Symposia, Wiley Online Library: 2016; pp 30-34.
51. Mittal, H.; Kaith, B. S.; Jindal, R., Synthesis, characterization and swelling behaviour of poly (acrylamide-comethacrylic acid) grafted Gum ghatti based superabsorbent hydrogels. *Adv. Appl. Sci. Res.* **2010**, *1* (3), 56-66, DOI 10.1002/app.35238.
52. Ahearne, M.; Yang, Y.; El Haj, A. J.; Then, K. Y.; Liu, K. K., Characterizing the viscoelastic properties of thin hydrogel-based constructs for tissue engineering applications. *J. R. Soc. Interface* **2005**, *2* (5), 455-463, DOI 10.1098/rsif.2005.0065.
53. Drury, J. L.; Dennis, R. G.; Mooney, D. J., The tensile properties of alginate hydrogels. *Biomaterials* **2004**, *25* (16), 3187-3199, DOI 10.1016/j.biomaterials.2003.10.002.
54. Liu, Y. J.; Fu, L. H.; Liu, S.; Meng, L. Y.; Li, Y. Y.; Ma, M. G., Synthetic self-assembled homogeneous network hydrogels with high mechanical and recoverable properties for tissue replacement. *J. Mater. Chem B* **2016**, *4* (28), 4847-4854, DOI 10.1039/c6tb01249c.
55. Lee, D.; Zhang, H.; Ryu, S., *Elastic Modulus Measurement of Hydrogels*. 2018; p 1-21.
56. Anseth, K. S.; Bowman, C. N.; Brannon-Peppas, L., Mechanical properties of hydrogels and their experimental determination. *Biomaterials* **1996**, *17* (17), 1647-1657, DOI 10.1016/0142-9612(96)87644-7.
57. Mulder, M.; Mulder, J., *Basic principles of membrane technology*. Springer science & business media: 1996.
58. Marc, M.; Ravi, S. S.; Robert, R., Complementary life cycle assessment of wastewater treatment plants: An integrated approach to comprehensive upstream and downstream impact

assessments and its extension to building-level wastewater generation. *Sustainable Cities and Society* **2016**, *23*, 37-49, DOI 10.1016/j.scs.2016.02.013.

59. Zhang, X.; Minear, R. A., Removal of low-molecular weight DBPs and inorganic ions for characterization of high-molecular weight DBPs in drinking water. *Water Res.* **2006**, *40* (5), 1043-1051, DOI 10.1016/j.watres.2005.12.040.

60. Park, N.; Kwon, B.; Sun, M.; Ahn, H.; Kim, C.; Kwoak, C.; Lee, D.; Chae, S.; Hyung, H.; Cho, J., Application of various membranes to remove NOM typically occurring in Korea with respect to DBP, AOC and transport parameters. *Desalination* **2005**, *178* (1), 161-169, DOI 10.1016/j.desal.2004.11.035.

61. Guo, W.; Ngo, H.-H.; Li, J., A mini-review on membrane fouling. *Bioresource Technology* **2012**, *122*, 27-34, DOI 10.1016/j.biortech.2012.04.089.

62. Van der Bruggen, B.; Verberk, J.; Verhack, J., Comparison of pressure-driven membrane processes and traditional processes for drinking water production in Europe based on specific impact criteria. *Water SA* **2004**, *30* (3), 413-419, DOI 10.4314/wsa.v30i3.5091.

63. de Morais Coutinho, C.; Chiu, M. C.; Basso, R. C.; Ribeiro, A. P. B.; Gonçalves, L. A. G.; Viotto, L. A., State of art of the application of membrane technology to vegetable oils: A review. *Food Research International* **2009**, *42* (5-6), 536-550, DOI 10.1016/j.foodres.2009.02.010.

64. Li, N. N.; Fane, A. G.; Ho, W. W.; Matsuura, T., *Advanced membrane technology and applications*. John Wiley & Sons: 2011.

65. Ketola, A. Determination of surfactants in industrial waters of paper- and board mills. 2016.

66. Singh, R., *Chapter 1 - Introduction to Membrane Technology-Membrane Technology and Engineering for Water Purification (Second Edition)*. Butterworth-Heinemann: 2015; p 1-80.

67. Xiarchos, I.; Doulia, D.; Gekas, V.; Trägårdh, G., Polymeric Ultrafiltration Membranes and Surfactants. *Separation & Purification Reviews* **2003**, *32* (2), 215-278, DOI 10.1081/SPM-120026628.

68. Hinkov, A.; ÍK, Z.; Henke, S.; Kadlec, P., Application of Cross-Flow Ultrafiltration on Inorganic Membranes in Purification of Food Materials. *Czech Journal of Food Sciences* **2005**, *23*, 103-110, DOI 10.17221/3378-CJFS.

69. Hofs, B.; Ogier, J.; Vries, D.; Beerendonk, E.; Cornelissen, E., Comparison of ceramic and polymeric membrane permeability and fouling using surface water. *Separation and Purification Technology* **2011**, *79*, 365-374, DOI 10.1016/j.seppur.2011.03.025.

70. Rasouli, Y.; Abbasi, M.; Hashemifard, S. A., Fabrication, characterization, fouling behavior and performance study of ceramic microfiltration membranes for oily wastewater treatment. *Journal of Asian Ceramic Societies* **2019**, *7* (4), 476-495, DOI 10.1080/21870764.2019.1667070.
71. Hankins, N. P.; Lu, N.; Hilal, N., Enhanced removal of heavy metal ions bound to humic acid by polyelectrolyte flocculation. *Separation and Purification Technology* **2006**, *51* (1), 48-56, DOI 10.1016/j.seppur.2005.12.022.
72. Hsu, B.-M.; Yeh, H.-H., Removal of Giardia and Cryptosporidium in drinking water treatment: a pilot-scale study. *Water Research* **2003**, *37* (5), 1111-1117, DOI 10.1016/S0043-1354(02)00466-9.
73. Ciora, R.; Liu, P., Ceramic membranes for environmental related applications. *Fluid/Particle Separation Journal* **2003**, *15*, 51-60,
74. Goosen, M. F. A.; Sablani, S. S.; Al-Hinai, H.; Al-Obeidani, S.; Al-Belushi, R.; Jackson, D., Fouling of Reverse Osmosis and Ultrafiltration Membranes: A Critical Review. *Separation Science and Technology* **2005**, *39* (10), 2261-2297, DOI 10.1081/SS-120039343.
75. Agenson, K.; Urase, T., Change in membrane performance due to organic fouling in nanofiltration (NF)/reverse osmosis (RO) applications. *Separation and Purification Technology* **2007**, *55*, 147-156, DOI 10.1016/j.seppur.2006.11.010.
76. Li, H.; Wu, S.; Du, C.; Zhong, Y.; Yang, C., Preparation, Performances, and Mechanisms of Microbial Flocculants for Wastewater Treatment. *Int. J. Environ. Res. Public Health* **2020**, *17* (4), 1360, DOI 10.3390/ijerph17041360.
77. Yiantsios, S. G.; Karabelas, A. J., An experimental study of humic acid and powdered activated carbon deposition on UF membranes and their removal by backwashing. *Desalination* **2001**, *140* (2), 195-209, DOI 10.1016/S0011-9164(01)00368-X.
78. Ahmad, A. L.; Mariadas, A., Baffled microfiltration membrane and its fouling control for feed water of desalination. *Desalination* **2004**, *168*, 223-230, DOI 10.1016/j.desal.2004.07.002.
79. Ma, J.; Liu, W., Effectiveness of ferrate (VI) preoxidation in enhancing the coagulation of surface waters. *Water Res.* **2002**, *36* (20), 4959-4962, DOI 10.1016/S0043-1354(02)00224-5.
80. Al-Ahmad, M. J.; Farag Abdul, A.; Mutiri, A.; Ubaisy, A., Biofouling in RO membrane systems Part 1: Fundamentals and control. *Desalination* **2000**, *132*, 173-179, DOI 10.1016/S0011-9164(00)00146-6.

81. Hallé, C. Biofiltration in Drinking Water Treatment: Reduction of Membrane Fouling and Biodegradation of Organic Trace Contaminants. 2022.
82. Song, L.; Elimelech, M., Theory of concentration polarization in crossflow filtration. *Journal of the Chemical Society, Faraday Transactions* **1995**, *91* (19), 3389-3398, DOI 10.1039/FT9959103389.
83. Katsoufidou, K.; Yiantsios, S. G.; Karabelas, A. J., An experimental study of UF membrane fouling by humic acid and sodium alginate solutions: the effect of backwashing on flux recovery. *Desalination* **2008**, *220* (1), 214-227, DOI 10.1016/j.desal.2007.02.038.
84. Sablani, S. S.; Goosen, M. F. A.; Al-Belushi, R.; Wilf, M., Concentration polarization in ultrafiltration and reverse osmosis: a critical review. *Desalination* **2001**, *141* (3), 269-289, DOI 10.1016/S0011-9164(01)85005-0.
85. Zhou, Y.; Yu, S.; Gao, C.; Feng, X., Surface modification of thin film composite polyamide membranes by electrostatic self deposition of polycations for improved fouling resistance. *Separation and Purification Technology* **2009**, *66* (2), 287-294, DOI 10.1016/j.seppur.2008.12.021.
86. Ang, W. S.; Tiraferri, A.; Chen, K. L.; Elimelech, M., Fouling and cleaning of RO membranes fouled by mixtures of organic foulants simulating wastewater effluent. *Journal of Membrane Science* **2011**, *376* (1), 196-206, DOI 10.1016/j.memsci.2011.04.020.
87. Xing, C. H.; Wen, X. H.; Qian, Y.; Sun, D.; Klose, P. S.; Zhang, X. Q., Fouling and cleaning of microfiltration membrane in municipal wastewater reclamation. *Water Sci. Technol.* **2003**, *47* (1), 263-270, DOI 10.2166/wst.2003.0065.
88. Machenbach, I. Drinking Water Production by Coagulation and Membrane Filtration. 2007.
89. Ogunbiyi, O. O.; Miles, N. J.; Hilal, N., Comparison of Different Pitch Lengths on Static Promoters for Flux Enhancement in Tubular Ceramic Membrane. *Separation Science and Technology* **2007**, *42* (9), 1945-1963, DOI 10.1080/01496390701401576.
90. Amsden, B., Solute diffusion within hydrogels. Mechanisms and models. *Macromolecules* **1998**, *31* (23), 8382-8395, DOI 10.1021/ma980765f.
91. Ogston, A., The spaces in a uniform random suspension of fibres. *Trans. Faraday. Soc.* **1958**, *54*, 1754-1757, DOI 10.1039/TF9585401754.
92. Johansson, L.; Elvingsson, C.; Loeffroth, J. E., Diffusion and interaction in gels and solutions. 3. Theoretical results on the obstruction effect. *Macromolecules* **1991**, *24* (22), 6024-6029, DOI 10.1021/ma00022a019.

93. Cukier, R. I., Diffusion of Brownian spheres in semidilute polymer solutions. *Macromolecules* **1984**, *17* (2), 252-255, DOI 10.1021/ma00132a023.
94. Yasuda, H.; Lamaze, C.; Ikenberry, L., Permeability of solutes through hydrated polymer membranes. Part I. Diffusion of sodium chloride. *Makromol. Chem.* **1968**, *118* (1), 19-35, DOI 10.1002/macp.1968.021180102.
95. Lustig, S. R.; Peppas, N. A., Solute diffusion in swollen membranes. IX. Scaling laws for solute diffusion in gels. *Journal of Applied Polymer Science* **1988**, *36* (4), 735-747, DOI 10.1002/app.1988.070360401.
96. Fujiyabu, T.; Li, X.; Chung, U.-i.; Sakai, T., Diffusion behavior of water molecules in hydrogels with controlled network structure. *Macromolecules* **2019**, *52* (5), 1923-1929, DOI 10.1021/acs.macromol.8b02488.
97. Witten, J.; Ribbeck, K., The particle in the spider's web: transport through biological hydrogels. *Nanoscale* **2017**, *9* (24), 8080-8095, DOI 10.1039/C6NR09736G.
98. Lieleg, O.; Ribbeck, K., Biological hydrogels as selective diffusion barriers. *Trends in Cell Biology* **2011**, *21* (9), 543-551, DOI 10.1016/j.tcb.2011.06.002.
99. Lieleg, O.; Vladescu, I.; Ribbeck, K., Characterization of particle translocation through mucin hydrogels. *Biophysical journal* **2010**, *98* (9), 1782-1789, DOI 10.1016/j.bpj.2010.01.012.
100. Hansing, J.; Netz, R. R., Hydrodynamic Effects on Particle Diffusion in Polymeric Hydrogels with Steric and Electrostatic Particle–Gel Interactions. *Macromolecules* **2018**, *51* (19), 7608-7620, DOI 10.1021/acs.macromol.8b01494.
101. Fu, W.; Pei, T.; Mao, Y.; Li, G.; Zhao, Y.; Chen, L., Highly hydrophilic poly(vinylidene fluoride) ultrafiltration membranes modified by poly(N-acryloyl glycinamide) hydrogel based on multi-hydrogen bond self-assembly for reducing protein fouling. *J. Membr. Sci.* **2019**, *572*, 453-463, DOI 10.1016/j.memsci.2018.11.022.
102. Meng, J.; Xie, Y.; Gu, Y.-H.; Yan, X.; Chen, Y.; Guo, X.-J.; Lang, W.-Z., PVDF-CaAlg nanofiltration membranes with dual thin-film-composite (TFC) structure and high permeation flux for dye removal. *Separation and Purification Technology* **2021**, *255*, 117739, DOI 10.1016/j.seppur.2020.117739.
103. Xu, S.-J.; Chen, G.-E.; Xu, Z.-L., Excellent anti-fouling performance of PVDF polymeric membrane modified by enhanced CaA gel-layer. *Journal of industrial and engineering chemistry* **2018**, *58*, 179-188, DOI 10.1016/j.jiec.2017.09.023.
104. Chang, Y.; Ko, C.-Y.; Shih, Y.-J.; Quémener, D.; Deratani, A.; Wei, T.-C.; Wang, D.-M.; Lai, J.-Y., Surface grafting control of PEGylated poly (vinylidene fluoride) antifouling

membrane via surface-initiated radical graft copolymerization. *Journal of Membrane Science* **2009**, *345* (1-2), 160-169, DOI 10.1016/j.memsci.2009.08.039.

105. Shen, X.; Yin, X.; Zhao, Y.; Chen, L., Antifouling enhancement of PVDF membrane tethered with polyampholyte hydrogel layers. *Polymer Engineering & Science* **2015**, *55* (6), 1367-1373, DOI 10.1002/pen.24077.

106. Bernstein, R.; Antón, E.; Ulbricht, M., Tuning the nanofiltration performance of thin film strong polyelectrolyte hydrogel composite membranes by photo-grafting conditions. *Journal of Membrane Science* **2013**, *427*, 129–138, DOI 10.1016/j.memsci.2012.09.034.

107. Zhang, W.; Yang, Z.; Kaufman, Y.; Bernstein, R., Surface and anti-fouling properties of a polyampholyte hydrogel grafted onto a polyethersulfone membrane. *Journal of colloid and interface science* **2018**, *517*, 155-165, DOI 10.1016/j.jcis.2018.01.106.

108. La, Y.-H.; Sooriyakumaran, R.; McCloskey, B. D.; Allen, R. D.; Freeman, B. D.; Al-Rasheed, R., Enhancing water permeability of fouling-resistant POSS–PEGM hydrogels using ‘addition–extraction’ of sacrificial additives. *Journal of membrane science* **2012**, *401*, 306-312, DOI 10.1016/j.memsci.2012.02.021.

109. Qin, D.; Liu, Z.; Liu, Z.; Bai, H.; Sun, D. D., Superior antifouling capability of hydrogel forward osmosis membrane for treating wastewaters with high concentration of organic foulants. *Environmental science & technology* **2018**, *52* (3), 1421-1428, DOI 10.1021/acs.est.7b04838.

110. Peng, F.; Huang, X.; Jawor, A.; Hoek, E. M., Transport, structural, and interfacial properties of poly (vinyl alcohol)–polysulfone composite nanofiltration membranes. *Journal of Membrane Science* **2010**, *353* (1-2), 169-176, DOI 10.1016/j.memsci.2010.02.044.

111. Sadeghi, I.; Yi, H.; Asatekin, A., A method for manufacturing membranes with ultrathin hydrogel selective layers for protein purification: Interfacially initiated free radical polymerization (IIFRP). *Chemistry of Materials* **2018**, *30* (4), 1265-1276, DOI 10.1021/acs.chemmater.7b04598.

112. La, Y.-H.; McCloskey, B. D.; Sooriyakumaran, R.; Vora, A.; Freeman, B.; Nassar, M.; Hedrick, J.; Nelson, A.; Allen, R., Bifunctional hydrogel coatings for water purification membranes: improved fouling resistance and antimicrobial activity. *J. Membr. Sci.* **2011**, *372* (1-2), 285-291, DOI 10.1016/j.memsci.2011.02.005.

113. Ju, H.; McCloskey, B. D.; Sagle, A. C.; Wu, Y.-H.; Kusuma, V. A.; Freeman, B. D., Crosslinked poly (ethylene oxide) fouling resistant coating materials for oil/water separation. *J. Membr. Sci.* **2008**, *307* (2), 260-267, DOI 10.1016/j.memsci.2007.09.028.

114. Kang, G.; Cao, Y.; Zhao, H.; Yuan, Q., Preparation and characterization of crosslinked poly (ethylene glycol) diacrylate membranes with excellent antifouling and solvent-resistant properties. *J. Membr. Sci.* **2008**, *318* (1-2), 227-232, DOI 10.1016/j.memsci.2008.02.045.
115. Kang, S.; Asatekin, A.; Mayes, A. M.; Elimelech, M., Protein antifouling mechanisms of PAN UF membranes incorporating PAN-g-PEO additive. *Journal of Membrane Science* **2007**, *296* (1-2), 42-50, DOI 10.1016/j.memsci.2007.03.012.
116. Ostuni, E.; Chapman, R. G.; Holmlin, R. E.; Takayama, S.; Whitesides, G. M., A survey of structure– property relationships of surfaces that resist the adsorption of protein. *Langmuir* **2001**, *17* (18), 5605-5620, DOI 10.1021/la010384m.
117. Zhang, X.; Lin, B.; Zhao, K.; Wei, J.; Guo, J.; Cui, W.; Jiang, S.; Liu, D.; Li, J., A free-standing calcium alginate/polyacrylamide hydrogel nanofiltration membrane with high anti-fouling performance: preparation and characterization. *Desalination* **2015**, *365*, 234-241, DOI 10.1016/j.desal.2015.03.015.
118. Sun, J.-Y.; Zhao, X.; Illeperuma, W. R.; Chaudhuri, O.; Oh, K. H.; Mooney, D. J.; Vlassak, J. J.; Suo, Z., Highly stretchable and tough hydrogels. *Nature* **2012**, *489* (7414), 133-136, DOI 10.1038/nature11409.
119. Xiao-lei, W.; Wei, Q.; Li-xin, W.; Kong-yin, Z.; Hui-cai, W.; Hong-yu, L.; Jun-fu, W., Desalination of dye utilizing carboxylated TiO₂/calcium alginate hydrogel nanofiltration membrane with high salt permeation. *Sep. Purif. Technol.* **2020**, *253*, 117475, DOI 10.1016/j.seppur.2020.117475.
120. Tessmar, J. K.; Göpferich, A. M., Customized PEG-derived copolymers for tissue-engineering applications. *Macromolecular bioscience* **2007**, *7* (1), 23-39, DOI 10.1002/mabi.200600096.
121. Veronese, F. M.; Mero, A., The impact of PEGylation on biological therapies. *BioDrugs* **2008**, *22* (5), 315-329, DOI 10.2165/00063030-200822050-00004.
122. Ju, H.; McCloskey, B. D.; Sagle, A. C.; Kusuma, V. A.; Freeman, B. D., Preparation and characterization of crosslinked poly(ethylene glycol) diacrylate hydrogels as fouling-resistant membrane coating materials. *J. Membr. Sci.* **2009**, *330* (1), 180-188, DOI 10.1016/j.memsci.2008.12.054.
123. Lin, H.; Van Wagner, E.; Swinnea, J. S.; Freeman, B. D.; Pas, S. J.; Hill, A. J.; Kalakkunnath, S.; Kalika, D. S., Transport and structural characteristics of crosslinked poly (ethylene oxide) rubbers. *J. Membr. Sci.* **2006**, *276* (1-2), 145-161, DOI 10.1016/j.memsci.2005.09.040.

124. Wu, Y.-H.; Park, H. B.; Kai, T.; Freeman, B.; Kalika, D., Water uptake, transport and structure characterization in poly(ethylene glycol) diacrylate hydrogels. *J. Membr. Sci.* **2010**, *347*, 197-208, DOI 10.1016/j.memsci.2009.10.025.
125. Nemir, S.; Hayenga, H. N.; West, J. L., PEGDA hydrogels with patterned elasticity: Novel tools for the study of cell response to substrate rigidity. *Biotechnol. Bioeng.* **2010**, *105* (3), 636-644, DOI 10.1002/bit.22574.
126. Pereira, R. F.; Bártolo, P. J., 3D photo-fabrication for tissue engineering and drug delivery. *Engineering* **2015**, *1* (1), 090-112, DOI 10.15302/J-ENG-2015015.
127. Gou, M.; Qu, X.; Zhu, W.; Xiang, M.; Yang, J.; Zhang, K.; Wei, Y.; Chen, S., Bio-inspired detoxification using 3D-printed hydrogel nanocomposites. *Nature Communications* **2014**, *5* (1), 3774, DOI 10.1038/ncomms4774.
128. Liu, S.; Yeo, D. C.; Wiraja, C.; Tey, H. L.; Mrksich, M.; Xu, C., Peptide delivery with poly(ethylene glycol) diacrylate microneedles through swelling effect. *Bioeng Transl Med* **2017**, *2* (3), 258-267, DOI 10.1002/btm2.10070.
129. Nguyen, K. T.; West, J. L., Photopolymerizable hydrogels for tissue engineering applications. *Biomaterials* **2002**, *23* (22), 4307-4314, DOI 10.1016/S0142-9612(02)00175-8.
130. González-Méijome, J. M.; López-Alemany, A.; Almeida, J. B.; Parafita, M. A.; Refojo, M. F., Microscopic observations of superficial ultrastructure of unworn siloxane-hydrogel contact lenses by cryo-scanning electron microscopy. *Journal of Biomedical Materials Research Part B: Applied Biomaterials: An Official Journal of The Society for Biomaterials, The Japanese Society for Biomaterials, and The Australian Society for Biomaterials and the Korean Society for Biomaterials* **2006**, *76* (2), 419-423, DOI 10.1002/jbm.b.30386.
131. Dusek, K., Inhomogeneities induced by crosslinking in the course of crosslinking copolymerization. In *Polymer Networks*, Springer: 1971; pp 245-260.
132. Dušek, K. In *Phase separation during the formation of three-dimensional polymers*, J. Polym. Sci., Part C: Polym. Symp., Wiley Online Library: 1967; pp 1289-1299.
133. Okada, M.; Sun, J.; Tao, J.; Chiba, T.; Nose, T., Phase separation kinetics and morphology in the critical to off-critical crossover region. *Macromolecules* **1995**, *28* (22), 7514-7518, DOI 10.1021/ma00126a031.
134. Okada, M.; Fujimoto, K.; Nose, T., Phase separation induced by polymerization of 2-chlorostyrene in a polystyrene/dibutyl phthalate mixture. *Macromolecules* **1995**, *28* (6), 1795-1800, DOI 10.1021/ma00110a011.

135. Lin-Gibson, S.; Jones, R. L.; Washburn, N. R.; Horkay, F., Structure– property relationships of photopolymerizable poly (ethylene glycol) dimethacrylate hydrogels. *Macromolecules* **2005**, *38* (7), 2897-2902, DOI 10.1021/ma0487002.
136. Waters, D. J.; Engberg, K.; Parke-Houben, R.; Hartmann, L.; Ta, C. N.; Toney, M. F.; Frank, C. W., Morphology of photopolymerized end-linked poly (ethylene glycol) hydrogels by small-angle X-ray scattering. *Macromolecules* **2010**, *43* (16), 6861-6870, DOI 10.1021/ma101070s.
137. Malo de Molina, P.; Lad, S.; Helgeson, M. E., Heterogeneity and its Influence on the Properties of Difunctional Poly(ethylene glycol) Hydrogels: Structure and Mechanics. *Macromolecules* **2015**, *48* (15), 5402-5411, DOI 10.1021/acs.macromol.5b01115.
138. Boots, H.; Kloosterboer, J.; Serbutoviez, C.; Touwslager, F., Polymerization-Induced Phase Separation. 1. Conversion– Phase Diagrams. *Macromolecules* **1996**, *29* (24), 7683-7689, DOI 10.1021/ma960292h.
139. Al-Nasassrah, M. A.; Podcizek, F.; Newton, J. M., The effect of an increase in chain length on the mechanical properties of polyethylene glycols. *European journal of pharmaceutics and biopharmaceutics* **1998**, *46* (1), 31-38, DOI 10.1016/S0939-6411(97)00151-3.
140. Gunn, J. W.; Turner, S. D.; Mann, B. K., Adhesive and mechanical properties of hydrogels influence neurite extension. *Journal of Biomedical Materials Research Part A: An Official Journal of The Society for Biomaterials, The Japanese Society for Biomaterials, and The Australian Society for Biomaterials and the Korean Society for Biomaterials* **2005**, *72* (1), 91-97, DOI 10.1002/jbm.a.30203.
141. Padmavathi, N. C.; Chatterji, P., Structural characteristics and swelling behavior of poly (ethylene glycol) diacrylate hydrogels. *Macromolecules* **1996**, *29* (6), 1976-1979, DOI 10.1021/ma950827r.
142. Gabler, S.; Stampfl, J.; Koch, T.; Seidler, S.; Schuller, G.; Redl, H.; Juras, V.; Trattnig, S.; Weidisch, R., Determination of the viscoelastic properties of hydrogels based on polyethylene glycol diacrylate (PEG-DA) and human articular cartilage. *International Journal of Materials Engineering Innovation* **2009**, *1* (1), 3-20, DOI 10.1504/IJMatEI.2009.024024.
143. Van Hove, A. H.; Wilson, B. D.; Benoit, D. S., Microwave-assisted functionalization of poly (ethylene glycol) and on-resin peptides for use in chain polymerizations and hydrogel formation. *Journal of Visualized Experiments* **2013**, (80), e50890, DOI 10.3791/50890

144. Choi, J. R.; Yong, K. W.; Choi, J. Y.; Cowie, A. C., Recent advances in photocrosslinkable hydrogels for biomedical applications. *BioTechniques* **2019**, *66* (1), 40-53, DOI 10.2144/btn-2018-0083.
145. Chen, J.; Park, H.; Park, K., Synthesis of superporous hydrogels: Hydrogels with fast swelling and superabsorbent properties. *Journal of Biomedical Materials Research: An Official Journal of The Society for Biomaterials, The Japanese Society for Biomaterials, and the Australian Society for Biomaterials* **1999**, *44* (1), 53-62, DOI 10.1002/(SICI)1097-4636(199901)44:1<53::AID-JBM6>3.0.CO;2-W.
146. Okay, O., Macroporous copolymer networks. *Progress in polymer science* **2000**, *25* (6), 711-779, DOI 10.1016/S0079-6700(00)00015-0.
147. Kabiri, K.; Omidian, H.; Hashemi, S.; Zohuriaan-Mehr, M., Synthesis of fast-swelling superabsorbent hydrogels: effect of crosslinker type and concentration on porosity and absorption rate. *European Polymer Journal* **2003**, *39* (7), 1341-1348, DOI 10.1016/S0014-3057(02)00391-9.
148. Chiu, Y. C.; Larson, J. C.; Isom, A., Jr.; Brey, E. M., Generation of porous poly(ethylene glycol) hydrogels by salt leaching. *Tissue Eng. Part C: Methods* **2010**, *16* (5), 905-912, DOI 10.1089/ten.TEC.2009.0646.
149. Turani-i-Belloto, A.; Meunier, N.; Lopez, P.; Leng, J., Diffusion-limited dissolution of calcium carbonate in a hydrogel. *Soft Matter* **2019**, *15* (14), 2942-2949, DOI 10.1039/C8SM02625D.
150. Lee, A. G.; Arena, C. P.; Beebe, D. J.; Palecek, S. P., Development of macroporous poly(ethylene glycol) hydrogel arrays within microfluidic channels. *Biomacromolecules* **2010**, *11* (12), 3316-3324, DOI 10.1021/bm100792y.
151. Choi, N. W.; Kim, J.; Chapin, S. C.; Duong, T.; Donohue, E.; Pandey, P.; Broom, W.; Hill, W. A.; Doyle, P. S., Multiplexed detection of mRNA using porosity-tuned hydrogel microparticles. *Analytical chemistry* **2012**, *84* (21), 9370-9378, DOI 10.1021/ac302128u.
152. Caykara, T.; Bulut, M.; Dilsiz, N.; Akyüz, Y., Macroporous poly (acrylamide) hydrogels: Swelling and shrinking behaviors. *Journal of Macromolecular Science Part A--Pure and Applied Chemistry* **2006**, *43* (6), 889-897, DOI 10.1080/10601320600653699.
153. Courtois, J.; Byström, E.; Irgum, K., Novel monolithic materials using poly (ethylene glycol) as porogen for protein separation. *Polymer* **2006**, *47* (8), 2603-2611, DOI 10.1016/j.polymer.2006.01.096.
154. Annabi, N.; Nichol, J. W.; Zhong, X.; Ji, C.; Koshy, S.; Khademhosseini, A.; Dehghani, F., Controlling the porosity and microarchitecture of hydrogels for tissue

engineering. *Tissue Engineering Part B: Reviews* **2010**, *16* (4), 371-383, DOI 10.1089/ten.teb.2009.0639.

155. Ulbricht, M.; Matuschewski, H.; Oechel, A.; Hicke, H.-G., Photo-induced graft polymerization surface modifications for the preparation of hydrophilic and low-protein-adsorbing ultrafiltration membranes. *Journal of Membrane Science* **1996**, *115* (1), 31-47, DOI 10.1016/0376-7388(95)00264-2.

156. Susanto, H.; Balakrishnan, M.; Ulbricht, M., Via surface functionalization by photograft copolymerization to low-fouling polyethersulfone-based ultrafiltration membranes. *Journal of Membrane Science* **2007**, *288* (1), 157-167, DOI 10.1016/j.memsci.2006.11.013.

157. Decock, J.; Schlenk, M.; Salmon, J. B., In situ photo-patterning of pressure-resistant hydrogel membranes with controlled permeabilities in PEGDA microfluidic channels. *Lab on a chip* **2018**, *18* (7), 1075-1083, DOI 10.1039/c7lc01342f.

158. Zhang, Y.; Benes, N. E.; Lammertink, R. G., Performance study of pervaporation in a microfluidic system for the removal of acetone from water. *Chemical Engineering Journal* **2016**, *284*, 1342-1347, DOI 10.1016/j.cej.2015.09.084.

159. Ziemecka, I.; Haut, B.; Scheid, B., Hydrogen peroxide concentration by pervaporation of a ternary liquid solution in microfluidics. *Lab on a chip* **2015**, *15* (2), 504-511, DOI 10.1039/C4LC00886C.

160. Hatch, A. V.; Herr, A. E.; Throckmorton, D. J.; Brennan, J. S.; Singh, A. K., Integrated preconcentration SDS-PAGE of proteins in microchips using photopatterned cross-linked polyacrylamide gels. *Analytical Chemistry* **2006**, *78* (14), 4976-4984, DOI 10.1021/ac0600454.

161. Song, S.; Singh, A. K.; Kirby, B. J., Electrophoretic concentration of proteins at laser-patterned nanoporous membranes in microchips. *Analytical Chemistry* **2004**, *76* (15), 4589-4592, DOI 10.1021/ac0497151.

162. Ngene, I. S.; Lammertink, R. G.; Wessling, M.; van der Meer, W., A microfluidic membrane chip for in situ fouling characterization. *Journal of membrane science* **2010**, *346* (1), 202-207, DOI 10.1016/j.memsci.2009.09.035.

163. Beebe, D. J.; Moore, J. S.; Bauer, J. M.; Yu, Q.; Liu, R. H.; Devadoss, C.; Jo, B.-H., Functional hydrogel structures for autonomous flow control inside microfluidic channels. *Nature* **2000**, *404* (6778), 588-590, DOI 10.1038/35007047.

164. Cuchiara, M. P.; Allen, A. C.; Chen, T. M.; Miller, J. S.; West, J. L., Multilayer microfluidic PEGDA hydrogels. *Biomaterials* **2010**, *31* (21), 5491-5497, DOI 10.1016/j.biomaterials.2010.03.031.

Chapter 2

Large and non-linear permeability amplification with polymeric additives in hydrogel membranes

This Chapter is a copy of an article published in *Macromolecules* (Eddine, M. A.; Belbekhouche, S.; de Chateauneuf-Randon, S.; Salez, T.; Kovalenko, A.; Bresson, B.; Monteux, C., Large and Nonlinear Permeability Amplification with Polymeric Additives in Hydrogel Membranes. *Macromolecules* **2022**, 55 (21), 9841-9850, DOI 10.1021/acs.macromol.2c01462).

2.1 ABSTRACT

Hydrogels which are hydrophilic and porous materials have recently emerged as promising systems for filtration applications. In our study, we prepare hydrogel membranes by the photopolymerization of a mixture of poly (ethylene glycol) diacrylate (PEGDA) and large poly (ethylene glycol) (PEG) chains of 300 000 g.mol⁻¹ in the presence of a photoinitiator. We find that this addition of free PEG chains induces a large and non-linear increase of the water permeability. Indeed, by changing the content of PEG chains added, we obtain variations of the hydrogel water permeability over two orders of magnitude. The highest water permeability values are obtained for the membranes when the PEG concentration is equal to its critical overlap concentration C^* . Moreover, we find that the flow rate of water through the membranes varies non-linearly with the pressure. We relate this result to the deformability of the membranes as the applied pressure leads to a compression of the pores. This study provides new perspectives for the design of flexible hydrogel membranes with controlled permeability and their application in water treatment and bioseparation.

2.2 KEYWORDS

hydrogel, poly (ethylene glycol) diacrylate, poly (ethylene glycol), permeability, critical overlap concentration

2.3 INTRODUCTION

Pressure-driven membrane technologies, such as microfiltration, ultrafiltration, nanofiltration and reverse osmosis, have proven their effectiveness in a broad range of water treatment applications^{1,2}. The porous structure of membranes, either composed of ceramics or polymers, controls the size of the particles that permeates through the membrane. Fouling of membranes with bio-organisms and proteins usually limits the life time and permeability of membranes^{3,4}.

Hydrogels, which are networks of polymer chains in water, have a porous and hydrophilic structure which has recently attracted the attention of researchers in the context of filtration and separation⁵. Their network structure also enables ones to control the Brownian diffusion of species through them⁶⁻¹⁰ which can be used for drug delivery purpose¹¹. Controlling the transport of solvents, ions, solutes and particles in such polymer networks is also desirable for other applications such as catalysis, fuel cells and batteries and can be done by controlling their microscopic morphology and porosity¹². In the context of water treatment¹³, biomolecular separation^{14,15}, virus filtration¹⁶ or even crude oil emulsion separation¹⁷, thin coatings of hydrogels deposited on conventional filtration membranes have been used to prevent fouling of membranes by proteins. Indeed, classical hydrophobic membranes made of polysulfone (PSF)¹⁸, polyethersulfone (PES)¹⁹, or polyvinylidene fluoride (PVDF)²⁰, and coated with a hydrogel layer enable both to increase the hydrophilicity of the membranes and to decrease their affinity with hydrophobic proteins.

Recently poly (ethylene glycol) diacrylate (PEGDA)-based hydrogels have been used either as thin coatings on hydrophobic membranes^{18,21} or as stand-alone thick membranes^{22,23}. Ju and colleagues²² studied the water permeability of a family of cross-linked poly (ethylene glycol) diacrylate (PEGDA) membranes. PEGDA is particularly suitable for filtration experiments as it can sustain high filtration pressures owed to its excellent mechanical properties²⁴.

Micron-sized PEGDA/PEG hydrogels are also used for microfluidic filtration applications²⁵⁻²⁷ where small free PEG chains ($\overline{Mw} \sim 1000 \text{ g.mol}^{-1}$) are added in the prepolymerization mixture in the context of protein crystallization²⁸. After polymerization, the small free PEG chains are expected to be rinsed out of the membranes hence enabling the increase of the permeability of PEGDA hydrogels over one order of magnitude depending on the PEG concentration²⁷. To control the permeability of PEGDA hydrogels, other studies report the polymerization of PEGDA in the presence of a sacrificial template (or porogens) such as salt crystals²⁹, or

sacrificial particles³⁰ which are dissolved after polymerization. Although these methods allow the formation of larger porosities in the hydrogels, some of them involve removing these templates using a chemical treatment which limits their application.

In our study, we focus on the filtration properties of free-standing hydrogel membranes, of millimetric thickness, composed of a PEGDA matrix in which large free PEG chains ($\overline{M}_w=300\,000\text{ g.mol}^{-1}$) are added at varying concentrations. Here, the free PEG chains are not used as templates but remain trapped inside the PEGDA matrix. Hence, a great advantage of these membranes is that they can be prepared in a one-step process. We show that varying the PEG concentration enables tuning the PEG/PEGDA hydrogel's permeability over two orders of magnitude, including an optimum with the PEG concentration corresponding to the critical overlap concentration of PEG solutions. Moreover, we show that the permeability of the PEG/PEGDA membranes strongly depends on the applied pressure. We suggest that this non-linear behavior is due to a deformation of the hydrogel matrix induced by the confined viscous flow. These results are promising for the development of versatile macroporous hydrogel membranes with tunable and non-linear water permeabilities.

2.4 EXPERIMENTAL SECTION

2.4.1 Materials

We use poly (ethylene glycol) diacrylate PEGDA ($\overline{M}_w=700\text{ g.mol}^{-1}$) oligomers with 13 ethylene oxide units and 4-(2-hydroxyethoxy) phenyl 2-hydroxy-2-propyl ketone (Irgacure 2959) photoinitiator which are purchased from Sigma–Aldrich. Linear poly (ethylene glycol) (PEG) ($\overline{M}_w=300\,000\text{ g.mol}^{-1}$, $D=2.1$) is purchased from Serva. Water is purified with a Milli-Q reagent system (Millipore).

2.4.2 PEGDA hydrogels preparation

The PEGDA and PEG/PEGDA membranes are synthesized via UV-initiated free-radical photopolymerization, using Irgacure 2959 as the photoinitiator. The prepolymerization solution is prepared by adding 0.1 wt% photoinitiator (Irgacure 2959) into pure PEGDA. After stirring, the solution is mixed with water to obtain a prepolymerization solution composed of 16 wt% PEGDA and 84 wt% water. The prepolymerization solution is then sandwiched between two glass plates ($120\times 80\text{ mm}^2$) which are separated by 1-mm-thick spacers to obtain a membrane thickness of 1 mm. Then the solution is polymerized under irradiation with UV light (Intensity = $1800\text{ }\mu\text{W/cm}^2$) with a wavelength of 365 nm for 10 min. After polymerization, the obtained

hydrogels are placed in a Petri dish with pure water for at least 24 hours prior to filtration experiments, in order to remove any unreacted PEGDA oligomers or untrapped PEG chains. As explained in Figure S2.1, the obtained hydrogels right after polymerization contain 82% of water and 18% of PEGDA. Moreover, once immersed in deionized water, they do not swell or deswell over four days at room temperature, consistently with the study of Ju *et al.*²².

To obtain the PEG/PEGDA hydrogels, PEG-300 000 g.mol⁻¹ is dissolved in the prepolymerization solution. To prepare the sample, we keep the masses of PEGDA and water constant and add varying quantities of PEG-300 000 g.mol⁻¹ in the prepolymerization solution so that the PEG weight percentage Φ_{PEG} in the prepolymerization solution ranges between 0.4 wt% and 7.7 wt%. For the filtration and mechanical measurements, the membranes are then cut to obtain 1-mm-thick disks of diameter either 14 mm or 45 mm using punch cutters with corresponding diameters. As shown in Figure S2.1, by weighing the hydrogel disks in the preparation state, and after drying, we find that the water content is comprised between 80 and 82% for all the prepared hydrogels. Moreover, no significant swelling is measured when the hydrogels are immersed in pure water at room temperature.

2.4.3 Chemical composition of hydrogels

The chemical composition was analyzed by Fourier-transform infrared spectroscopy FTIR (Bruker, Tensor 27 instrument equipped with a Digitec DLaTGS detector). The FTIR spectroscopy resolution is about 4 cm⁻¹ and the infrared radiation ranging approximately from 4000 to 400 cm⁻¹. The number of averaged scans is 32.

2.4.4 Atomic Force Microscopy (AFM) measurements

AFM images were obtained with a Bruker Icon microscope driven by a Nanoscope V controller. The surface of the hydrogel membrane immersed in water was observed in Peak Force mode. The height images were acquired with a cantilever of spring constant 0.7 N.m⁻¹ specially designed for this application. In this mode, similar to a rapid approach-retract experiment, the cantilever oscillates at a frequency of 1 kHz. The scanning frequency was 0.7 Hz and the maximum force was set to 500 pN.

2.4.5 Mechanical measurements

Disc-shaped hydrogel membranes were used to test the mechanical properties. Before mechanical testing, the gels were conserved in water overnight. Discs were 14 mm in diameter and ~1 mm in thickness. Samples were tested under compression using an Instron 5565 testing

machine at a deformation speed of $0.01 \text{ mm}\cdot\text{s}^{-1}$. Discs were compressed between 10 and 40% of their original thickness and then unloaded to determine their elastic recoil capacity. The stress σ (Pa) was calculated from the ratio between the force F and the initial sample area S_0 using the (Equation 2.1):

$$\sigma = \frac{F}{S_0} \quad (2.1)$$

The strain ε (%) was calculated from the sample thickness in the initial state (h_0) and in the compressed state (h) as given in (Equation 2.2):

$$\varepsilon = \frac{h}{h_0} \times 100 \quad (2.2)$$

The effective Young's modulus of each gel was calculated from the slope of the stress–strain curve, in the range of >1-4 % in strain, in the loading phase, using the Hooke's law given in (Equation 2.3):

$$E = \frac{\sigma}{\varepsilon} \quad (2.3)$$

For all samples, E was calculated from adjusting the stress-strain data at strain >1-4%, while some curve variability was observed at the very low strains (0-1%) because of parallelism issues.

2.4.6 Filtration experiments

Water permeability through conventional and PEG-modified PEGDA hydrogels was measured using a dead-end ultrafiltration UF cell obtained from Fisher Scientific S.A.S. (Amicon Model 8050, 50 mL for 45 mm Filters), as shown in Figure 2.1. The filtration was performed at ambient temperature, with Milli-Q water as the feed solution. A maximum feed pressure of 1 bar was used. The membrane with the area 15.90 cm^2 was fixed in the membrane holder of the cell. We first checked that the flow rate at a given pressure ΔP was constant during hours for all the samples. Then, standard filtration experiments were performed by increasing the pressure from 100 mbar to 1 bar and waiting 10 minutes at each pressure, while weighing the liquid permeate as a function of time with a balance (Sartorius) to obtain a precise measurement of the flow rate Q .

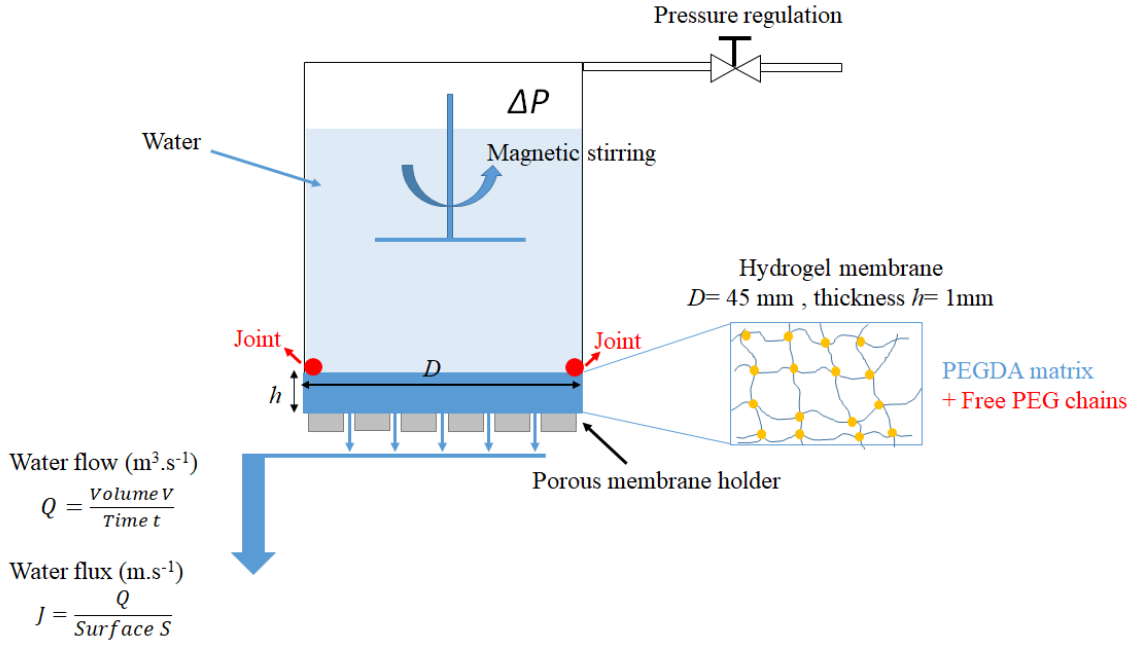


Figure 2.1. Representative schematic of the filtration experiments using an ultrafiltration stirred cell.

Permeate flow rate Q was recorded, and the water intrinsic permeability K was calculated by the following (Equation 2.4):

$$K = \frac{Q\mu h}{\Delta P S} \quad (2.4)$$

where Q is the water flow rate ($\text{m}^3 \cdot \text{s}^{-1}$) calculated from the slope of the variation of the accumulated permeate volume (m^3) as a function of time (s), μ is the water viscosity (Pa.s), h is the hydrogel thickness (m), S is the surface area of the hydrogel membrane (m^2) and ΔP is the pressure difference across the membrane (Pa). The water flux is calculated from the value of water flow rate according to (Equation 2.5):

$$J = \frac{Q}{S} \quad (2.5)$$

Permeate samples were analyzed using a total organic carbon (TOC-L series from Shimadzu) in order to determine if PEG-300 000 $\text{g} \cdot \text{mol}^{-1}$ chains were washed out of the gel during the filtration experiments.

2.5 RESULTS

2.5.1 Hydrogel membranes characterization

In order to follow the polymerization reaction of PEGDA oligomers, FTIR spectra were acquired for the as-received PEGDA oligomer, conventional PEGDA sample and PEG-modified PEGDA samples. The analyzed samples were obtained from hydrogels via drying in a vacuum oven at 80° C for 2-3 h. Figure 2.2 presents the FTIR spectra of dried PEGDA hydrogels membranes prepared with 16 wt % of PEGDA and various PEG-300 000 g.mol⁻¹ contents in prepolymerization mixture.

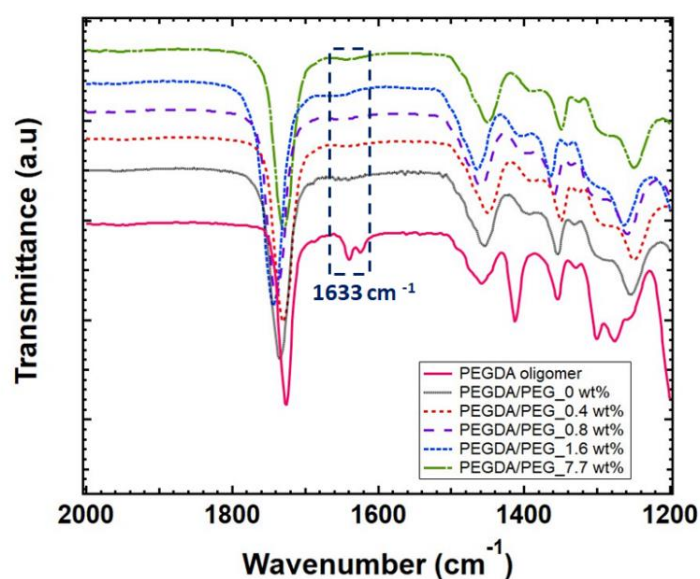


Figure 2.2. FTIR spectra of dried PEGDA hydrogels membranes prepared with 16 wt% of PEGDA and various PEG-300 000 g.mol⁻¹ contents in prepolymerization mixture compared to the spectrum of the as-received PEGDA oligomer.

In the PEGDA oligomer spectrum, we find the characteristic peaks that are attributed to the carbonyl groups C=O at 1724 cm⁻¹ and the C=C bonds at 1633 cm⁻¹. For the cross-linked PEGDA or mixture of PEGDA/PEG samples, we observe that the peaks of carbonyl groups remain the same, while the characteristic peak of the C=C bonds at 1633 cm⁻¹ from PEGDA has disappeared. This suggests that the hydrogel films were successfully synthesized after UV cross-linking. Our results confirm that the PEGDA polymerization reaction is complete even after the addition of free PEG-300 000 g.mol⁻¹ chains of different concentrations.

While the membrane of PEGDA/PEG_0 wt% is colorless and transparent, the addition of free PEG chains induces a strong turbidity of the samples as shown in Figure 2.3 a, b, c consistently

with a heterogeneous structure with spatial variations of the index of refraction that scatter light and which size ranges from several hundreds of nanometers to micron size.

To further characterize the hydrogels structure, AFM measurements were performed in water for a series of PEGDA hydrogel membranes prepared with various PEG-300 000 g.mol⁻¹ contents (Figure 2.3 d to i). For PEGDA/PEG_0 wt %, the hydrogel presents a surface with heterogeneities of the order of 100 to 200 nm in diameter which can be seen in Figure 2.3 d with a field of view of 20 μm and more precisely in Figure 2.3 g with a field of view of 5 μm. This is consistent with the work of Molina *et al.* who evidenced a structure with PEGDA rich zones coexisting with 200 nm voids filled with water³¹. The authors showed that the volume fraction of the water voids decreases when the PEGDA concentration increases.

For the PEGDA/PEG samples 0.8 wt% and 4 wt%, the AFM images with a field of view of 20 μm Figure 2.3 (e-f) show micron size heterogeneities consistently with the increase in turbidity observed upon addition of PEG in the PEGDA samples.

When imaging the 0.8 wt% PEG/PEGDA sample with a 5 μm field of view Figure 2.3 h we find that the micron sized zones contain voids of diameter of the order of 40 nm, which is smaller than the voids observed for pure PEGDA. Several 200 nm large voids can also be seen and seem to be located in the periphery of the micron size areas. From these results we suggest that a phase separation between PEGDA and PEG controls the heterogeneous structure of the samples. According to Molina *et al.*³¹ who showed that the volume fraction of the voids reflects the PEGDA content we suggest that the micron sized zones that contain 40 nm large voids are enriched in PEGDA with respect to the areas at their periphery.

As the PEG content increases to 4 wt%, the micron sized heterogeneities can still be seen on the 20 μm field of view image (Figure 2.3 f). However, the nanometric voids can no longer be seen on the 5 μm field of view image (Figure 2.3 i) neither in the micron sized zones nor at their periphery. The absence of voids in the micron sized zones may be due to an enrichment in PEGDA of the PEGDA rich zones. We note that the absence of nanometric water voids may also be due to a strong increase of the PEG concentration, filling the water voids either in the PEGDA rich areas or at their periphery.

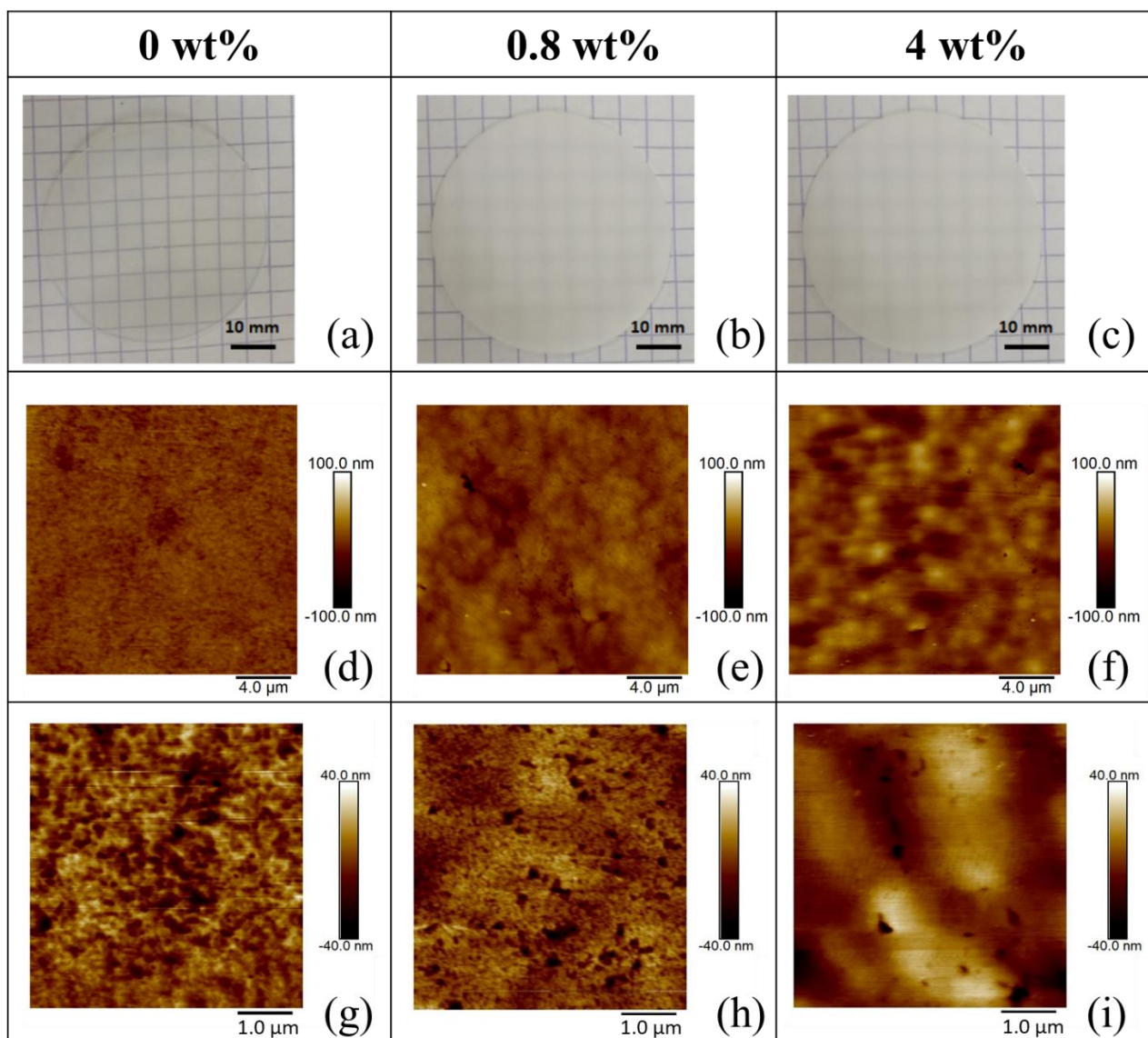


Figure 2.3. Photographs of PEGDA hydrogel membranes prepared with PEGDA and a) 0 wt%; b) 0.8wt% and c) 4wt% of PEG-300 000 g.mol^{-1} in the prepolymerization mixture.

Surface AFM images with 20 μm of field of view of PEGDA hydrogel membranes prepared with PEGDA and a) 0 wt%; b) 0.8 wt% and c) 4 wt% of PEG-300 000 g.mol^{-1} in the prepolymerization mixture.

Surface AFM images with 5 μm of field of view of PEGDA hydrogel membranes prepared with PEGDA and a) 0 wt%; b) 0.8 wt% and c) 4 wt% of PEG-300 000 g.mol^{-1} in the prepolymerization mixture.

2.5.2 Mechanical characterization

To further characterize the membranes samples, compression experiments were carried out for PEGDA/PEG hydrogel membranes prepared with various contents of PEG-300 000 $\text{g}\cdot\text{mol}^{-1}$.

Figure 2.4 a presents the variation of the stress as a function of the strain in the linear regime (0-4%) at a deformation rate of $0.01 \text{ mm}\cdot\text{s}^{-1}$, for deformations between 0 and 4% and stresses below 0.05 MPa, which are relevant to the filtration experiments where pressures below 1 Bar (i.e. 0.1 MPa) are applied.

For PEGDA membranes prepared without PEG (0 wt%), the effective Young's modulus value, calculated from the slope of the stress-strain curve at low strain (>1-4%), is 1 MPa, which is of the same order of magnitude as the values reported in the literature^{32, 33}. The addition of free PEG chains, from 0.4 wt% to 7.7 wt%, to the PEGDA matrix increases the compliance of the gel. The values of the effective Young's moduli calculated for low strains decrease from 0.75 MPa to 0.05 MPa when the PEG-300 000 $\text{g}\cdot\text{mol}^{-1}$ percentage increases from 0.4 to 7.7 wt%, as represented in Figure 2.4 b.

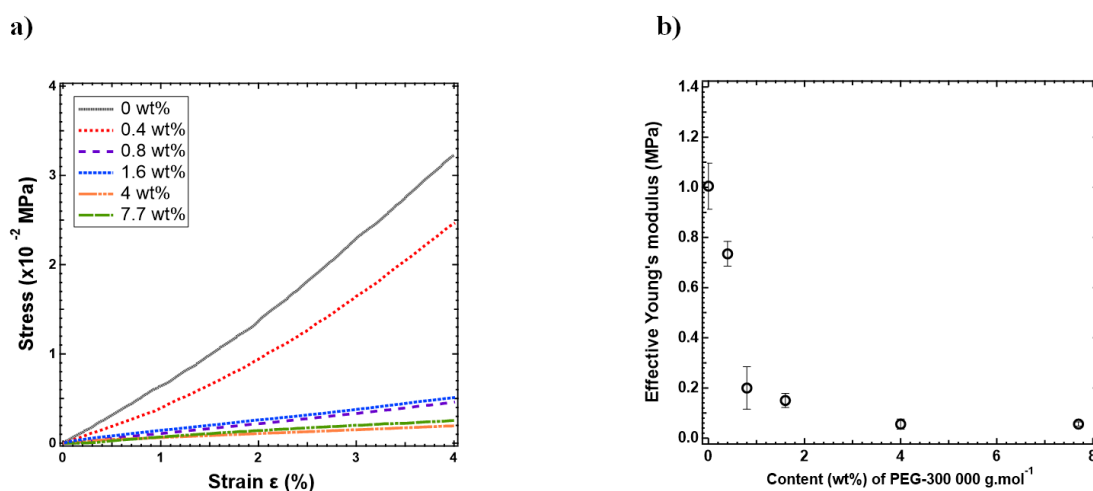


Figure 2.4. a) Stress versus strain for PEGDA hydrogel membranes prepared with 16 wt% of PEGDA and various PEG-300 000 $\text{g}\cdot\text{mol}^{-1}$ contents in the prepolymerization mixture. b) Variation of the effective Young's modulus as a function of PEG-300 000 $\text{g}\cdot\text{mol}^{-1}$ content.

During the compression experiments, water is expelled from the PEGDA/PEG samples (see video in S2.2) while almost no water is expelled in the case of pure PEGDA hydrogels. The fast transport of water expelled from the PEG/PEGDA hydrogels suggests the formation of large and interconnected pores which leads to a larger compressibility and thus lower effective Young's moduli in contrast with pure PEGDA samples.

2.5.3 Roles of pressure and PEG concentration on water intrinsic permeability

Filtration experiments were conducted to investigate water intrinsic permeability properties of PEGDA hydrogels membranes prepared with various contents of PEG-300 000 $\text{g}\cdot\text{mol}^{-1}$. Figure 2.5 shows the results of the water filtration experiments through a hydrogel membrane composed of 16 wt% of PEGDA which does not contain any free PEG chains. We first notice that the volume of water recovered at constant pressure increases linearly with time, during the filtration process (see Figure 2.5 a). From the slope of the line, we can deduce the value of the water flow rate which remains constant over time at a given pressure, and increases from $3.26 \times 10^{-12} \text{ m}^3 \cdot \text{s}^{-1}$ to $1.36 \times 10^{-10} \text{ m}^3 \cdot \text{s}^{-1}$ when the pressure increases from 2000 Pa to 80000 Pa.

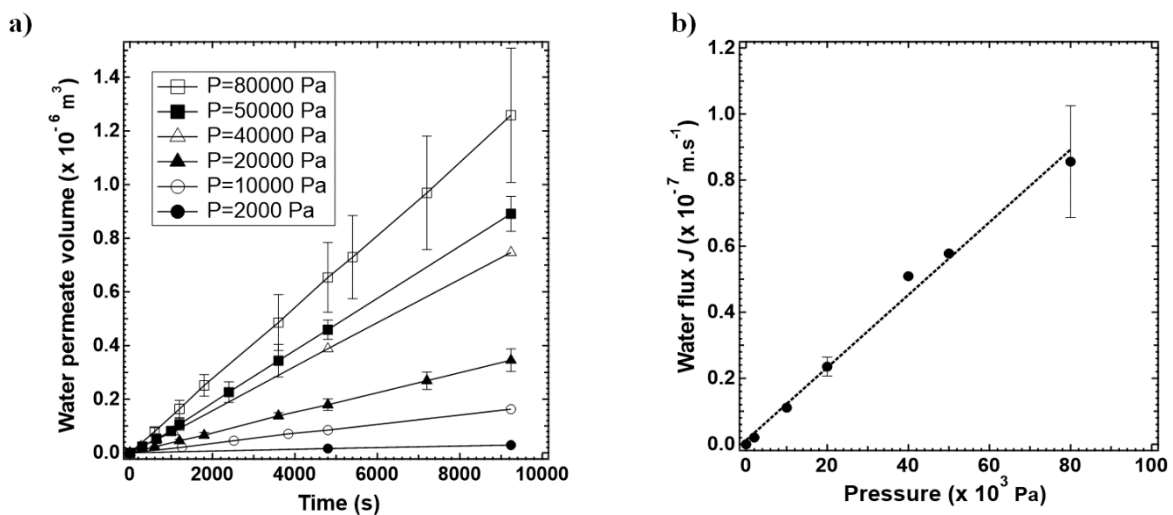


Figure 2.5. a) Water permeate volume variation of PEGDA hydrogel membranes prepared with 16 wt% of PEGDA as a function of time for different pressures. (●) 2000 Pa; (○) 10000 Pa; (▲) 20000 Pa; (△) 40000 Pa ;(■) 50000 Pa and (□) 80000 Pa. b) Water flux variation of a PEGDA hydrogel membrane prepared with 16 wt% of PEGDA as a function of pressure.

We plot the water flux J as a function of pressure in Figure 2.5 b. We obtain a linear variation between J and the pressure. The slope of this line enables us to deduce the water intrinsic permeability K using (Equation 2.4). We find that $K \sim 10^{-18} \text{ m}^2$ which is of the same order of magnitude as the values found by Ju and co-workers for a membrane of PEGDA-700 $\text{g}\cdot\text{mol}^{-1}$ 22.

In the presence of free PEG chains with a molar mass of 300 000 $\text{g}\cdot\text{mol}^{-1}$ at 1.6 wt%, we first notice that the volume of water recovered at constant pressure increases linearly with time, during the filtration process (see Figure 2.6 a) as in the previous case of PEGDA hydrogels.

Thus, we obtain a constant value of the water flux, J , at a constant pressure. As shown in Figure 2.6 b the water flux for these PEG/PEGDA hydrogels is two orders of magnitude higher than the one obtained for a PEGDA membrane. Interestingly, in contrast to the PEGDA hydrogel, we observe a non-linear variation of the water flux as a function of the applied pressure, as shown in Figure 2.6 b, and the water flux reaches a plateau at pressures above ~ 400 mbar. We calculate the intrinsic permeability value for each pressure by using (Equation 2.4). As shown in Figure 2.6 c, the value of the water intrinsic permeability K decreases by a factor five when increasing the applied pressure by a factor ~ 40 . We will discuss this effect later.

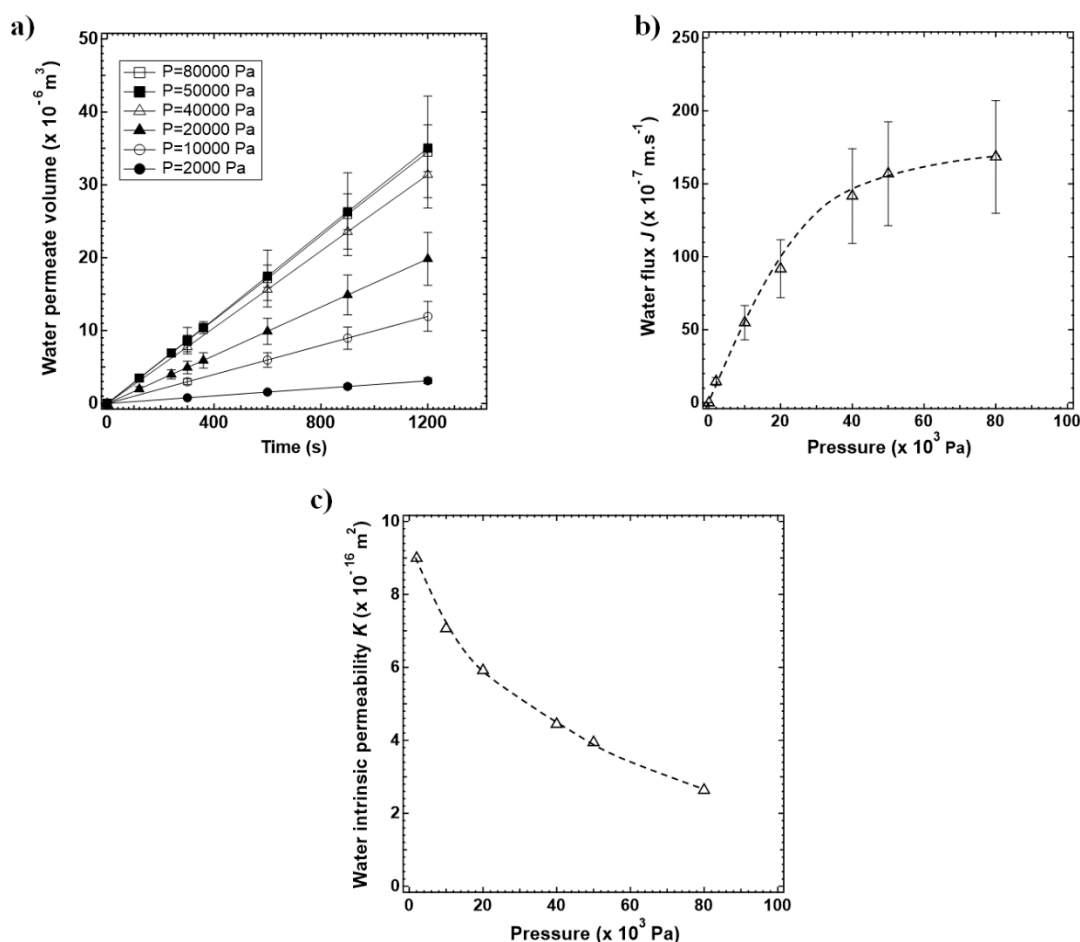


Figure 2.6. a) Water permeate volume variation of PEGDA hydrogel membranes prepared with 16 wt% of PEGDA and 1.6 % of PEG-300 000 g.mol⁻¹ as a function of time for different pressures. b) Water flux and c) Water permeability versus pressure for PEGDA hydrogel membranes prepared with 16 wt% of PEGDA and 1.6 wt% of PEG-300 000 g.mol⁻¹ contents in the prepolymerization mixture.

The dashed lines are represented as guides for the eyes.

We tested the robustness and reproducibility of the results by performing up to ten filtration cycles between 0 and 1 bar rising and decreasing the pressure. Within each cycle, the water flux-pressure dependence was similar within a 25% deviation, as shown in (Figure 2.7 a).

By analyzing the PEG content of the permeate after one filtration cycle by total organic carbon (TOC) analysis, we detect a small portion of PEG in the permeate. From the obtained concentration equal to 63 mg.L^{-1} in the permeate, we may estimate the fraction of the PEG that was washed out from the hydrogels, knowing the total quantity of PEG in the hydrogel disks. The fraction therefore reads in (Equation 2.6):

$$f = \frac{C_{\text{permeate}} * V_{\text{permeate}}}{\Phi_{\text{PEG}} * \rho_{\text{hydrogel}} * V_{\text{hydrogel}}} \quad (2.6)$$

with C_{permeate} (mg.L^{-1}) the concentration in the permeate measured by TOC, V_{permeate} (L) the volume of permeate, Φ_{PEG} (wt%) the weight fraction of PEG in the hydrogel, ρ_{hydrogel} the volumic mass of the hydrogel taken equal to $\rho_{\text{water}} = 10^6 \text{ mg.L}^{-1}$ and V_{hydrogel} the volume of the hydrogel membrane (L).

The fraction f is about 3% for the first filtration cycle which shows that most of the PEG remains in the hydrogel. For the nine following filtration cycles, the amount of free PEG chains rinsed out of the hydrogel becomes lower than 0.3 % as represented in Figure 2.7 b.

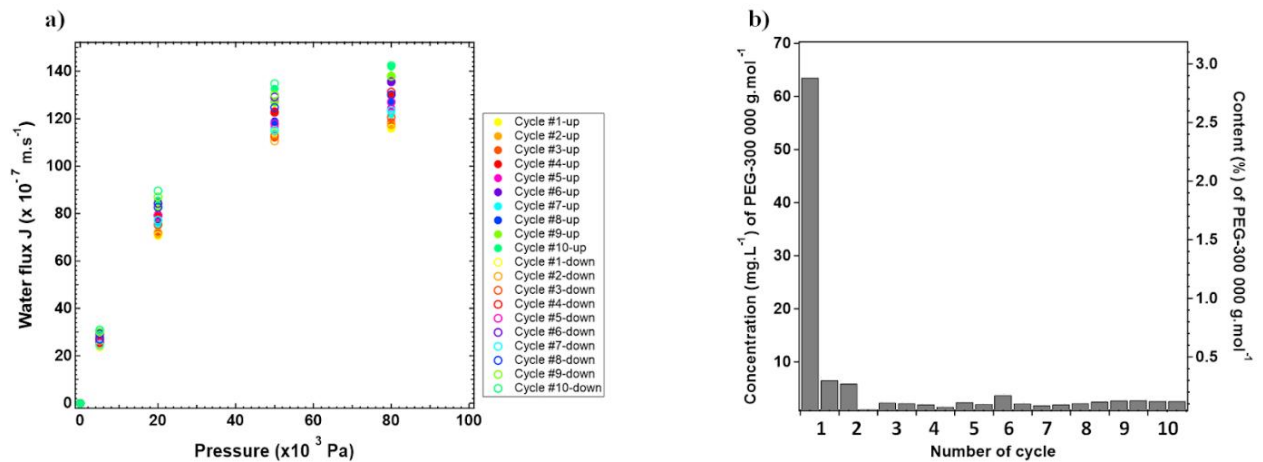


Figure 2.7. a) Variation of the water flux for PEGDA hydrogel membrane prepared with 16 wt% of PEGDA and 1.6 wt% of PEG-300 000 g.mol^{-1} as a function of the applied pressure during ten filtration cycles. b) Effect of the number of filtration cycles on the concentration and the content of PEG-300 000 g.mol^{-1} measured in the permeate volume. The right axis represents the ratio of PEG leaving the hydrogel membrane to the total quantity contained in the membrane.

These results show that the high molar mass PEG chains are not rinsed out of the hydrogel during filtration, in contrast to what the data from the literature suggest for short PEG chains that act as templates during the polymerization reaction and get rinsed away afterwards³⁴⁻³⁶. We may attribute this difference to entanglements between the PEG chains and the PEGDA matrix, that resist to the chain withdrawal.

Figure 2.8 a shows the comparison of the measured water fluxes for PEGDA/PEG hydrogel membranes as a function of pressure at different contents of PEG-300 000 g.mol⁻¹. When the PEG percentage increases, the values of J exhibit a maximum for a PEG weight fraction of 1.6 wt%. Moreover, for all PEG concentrations, we find a non-linear relation between the water flux and the applied pressure as the water flux reaches a plateau at the highest pressures. In Figure 2.8 b, we plot the water permeability calculated at $P=100$ mbar according to (Equation 2.4). We observe that K varies over two orders of magnitude with the PEG concentration and presents a maximum for a PEG concentration of 1.6 wt%. The possible origins of this behavior will be discussed in the next Section.

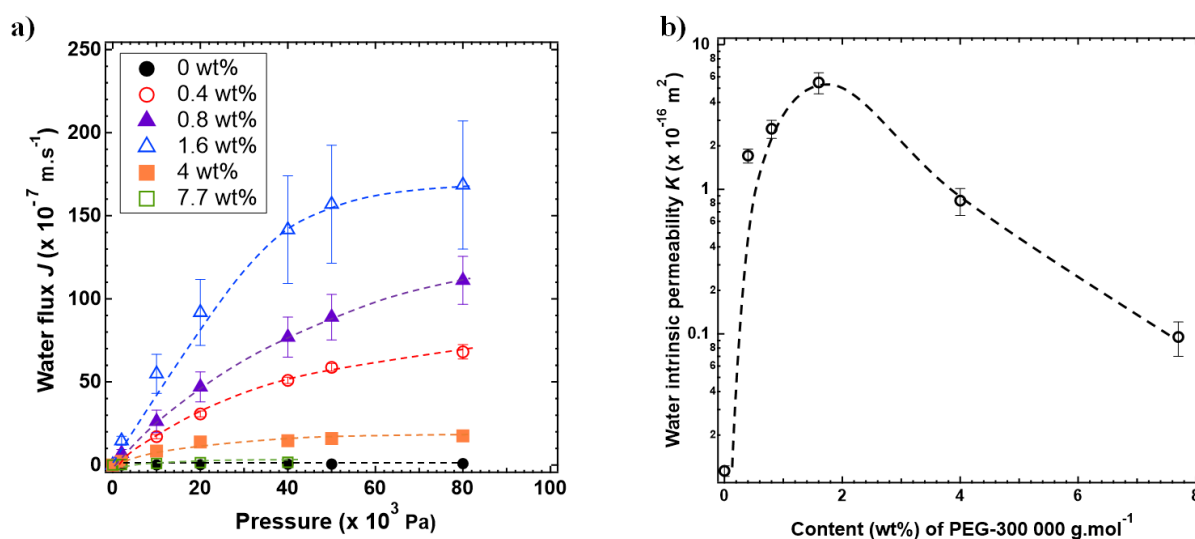


Figure 2.8. a) Water flux versus pressure for PEGDA hydrogel membranes prepared with 16 wt% of PEGDA and various PEG-300 000 g.mol⁻¹ contents in the prepolymerization mixture. (●) 0 wt%; (○) 0.4 wt%; (▲) 0.8 wt%; (△) 1.6 wt%; (■) 4 wt% and (□) 7.7 wt%. b) Water intrinsic permeability at $P=10000 \text{ Pa}$ versus content of PEG-300 000 g.mol⁻¹ in the prepolymerization mixture of hydrogel membranes prepared with 16 wt% of PEGDA. The dashed lines are guides for the eyes.

In summary of the permeability measurements, we have shown that addition of free PEG chains to the PEGDA hydrogel network strongly modifies its permeation properties to water. The pressure dependence of the water flux J for PEGDA/PEG hydrogels is non-linear, showing a saturation-like behavior at high pressures. The low-pressure permeability strongly varies with PEG concentration and presents a maximum at about 1.6 wt% of free PEG concentration.

2.6 DISCUSSION

2.6.1 Permeability variation with the PEG concentration

As for any porous material, the intrinsic permeability K of a membrane should depend on the pore size d_p , the tortuosity τ and the fraction of open pores³⁷. Moreover in the case of a hydrogel, the permeability and kinetics of water transport is known to decrease with the polymer concentration³⁸. The permeability of our PEDGA/PEG hydrogels is therefore related to the structure of the hydrogels, which we discuss below.

For the pure PEGDA hydrogels, the AFM images show 200 nm voids which, according to Molina *et al.*³¹, are water cavities dispersed in a polymerized PEGDA matrix. Interestingly, the permeability of the pure PEGDA hydrogels is the lowest of the systems studied here, of the order of 10^{-18} m². Assuming that $K \sim d_p^2$ with d_p the pore size of the membrane we deduce pore sizes of the order of 1 nm which is two orders of magnitude below the 200 nm diameter of the voids observed with the AFM. This 1 nm value seems to correspond to the length of the PEG spacers between the diacrylate groups measured by Molina *et al.*³¹, which are composed of 13 ethylene glycol monomer units. We therefore suggest that for the pure PEGDA samples the 200 nm water voids are mostly closed cavities that do not contribute to the permeability and that in these samples the water permeates through the PEGDA spacers.

When PEG is added to the PEGDA prepolymerization solution, the permeability of the PEG/PEGDA hydrogels increases by two orders of magnitude and reaches a maximum at a PEG concentration of 1.6 wt% which corresponds to the critical overlap concentration C^* of PEG 300 000 g.mol⁻¹ chains, as measured by a rheological measurement of the PEG solutions and PEG/PEGDA prepolymerization solutions (Figure S2.2). Note that the same value of C^* has been obtained by the following (Equation 2.7)³⁹:

$$C^* = \frac{\overline{Mw}}{\frac{4}{3}\pi r_g^3 N_A} \quad (2.7)$$

where \overline{Mw} is the average molar mass of the polymer, r_g is the gyration radius (of the order of 20 nm for PEG-300 000 g.mol⁻¹) of polymer coils and N_A is Avogadro number: $N_A = 6.023 \times 10^{23}$ mol⁻¹.

At concentrations below C^* , the AFM measurements performed on the PEGDA/PEG samples showed micron sized zones containing 40 nm large water voids which are smaller than the 200 nm voids observed in PEGDA/water samples. At C^* , the permeability reaches 10^{-16} m², from which we get a rough estimation of the pore size, $d_p \sim K^{1/2} \sim 20$ nm neglecting parameters as tortuosity and pore volume fraction. Interestingly this value is the same order of magnitude as the pore sizes obtained by AFM. We therefore suggest that the 40 nm pores present some level of connectivity and contribute to the permeation of water.

Based on Molina's article which showed that increasing the PEGDA content in PEGDA/water systems leads to a decrease of the void volume fraction, we hypothesize that PEGDA rich micron-sized zones coexist with zones that have a lower PEGDA concentration and may consequently be enriched in PEG. The PEGDA poor phases, which are more permeable than the PEGDA-rich zones, would then lead to an increase of the permeability of the hydrogel membranes.

Above C^* , the permeability drops with the PEG concentration. We suggest that the addition of PEG above C^* leads to an increase of the PEG concentration in the PEGDA-poor areas above the entanglement concentration, which may retard the water transportation due to the polymer-solvent friction, similarly to the work reported by Fujiki *et al.*⁴⁰ who evidenced that the friction coefficient f -corresponding to $\frac{\mu}{K}$ in our study- is governed by the polymer concentration.

2.6.2 Non-linear variation of the flow rate-pressure curve

We reported in Figure 2.6 and Figure 2.8 a non-linear variation of the water flow rate with the applied pressure as the flow rate reaches a plateau at large pressures. We emphasize that the water flow rates measured for all samples at all pressures are constant over time for several hours (examples of time evolution of the water volume are shown Figure 2.6 a). Hence this levelling of the water flow rate with pressure is not due to any transient clogging phenomenon nor to the transfer of free PEG chains through the matrix which are shown to remain in the matrix in Figure 2.7.

To account for the non-linear variation of the flow rate with the applied pressure, we suggest that the membrane compression under the action of a high pressure may lead to the expulsion

of water and compression of the pores resulting in a decrease in the gel permeability. The solvent release from hydrogels under compression is a well-known phenomenon and has been studied in detail by Vervoort *et al.*⁴¹. They demonstrated that under uniaxial compression test, gel deformation, volume loss and solvent expulsion can be observed. This simple experiment shows that the PEGDA/PEG hydrogel structure presents some compressibility.

Assuming that the hydrogel compression is responsible for the permeability loss of the hydrogel with increasing pressure, we expect that the permeability loss should increase with the PEG concentration. The relative variation of permeability is given by (Equation 2.8):

$$\frac{\Delta K}{K_{max}} = \frac{(K_{max}-K)}{K_{max}} \quad (2.8)$$

where K_{max} is the maximum intrinsic permeability obtained at low applied pressure (i.e. P=2000 Pa). In Figure 2.9, we plot the relative variation of permeability as a function of the pressure for several PEG concentrations. The relative variation of the permeability with pressure increases with the PEG concentration, which correlates well with the fact that the hydrogel tends to be more easily deformed when the PEG content increases in the PEGDA hydrogel.

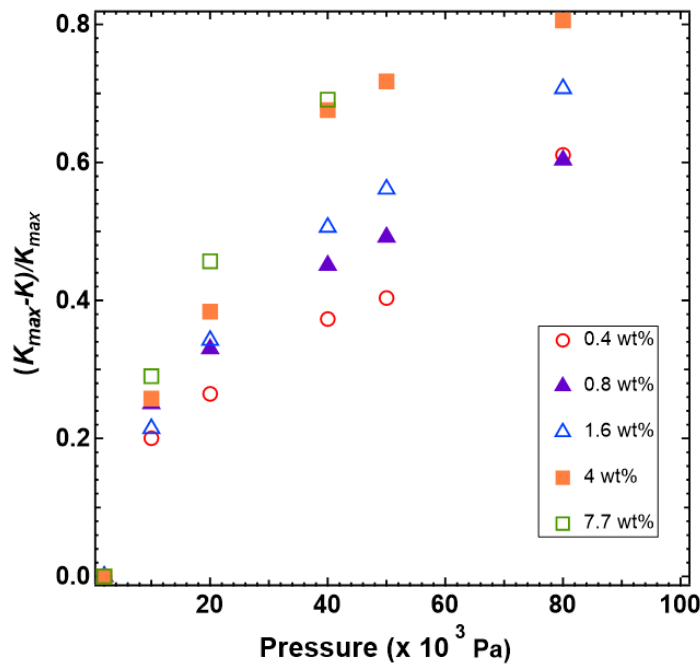


Figure 2.9. Water permeability variation versus pressure for PEGDA hydrogel membranes prepared with 16 wt% of PEGDA and various PEG-300 000 g.mol⁻¹ contents in the prepolymerization mixture: (○) 0.4 wt%; (▲) 0.8 wt%; (△) 1.6 wt%; (■) 4 wt% and (◻) 7.7 wt%.

Assuming that the permeability loss is due to the hydrogel compression under the action of the applied pressure difference across the membrane during filtration, we can estimate the variation of the pore size corresponding to the permeability variation. Taking $K \sim d_p^2$ with d_p the pore size of the membrane, according to the Hagen-Poiseuille law, the relative compression of the pores should scale as (Equation 2.9):

$$\frac{\Delta d_p}{d_p} \sim \frac{1}{2} \frac{\Delta K}{K_{max}} \quad (2.9)$$

From the permeability variations reported in Figure 2.9 we can estimate the range of pore-size variation to be $\frac{\Delta d_p}{d_p} \sim 0.1 - 0.4$ depending on the applied pressure and PEG content in the hydrogel.

The pore compression can also be estimated from the effective Young's modulus E and the pressure as given in (Equation 2.10):

$$\frac{\Delta d_p}{d_p} \sim (1 - 2\nu) \frac{P}{E} \quad (2.10)$$

with ν the effective Poisson's ratio (see details in supporting information : Model of pore compression). We take $\nu = 0.2$ according to Cappello *et al.* who measured the Poisson's ratio of PEGDA/ PEG-1000 g.mol⁻¹ hydrogels⁴².

For a pressure of the order of 10⁴ Pa and taking $E \sim 0.1$ to 1 MPa, we find a pore variation of $\frac{\Delta d_p}{d_p} \sim 0.02$ to 0.2 which is, given the rough scaling approach used here, in reasonable agreement with the values of $\frac{\Delta d_p}{d_p}$ estimated above from the permeability variations. This simple argument tells us that the non-linear variation of the permeability with the pressure seems to be mostly due to the compression of the hydrogels and the reduction of the pore size, an effect which increases with the PEG content as these hydrogels have a lower effective modulus than PEGDA hydrogels without PEG.

2.7 CONCLUSION

We synthesized a PEGDA/PEG composite hydrogel membrane by introducing free PEG-300 000 g.mol⁻¹ chains to a PEGDA matrix. FTIR measurement showed that the PEGDA polymerization reaction still occurs even after adding free PEG-300 000 g.mol⁻¹ chains of different concentrations. The water flux recovery rate after the cyclic filtration experiments shows that the PEG chains are not flushed out of the gel and thus do not behave as a porogen agent.

Water permeability studies confirmed the validity of Darcy's law for the conventional PEGDA membranes, whereas this law is no longer valid for the PEGDA/PEG composite hydrogels. We assumed in this case that the pressure-induced compression of the hydrogel induces the closure of some pores at high pressure during filtration experiments. Furthermore, increasing the content of PEG chains in the hydrogel system, allows tuning the water permeability over 2 orders of magnitude. The maximum of water permeability is obtained with a hydrogel composite composed of 1.6 wt% of PEG corresponding to the critical overlap concentration C^* of PEG-300 000 g.mol⁻¹. Combining these results, as well as turbidity observations and AFM measurements, we hypothesize that the hydrogel structure is controlled by a phase separation between PEGDA rich and PEGDA poor zones, the latter being more permeable to water than the PEGDA rich areas. Below C^* , we suggest that the increase of the permeability is obtained because of an increase of the fraction of connected pores in which the water can be transported. Above C^* , we suggest that the increase of the PEG concentration in the PEGDA-poor pores may delay the transport of water in the hydrogels leading to a decrease of the permeability.

Acknowledgements

We thank A. Marcellan, J. Comtet, G. Ducouret, L. Jorgensen, L. Bocquet and E. Barthel for many fruitful discussions. We thank M. Hanafi for the SEC measurements. We gratefully acknowledge Institut Carnot for microfluidics for the financial support during this research project, as well as the Agence Nationale de la Recherche (grants ANR-21-ERCC-0010-01 *EMetBrown*, ANR-21-CE06-0029 *Softer*, ANR-21-CE06-0039 *Fricolas*). We also thank the Soft Matter Collaborative Research Unit, Frontier Research Center for Advanced Material and Life Science, Faculty of Advanced Life Science at Hokkaido University, Sapporo, Japan.

References

1. Petersen, R. J., Composite reverse osmosis and nanofiltration membranes. *J. Membr. Sci.* **1993**, 83 (1), 81-150, DOI 10.1016/0376-7388(93)80014-O.
2. Freeman, B.; Pinnau, I., Gas and Liquid Separations Using Membranes: An Overview. *ACS Symp. Ser.* **2004**, 876, 1-23, DOI 10.1021/bk-2004-0876.ch001.
3. Tul Muntha, S.; Kausar, A.; Siddiq, M., Advances in Polymeric Nanofiltration Membrane: A Review. *Polym Plast. Technol. Eng.* **2017**, 56 (8), 841-856, DOI 10.1080/03602559.2016.1233562.
4. Kayvani Fard, A.; McKay, G.; Buekenhoudt, A.; Al Sulaiti, H.; Motmans, F.; Khraisheh, M.; Atieh, M., Inorganic Membranes: Preparation and Application for Water Treatment and Desalination. *Materials* **2018**, 11 (1), DOI 10.3390/ma11010074.
5. Tokarev, I.; Minko, S., Stimuli-responsive porous hydrogels at interfaces for molecular filtration, separation, controlled release, and gating in capsules and membranes. *Adv. Mater.* **2010**, 22 (31), 3446-3462, DOI 10.1002/adma.201000165.
6. Latreille, P.-L.; Adibnia, V.; Nour, A.; Rabanel, J.-M.; Lalloz, A.; Arlt, J.; Poon, W. C. K.; Hildgen, P.; Martinez, V. A.; Banquy, X., Spontaneous shrinking of soft nanoparticles boosts their diffusion in confined media. *Nat. Commun.* **2019**, 10 (1), 4294, DOI 10.1038/s41467-019-12246-x.
7. Yu, M.; Xu, L.; Tian, F.; Su, Q.; Zheng, N.; Yang, Y.; Wang, J.; Wang, A.; Zhu, C.; Guo, S.; Zhang, X.; Gan, Y.; Shi, X.; Gao, H., Rapid transport of deformation-tuned nanoparticles across biological hydrogels and cellular barriers. *Nat. Commun.* **2018**, 9 (1), 2607, DOI 10.1038/s41467-018-05061-3.
8. Refojo, M.; Yasuda, H., Hydrogels from 2-hydroxyethyl methacrylate and propylene glycol monoacrylate. *J. Appl. Polym. Sci.* **1965**, 9 (7), 2425-2435, DOI 10.1002/app.1965.070090707.
9. Yasuda, H.; Gochin, M.; Stone Jr, W., Hydrogels of poly (hydroxyethyl methacrylate) and hydroxyethyl methacrylate—glycerol monomethacrylate copolymers. *J. Polym. Sci. A-1 Polym. Chem.* **1966**, 4 (12), 2913-2927, DOI 10.1002/pol.1966.150041201.
10. Yasuda, H.; Lamaze, C.; Ikenberry, L., Permeability of solutes through hydrated polymer membranes. Part I. Diffusion of sodium chloride. *Makromol. Chem.* **1968**, 118 (1), 19-35, DOI 10.1002/macp.1968.021180102.

11. Vashist, A.; Sharif, A., Hydrogels: smart materials for drug delivery. *Orient. J. Chem.* **2013**, *29* (3), 861-870, DOI 10.13005/ojc/290303.
12. Fernández-Rico, C.; Sai, T.; Sicher, A.; Style, R. W.; Dufresne, E. R., Putting the Squeeze on Phase Separation. *JACS Au.* **2022**, *2* (1), 66-73, DOI 10.1021/jacsau.1c00443.
13. Mohammadzadeh Pakdel, P.; Peighambaroust, S. J., Review on recent progress in chitosan-based hydrogels for wastewater treatment application. *Carbohydr. Polym.* **2018**, *201*, 264-279, DOI 10.1016/j.carbpol.2018.08.070.
14. Zhao, K.; Zhang, X.; Wei, J.; Li, J.; Zhou, X.; Liu, D.; Liu, Z.; Li, J., Calcium alginate hydrogel filtration membrane with excellent anti-fouling property and controlled separation performance. *J. Membr. Sci.* **2015**, *492*, 536-546, DOI 10.1016/j.memsci.2015.05.075.
15. Zhao, Y.-F.; Zhu, L.-P.; Yi, Z.; Zhu, B.-K.; Xu, Y.-Y., Zwitterionic hydrogel thin films as antifouling surface layers of polyethersulfone ultrafiltration membranes anchored via reactive copolymer additive. *J. Membr. Sci.* **2014**, *470*, 148-158, DOI 10.1016/j.memsci.2014.07.023.
16. Lu, R.; Zhang, C.; Piatkovsky, M.; Ulbricht, M.; Herzberg, M.; Nguyen, T. H., Improvement of virus removal using ultrafiltration membranes modified with grafted zwitterionic polymer hydrogels. *Water Res.* **2017**, *116*, 86-94, DOI 10.1016/j.watres.2017.03.023.
17. Gao, S.; Zhu, Y.; Wang, J.; Zhang, F.; Li, J.; Jin, J., Layer-by-Layer Construction of Cu²⁺/Alginate Multilayer Modified Ultrafiltration Membrane with Bioinspired Superwetting Property for High-Efficient Crude-Oil-in-Water Emulsion Separation. *Adv. Funct. Mater.* **2018**, *28* (49), 1801944, DOI 10.1002/adfm.201801944.
18. La, Y.-H.; McCloskey, B. D.; Sooriyakumaran, R.; Vora, A.; Freeman, B.; Nassar, M.; Hedrick, J.; Nelson, A.; Allen, R., Bifunctional hydrogel coatings for water purification membranes: improved fouling resistance and antimicrobial activity. *J. Membr. Sci.* **2011**, *372* (1-2), 285-291, DOI 10.1016/j.memsci.2011.02.005.
19. Peeva, P.; Million, N.; Ulbricht, M., Factors affecting the sieving behavior of anti-fouling thin-layer cross-linked hydrogel polyethersulfone composite ultrafiltration membranes. *J. Membr. Sci.* **2012**, *390-391*, 99-112, DOI 10.1016/j.memsci.2011.11.025.
20. Fu, W.; Pei, T.; Mao, Y.; Li, G.; Zhao, Y.; Chen, L., Highly hydrophilic poly(vinylidene fluoride) ultrafiltration membranes modified by poly(N-acryloyl glycinamide) hydrogel based on multi-hydrogen bond self-assembly for reducing protein fouling. *J. Membr. Sci.* **2019**, *572*, 453-463, DOI 10.1016/j.memsci.2018.11.022.

21. Sadeghi, I.; Yi, H.; Asatekin, A., A Method for Manufacturing Membranes with Ultrathin Hydrogel Selective Layers for Protein Purification: Interfacially Initiated Free Radical Polymerization (IIFRP). *Chem. Mater.* **2018**, *30* (4), 1265-1276, DOI 10.1021/acs.chemmater.7b04598.
22. Ju, H.; McCloskey, B. D.; Sagle, A. C.; Kusuma, V. A.; Freeman, B. D., Preparation and characterization of crosslinked poly(ethylene glycol) diacrylate hydrogels as fouling-resistant membrane coating materials. *J. Membr. Sci.* **2009**, *330* (1), 180-188, DOI 10.1016/j.memsci.2008.12.054.
23. Wu, Y.-H.; Park, H. B.; Kai, T.; Freeman, B.; Kalika, D., Water uptake, transport and structure characterization in poly(ethylene glycol) diacrylate hydrogels. *J. Membr. Sci.* **2010**, *347*, 197-208, DOI 10.1016/j.memsci.2009.10.025.
24. Nemir, S.; Hayenga, H. N.; West, J. L., PEGDA hydrogels with patterned elasticity: Novel tools for the study of cell response to substrate rigidity. *Biotechnol. Bioeng.* **2010**, *105* (3), 636-644, DOI 10.1002/bit.22574.
25. Lee, A. G.; Arena, C. P.; Beebe, D. J.; Palecek, S. P., Development of macroporous poly(ethylene glycol) hydrogel arrays within microfluidic channels. *Biomacromolecules* **2010**, *11* (12), 3316-3324, DOI 10.1021/bm100792y.
26. Bacchin, P.; Leng, J.; Salmon, J. B., Microfluidic Evaporation, Pervaporation, and Osmosis: From Passive Pumping to Solute Concentration. *Chem. Rev.* **2021**, *122* (7), 6938-6985, DOI 10.1021/acs.chemrev.1c00459.
27. Decock, J.; Schlenk, M.; Salmon, J. B., In situ photo-patterning of pressure-resistant hydrogel membranes with controlled permeabilities in PEGDA microfluidic channels. *Lab on a chip* **2018**, *18* (7), 1075-1083, DOI 10.1039/c7lc01342f.
28. Junius, N.; Jaho, S.; Sallaz-Damaz, Y.; Borel, F.; Salmon, J.-B.; Budayova-Spano, M., A microfluidic device for both on-chip dialysis protein crystallization and in situ X-ray diffraction. *Lab on a chip* **2020**, *20* (2), 296-310, DOI 10.1039/C9LC00651F.
29. Chiu, Y. C.; Larson, J. C.; Isom, A., Jr.; Brey, E. M., Generation of porous poly(ethylene glycol) hydrogels by salt leaching. *Tissue Eng. Part C: Methods* **2010**, *16* (5), 905-912, DOI 10.1089/ten.TEC.2009.0646.
30. Turani-i-Belloto, A.; Brunet, T.; Khaldi, A.; Leng, J., A Sacrificial Route for Soft Porous Polymers Synthesized via Frontal Photo-Polymerization. *Polymers* **2020**, *12* (5), 1008, DOI 10.3390/polym12051008.

31. Malo de Molina, P.; Lad, S.; Helgeson, M. E., Heterogeneity and its Influence on the Properties of Difunctional Poly(ethylene glycol) Hydrogels: Structure and Mechanics. *Macromolecules* **2015**, *48* (15), 5402-5411, DOI 10.1021/acs.macromol.5b01115.
32. Lin, H.; Van Wagner, E.; Swinnea, J. S.; Freeman, B. D.; Pas, S. J.; Hill, A. J.; Kalakkunnath, S.; Kalika, D. S., Transport and structural characteristics of crosslinked poly(ethylene oxide) rubbers. *J. Membr. Sci.* **2006**, *276* (1-2), 145-161, DOI 10.1016/j.memsci.2005.09.040.
33. Duprat, C.; Berthet, H.; Wexler, J. S.; Du Roure, O.; Lindner, A., Microfluidic in situ mechanical testing of photopolymerized gels. *Lab on a chip* **2015**, *15* (1), 244-252, DOI 10.1039/C4LC01034E.
34. Choi, N. W.; Kim, J.; Chapin, S. C.; Duong, T.; Donohue, E.; Pandey, P.; Broom, W.; Hill, W. A.; Doyle, P. S., Multiplexed Detection of mRNA Using Porosity-Tuned Hydrogel Microparticles. *Anal. Chem.* **2012**, *84* (21), 9370-9378, DOI 10.1021/ac302128u.
35. Courtois, J.; Byström, E.; Irgum, K., Novel monolithic materials using poly(ethylene glycol) as porogen for protein separation. *Polymer* **2006**, *47* (8), 2603-2611, DOI 10.1016/j.polymer.2006.01.096.
36. Caykara, T.; Bulut, M.; Dilsiz, N.; Ksel, A., Macroporous Poly(Acrylamide) Hydrogels: Swelling and Shrinking Behaviors. *J. Macromol. Sci. A* **2006**, *43*, 889-897, DOI 10.1080/10601320600653699.
37. Li, W.; Xing, W.; Xu, N., Modeling of relationship between water permeability and microstructure parameters of ceramic membranes. *Desalination* **2006**, *192* (1-3), 340-345, DOI 10.1016/j.desal.2005.07.042.
38. Tokita, M.; Tanaka, T., Reversible decrease of gel-solvent friction. *Science* **1991**, *253* (5024), 1121-1123, DOI 10.1126/science.253.5024.1121.
39. Rubinstein, M.; Colby, R. H., *Polymer physics*. Oxford university press New York: 2003; Vol. 23.
40. Fujiki, M.; Ito, M.; Mortensen, K.; Yashima, S.; Tokita, M.; Annaka, M., Friction coefficient of well-defined hydrogel networks. *Macromolecules* **2016**, *49* (2), 634-642, DOI 10.1021/acs.macromol.5b01997.
41. Vervoort, S.; Patlazhan, S.; Weyts, J.; Budtova, T., Solvent release from highly swollen gels under compression. *Polymer* **2005**, *46* (1), 121-127, DOI 10.1016/j.polymer.2004.10.046.
42. Cappello, J.; d'Herbement, V.; Lindner, A.; Du Roure, O., Microfluidic In-Situ Measurement of Poisson's Ratio of Hydrogels. *Micromachines* **2020**, *11* (3), 318, DOI 10.3390/mi11030318.

Chapter 3

Sieving and clogging in PEG-PEGDA hydrogel membranes

3.1 ABSTRACT

Hydrogels are promising systems for separation applications due to their structural characteristics (i.e. hydrophilicity and porosity). In our study, we investigate the filtration of rigid latex particles of different sizes through free-standing hydrogel membranes prepared by photopolymerization of a mixture of poly (ethylene glycol) diacrylate (PEGDA) and large poly (ethylene glycol) (PEG) chains of $300\,000\text{ g}\cdot\text{mol}^{-1}$ in the presence of a photoinitiator. Atomic force microscopy (AFM) and cryoscanning electron microscopy (cryoSEM) were employed to characterize the structure of the hydrogel membrane. We find that the 20 nm particle permeation depends on both the PEGDA/PEG composition and the pressure applied during filtration. However, particles of 100 nm and $1\ \mu\text{m}$ do not permeate any of the PEG containing samples, despite the presence of large cavities of $1\ \mu\text{m}$ evidenced by cryoSEM images. We suggest that the PEG chains induce local nanoscale defects in the cross-linking of PEGDA-rich walls separating the micron size cavities, that control the permeation of particles and water. Moreover, we discuss the decline of the permeation flux observed in the presence of latex particles, compared to that of pure water. We suggest an irreversible clogging of the nanometric structure by the nanoparticle of 20 and 100 nm, and the formation of layer of constant thickness with the $1\ \mu\text{m}$ particles.

3.2 KEYWORDS

Hydrogel, poly (ethylene glycol) diacrylate, poly (ethylene glycol), latex particles, AFM, cryoSEM, clogging, filtration, porous flows.

3.3 INTRODUCTION

Hydrogels are networks of polymer chains swollen in water in which molecular species and nanoparticles can diffuse under an imposed concentration gradient or can be transported through a hydrodynamic flux obtained by applying a pressure gradient¹. Inversely, the molecular network structure of hydrogels provides them with promising filtration properties². The diffusive transport of species in hydrogels has been the object of numerous experimental and theoretical studies in the past, often motivated by drug release applications³. Several theories have been developed such as the obstruction, hydrodynamic or free volume theories with various assumptions. While the obstruction theory based on the Ogston model assumes that the hydrogel is a rigid network with a fixed mesh size⁴, other theories take into account hydrodynamic interactions between the network and the solvent or the thermal fluctuations of the network^{5,6}. Several experimental studies provided measurements of diffusion coefficients of molecules in hydrogels and compared them with the available theories⁷. Overall, the size of the solute, its charge and its interactions with the components of the gel, control its transport through a hydrogel membrane^{2, 8-10}. While various studies exist on the particle transport through porous filtration membrane systems under the effect of applied pressure gradients¹¹⁻¹⁴, the transport of particles through hydrogel membranes is relatively poorly studied¹⁵.

The use of hydrogels as coating layers on classical hydrophobic filtration membranes has attracted attention for wastewater treatment¹⁶⁻¹⁸. They have proven their effectiveness as ideal materials for modifying filtration membranes, to achieve robust anti-fouling and long stability¹⁸⁻²⁰. However, coating or grafting hydrogels on membranes still presents some issues, mainly by the partial adsorption of the pollutants that pass through the hydrogel layer on the hydrophobic substrate during filtration^{21,22}. A great interest has been paid in recent years to self-supporting hydrogel films with a thickness of several hundreds of microns, in order to avoid surface-coated membrane problems^{23,24}. Free-standing hydrogels have been used for water permeability studies and the rejection of dyes, proteins and salts^{25,26}. Since common hydrogels have poor mechanical properties²⁷, it is important to develop new hydrogel systems that could be used as free-standing membranes without support.

Poly (ethylene glycol) diacrylate (PEGDA)-based hydrogels are resistant hydrogels which have been widely used as scaffolds for tissue engineering applications^{28,29}, drug delivery³⁰ and microfluidic devices^{31,32}. In the context of filtration, PEGDA hydrogels have proven their effectiveness as protein-fouling resistant films^{30,33}. In addition, they have shown a well-controlled water permeability through the porous PEGDA films complemented with porogens

(e.g. poly (ethylene glycol) PEG chains with low molar mass) ^{34, 35}. PEG-based hydrogel membranes are known for their size-dependent particle permeabilities, and used as simple models for mucus ^{1, 36, 37}. Recently, we have developed new PEGDA/PEG composite hydrogel membranes by introducing large free PEG-300 000 g.mol⁻¹ chains to a PEGDA matrix³⁸. We have shown that these large PEG chains remain trapped in the hydrogel matrix during multiple filtration cycles. Using a frontal filtration cell we were able to control the water permeability over two orders of magnitude depending on PEG concentration (1×10^{-18} to 5.5×10^{-16} m²).

In the present study, we investigate the filtration of rigid latex particles with different sizes (20 nm, 100 nm and 1 μ m) through these PEGDA/PEG hydrogel membranes. We focus on how to control the cut-off size rejection of particles depending on the applied pressure and the composition of the hydrogel system. In addition, we study the structural properties of the composite PEGDA/PEG hydrogel membranes by AFM and cryoSEM measurements in order to obtain more insight into the hydrogel structure. We show that despite the presence of similar large micron sized cavities for all PEG containing samples, large particles of 100 nm and 1 μ m do not permeate through the membranes. We suggest therefore that these micron size cavities do not form a percolating network and that the permeation of water and nanoparticles is rather controlled by the nanostructure present in the PEGDA rich walls between these micron size cavities.

Furthermore, we study the reasons of the decrease of the permeation fluxes in the presence of nano and microparticles through the PEGDA/PEG hydrogel membranes.

3.4 EXPERIMENTAL SECTION

3.4.1 Materials

We use poly (ethylene glycol) diacrylate PEGDA ($\overline{M}_w=700$ g.mol⁻¹) with 13 ethylene oxide units and 4-(2-hydroxyethoxy) phenyl 2-hydroxy-2-propyl ketone (Irgacure 2959) which are purchased from Sigma–Aldrich. Linear poly (ethylene glycol) (PEG) ($\overline{M}_w=300\ 000$ g.mol⁻¹, $\overline{D}=2.1$) is purchased from Serva. FluoSpheres™ carboxylate-modified polystyrene particles ((20 nm, 100 nm and 1 μ m of diameter), red fluorescent (580/605), 2% solids) are purchased from thermoFisher scientific. Water is purified with a Milli-Q reagent system (Millipore).

3.4.2 PEGDA hydrogels preparation

The PEGDA and PEG/PEGDA membranes are synthesized via UV-initiated free-radical photopolymerization, using Irgacure 2959 as the photoinitiator. The prepolymerization solution is prepared by adding 0.1 wt% photoinitiator into pure PEGDA solution. After stirring, the

solution is mixed with water to obtain 16 wt% PEGDA and 84 wt% water. The prepolymerization solution is then sandwiched between two glass plates (120 mm x 80 mm) which are separated by 1 mm thick spacers to obtain a membrane thickness of 1 mm. Then the solution is polymerized under irradiation of UV light (intensity =1800 $\mu\text{w}/\text{cm}^2$) with a wavelength of 365 nm for 10 min. After polymerization, the obtained hydrogels are placed in a petri dish with pure water for at least 24 hours prior filtration to eliminate any unreacted PEGDA monomers or small free PEG chains.

To obtain the PEG/PEGDA hydrogels, PEG-300 000 $\text{g}\cdot\text{mol}^{-1}$ is dissolved in the prepolymerization solution. We use PEGDA/PEG hydrogel membranes prepared with 0.4; 1.6 and 4 wt% of PEG-300 000 $\text{g}\cdot\text{mol}^{-1}$ chains for the filtration of modified polystyrene particles with different sizes. For the filtration measurements, the membranes are then cut to obtain 1 mm thick disks of 45 mm diameter.

3.4.3 Particles characterization

Zeta potential and particles size measurements of carboxylate-modified polystyrene particles (Fluospheres) were recorded by Zetasizer Nano-ZS90 from Malvern. The samples used for these measurements were 100-fold diluted in Milli-Q water to reach a particle concentration of $2 \times 10^{-4} \text{ g}\cdot\text{mL}^{-1}$ and to avoid multiple scattering of light. The results are presented in Table S3.1 and Figure S3.1. The optical absorbance measurements of the modified polystyrene particles were carried out with a UV-vis Hewlett-Packard 8453 spectrophotometer using a 1 cm path length quartz cell, in a wavelength range from 190 to 1100 nm.

3.4.4 AFM characterization

AFM images were obtained with a Bruker Icon microscope driven by a Nanoscope V controller. The surface of the hydrogel membrane immersed in water before filtration was observed in Peak Force mode. The height images were acquired with a cantilever of spring constant $0.7 \text{ N}\cdot\text{m}^{-1}$ specially designed for this application. In this mode, similar to a rapid approach-retract experiment, the cantilever oscillates at a frequency of 1 kHz. The scanning frequency was 0.7 Hz and the maximum force was set to 500 pN.

3.4.5 CryoSEM characterization

PEGDA and PEGDA/PEG hydrogel membranes with a thickness of 1 mm were placed on a home-made cryo-holder to be quickly plunged into an ethane slush. As the sample is free-standing over the holder, the sample is rapidly frozen during the plunging by direct contact with the liquid ethane, in order to form amorphous glaze. Subsequently, the sample is transferred

into the Quorum PT 3010 chamber attached to the microscope. There, the frozen sample is fractured with a razor blade. A slight etching at -90°C may be performed to render the sample more visible. The sample is eventually transferred in the FEG-cryoSEM (Hitachi SU8010) and observed at 1 kV at -150°C . No further metallization step is required before transferring the sample to the SEM chamber. Several sublimation cycles were performed on each sample to ensure the removal of the glaze from the hydrogel.

3.4.6 Particles filtration experiments

Particle filtration through conventional (pristine PEGDA hydrogels) and PEG-modified PEGDA hydrogels was measured using a dead-end ultrafiltration (UF) cell obtained from Fisher Scientific S.A.S. (Model 8050, 50 mL for 45 mm Filters) as represented in Figure 3.1. The filtrations are performed at ambient temperature, with 60 ml of carboxylate-modified polystyrene particles (Fluospheres) solution as the feed solution. The solution used for this experiment was 100-fold diluted in Milli-Q water to reach a particle concentration of $2 \times 10^{-4} \text{ g.mL}^{-1}$. The maximum feed pressure rating of 1 bar is used. The membrane area was 15.90 cm^2 fixed in the membrane holder of the cell. Standard filtration experiments are performed at a constant pressure (from 20 mBar to 800 mBar) and the liquid permeates are weighted as a function of time with a balance (Sartorius) to obtain a precise measurement of the flow rate Q in $\text{m}^3.\text{s}^{-1}$. Permeate samples were analyzed using a UV-vis spectrophotometer to determine the concentration of the latex particles that passed through the gels during the filtration experiments.

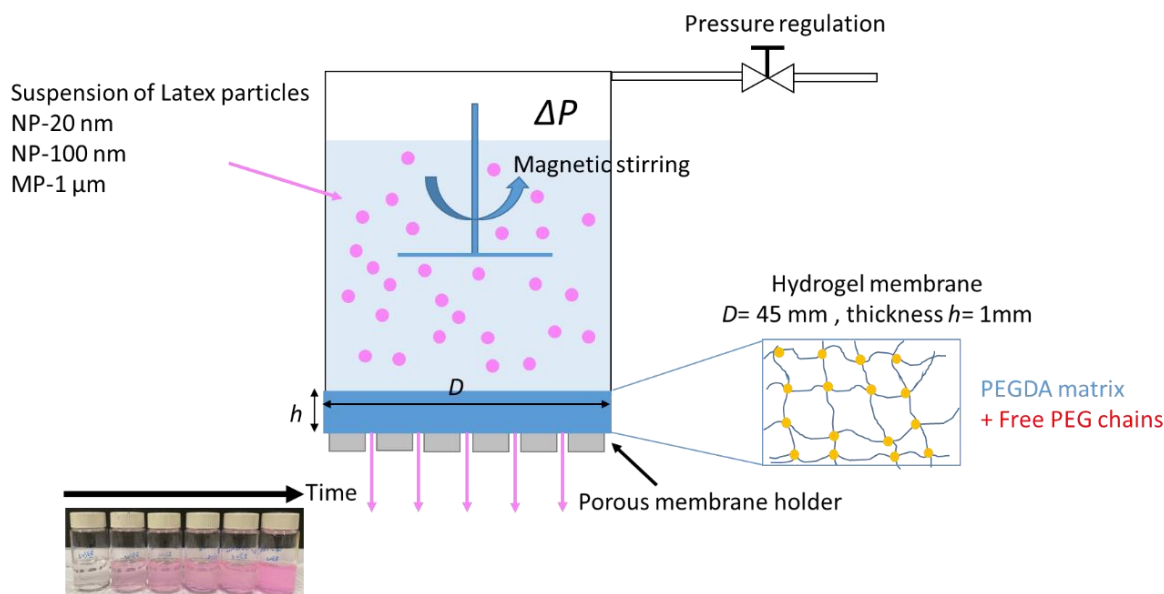


Figure 3.1. Representative schematic of the filtration experiments of latex particle suspension using an ultrafiltration stirred cell.

3.5 RESULTS AND DISCUSSION

3.5.1 Sieving of nanometric and micrometric particles by PEG/PEGDA hydrogels and relation to the hydrogels structure

In this section we study the filtration of latex particles of sizes 20 nm, 100 nm and 1 μm through PEG/PEGDA hydrogel membranes prepared with varying PEG concentrations. We also present structural measurements obtained by AFM and cryoSEM which enables us to obtain a better insight into the structure of the hydrogels.

3.5.1.1 Filtration experiments

We start by measuring the permeation of 20 nm particles through PEG/PEGDA hydrogels of varying PEG contents by measuring the particle concentrations in the permeate as a function of the volume filtered, for different applied pressures. The choice of the hydrogels samples studied is based on our previous work³⁸, in which we had found that the permeability of PEGDA/PEG hydrogels presents an optimum at a weight fraction of PEG of $C^* = 1.6$ wt% corresponding to the overlap concentration of the PEG chains. We therefore choose PEGDA/PEG compositions that range below and above this maximum permeability (i.e. $K = 5.5 \times 10^{-16} \text{ m}^2$). We compare the case of pure PEGDA hydrogels and PEGDA/PEG hydrogels containing 0.4 wt%, 1.6 wt% and 4 wt% of PEG (Figure 3.2). For pure PEGDA hydrogel (Figure 3.2 a), we find that the nanoparticles of 20 nm (NP-20 nm) do not permeate through the hydrogels and their concentration in the permeate is zero. For the 0.4 wt% PEG samples (Figure 3.2 b), the

concentration of NP-20 nm in the permeate increases with the permeate volume and depends on the applied pressure P . This concentration is almost zero at $P = 50$ mBar and increases with the pressure.

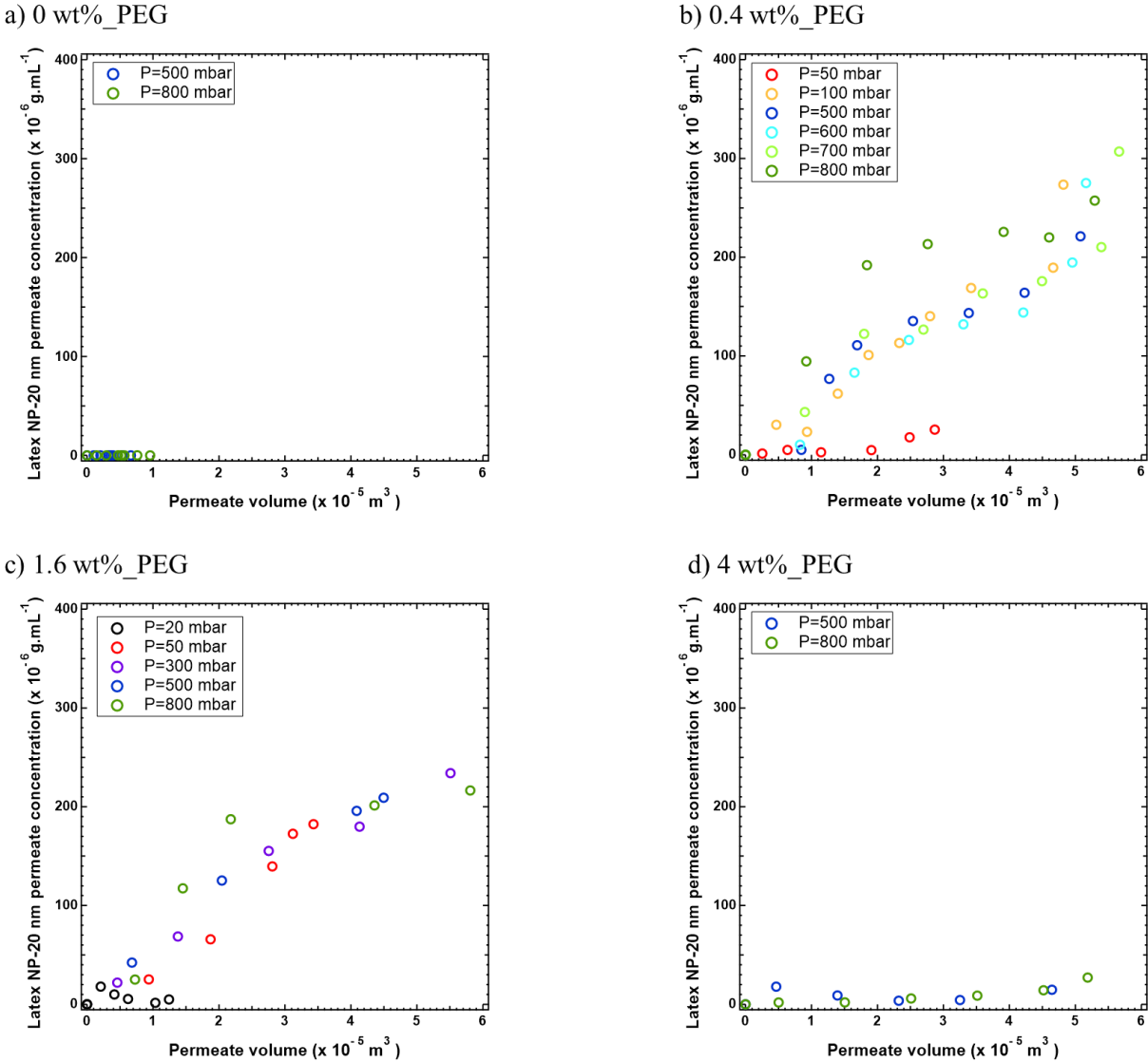


Figure 3.2. Variation of latex nanoparticle of 20 nm concentration in the permeate as a function of the permeate volume under different applied pressures for hydrogel membrane prepared with PEGDA and a) 0 wt%, b) 0.4 wt%, c) 1.6 wt% and d) 4 wt% of PEG-300 000 g.mol^{-1} .

For the most permeable PEGDA hydrogel containing 1.6 wt% of PEG, we notice that the concentration of NP in the permeate is negligible for $P < 50$ mBar and becomes non zero above 50 mBar (Figure 3.2 c). It therefore seems that there is a critical pressure above which the nanoparticles permeate. In the case of 4 wt% of PEG content in the hydrogel (Figure 3.2 d),

we find that the NP-20 nm do not permeate through the hydrogel membrane even for the largest applied pressure (800 mBar).

For the 1.6 wt% PEG hydrogel we also filtrate larger particles, of diameter 100 nm and 1 μm . As can be seen in Figure 3.3, neither the 100 nm nor the 1 μm particles permeate through the hydrogel with 1.6 wt% of PEG, suggesting that the water and nanoparticle permeation operates through a nanometric structure with typical size ranging between 20 nm and 100 nm.

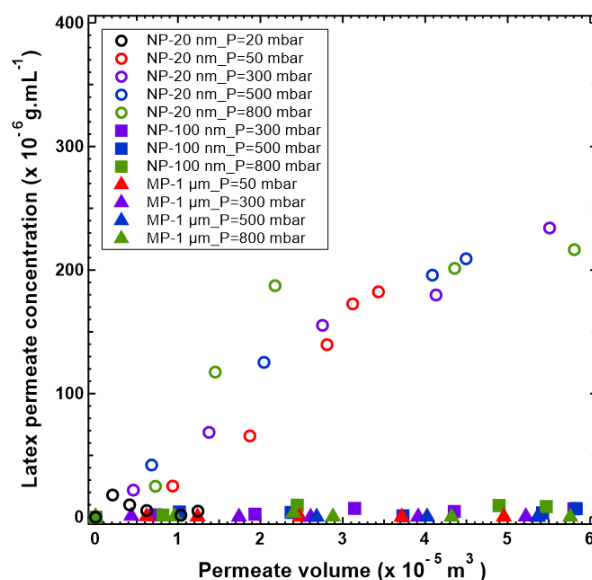


Figure 3.3. Variation of latex nanoparticles of 100 nm (NP-100 nm) and microparticles of 1 μm (MP-1 μm) concentration in the permeate as a function of the permeate volume under different applied pressures for hydrogel membranes prepared with PEGDA and 1.6 wt% of PEG-300 000 g.mol^{-1} . The empty symbols correspond to the concentration of latex nanoparticles of 20 nm (NP-20 nm).

3.5.1.2 Link between particles filtration and the structure of PEG/PEGDA hydrogels

In this section, we discuss the filtration results presented in relation with AFM and cryoSEM measurements presented in Figure 3.4, to obtain more insight into the structure of the hydrogels. As can be seen in Figure 3.4, the PEGDA hydrogels, with no added PEG, present cavities of diameter $d_{cavity} \sim 200$ nm, which according to the SANS study of Molina *et al.*³⁹, are filled with water due to a phase separation between PEGDA ($\overline{Mw}=700$ g.mol^{-1}) and water. This phase separation occurs when the water content in the prepolymerization solution is above 50 wt%, which is the equilibrium water content of the PEGDA matrix of molar mass of 700 g.mol^{-1} . In our case, the total amount of water in the prepolymerization solution is 84 wt%, hence during polymerization, the water in excess, with respect to the equilibrium content of 50 %, is expelled

from the polymerizing PEGDA/water network and is trapped in cavities of diameter $d_{cavity} \sim 200$ nm. The rejection of the 20 nm particles by these PEGDA hydrogels suggests that these 200 nm water cavities are closed.

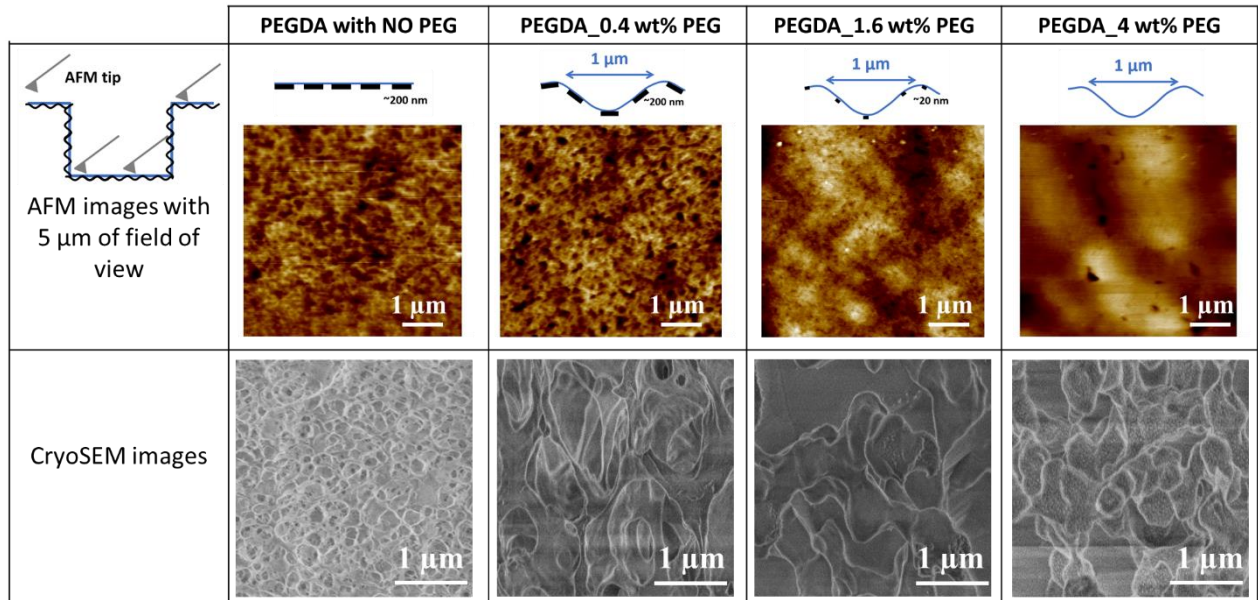


Figure 3.4. AFM images and cryoSEM images for hydrogel membranes prepared with PEGDA and various contents of PEG-300 000 $g.mol^{-1}$.

The average Z-scale in AFM images is ± 50 nm

For all three PEG containing samples investigated, larger cavities of size $d_{cavity} \sim \mu m$ are evidenced by cryoSEM images in Figure 3.4. The walls of these micrometric cavities can be observed by AFM with a field of view of 5 μm . For reasons of image clarity, the Z-scales are not identical for all images. The average Z-scale is ± 50 nm. The AFM images evidence smaller cavities of diameter $d_{cavity} \sim 200$ nm for the 0.4 wt% hydrogels which are very similar to the case of the reference PEGDA sample, hence suggesting that the walls of the micron size cavities are mainly composed of PEGDA and water. For the 1.6 wt% sample, the PEGDA rich walls do not present 200 nm cavities but present nanometric heterogeneities of a few tens of nanometers, while for the 4 wt% PEG sample the walls of the micron size cavities seem to be homogenous at a nanometric scale.

To summarize, the three PEG containing samples present similar micron sized cavities but only the 0.4 wt% and 1.6 wt% allow for the permeation of the 20 nm particles while none of the three samples enables the permeation of the 100 nm or 1 μm particles. In Figure 3.5 a and b, we suggest possible elements of the structure that may account for such results depending on the PEG concentration. We showed in a previous article³⁸ that the PEG chains remain

irreversibly trapped in the hydrogels and are not washed out during filtration cycles at the highest pressures. Hence we suggest that the PEG chains get trapped inside the PEGDA rich walls separating the micron size cavities during the polymerization process. The PEG chains would then induce local defects in the cross-linking density allowing the permeation of the 20 nm nanoparticles but not the 100 nm ones. In such scenario, the PEG-containing walls would therefore provide some level of connectivity between the large micron cavities and control the permeation of both the particles and water. The PEG chains may also be partially trapped in the PEGDA walls and decorate the inner surface of the micron size cavities. For PEG concentrations close to or above the overlap concentration of 1.6 wt%, these chains would then form a dense brush of elongated chains which traps the particles and reduces the permeability. The end-to-end distance of an elongated PEG chain of molar mass 300 000 g.mol⁻¹ can indeed reach a length of the order of one micron which would be sufficient to slow down or even prevent the permeation of the particles. Such a trapping of the PEG chains in the cavities walls can therefore account for the observed maximum of intrinsic permeability with the PEG concentration.

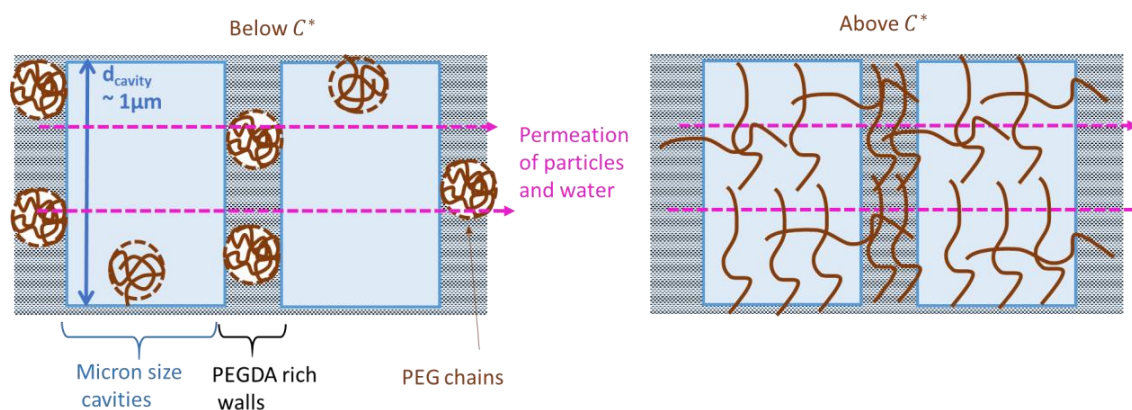


Figure 3.5. Schematic propositions of the hydrogel structure that may account for our results. Illustration of the permeation of water and nanoparticles through the PEGDA/PEG hydrogel membranes. a) At low PEG concentrations, PEG chains trapped in the walls separating the micron sized cavities control the permeation of the particles and water through the hydrogels. b) At higher PEG concentration, PEG chains partially trapped in the PEGDA matrix decorate the PEGDA rich inner walls of the cavities and form dense brushes that slow down the permeation of water and particles.

The value of the critical pressure needed to allow the permeation of the 20 nm particles for the 1.6 wt% PEG hydrogel enables to give information about the hydrogel structure. Indeed the pressure (P) needed to force a particle of radius R_{partic} to go through a cavity of radius λ in a material of elastic modulus (E) scales as (Equation 3.1):

$$\frac{P}{E} \approx \frac{R_{partic}}{\lambda} - 1 \quad (3.1)$$

This equation can be rewritten as:

$$\frac{R_{partic}}{\lambda} \approx \frac{P}{E} + 1 \quad (3.2)$$

In the case of the 1.6 wt% PEG sample, a low pressure of 50 mBar is required to force the particles to permeate through the hydrogel. Interestingly this low pressure is much lower than the elastic modulus of the PEGDA/PEG hydrogels, of the order of 0.2 MPa³⁸. Consequently, one has $\frac{P}{E} \ll 1$ meaning that $\lambda \approx R_{partic} \approx 20$ nm. This estimated value of λ is orders of magnitude lower than $d_{cavity} \sim \mu\text{m}$ observed in the cryoSEM images, and also much lower than $d_{cavity} \sim 200$ nm, the size of the water cavities observed in the pure PEGDA sample. It is, however, the same order of magnitude as the heterogeneities observed by AFM in the walls of the micrometric cavities for the 1.6 wt% PEG samples. Therefore, this result suggests that the permeation of the 20 nm nanoparticles through the hydrogel membranes is probably controlled by heterogeneities of the order of 20 nm in the PEGDA-rich walls connecting the micron sized cavities. The existence of a non-zero critical pressure needed to allow the permeation of the 20 nm particles is possibly due to an energy barrier required to deform the PEG chains.

Finally, considering the value of the permeability K , for the 1.6 wt% PEG/PEGDA sample and knowing the pore sizes from AFM experiments, one can deduce the fraction ε of open cavities, using the Carman-Kozeny equation^{40, 41}, which describes the permeation of water through a bed of beads of diameter d , given in (Equation 3.3):

$$\frac{\varepsilon^3}{(1-\varepsilon)^2} = \frac{180.K}{d^2} \quad (3.3)$$

Although the situation described by the Carman Kozeny equation is obviously different from our system, this equation has already been used to predict the permeability of hydrogels⁴²⁻⁴⁴, taking for d the distance between two cross-links in the case of a simple hydrogel. In our case, we first take $d \sim 20$ nm, i.e. the typical size discussed above. For the 1.6 wt% of PEG hydrogel, the permeability is $K \sim 5 \times 10^{-16}$ m², from which we can deduce a cavity fraction of $\phi \sim 0.95$. This means that the nanometric heterogeneities in the walls of the micron sized cavities may control water permeation in the hydrogels.

3.5.2 Clogging of the PEG/PEGDA hydrogels by nano and microparticles

We compare the water permeation flux through the PEG/PEGDA hydrogels when the feed solution is either pure water or the nano and microparticle suspension. For the pure PEGDA hydrogels and the 4 wt% PEG hydrogels, the permeation flux is identical for pure water and for the 20 nm particle suspension (Figure 3.6 a and d). However, for the 0.4 wt% (Figure 3.6 b) and 1.6 wt% (Figure 3.6 c) hydrogels, the permeation flux of the 20 nm suspension is lower than the one measured for pure water. For these two hydrogels, we showed earlier that the 20 nm particles permeate through the samples, hence we suggest that there might be some clogging of the smallest cavities of the hydrogels by the 20 nm particles, thus reducing the permeation flux.

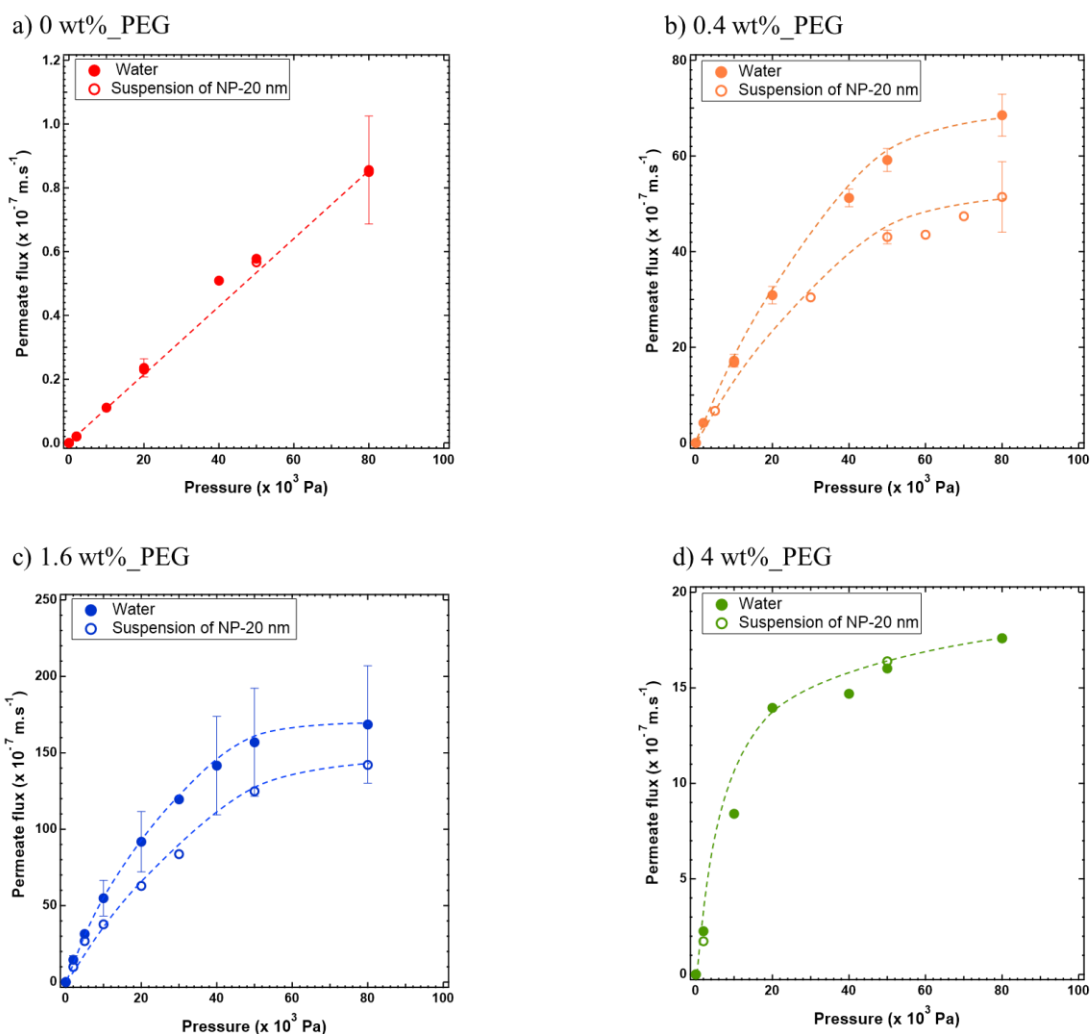
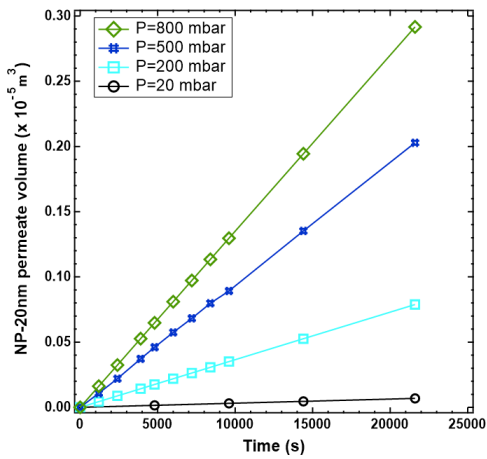


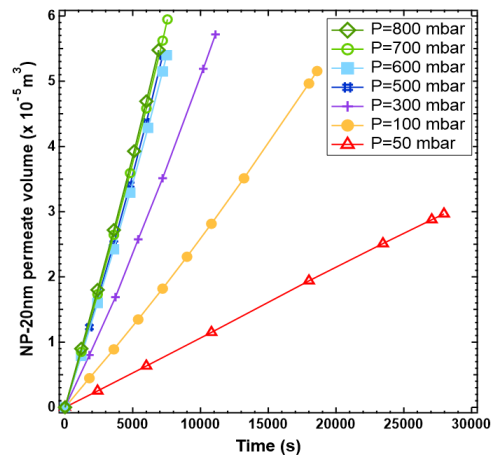
Figure 3.6. Variation of the water and latex nanoparticles of 20 nm (NP-20 nm) permeate fluxes as a function of applied pressure for hydrogel membranes prepared with PEGDA and a) 0 wt%, b) 0.4 wt%, c) 1.6 wt% and d) 4 wt% of PEG-300 000 $\text{g}\cdot\text{mol}^{-1}$. The dashed lines are guides for the eye.

We measure the variation of the permeate volume as a function of time under different applied pressures (Figure 3.7) and find that the permeate volume varies linearly with the time, regardless of the applied pressure. This observation suggests that the saturation of the cavities by the 20 nm nanoparticles permeating through the 0.4 and 1.6 wt% hydrogels is a fast process occurring early during the filtration process.

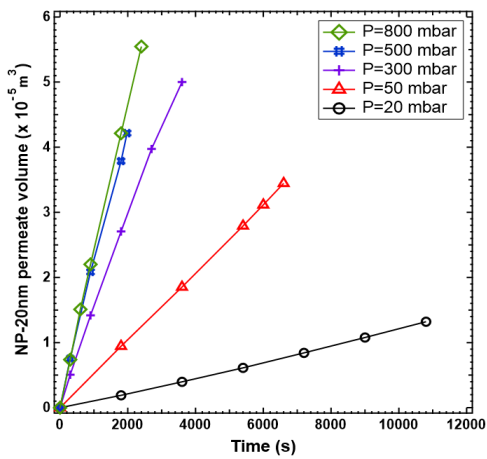
a) 0 wt%_PEG



b) 0.4 wt%_PEG



c) 1.6 wt%_PEG



d) 4 wt%_PEG

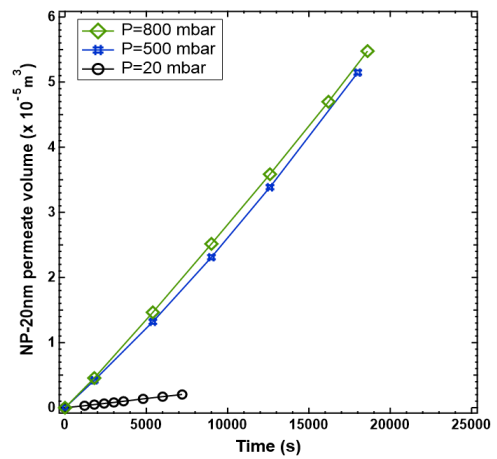


Figure 3.7. Variation of the latex nanoparticles of 20 nm (NP-20 nm) permeate volume as a function of the time under different applied pressures, for hydrogel membrane prepared with PEGDA and a) 0 wt%, b) 0.4 wt%, c) 1.6 wt% and d) 4 wt% of PEG-300 000 $g \cdot mol^{-1}$.

In Figure 3.8, we compare the permeation fluxes of the suspensions containing the 20, 100 nm and 1 μm particles with the case of pure water for the 1.6 wt% PEG/PEGDA hydrogels. The presence of latex particles decreases the permeate flux for the three types of particles investigated, the largest effect being the one measured for the large particles of 100 nm and 1 μm . Unlike in the case of the 20 nm particles, the 100 nm and 1 μm do not permeate through the 1.6 wt% hydrogels. Hence, the flux reduction can either be due to the gradual building of a “cake” of particles above the hydrogel membranes or to a clogging of the particles inside the cavities of the membrane.

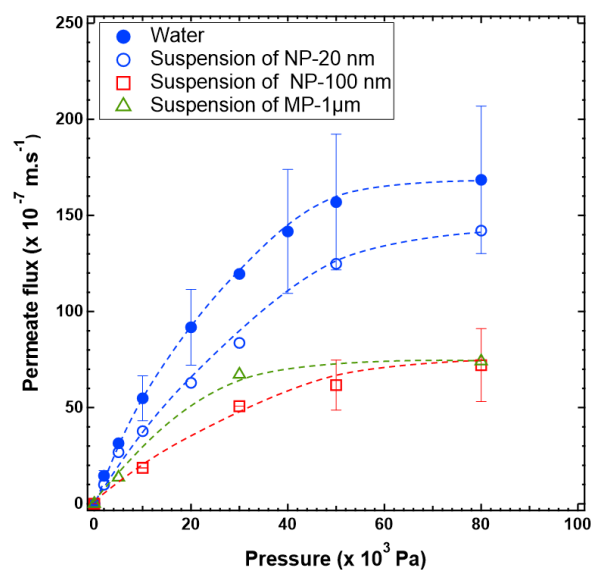


Figure 3.8. Variation of the water, latex nanoparticles of 20 nm (NP-20 nm), nanoparticles of 100 nm (NP-100 nm) and microparticles of 1 μm (MP-1 μm) permeate flux as a function of applied pressure for hydrogel membranes prepared with PEGDA and 1.6 wt% of PEG-300 000 g.mol^{-1} . The dashed lines are guides for the eye.

In the case of the formation of such a cake, one expects that the permeability of the cake will decrease over time as the cake thickness will increase, and hence we should observe a temporal decay of the permeation flux. However, as shown in Figure 3.9, the permeation volume increases linearly with time, meaning that the permeation flux is constant with time, excluding the possibility of a gradual building of a cake of rejected particles above the membrane.

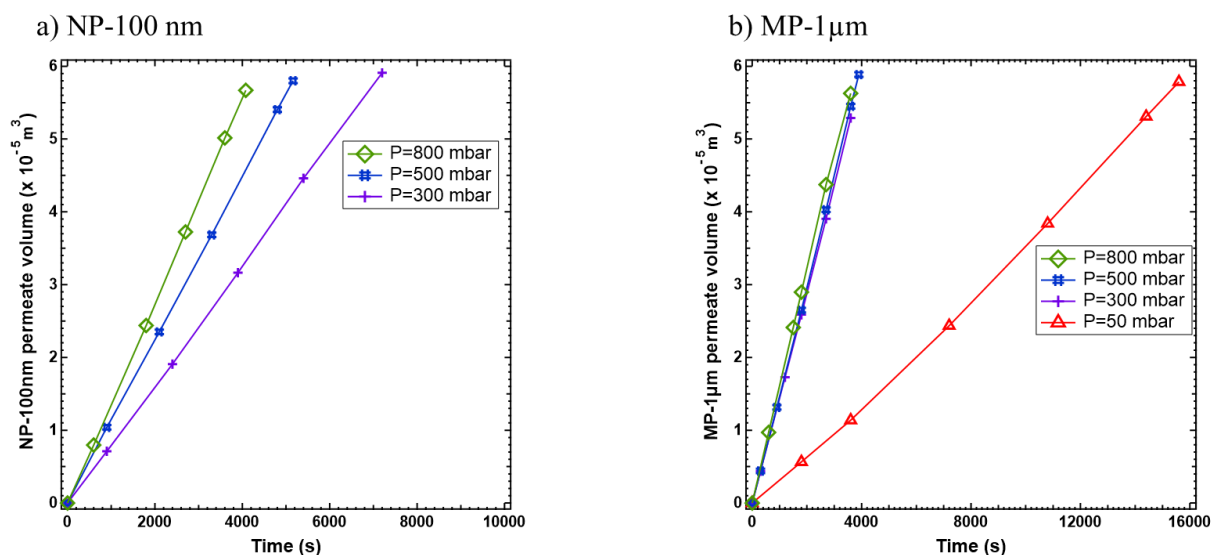


Figure 3.9. Variation of latex a) nanoparticles of 100 nm (NP-100 nm) and b) microparticles of 1 μm (MP-1 μm) permeate volume as a function of time under different applied pressures for hydrogel membranes prepared with PEGDA and 1.6 wt% of PEG-300 000 g.mol^{-1} .

To determine whether the 100 nm particles enter into the cavities and clog them, we perform cryoSEM experiments of the 1.6 wt% PEG hydrogels after the filtration of the 100 nm particles to observe the location of the particles in the cavities. Figure 3.10 a and b show that some of the 100 nm are trapped inside the hydrogels at the walls of the micron sized cavities. The 100 nm particles probably clog the nanometric structure of the walls connecting the micron sized cavities, which reduces the permeability of the hydrogels.

In the case of the 1 μm particles, the cryoSEM images obtained after the MP-1 μm filtration do not show the presence of microparticles in the hydrogel network (see Figure S3.2).

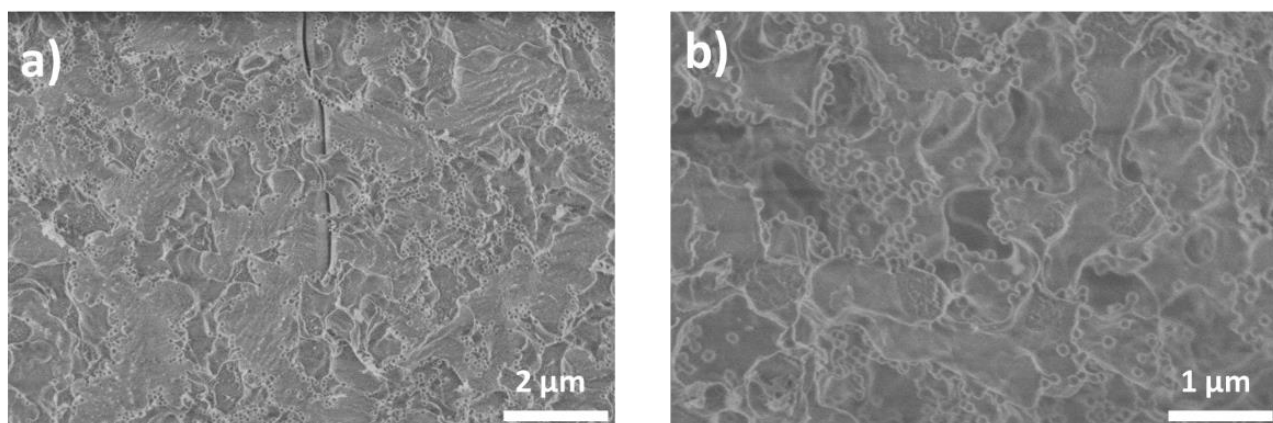


Figure 3.10. CryoSEM images of the cross-section of PEGDA/1.6 wt% PEG hydrogel membrane after filtration experiments of nanoparticle of 100 nm (NP-100 nm).

We therefore suggest that the permeability reduction in the case of the 1 μm particles is due to a deposition of a cake of particles on the hydrogel membrane surface. The magnetic stirrer rotating above the hydrogels during the filtration experiments may prevent the growth of this deposited layer over time, hence leading to a constant water flux over time.

To confirm these hypotheses, we can estimate the reversibility of the clogging process of the hydrogels by the particles by performing filtration cycles, increasing and then reducing the pressure and measuring the permeation flux (Figure 3.11). In the case of the 100 nm particles (Figure 3.11 a), after a first increase of the pressure to 800 mBar, decreasing the pressure back to lower values does not enable to recover the same value of the permeation flux as the one measured as the pressure is increased. This means that the clogging of the cavities by the 100 nm is irreversible and that the particles are trapped inside the cavities, as shown with cryoSEM images. However, the cyclic filtration of MP-1 μm through the hydrogel does not affect significantly the permeate flux, as shown in Figure 3.11 b. This result confirms that these micron sized particles do not enter into the hydrogel and that the flux reduction is due to a reversible deposition of a layer of particles of constant thickness on the hydrogel membrane.

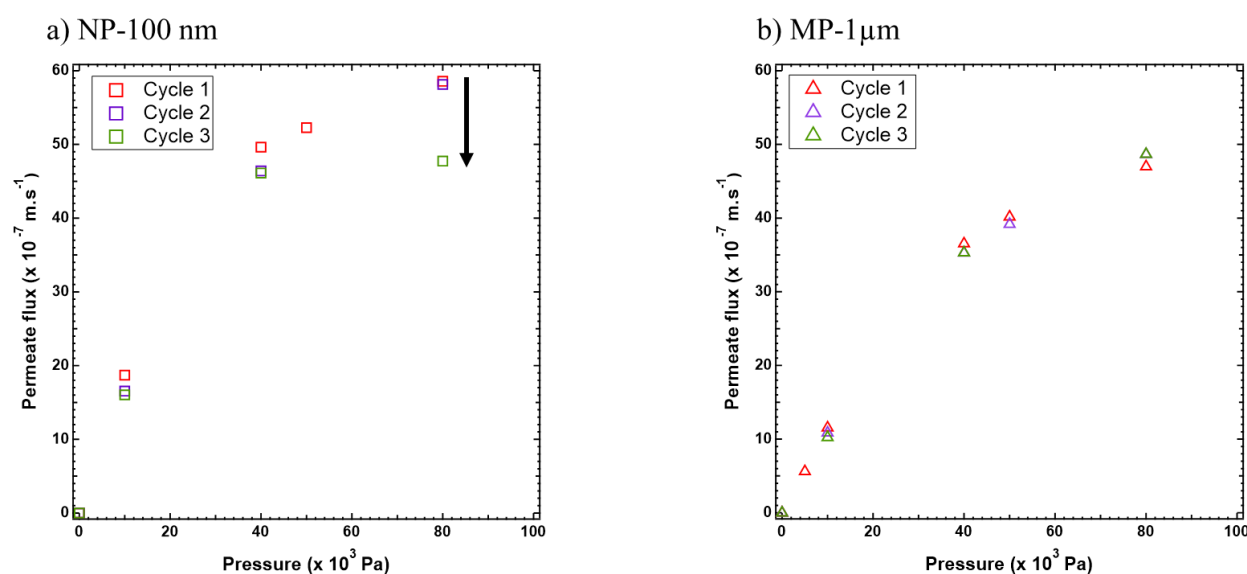


Figure 3.11. Cyclic filtration of a) nanoparticles of 100 nm (NP-100 nm) and b) microparticles of 1 μm (MP-1 μm) through PEGDA hydrogels prepared with 1.6 wt% of PEG chains.

3.6 CONCLUSION

We address the filtration of latex particles with different sizes through a novel composite hydrogel system prepared by photopolymerization of a mixture of PEGDA and large PEG chains of $300\,000\text{ g}\cdot\text{mol}^{-1}$. By investigating the filtration of nano and microparticles and combining these results with AFM and cryoSEM images we are able to obtain insight into the structure of the PEG/PEGDA hydrogels. We show that particles of 20 nm can pass through the PEGDA/PEG hydrogels membranes depending on the PEG content and the applied pressure during filtration. However, despite the presence of micron size cavities for the PEG containing samples, particles of 100 nm and $1\ \mu\text{m}$ do not pass through the PEGDA/PEG hydrogel membranes. Consequently, we suggest that the presence of PEG chains induces local nanoscale defects in the cross-linking of PEGDA-rich walls separating the micron size cavities, that control the permeation of particles and water.

We also investigated the decrease of the water flux in the presence of the latex particles of different sizes. The reducing of the permeation flux in the case of nanoparticles of 20 nm and 100 nm is due to the clogging of the nanometric structure of the hydrogels. In contrast, the permeability reduction in the case of the microparticles of $1\ \mu\text{m}$ is due to the deposition of a layer of particles of constant thickness on the hydrogel membrane.

References

1. Witten, J.; Ribbeck, K., The particle in the spider's web: transport through biological hydrogels. *Nanoscale* **2017**, *9* (24), 8080-8095, DOI 10.1039/C6NR09736G.
2. Tokarev, I.; Minko, S., Stimuli-responsive porous hydrogels at interfaces for molecular filtration, separation, controlled release, and gating in capsules and membranes. *Adv. Mater.* **2010**, *22* (31), 3446-3462, DOI 10.1002/adma.201000165.
3. Siepmann, J.; Peppas, N. A., Modeling of drug release from delivery systems based on hydroxypropyl methylcellulose (HPMC). *Adv. Drug Deliv. Rev.* **2012**, *64*, 163-174, DOI 10.1016/j.addr.2012.09.028.
4. Ogston, A., The spaces in a uniform random suspension of fibres. *Trans. Faraday. Soc* **1958**, *54*, 1754-1757, DOI 10.1039/TF9585401754.
5. Cukier, R. I., Diffusion of Brownian spheres in semidilute polymer solutions. *Macromolecules* **1984**, *17* (2), 252-255, DOI 10.1021/ma00132a023.
6. Sarfati, R.; Calderon, C. P.; Schwartz, D. K., Enhanced Diffusive Transport in Fluctuating Porous Media. *ACS Nano* **2021**, *15* (4), 7392-7398, DOI 10.1021/acsnano.1c00744.
7. Fujiyabu, T.; Li, X.; Chung, U.-i.; Sakai, T., Diffusion behavior of water molecules in hydrogels with controlled network structure. *Macromolecules* **2019**, *52* (5), 1923-1929, DOI 10.1021/acs.macromol.8b02488.
8. Hansing, J.; Netz, R. R., Hydrodynamic Effects on Particle Diffusion in Polymeric Hydrogels with Steric and Electrostatic Particle–Gel Interactions. *Macromolecules* **2018**, *51* (19), 7608-7620, DOI 10.1021/acs.macromol.8b01494.
9. Hansing, J.; Ciemer, C.; Kim, W. K.; Zhang, X.; DeRouchey, J. E.; Netz, R. R., Nanoparticle filtering in charged hydrogels: Effects of particle size, charge asymmetry and salt concentration. *EUR. Phys. J.E* **2016**, *39* (5), 1-13, DOI 10.1140/epje/i2016-16053-2.
10. Lieleg, O.; Ribbeck, K., Biological hydrogels as selective diffusion barriers. *Trends in Cell Biology* **2011**, *21* (9), 543-551, DOI 10.1016/j.tcb.2011.06.002.
11. Benet, E.; Badran, A.; Pellegrino, J.; Vernerey, F., The porous media's effect on the permeation of elastic (soft) particles. *J. Membr. Sci.* **2017**, *535*, 10-19, DOI 10.1016/j.memsci.2017.04.014.
12. Helling, A.; Kubicka, A.; Schaap, I. A.; Polakovic, M.; Hansmann, B.; Thiess, H.; Strube, J.; Thom, V., Passage of soft pathogens through microfiltration membranes scales with

transmembrane pressure. *J. Membr. Sci.* **2017**, *522*, 292-302, DOI 10.1016/j.memsci.2016.08.016.

13. Hendrickson, G. R.; Lyon, L. A., Microgel translocation through pores under confinement. *Angew. Chem. Int. Ed.* **2010**, *49* (12), 2193-2197, DOI 10.1002/anie.200906606.

14. Christensen, M. L.; Johansson, C.; Sedin, M.; Keiding, K., Nonlinear filtration behavior of soft particles: Effect of dynamic cake compression. *Powder technol.* **2011**, *207* (1-3), 428-436, DOI 10.1016/j.powtec.2010.11.031.

15. Valade, D.; Wong, L. K.; Jeon, Y.; Jia, Z.; Monteiro, M. J., Polyacrylamide hydrogel membranes with controlled pore sizes. *J. Polym. Sci. A. Polym. Chem.* **2013**, *51* (1), 129-138, DOI 10.1002/pola.26311.

16. Lei, J.; Ulbricht, M., Macroinitiator-mediated photoreactive coating of membrane surfaces with antifouling hydrogel layers. *J. Membr. Sci.* **2014**, *455*, 207-218, DOI 10.1016/j.memsci.2013.12.059.

17. Tang, Z.; Wei, J.; Yung, L.; Ji, B.; Ma, H.; Qiu, C.; Yoon, K.; Wan, F.; Fang, D.; Hsiao, B. S.; Chu, B., UV-cured poly(vinyl alcohol) ultrafiltration nanofibrous membrane based on electrospun nanofiber scaffolds. *J. Membr. Sci.* **2009**, *328* (1), 1-5, DOI 10.1016/j.memsci.2008.11.054.

18. Wang, X.; Fang, D.; Yoon, K.; Hsiao, B. S.; Chu, B., High performance ultrafiltration composite membranes based on poly(vinyl alcohol) hydrogel coating on crosslinked nanofibrous poly(vinyl alcohol) scaffold. *J. Membr. Sci.* **2006**, *278* (1), 261-268, DOI 10.1016/j.memsci.2005.11.009.

19. La, Y.-H.; McCloskey, B.; Sooriyakumaran, R.; Vora, A.; Freeman, B.; Nassar, M.; Hedrick, J.; Nelson, A.; Allen, R., Bifunctional hydrogel coatings for water purification membranes: Improved fouling resistance and antimicrobial activity. *Fuel and Energy Abstracts* **2011**, *372*, 285-291, DOI 10.1016/j.memsci.2011.02.005.

20. Zhao, Y.-F.; Zhu, L.-P.; Yi, Z.; Zhu, B.-K.; Xu, Y.-Y., Zwitterionic hydrogel thin films as antifouling surface layers of polyethersulfone ultrafiltration membranes anchored via reactive copolymer additive. *J. Membr. Sci.* **2014**, *470*, 148-158, DOI 10.1016/j.memsci.2014.07.023.

21. Zhang, X.; Lin, B.; Zhao, K.; Wei, J.; Guo, J.; Cui, W.; Jiang, S.; Liu, D.; Li, J., A free-standing calcium alginate/polyacrylamide hydrogel nanofiltration membrane with high anti-fouling performance: preparation and characterization. *Desalination* **2015**, *365*, 234-241, DOI 10.1016/j.desal.2015.03.015.

22. Xiao-lei, W.; Wei, Q.; Li-xin, W.; Kong-yin, Z.; Hui-cai, W.; Hong-yu, L.; Jun-fu, W., Desalination of dye utilizing carboxylated TiO₂/calcium alginate hydrogel nanofiltration membrane with high salt permeation. *Sep. Purif. Technol.* **2020**, *253*, 117475, DOI 10.1016/j.seppur.2020.117475.
23. Ju, H.; McCloskey, B. D.; Sagle, A. C.; Kusuma, V. A.; Freeman, B. D., Preparation and characterization of crosslinked poly(ethylene glycol) diacrylate hydrogels as fouling-resistant membrane coating materials. *J. Membr. Sci.* **2009**, *330* (1), 180-188, DOI 10.1016/j.memsci.2008.12.054.
24. Wu, Y.-H.; Park, H. B.; Kai, T.; Freeman, B.; Kalika, D., Water uptake, transport and structure characterization in poly(ethylene glycol) diacrylate hydrogels. *J. Membr. Sci.* **2010**, *347*, 197-208, DOI 10.1016/j.memsci.2009.10.025.
25. Ju, H.; McCloskey, B. D.; Sagle, A. C.; Wu, Y.-H.; Kusuma, V. A.; Freeman, B. D., Crosslinked poly (ethylene oxide) fouling resistant coating materials for oil/water separation. *J. Membr. Sci.* **2008**, *307* (2), 260-267, DOI 10.1016/j.memsci.2007.09.028.
26. Ju, H.; Sagle, A. C.; Freeman, B. D.; Mardel, J. I.; Hill, A. J., Characterization of sodium chloride and water transport in crosslinked poly(ethylene oxide) hydrogels. *J. Membr. Sci.* **2010**, *358* (1), 131-141, DOI 10.1016/j.memsci.2010.04.035.
27. Oyen, M., Mechanical characterisation of hydrogel materials. *Int. Mater. Rev.* **2014**, *59* (1), 44-59, DOI 10.1179/1743280413Y.0000000022.
28. Durst, C. A.; Cuchiara, M. P.; Mansfield, E. G.; West, J. L.; Grande-Allen, K. J., Flexural characterization of cell encapsulated PEGDA hydrogels with applications for tissue engineered heart valves. *Acta Biomater.* **2011**, *7* (6), 2467-2476, DOI 10.1016/j.actbio.2011.02.018.
29. Yasar, O.; Orock, A.; Tarantini, S.; White, J.; Khandaker, M., Mechanical characterization of polyethylene glycol diacrylate (PEGDA) for tissue engineering applications. In *Mechanics of Biological Systems and Materials*, Springer: 2013; Vol. 5, pp 189-195.
30. Gao, Y.; Hou, M.; Yang, R.; Zhang, L.; Xu, Z.; Kang, Y.; Xue, P., Highly porous silk fibroin scaffold packed in PEGDA/sucrose microneedles for controllable transdermal drug delivery. *Biomacromolecules* **2019**, *20* (3), 1334-1345, DOI 10.1021/acs.biomac.8b01715.
31. Lee, A. G.; Arena, C. P.; Beebe, D. J.; Palecek, S. P., Development of macroporous poly(ethylene glycol) hydrogel arrays within microfluidic channels. *Biomacromolecules* **2010**, *11* (12), 3316-3324, DOI 10.1021/bm100792y.

32. Bacchin, P.; Leng, J.; Salmon, J. B., Microfluidic Evaporation, Pervaporation, and Osmosis: From Passive Pumping to Solute Concentration. *Chem. Rev.* **2021**, *122* (7), 6938-6985, DOI 10.1021/acs.chemrev.1c00459.
33. Baek, K.; Liang, J.; Lim, W. T.; Zhao, H.; Kim, D. H.; Kong, H., In situ assembly of antifouling/bacterial silver nanoparticle-hydrogel composites with controlled particle release and matrix softening. *ACS Appl. Mater. Interfaces* **2015**, *7* (28), 15359-15367, DOI 10.1021/acsami.5b03313.
34. Calì, A.; Leng, J.; Decock, J.; De Stefano, L.; Salmon, J. B., *Microscopy assisted fabrication of a hydrogel-based microfluidic filter*. 2015; Vol. 10.
35. Decock, J.; Schlenk, M.; Salmon, J. B., In situ photo-patterning of pressure-resistant hydrogel membranes with controlled permeabilities in PEGDA microfluidic channels. *Lab on a chip* **2018**, *18* (7), 1075-1083, DOI 10.1039/c7lc01342f.
36. Herrmann, A.; Rödiger, S.; Schmidt, C.; Schierack, P.; Schedler, U., Spatial Separation of Microbeads into Detection Levels by a Bioorthogonal Porous Hydrogel for Size-Selective Analysis and Increased Multiplexity. *Anal. Chem.* **2019**, *91* (13), 8484-8491, DOI 10.1021/acs.analchem.9b01586.
37. Wolde-Kidan, A.; Herrmann, A.; Prause, A.; Gradzielski, M.; Haag, R.; Block, S.; Netz, R. R., Particle Diffusivity and Free-Energy Profiles in Hydrogels from Time-Resolved Penetration Data. *Biophys. J.* **2021**, *120* (3), 463-475, DOI 10.1016/j.bpj.2020.12.020.
38. Eddine, M. A.; Belbekhouche, S.; de Chateaufneuf-Randon, S.; Salez, T.; Kovalenko, A.; Bresson, B.; Monteux, C., Large and Nonlinear Permeability Amplification with Polymeric Additives in Hydrogel Membranes. *Macromolecules* **2022**, *55* (21), 9841-9850, DOI 10.1021/acs.macromol.2c01462.
39. Malo de Molina, P.; Lad, S.; Helgeson, M. E., Heterogeneity and its Influence on the Properties of Difunctional Poly(ethylene glycol) Hydrogels: Structure and Mechanics. *Macromolecules* **2015**, *48* (15), 5402-5411, DOI 10.1021/acs.macromol.5b01115.
40. Carman, P. C., Fluid flow through granular beds. *Trans. Inst. Chem. Eng.* **1937**, *15*, 150-166,
41. Ollivier, J.; Massat, M., Permeability and microstructure of concrete: a review of modelling. *Cement and Concrete Research* **1992**, *22* (2-3), 503-514,
42. Gao, Y.; Cho, H.-J. J., Quantifying the trade-off between stiffness and permeability in hydrogels. *Soft Matter* **2022**, *18*, 7735-7740, DOI 10.1039/D2SM01215D.

43. Nakao, S. I.; Nomura, T.; Kimura, S., Characteristics of macromolecular gel layer formed on ultrafiltration tubular membrane. *AIChE. J.* **1979**, 25 (4), 615-622, DOI 10.1002/aic.690250407.
44. Isobe, N.; Kimura, S.; Wada, M.; Deguchi, S., Poroelasticity of cellulose hydrogel. *J.Taiwan. Inst. Chem. Eng.* **2018**, 92, 118-122, DOI 10.1016/j.jtice.2018.02.017.

Chapter 4

Effect of PEG content and molar mass on the morphological structure and water permeability properties of PEGDA/PEG composite hydrogel membranes

4.1 ABSTRACT

In our study, we explore the effect of poly (ethylene glycol) (PEG) molar mass on the permeability and structure of poly (ethylene glycol) diacrylate PEGDA/PEG composite hydrogel membranes. We find that the variation of PEG contents and molar masses allowed tuning the water permeability properties over several orders of magnitude. We show that the maximum of water permeability measured at the critical overlap concentration C^* of PEG chains in a previous study is a robust phenomenon. Moreover, the maximum permeability measured at C^* follows a non-monotonic evolution with the molar mass and presents a maximum for a molar mass of PEG-35 000 g.mol⁻¹. Our results show that most PEG chains are irreversibly trapped in the PEGDA matrix even for the shortest molar masses down to 600 g.mol⁻¹ suggesting that the PEG chains may be covalently grafted to the PEGDA matrix. CryoSEM and AFM measurements show large micron size cavities separated by PEGDA rich walls which nanometric structure strongly depends on the PEG content. Combining our permeability and structural measurements, we suggest that the PEG chains trapped inside the PEGDA rich walls induce nanometric defects in the cross-linking density that result in the increase of the permeability below C^* . Above C^* we suggest that partially trapped PEG chains may form a brush decorating the surface of the PEGDA rich walls leading to a decrease of the permeability. These two opposite effects are expected to depend on the molar mass with opposite trends which may account for the non-monotonic variation of the maximum

permeability at C^* with the molar mass. These results show the possibility to tune the hydrogel membrane properties to provide new perspectives in separation application.

4.2 KEYWORDS

CryoSEM, AFM, phase separation, morphology, hydrogel, permeability.

4.3 INTRODUCTION

Macroporous polymer hydrogels have been the subject of research applied to a wide range of areas¹ such as drug delivery^{2, 3}, scaffold for tissue engineering⁴ as well as membrane for filtration process and environmental application^{5,6}. The porosity of the polymeric network can be obtained by various methods, such as foaming⁷, emulsion templating⁸, sacrificial templates such as salt crystals⁹⁻¹¹ or sacrificial particles (such as calcium carbonate particles¹², gelatin microparticles¹³⁻¹⁶,...) and cryogelation¹⁷. While these methods involve several steps, phase separation is another simple approach to produce porous materials¹⁸⁻²⁰. Polymerization induced phase separation (PIPS) is a simpler method where phase separation occurs during the polymerization of an initially homogeneous solution of monomer and solvent²¹⁻³⁰ and is subsequently kinetically frozen. This method allows production of hydrogels network of varying morphology, mechanical properties and permeability³¹.

PEGDA based hydrogels have been shown to undergo PIPS which generates water cavities in the PEGDA network. Alternatively, adding incompatible polymers in the PEGDA solution such as polyurethane (PU), polyetherimide (PEI) or hyaluronic acid (HA)³²⁻³⁴ also enables to induce a porous structure. PEGDA based membranes are promising for filtration, gas separation, tissue engineering or drug delivery applications because they are hydrophilic, resistant and their macroporous structure enables a good control of their transport properties with respect to water, gases or nutrients^{35,36}.

We have shown in Chapters 2 and 3 that adding long PEG chains in the PEGDA prepolymerization solution also enables to obtain macroporous hydrogels with controlled permeability. We found that the resulting hydrogels present micron size cavities separated by PEGDA rich walls. Unlike previous studies which incorporate PEG chains as porogens, we showed that these long PEG chains remain irreversible trapped in the hydrogels and are not rinsed out even after several filtration cycles up to 1 bar. The intrinsic permeability of these composite PEG/PEGDA hydrogels can be varied by orders of magnitude by varying the PEG content and presents a maximum with the PEG concentration, obtained at the critical overlap

concentration C^* of the PEG chains. In Chapter 3, we further showed that 20 nm nanoparticles permeate through the most permeable PEG/PEGDA hydrogel while the 100 nm and 1 μ m particles do not, suggesting that the PEG chains trapped in the PEGDA matrix induce local nanometric defects in the cross-linking density leading to the increased permeability below C^* . Above C^* , we suggested that some PEG chains which are only partially anchored in the PEGDA matrix form a dense brush at the surface of the micron size cavities that disturbs the permeation of the largest particles. We expect that these two scenarios will be influenced by the molar mass in different manners. Hence in this Chapter our goal is to determine how the molar mass of the PEG chains influences the intrinsic permeability and structure of the PEG/PEGDA hydrogels. We show that the permeability maximum obtained at $C = C^*$ is a general phenomenon and that the molar mass has only a weak influence on the fraction of PEG chains irreversibly trapped in the PEGDA matrix.

4.4 EXPERIMENTAL

4.4.1 Materials

We use poly (ethylene glycol) diacrylate PEGDA ($\overline{M}_w=700$ g.mol⁻¹) oligomers with 13 ethylene oxide units and 4-(2-hydroxyethoxy) phenyl 2-hydroxy-2-propyl ketone (Irgacure 2959) photoinitiator which are purchased from Sigma–Aldrich. Linear poly (ethylene glycol)s (PEG) ($\overline{M}_w = 600$; 3000 ($\overline{D} = 1.031$) ; 10 000 ($\overline{D} = 1.031$) ; 35 000 ($\overline{D} = 1.026$)) are purchased from Sigma–Aldrich. Linear poly (ethylene glycol)s (PEG) ($\overline{M}_w = 300\ 000$ g.mol⁻¹, $\overline{D} = 2.1$) and ($\overline{M}_w = 600\ 000$ g.mol⁻¹) are purchased from Serva and Acros Organics, respectively. Poly (ethylene glycol) monomethacrylate PEGMA ($\overline{M}_w=2000$ g.mol⁻¹) is purchased from Polysciences. Water is purified with a Milli-Q reagent system (Millipore).

4.4.2 PEGDA hydrogels preparation

The PEGDA and PEGDA/PEG membranes are synthesized via UV-initiated free-radical photopolymerization, using Irgacure 2959 as the photoinitiator, as described in our previous study³⁷. Briefly, the prepolymerization solution is prepared by adding 0.1 wt% photoinitiator (Irgacure 2959) into pure PEGDA-oligomer. After stirring, PEG is dissolved in the prepolymerization solution, and the solution is mixed with water to obtain a prepolymerization solution composed of 16 wt% PEGDA and 84 wt% water with varying quantities of PEG chains. The prepolymerization solution is then sandwiched between two glass plates (120x80 mm²) which are separated by 1 mm thick spacers to obtain a membrane thickness of 1 mm. Then the solution is polymerized under irradiation with the UV-light (Intensity = 1800 μ W/cm²)

with a wavelength of 365 nm for 10 min. After polymerization, the obtained hydrogels are placed in a Petri dish with pure water for at least 24 hours prior to filtration experiments to remove any unreacted PEGDA oligomers or untrapped PEG chains.

In order to confirm that the addition of PEG with different molar mass does not affect the polymerization reaction of PEGDA, as in Chapter 2, we follow the polymerization reaction of PEGDA hydrogels prepared with different concentrations of PEG-3000 g.mol⁻¹. We obtain that the PEGDA polymerization was complete even after the addition of PEG chains with a concentration ranged between 0 and 20 wt%. The results are presented in Figure S4.1.

4.4.3 Morphological characterization of hydrogel membranes

CryoScanning Electron Microscopy (CryoSEM)

The PEGDA/PEG hydrogel membranes with a thickness of 1 mm were placed on a home-made cryo-holder to be quickly plunged into an ethane slush. As the sample is frestanding over the holder, the sample is rapidly frozen during the plunging by direct contact with the liquid ethane, in order to form amorphous glace. Subsequently, the sample is transferred into the Quorum PT 3010 chamber attached to the microscope. There, the frozen sample is fractured with a razor blade. A slight etching at -90°C may be performed. The sample is eventually transferred in the FE-cryo SEM (Hitachi SU8010) and observed at 1 kV at -150°C. No further metallization step is required before transferring the sample to the SEM chamber. Several sublimation cycles were performed on each sample to ensure the removal of the glace from the hydrogel.

Atomic Force Microscopy (AFM)

AFM images are obtained with a Bruker Icon microscope driven by a Nanoscope V controller. The surface of PEGDA/PEG hydrogel membranes is probed in water at room temperature in Peak Force mode. The cantilever and the sample were immersed in deionized water. We used a scan assist Bruker probe with a spring constant of 0.7 N/m. The peak force frequency was of 1 kHz.

4.4.4 Permeability experiments

Water permeability through conventional and PEG-modified PEGDA hydrogels was measured using a dead-end ultrafiltration UF cell obtained from Fisher Scientific S.A.S. (Amicon Model 8050, 50 mL for 45 mm Filters) as described in our previous study³⁷. The filtrations were performed at ambient temperature, with Milli-Q water as the feed solution. The membrane with the area 15.90 cm² was fixed in the membrane holder of the cell. The standard filtration

experiments were performed at 100 mBar and the liquid permeate is weighted as a function of time with a balance to obtain a precise measurement of the flow rate Q .

Permeate flow rate Q was recorded, and the water intrinsic permeability K was calculated by the following (Equation 4.1):

$$K = \frac{Q\mu h}{\Delta P S} \quad (4.1)$$

where Q is the water flow rate ($\text{m}^3 \cdot \text{s}^{-1}$) calculated from the slope of the variation of the accumulated permeate volume (m^3) as a function of time (s), μ is the water viscosity (Pa.s), h is the hydrogel thickness (m), S is the surface area of the hydrogel membrane (m^2) and ΔP is the pressure difference across the membrane (Pa).

In this study, the values of permeability K that are presented are obtained from the slope of the $Q = f(\Delta P)$ curves for pressures ranging from 0 to 100 mBar where the flux varies linearly with the applied pressure.

4.5 RESULTS

4.5.1 Permeability variations around C^* for varying PEG molar masses

In this section, our goal is to determine whether this permeability maximum at C^* described before is a robust phenomenon and whether it applies to PEG chains of varying molar masses. To obtain the water intrinsic permeability K of the PEG/PEGDA hydrogels, we measure the water flux, Q , as a function of the applied pressure, for $P < 100$ mBar in the linear regime for which Q varies linearly with ΔP . In Figure 4.1, we report the intrinsic permeability measurements for a series of PEGDA/PEG hydrogel systems with molar mass of PEGs ranging from 600 to 600 000 $\text{g} \cdot \text{mol}^{-1}$. For molar masses between 600 and 3000 $\text{g} \cdot \text{mol}^{-1}$, the water permeability increases continuously with the PEG content in the hydrogel system. As an example for PEGDA prepared with PEG-600 $\text{g} \cdot \text{mol}^{-1}$ (Figure 4.1 a), the water permeability varies about two orders of magnitude from about $3.6 \pm 0.0015 \times 10^{-18} \text{ m}^2$ to $\sim 0.8 \pm 0.05 \times 10^{-16} \text{ m}^2$ when the PEG content increases from 7.7 to 29.5 wt%. In comparison, the water permeability for PEGDA/PEG-3000 $\text{g} \cdot \text{mol}^{-1}$ hydrogels varies by about three orders of magnitude with the PEG content, from $4.6 \pm 0.0025 \times 10^{-18} \text{ m}^2$ to $\sim 8.5 \pm 1.6 \times 10^{-16} \text{ m}^2$ when the PEG content increases from 1.6 to 20 wt% (Figure 4.1 b). For the highest PEGs molar mass (10 000; 35 000; 300 000 and 600 000 $\text{g} \cdot \text{mol}^{-1}$), the water permeability presents a maximum with the PEG concentration. For PEG-300 000 $\text{g} \cdot \text{mol}^{-1}$, we have already shown in Chapter 2 that this maximum is obtained for $C = C^* = 1.6 \text{ wt}\%$, the overlap concentration of PEG chains

which mark the transition between the semi-diluted and concentrated regime . For the other molar masses $\overline{M}_w=10\ 000\ \text{g}\cdot\text{mol}^{-1}$; $35\ 000\ \text{g}\cdot\text{mol}^{-1}$ and $600\ 000\ \text{g}\cdot\text{mol}^{-1}$, the permeability maximum are respectively obtained for $C \approx 8$; 4 and 1 wt% which correspond well to the values of C^* presented in Table 4.1. These values of C^* are obtained either by a change of slope in the viscosity measurements $\mu(C)$ (presented in Figure S4.2) or by using the following polymer physics scaling law (Equation 4.2):

$$C^* = \frac{\overline{M}_w}{\frac{4}{3}\pi r_g^3 N_A} \quad (4.2)$$

where \overline{M}_w is the average molar mass of the polymer, r_g is the gyration radius of polymer coils and N_A is Avogadro number: $N_A = 6.023 \times 10^{23}\ \text{mol}^{-1}$. The gyration radius r_g is calculated from the chain end-to-end distance R , in diluted conditions, by (Equation 4.3):

$$r_g = \frac{R^{1/2}}{\sqrt{6}} = \frac{(C_\infty n l^2)^{\frac{1}{2}}}{\sqrt{6}} \quad (4.3)$$

where l is the length of the C-C bond ($\sim 1.54\ \text{\AA}$), n is the number of ethylene glycol monomers (with $M_w=44\ \text{g}\cdot\text{mol}^{-1}$) in a polymer, and C_∞ is the Flory's characteristic ratio for PEG in water which increases with the chain length³⁸. For the highest molar masses, we take $C_\infty \sim 5$ consistently with Reference³⁹. For the lowest PEG molar masses, we take $C_\infty \sim 2.7$.

Table 4.1. The values of r_g and C^ for different PEGs molar mass.*

PEGs molar mass ($\text{g}\cdot\text{mol}^{-1}$)	600	3000	10 000	35 000	300 000	600 000
r_g (nm)	0.7	1.6	3.7	6.8	20.1	28.4
C^* (wt%)	above 50	~ 370	8	4.2	1.6	1

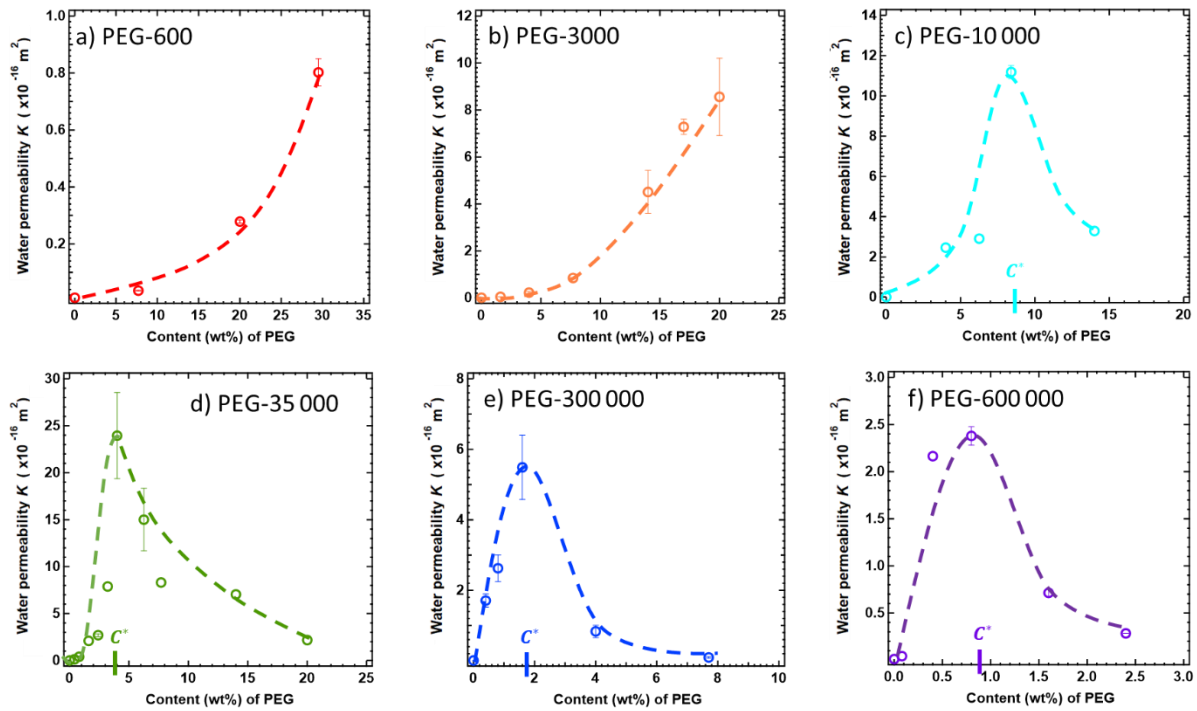


Figure 4.1. Water permeability at $P=10000$ Pa versus content of a) PEG-600 $\text{g}\cdot\text{mol}^{-1}$; b) PEG-3000 $\text{g}\cdot\text{mol}^{-1}$; c) PEG-10 000 $\text{g}\cdot\text{mol}^{-1}$; d) PEG-35 000 $\text{g}\cdot\text{mol}^{-1}$; e) PEG-300 000 $\text{g}\cdot\text{mol}^{-1}$ and f) PEG-600 000 $\text{g}\cdot\text{mol}^{-1}$ in the prepolymerization mixture of hydrogels membranes prepared with 16 wt% of PEGDA. The dashed lines are represented as a guide for the eyes.

In order to characterize in more details the dependence of the hydrogel permeability on the PEG molar mass, we plot the $K(C)$ curves on the same graph (Figure 4.2 a). At low PEG content we observe qualitatively that the slope of the $K(C)$ curves increases when the PEG molar mass increases. Figure 4.2 b which presents the slope of the $K(C)$ curves, dK/dC , as a function of the molar mass confirms that dK/dC increases monotonically with the PEG molar mass. Moreover Figure 4.2 c shows that the maximal water permeability K^* -obtained at the critical overlap concentration of PEG chains- presents a maximum for a PEG molar mass of 35 000 $\text{g}\cdot\text{mol}^{-1}$. Unlike the evolution of dK/dC which is monotonic with the molar mass, the variation of K^* is non monotonic, hence these two results prevent the possibility of rescaling easily the $K(C)$ curves on a single master curve.

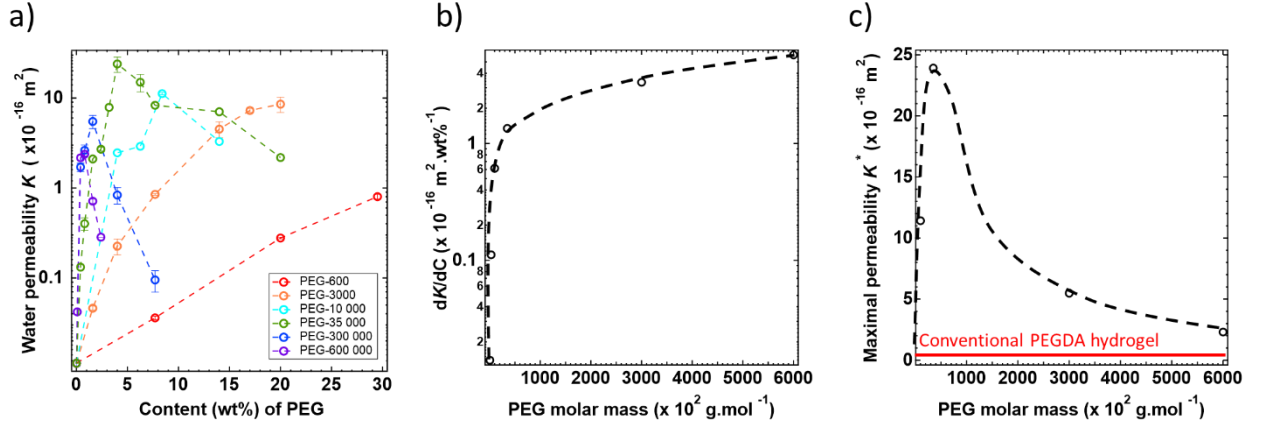


Figure 4.2. a) Variation of the water permeability as a function of the PEG concentration added to the hydrogel membrane with various molar mass. b) Variation of the slope of the curve (Permeability versus PEG content) at low PEG content as a function of PEG molar mass. c) Variation of the maximal water permeability as a function of PEG molar mass used in the composition of the PEGDA/PEG hydrogel membrane. The red solid line represents the water permeability of the conventional PEGDA hydrogel membrane without PEG chains ($K \sim 10^{-18} \text{ m}^2$). The dashed lines are represented as a guide for the eyes.

4.5.2 Fraction of the PEG chains trapped in the PEGDA matrix

In Chapter 2, we have shown that the chains of PEG-300 000 g.mol^{-1} are irreversibly trapped in the hydrogels and do not get flushed out even over several filtration cycles and play a key role in the permeability of the hydrogels. In this Section, our goal is to determine whether the molar mass of the PEG chains influences the amount of chains trapped.

We analyze the content of PEG released from the hydrogel in the water supernatant, where it is kept overnight, as well as in the permeate after a cyclic filtration, by total organic carbon (TOC) analysis. The fraction of PEG that we calculate is the ratio of PEG molecules found in the permeate divided by the total amount of PEG initially present in the hydrogels and is therefore calculated using (Equation 4.4):

$$f = \frac{C_{\text{permeate}} * V_{\text{permeate}}}{\phi_{\text{PEG}} * \rho_{\text{hydrogel}} * V_{\text{hydrogel}}} \quad (4.4)$$

where C_{permeate} (mg.L^{-1}) is the concentration in the permeate measured by TOC, V_{permeate} (L) is the volume of permeate, ϕ_{PEG} (wt%) is the weight fraction of PEG in the hydrogel, ρ_{hydrogel} is the volumic mass of the hydrogel taken equal to $\rho_{\text{water}} = 10^6 \text{ mg.L}^{-1}$ and V_{hydrogel} is the volume of the hydrogel membrane (L).

As presented in Figure 4.3, the fraction of PEG calculated in the supernatant depends on the PEG molar mass. For the small PEGs (i.e. PEG-600 and 3000 g.mol^{-1}), 20 % of the PEG initially

present in the PEGDA/PEG hydrogel are released from the hydrogel membranes into the supernatant (Figure 4.3 a and b) while 80% remain trapped in the sample. However, less than 4 % of PEG chains can be found in the supernatant for the large PEG chains of 300 000 g.mol⁻¹ (Figure 4.3 c). In contrast, the fraction of PEG calculated in the permeate after a cyclic filtration is negligible (< 1%), regardless the molar mass.

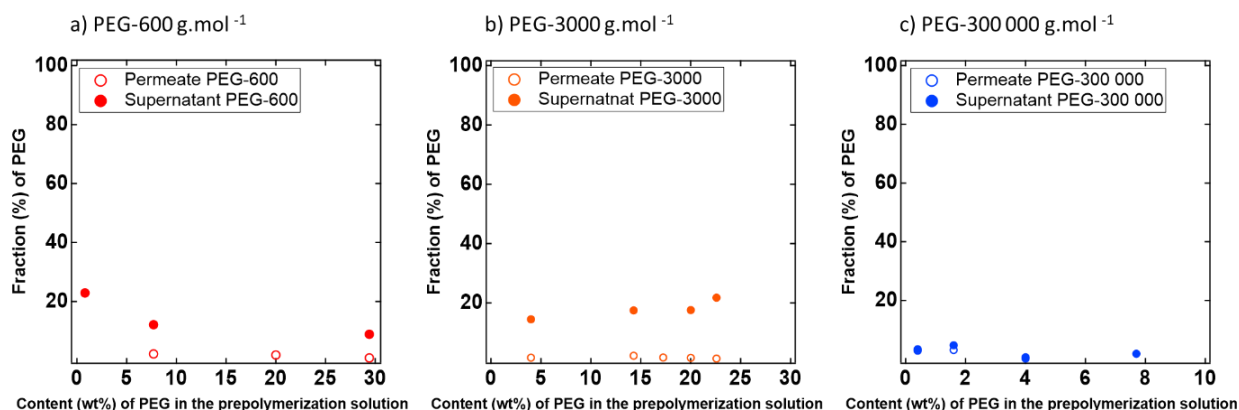


Figure 4.3. Variation of the fraction of PEG calculated in the supernatant liquid (solid symbol) and in the permeate after cyclic filtration (empty symbol) as a function of the content (wt%) of PEG in the prepolymerization solution for a) PEG-600, b) PEG-3000 and c) PEG-300 000 g.mol⁻¹.

To account for the irreversible incorporation of most PEG chains in the PEGDA matrix, we suggest that the PEG chains are chemically grafted to the PEGDA matrix and that this occurs through a chain transfer mechanism where the radicals transfer to the PEG chains. Such a chain transfer mechanism has been observed by Nandi *et al.*⁴⁰ during the radical polymerization of methyl methacrylate, MMA, in the presence of various glycols through the rupture of the C-H bonds of the glycol next to the OH group. As a result, the glycols get covalently grafted to the PMMA chains. We suggest that such a transfer reaction occurs between the PEG chains and the active PEGDA chains. To confirm this hypothesis, we propose a simple experiment. We prepare a solution containing poly (ethylene glycol) monomethacrylate, PEGMA, and PEG chains, in the presence of a photoinitiator, and illuminate with UV light. As PEGMA is monofunctional with only one acrylate function instead of two for the PEGDA oligomer (see Figure 4.4), we do not expect a hydrogel formation if the PEG chains remain free; we only expect the polymerization of PEGMA into PEGMA polymer chains hence a moderate increase of the viscosity. However, we obtain a hydrogel after about 10 min of UV irradiation, in the presence of PEG chains, while the pure PEGMA sample does not produce a hydrogel. This

simple experiment tells us that the PEG chains probably react chemically with the acrylate functions (see Figure S4.3) and get covalently grafted to the network. This experiment has been done by Sixtine de Chateauneuf-Randon.

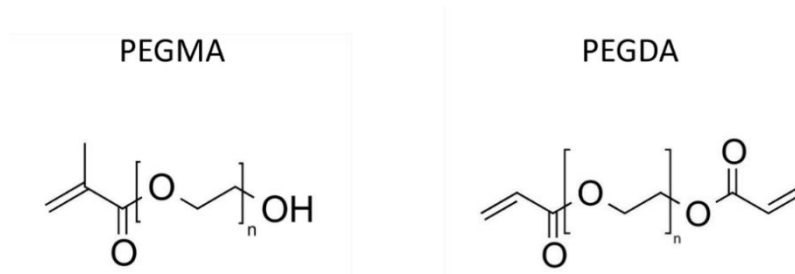


Figure 4.4. Chemical structure of poly (ethylene glycol) monomethacrylate PEGMA and poly (ethylene glycol) diacrylate PEGDA.

4.5.3 Role of PEG concentration and molar mass on hydrogel's structure

In order to understand the relation between the PEGDA/PEG hydrogel permeability and structure and how this depends on the PEG content, we perform AFM and cryoSEM measurements. CryoSEM measurements are performed with PEG molar mass of 600 g.mol⁻¹, 3000 g.mol⁻¹, 300 000 g.mol⁻¹ and 600 000 g.mol⁻¹. However, for the sake of clarity we only present in Figure 4.5 the results obtained with PEG 3000 g.mol⁻¹ and 600 000 g.mol⁻¹, while the other molar masses are presented in Figure S4.4. As a reference, the case of PEGDA without PEG is given in Figure 4.5 a.

As discussed in Molina's article⁴¹ and in Chapters 2 and 3, the 200 nm large cavities observed with the PEGDA sample correspond to the water in excess that is rejected from the PEGDA matrix whose equilibrium polymer/water fraction is 50/50 wt%/wt%. As discussed in the previous Chapters, these cavities are most probably closed leading to a low intrinsic permeability.

Adding 4 wt% of PEG-3000 $\text{g}\cdot\text{mol}^{-1}$ induces a slight increase in the size of the cavities up to ~ 500 nm (Figure 4.5 b). For some of the cavities, darker zones -marked with arrows- reveal areas which extend in depth in the direction perpendicular to the plane of observation and correspond to water that is sublimated during the successive sublimation cycles. These observations show that a weak fraction of these pores seems to be open in contrary to the case of pure PEGDA for which these cavities are closed. For the 17 wt% of PEG samples (Figure 4.5 c), the size of the cavities increases and reaches sizes of the order of one micron. In this case also, some of the cavities seem to extend in depth.

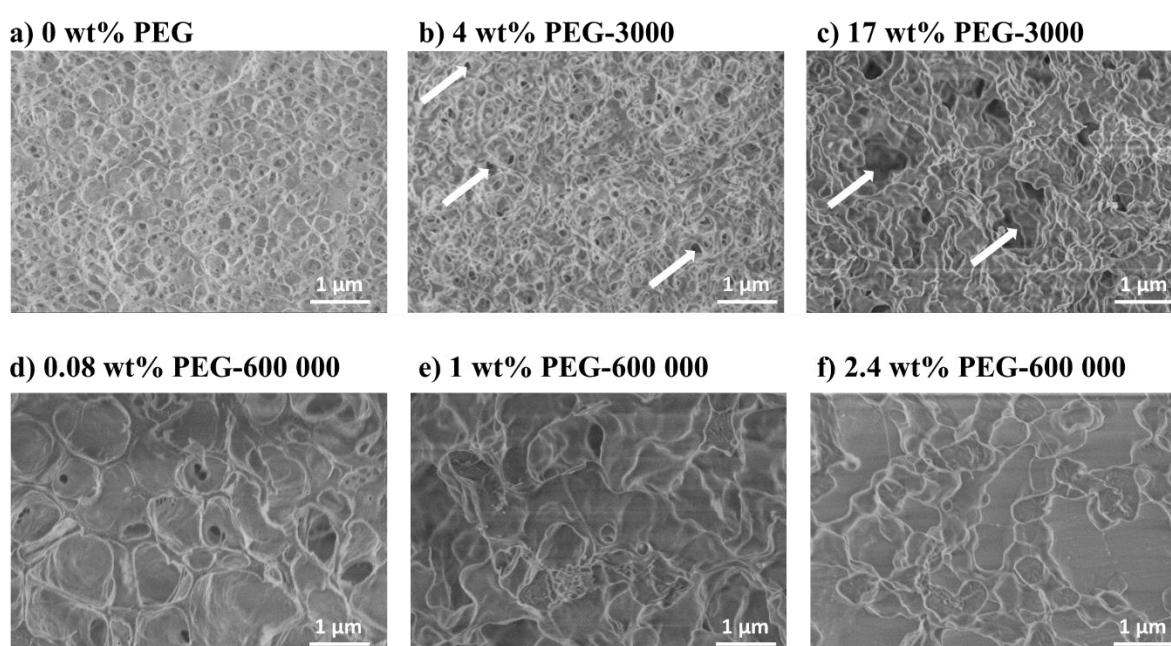


Figure 4.5. CryoSEM images of hydrogel membranes prepared with PEGDA and various content of PEG-3000 $\text{g}\cdot\text{mol}^{-1}$ a) 0; b) 4 and c) 17 wt% and PEG-600 000 $\text{g}\cdot\text{mol}^{-1}$ d) 0.08; e) 1 and f) 2.4 wt%.

For PEG-600 000 $\text{g}\cdot\text{mol}^{-1}$, micron size cavities are observed similarly to the results of PEG-300 000 $\text{g}\cdot\text{mol}^{-1}$ discussed in Chapter 3. In this case we do not detect an extension of the cavities in the direction perpendicular to the plane of observation. These results confirm previous filtration and permeation measurements from which we concluded that these micron size cavities probably do not form a percolating network and that the permeation of water and nanoparticles is rather controlled by the structure of the PEGDA rich walls between these micron size cavities. To obtain more insight into the wall structure, we perform AFM measurements with a field of view of $10\ \mu\text{m}$ for the various PEG molar mass at various concentrations below and above C^* .

For reasons of image clarity, the Z-scales are not identical for all images. The average Z-scale is ± 50 nm.

The AFM images obtained for PEGDA/PEG hydrogels prepared with various content of PEG-3000 $\text{g}\cdot\text{mol}^{-1}$ are represented in Figure 4.6. As shown in Figure 4.6 b, the addition of low content of PEG (i.e. 0.4 wt%) does not affect significantly the PEGDA hydrogel structure which present a distribution of pores of typical size ~ 200 nm. However, the addition of 0.8 wt% of PEG (Figure 4.6 c) leads to the formation of a small number of larger cavities of size ~ 500 nm, marked with dashed circle. For 4 wt% of PEG added, we observe an increased number of these large cavities (Figure 4.6 d). The same trend is observed for PEG 600 and 10 000 $\text{g}\cdot\text{mol}^{-1}$ as represented in Figure S4.5.

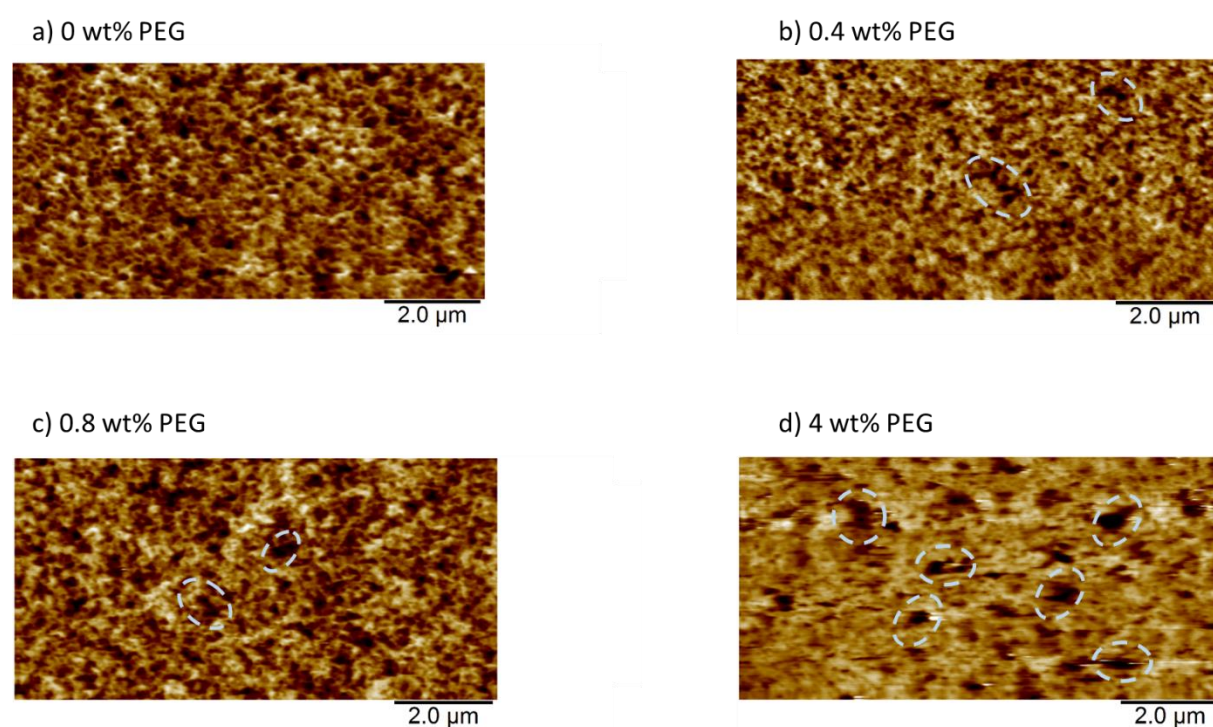


Figure 4.6. Surface AFM images of PEGDA hydrogels membranes prepared with 16 wt % of PEGDA and various content of PEG-3000 $\text{g}\cdot\text{mol}^{-1}$ a) 0; b) 0.4; c) 0.8 and d) 4 wt%.

The average Z-scale is ± 50 nm.

For hydrogel prepared with PEG-35 000 $\text{g}\cdot\text{mol}^{-1}$, a low content of PEG (i.e. 0.4 wt%) does not significantly modify the structure (Figure 4.7 a). When the PEG content increases to 0.8 wt%, some large cavities of size ~ 500 nm to $1\ \mu\text{m}$ can be seen as well as small cavities of the order of tens of nanometers. When the PEG content increases to 2.4 wt% and then 4 wt% (C^*), a micron size valleys and hills can be observed, which presumably correspond to the micron size cavities observed with cryoSEM. This micron size structure presents a very low rugosity at the nanometric scale, similarly to the results obtained with PEG-300 000 $\text{g}\cdot\text{mol}^{-1}$ and presented in Chapters 2 and 3.

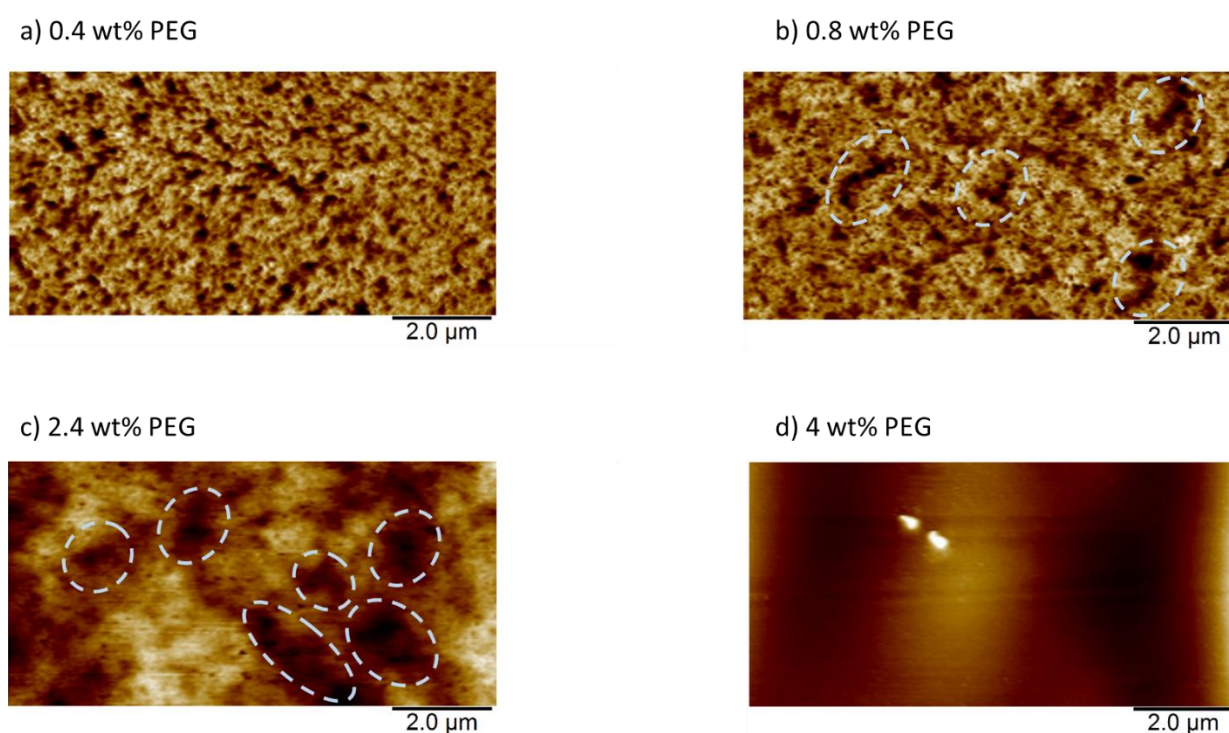


Figure 4.7. Surface AFM images of PEGDA hydrogels membranes prepared with 16 wt % of PEGDA and various content of PEG-35 000 $\text{g}\cdot\text{mol}^{-1}$ a) 0.4; b) 0.8; c) 2.4 and d) 4 wt%.

The average Z-scale is ± 50 nm.

4.6 DISCUSSION

In Chapter 3 we have proposed an evolution of the structure with the PEG concentration which is presented again in Figure 4.8 which we rediscuss now in light of the new results presented in Chapter 4. At PEG concentrations below C^* , we suggested that the PEG chains are trapped in the PEGDA rich walls separating the micron size heterogeneities and provide local defects in the cross-linking density which enables an increase of the water permeation flux. Some of the PEG chains trapped in the PEGDA walls may also decorate the internal surface of the micron

size cavities and form an elongated brush which slows down the water permeation above the PEG overlap concentration. Given the similar trend of the permeability curves and the AFM/cryoSEM measurements observed for the various molar masses this scenario seems robust.

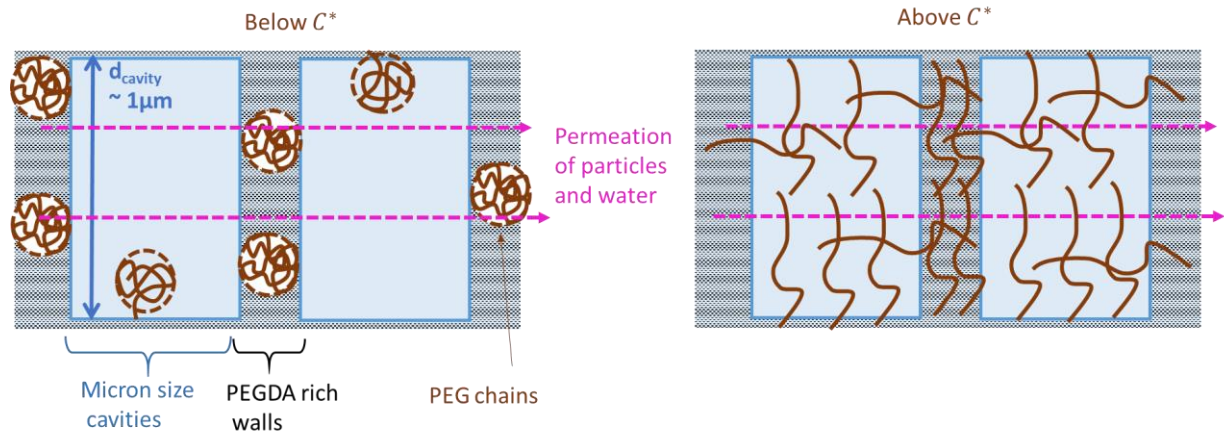


Figure 4.8. Schematic propositions of the hydrogel structure that may account for our results. Illustration of the permeation of water and nanoparticles through the PEGDA/PEG hydrogel membranes. a) At low PEG concentrations, PEG chains trapped in the walls separating the micron sized cavities control the permeation of the particles and water through the hydrogels. b) At higher PEG concentration, PEG chains partially trapped in the PEGDA matrix decorate the PEGDA rich inner walls of the cavities and form dense brushes that slow down the permeation of water and particles.

Nevertheless, we now would like to discuss the following questions:

- 1) What sets the size of the cavities and the wall structure? Why do micron size cavities are observed for PEG/PEGDA hydrogels while the PEGDA hydrogels present smaller cavities of the order of 200 nm? Why do the walls of these micron cavities become more homogeneous at the nanometric scale as the PEG concentration increases up to C^* and why does this correlate with an increase of the permeability ?
- 2) Why do we observe a maximum water permeability with the PEG molar mass obtained for PEG-35 000 g.mol⁻¹?

To answer these questions, we have to consider the study of Molina *et al.*⁴¹ concerning PEGDA/water systems which enables us to discuss the polymerization process with and without added PEG.

Molina *et al.* have shown using SANS measurements that PEGDA/water hydrogels are composed of water cavities coexisting with a PEGDA/water matrix that is characterized by a fixed ratio of water/PEGDA of 50/50 which does not depend significantly on the PEGDA molar mass. Adding water into the system at a weight fraction above this ratio results in a phase separation, where the water in excess forms cavities whose volume fraction is noted Φ_{cavities} hereafter (NB: it is noted Φ_{voids} in Molina's article, explained in Chapter 1 of this thesis manuscript, pages 40 and 41). When the total PEGDA content in the sample increases (noted Φ_0 in Molina's article), the fraction of water in the PEGDA/water matrix, called $\Phi_{\text{matrix water}}^{\text{matrix}}$ ($1 - \Phi_{0,n}$ in Molina's article) remains constant and equal to 50 wt% while by mass conservation Φ_{cavities} has to decrease (black lines in Figure 4.9). We suggested earlier in this thesis that these water cavities are closed and that they are trapped in the PEGDA matrix during the polymerization process. In other words, their coalescence or coarsening is probably "frozen" by the fast polymerization of the PEGDA matrix which is rigid and weakly permeable.

Let us now discuss the evolution of the water cavities and their walls when PEG is added in the system. We know from our TOC measurements that PEG chains are trapped irreversibly in the hydrogels and that they are probably covalently attached to the PEGDA polymerizing network. This phenomenon can have two main consequences on the polymerization process and final structure of the hydrogel:

- a) As the PEG chains are incorporated in the PEGDA polymerizing matrix, the PEG/PEGDA matrix becomes softer and more permeable, which would increase the probability for the water in excess expelled from the polymerizing matrix to coalesce or coarsen to form larger cavities. This phenomenon would explain why the 200 nm cavities are not observed in the walls between the micron cavities. Indeed, the water in excess gathers in micron large cavities.
- b) The incorporation of PEG chains induces local defects in the PEGDA cross-linking density which would enable the PEGDA/PEG matrix to incorporate a fraction of water $\Phi_{\text{matrix water}}^{\text{matrix}} > 50$ wt%. Indeed, in principle the water fraction results from a balance between entropic elasticity of the short PEGDA chains and enthalpic gain due to affinity

between the PEGDA and water. Adding long PEG chains may reduce the entropic cost associated with water incorporation. Increasing the equilibrium water fraction $\Phi_{\text{water}}^{\text{matrix}}$ of the PEGDA rich matrix above 50 wt% would then induce a lower amount of water in excess (we have 80 wt% of water in the solution) and a lower volume of water to be expelled to form the cavities explaining why the size of the cavities in the PEGDA rich walls decreases with the PEG content.

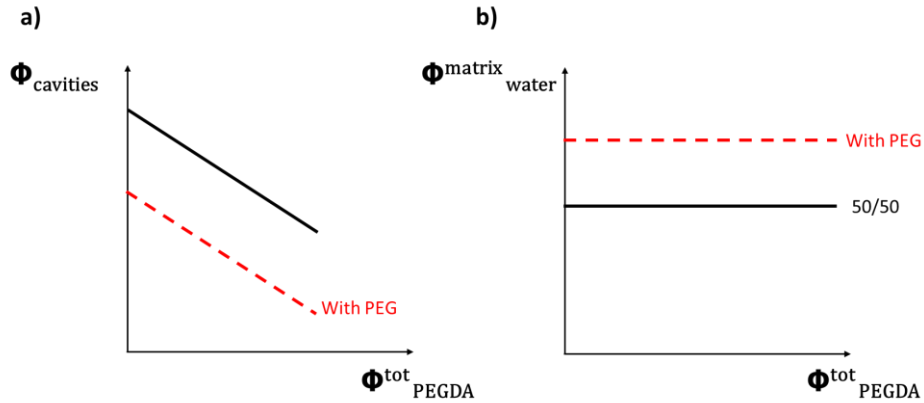


Figure 4.9. a) Variation of cavities volume fraction and b) Water volume fraction in the PEGDA matrix as a function of the total PEGDA polymer volume fraction.

Can we now explain why K presents a maximum with the PEG molar mass of $35\,000\text{ g}\cdot\text{mol}^{-1}$? Considering that PEG chains induce cross-linking defects in the PEGDA matrix we expect that the permeability will increase with the number of defects hence with the PEG content, C , and with r_g , the size of the polymer coils. This hypothesis would enable us to account for the fact that the slope of the $K(C)$ curves increases with the molar mass as shown in Figure 4.2 b. However, this hypothesis does not enable us to account easily for the non-monotonic evolution of K^* with the molar mass. However, if we now consider that close to C^* , the PEG chains form a dense brush at the surface of the micron size cavities we expect that the length of the brush will increase with the PEG molar mass, leading to a decrease of the permeability with the molar mass. These two effects depending on the molar mass in the opposite trend and being probably present at C^* may account for the non-monotonic variation of K^* with the PEG molar mass.

4.7 CONCLUSION

We developed a series of composite hydrogel membranes obtained by a simple photopolymerization of PEGDA under UV light in the presence of PEG chains with a wide range of molar mass (between 600 and 600 000 g.mol⁻¹). Compared to the literature studies, we have shown that regardless the molar mass, most PEG chains remain irreversibly trapped in the hydrogel matrix during filtration experiments. Increasing the content of PEG chains in the hydrogel system allowed tuning the PEGDA/PEG water permeability over several orders of magnitude. In addition, we showed that the existence of a maximum of the permeability obtained for the critical overlap concentration of PEG chains is a robust phenomenon observed for different PEG molar masses. We show that the maximum permeability at C^* follows a non-monotonic trend with the molar mass and is maximum for PEG-35 000 g.mol⁻¹. We suggest that the permeability increase below C^* is due to the PEG chains trapped in the PEGDA matrix that induce defect in the cross-linking density of the PEGDA walls between micron size cavities observed with cryoSEM. Above C^* the permeability decrease is probably due to the fact that the PEG chains partially trapped in the PEGDA matrix may form a brush decorating the interior of the cavities and slows down the permeation of water.

References

1. Okay, O., Macroporous copolymer networks. *Prog. Polym. Sci.* **2000**, *25* (6), 711-779, DOI 10.1016/S0079-6700(00)00015-0.
2. Lin, C. Y.; Wang, Y. R.; Lin, C. W.; Wang, S. W.; Chien, H. W.; Cheng, N. C.; Tsai, W. B.; Yu, J., Peptide-modified zwitterionic porous hydrogels for endothelial cell and vascular engineering. *Biores Open Access* **2014**, *3* (6), 297-310, DOI 10.1089/biores.2014.0048.
3. Simona, B. R.; Hirt, L.; Demkó, L.; Zambelli, T.; Vörös, J.; Ehrbar, M.; Milleret, V., Density gradients at hydrogel interfaces for enhanced cell penetration. *Biomater. Sci.* **2015**, *3* (4), 586-591, DOI 10.1039/C4BM00416G.
4. Chung, B. G.; Lee, K. H.; Khademhosseini, A.; Lee, S. H., Microfluidic fabrication of microengineered hydrogels and their application in tissue engineering. *Lab on a chip* **2012**, *12* (1), 45-59, DOI 10.1039/c1lc20859d.
5. Pi, J.-K.; Yang, H.-C.; Wan, L.-S.; Wu, J.; Xu, Z.-K., Polypropylene microfiltration membranes modified with TiO₂ nanoparticles for surface wettability and antifouling property. *J. Membr. Sci.* **2016**, *500*, 8-15, DOI 10.1016/j.memsci.2015.11.014.
6. Pourjavadi, A.; Nazari, M.; Kabiri, B.; Hosseini, S. H.; Bennett, C., Preparation of porous graphene oxide/hydrogel nanocomposites and their ability for efficient adsorption of methylene blue. *RSC Advances* **2016**, *6* (13), 10430-10437, DOI 10.1039/C5RA21629J.
7. Gama, N. V.; Ferreira, A.; Barros-Timmons, A., Polyurethane Foams: Past, Present, and Future. *Materials (Basel)* **2018**, *11* (10), DOI 10.3390/ma11101841.
8. Michael, S. S., PolyHIPEs: Recent advances in emulsion-templated porous polymers. *Prog. Polym. Sci.* **2014**, *39*, 199-234, DOI 10.1016/j.progpolymsci.2013.07.003.
9. Chiu, Y. C.; Larson, J. C.; Isom, A., Jr.; Brey, E. M., Generation of porous poly(ethylene glycol) hydrogels by salt leaching. *Tissue Eng. Part C: Methods* **2010**, *16* (5), 905-912, DOI 10.1089/ten.TEC.2009.0646.
10. Dadsetan, M.; Hefferan, T. E.; Szatkowski, J. P.; Mishra, P. K.; Macura, S. I.; Lu, L.; Yaszemski, M. J., Effect of hydrogel porosity on marrow stromal cell phenotypic expression. *Biomaterials* **2008**, *29* (14), 2193-2202, DOI 10.1016/j.biomaterials.2008.01.006.
11. Chiu, Y.-C.; Cheng, M.-H.; Engel, H.; Kao, S.-W.; Larson, J. C.; Gupta, S.; Brey, E. M., The role of pore size on vascularization and tissue remodeling in PEG hydrogels. *Biomaterials* **2011**, *32* (26), 6045-6051, DOI 10.1016/j.biomaterials.2011.04.066.

12. Turani-i-Belloto, A.; Brunet, T.; Khaldi, A.; Leng, J., A Sacrificial Route for Soft Porous Polymers Synthesized via Frontal Photo-Polymerization. *Polymers* **2020**, *12* (5), 1008, DOI 10.3390/polym12051008.
13. Orsi, S.; Guarnieri, D.; Netti, P. A., Design of novel 3D gene activated PEG scaffolds with ordered pore structure. *J. Mater. Sci : Mater. Med.* **2010**, *21* (3), 1013-1020, DOI 10.1007/s10856-009-3972-1.
14. Goh, M.; Kim, Y.; Gwon, K.; Min, K.; Hwang, Y.; Tae, G., In situ formation of injectable and porous heparin-based hydrogel. *Carbohydr. Polym.* **2017**, *174*, 990-998, DOI 10.1016/j.carbpol.2017.06.126.
15. Sokic, S.; Christenson, M.; Larson, J.; Papavasiliou, G., In Situ Generation of Cell-Laden Porous MMP-Sensitive PEGDA Hydrogels by Gelatin Leaching. *Macromol. Biosci.* **2014**, *14* (5), 731-739, DOI 10.1002/mabi.201300406.
16. Shao, L.; Gao, Q.; Xie, C.; Fu, J.; Xiang, M.; Liu, Z.; Xiang, L.; He, Y., Sacrificial microgel-laden bioink-enabled 3D bioprinting of mesoscale pore networks. *Bio-Des. Manuf.* **2020**, *3* (1), 30-39, DOI 10.1007/s42242-020-00062-y.
17. Savina, I. N.; Ingavle, G. C.; Cundy, A. B.; Mikhalovsky, S. V., A simple method for the production of large volume 3D macroporous hydrogels for advanced biotechnological, medical and environmental applications. *Sci. Rep.* **2016**, *6* (1), 21154, DOI 10.1038/srep21154.
18. Fernández-Rico, C.; Sai, T.; Sicher, A.; Style, R. W.; Dufresne, E. R., Putting the Squeeze on Phase Separation. *JACS Au.* **2022**, *2* (1), 66-73, DOI 10.1021/jacsau.1c00443.
19. Xue, L.; Zhang, J.; Han, Y., Phase separation induced ordered patterns in thin polymer blend films. *Prog. Polym. Sci.* **2012**, *37*, 564-594, DOI 10.1016/j.progpolymsci.2011.09.001.
20. Wang, D.-M.; Lai, J.-Y., Recent advances in preparation and morphology control of polymeric membranes formed by nonsolvent induced phase separation. *Curr. Opin. Chem. Eng.* **2013**, *2*, 229–237, DOI 10.1016/j.coche.2013.04.003.
21. Dušek, K., Phase separation during the formation of three-dimensional polymers. *J. Polym. Sci., Part B: Polym. Lett.* **1965**, *3* (3), 209-212, DOI 10.1002/pol.1965.110030311.
22. Dušek, K. In *Phase separation during the formation of three-dimensional polymers*, J. Polym. Sci., Part C: Polym. Symp., Wiley Online Library: 1967; pp 1289-1299.
23. Dusek, K., Inhomogeneities induced by crosslinking in the course of crosslinking copolymerization. In *Polymer Networks*, Springer: 1971; pp 245-260.
24. Okada, M.; Fujimoto, K.; Nose, T., Phase separation induced by polymerization of 2-chlorostyrene in a polystyrene/dibutyl phthalate mixture. *Macromolecules* **1995**, *28* (6), 1795-1800, DOI 10.1021/ma00110a011.

25. Okada, M.; Sun, J.; Tao, J.; Chiba, T.; Nose, T., Phase separation kinetics and morphology in the critical to off-critical crossover region. *Macromolecules* **1995**, *28* (22), 7514-7518, DOI 10.1021/ma00126a031.
26. Boots, H.; Kloosterboer, J.; Serbutoviez, C.; Touwslager, F., Polymerization-Induced Phase Separation. 1. Conversion– Phase Diagrams. *Macromolecules* **1996**, *29* (24), 7683-7689, DOI 10.1021/ma960292h.
27. Eliçabe, G. E.; Larrondo, H. A.; Williams, R. J., Polymerization-induced phase separation: A maximum in the intensity of scattered light associated with a nucleation-growth mechanism. *Macromolecules* **1997**, *30* (21), 6550-6555, DOI 10.1021/ma9707547.
28. Eliçabe, G. E.; Larrondo, H. A.; Williams, R. J., Light scattering in the course of a polymerization-induced phase separation by a nucleation-growth mechanism. *Macromolecules* **1998**, *31* (23), 8173-8182, DOI 10.1021/ma9805304.
29. Kwok, A. Y.; Prime, E. L.; Qiao, G. G.; Solomon, D. H., Synthetic hydrogels 2. Polymerization induced phase separation in acrylamide systems. *Polymer* **2003**, *44* (24), 7335-7344, DOI 10.1016/j.polymer.2003.09.026.
30. Chompff, A., *Polymer Networks: Structure and Mechanical Properties*. Springer Science & Business Media: 2013.
31. Wu, Y.-H.; Park, H. B.; Kai, T.; Freeman, B.; Kalika, D., Water uptake, transport and structure characterization in poly(ethylene glycol) diacrylate hydrogels. *J. Membr. Sci.* **2010**, *347*, 197-208, DOI 10.1016/j.memsci.2009.10.025.
32. Yoon, S.-S.; Kim, J.-H.; Kim, S.-C., Synthesis of biodegradable PU/PEGDA IPNs having micro-separated morphology for enhanced blood compatibility. *Polym. Bull.* **2005**, *53* (5), 339-347, DOI 10.1007/s00289-005-0355-8.
33. Saimani, S.; Kumar, A., Semi-IPN asymmetric membranes based on polyether imide (ULTEM) and polyethylene glycol diacrylate for gaseous separation. *J. Appl. Polym. Sci.* **2008**, *110* (6), 3606-3615, DOI 10.1002/app.28862.
34. Ouasti, S.; Donno, R.; Cellesi, F.; Sherratt, M. J.; Terenghi, G.; Tirelli, N., Network connectivity, mechanical properties and cell adhesion for hyaluronic acid/PEG hydrogels. *Biomaterials* **2011**, *32* (27), 6456-6470, DOI 10.1016/j.biomaterials.2011.05.044.
35. Kang, G.; Cao, Y.; Zhao, H.; Yuan, Q., Preparation and characterization of crosslinked poly (ethylene glycol) diacrylate membranes with excellent antifouling and solvent-resistant properties. *J. Membr. Sci.* **2008**, *318* (1-2), 227-232, DOI 10.1016/j.memsci.2008.02.045.

36. Susanto, H.; Balakrishnan, M.; Ulbricht, M., Via surface functionalization by photograft copolymerization to low-fouling polyethersulfone-based ultrafiltration membranes. *J. Membr. Sci.* **2007**, 288 (1-2), 157-167, DOI 10.1016/j.memsci.2006.11.013.
37. Eddine, M. A.; Belbekhouche, S.; de Chateauneuf-Randon, S.; Salez, T.; Kovalenko, A.; Bresson, B.; Monteux, C., Large and Nonlinear Permeability Amplification with Polymeric Additives in Hydrogel Membranes. *Macromolecules* **2022**, 55 (21), 9841-9850, DOI 10.1021/acs.macromol.2c01462.
38. Rubinstein, M.; Colby, R. H., *Polymer physics*. Oxford university press New York: 2003; Vol. 23.
39. Kawaguchi, S.; Imai, G.; Suzuki, J.; Miyahara, A.; Kitano, T.; Ito, K., Aqueous solution properties of oligo-and poly (ethylene oxide) by static light scattering and intrinsic viscosity. *Polymer* **1997**, 38 (12), 2885-2891, DOI 10.1016/S0032-3861(96)00859-2.
40. Nandi, U.; Kumar, G. S.; Bhaduri, C., Chain Transfer of Glycols in Polymerization of Methyl Methacrylate. *Indian Journal of Chemistry* **1981**, 20A, 759-763,
41. Malo de Molina, P.; Lad, S.; Helgeson, M. E., Heterogeneity and its Influence on the Properties of Difunctional Poly(ethylene glycol) Hydrogels: Structure and Mechanics. *Macromolecules* **2015**, 48 (15), 5402-5411, DOI 10.1021/acs.macromol.5b01115.

Conclusion & Perspectives

Hydrogels, which are networks of polymer chains in water, have porous and hydrophilic structures that have recently attracted the attention of researchers in the context of filtration and wastewater treatment. Their network structure, morphology and porosity enable the control of the diffusion and transport of different species and particles.

In this context, previous studies reported in the literature have mainly described the use of hydrogels as coating films on hydrophobic surfaces of conventional filtration membranes in order to improve their fouling resistance. However, the use of free-standing hydrogel membranes and the control of their porosity structure and permeability properties are rarely studied for filtration applications.

In this study, we were interested in developing a hydrogel system, with well-controlled permeability properties, formed in one-step process and capable of withstanding the pressure applied during the filtration experiment. For this purpose, we prepared different series of hydrogel membranes by the photopolymerization of a mixture of poly (ethylene glycol) diacrylate (PEGDA) and poly (ethylene glycol) (PEG) chains. We studied the effect of PEG concentration and molar mass (variable molar masses between 600 and 600 000 g.mol⁻¹) on the water permeability, mechanical properties and particles selective filtration of PEGDA/PEG composite membranes. Moreover, we investigated the evolution of the hydrogel structures, obtained by atomic force microscopy (AFM) and cryoscanning electron microscopy (cryoSEM) measurements. We further suggested an organization of the PEG chains in the PEGDA matrix that may account for most of our structural and permeability measurements.

The main conclusions obtained are highlighted below:

Roles of PEG concentration and molar mass on water intrinsic permeability at low applied pressure

In this study, the main objective was to investigate the effect of the addition of PEG chains on the water intrinsic permeability of PEGDA/PEG hydrogel membrane at low applied pressure. Compared to our reference PEGDA hydrogel membrane, we found that the addition of PEG chains, with different concentration and molar mass, allows to tune the water permeability over several orders of magnitude. For the low PEG chains added in the system

(e.g. 600 and 3000 g.mol⁻¹), we obtained a continuous increase of the permeability K with the PEG content. However, for the high PEG molar masses studied (10 000; 35 000; 300 000 and 600 000 g.mol⁻¹), the water permeability increases similarly with the content of PEG, until it reaches an optimum for a critical concentration of PEG. Above this critical concentration, the water permeability decreases as the PEG content increases. Interestingly, we found that this concentration corresponds to the critical overlap concentration of PEG chains, noted C^* , which marks the transition between a diluted and a semi-diluted regime for a polymer solution in water. Consequently, we obtained a robust phenomenon where the PEG concentration is a key parameter to control the water permeability of the composite hydrogel. In addition, the maximum of permeability obtained at C^* was applied to PEG chains of varying molar masses.

Non-linear intrinsic permeability variation with the pressure

We studied the effect of applied pressure on the water permeability for different PEGDA/PEG hydrogel membranes. In the presence of PEG chains, we obtained a non-linear variation of the water flux as a function of the applied pressure, in contrast to the case of the reference PEGDA sample. We observed that water fluxes reach a plateau above pressures of the order of 500 mBar, depending on PEG contents or molar masses. In addition, we obtained that the loss of permeability increases with the PEG concentration. We showed that the loss of permeability is due to the compression of the hydrogels upon applied pressure. We studied the mechanical properties of the hydrogels using compression experiments. We found first that the high strain imposed on the hydrogel membrane (e.g ~ 30 %), led to the expulsion of water from the hydrogel membrane containing different content of PEG chains, contrary to the pure PEGDA hydrogel without water expulsion. This result showed that adding PEG into the membranes leads to an opening of the hydrogel porosity. In addition, we found that the PEG-containing samples had a lower effective modulus than PEGDA hydrogels without PEG. The value of Young's moduli calculated for low strains decreased when the PEG content increases, for different molar mass. This softening of the hydrogels with the PEG content correlates well with the fact that the permeability loss increases with the PEG content. Consequently, we suggested that the non-linear variation of the permeability with the pressure was due to the compression of the hydrogels and the reduction of the pore size under the action of a large pressure.

Influence of PEG content on PEGDA/PEG hydrogel's morphological structure

The next challenge of this work was to understand the effect of PEG chains, with different content and molar mass, on the structuration of the PEGDA matrix. First, we confirmed that the PEGDA polymerization reaction was complete even after the addition of PEG chains of different concentrations. We then analyzed the content of PEG released from the hydrogel in the water supernatant, as well as in the permeate after a cyclic filtration. We found that for small PEG chains (i.e. 600 and 3000 g.mol⁻¹), most of the chains remain irreversibly trapped in the matrix. Moreover, for PEG with high molar mass (i.e. 300 000 g.mol⁻¹), 96 % of the chains remained trapped in the matrix during the complete rinsing and filtration process. To account for these results, we hypothesized that the PEG chains may be chemically grafted to the PEGDA matrix through a chain transfer mechanism where the radicals transfer to the PEG chains.

In order to obtain insight into the structure of the PEG/PEGDA hydrogels, we employed atomic force microscopy (AFM) and cryoscanning electron microscopy (cryoSEM) measurements. We showed first that the conventional PEGDA hydrogels, prepared without PEG, present a distribution of cavities of diameter ~ 200 nm, which are filled with water due to a phase separation between PEGDA ($\overline{M}_w=700$ g.mol⁻¹) and water, consistently with literature studies. Upon the addition of PEG, we observed a change in PEGDA hydrogel structure with the appearance of larger cavities of ~ 1 μ m, evidenced by cryoSEM images, for different PEG molar mass. Correlating these observations with our permeability results, we suggested that the 200 nm cavities for the reference PEGDA sample are closed and that the permeation of water is controlled by the PEGDA matrix. In addition, for the PEGDA/PEG hydrogel membranes, we assumed that the observed micron size cavities probably do not form a percolating network and that the permeation of water is rather controlled by the structure of the PEGDA rich walls between these micron size cavities. Using AFM measurements, we showed that the structure of PEGDA-rich wall was largely affected upon the addition of PEG chains. We observed the presence of nanoscale heterogeneities of a few tens of nanometers in the PEGDA rich walls between the micron size cavities. Moreover, for high PEG content (i.e. 4 wt% of PEG-35 000 g.mol⁻¹ and PEG-300 000 g.mol⁻¹), we noticed that the walls of the micron size cavities became homogenous at a nanometric scale. Correlating again these results with our permeability measurements, we proposed that the presence of PEG chains, trapped in the PEGDA rich walls, provides local nanoscale defects in the cross-linking density which enables an increase of the

water permeation flux at low PEG concentration. However, at high PEG content, some of the PEG chains may also decorate the internal surface of the micron size cavities and form an elongated brush which consequently slows down the water permeation and would account for the permeability decrease above C^* .

Filtration of particles through the PEGDA/PEG hydrogel membranes

We investigated the filtration of polystyrene particles of different size: 20 nm, 100 nm and 1 μm through a PEGDA membrane prepared with various content of PEG-300 000 $\text{g}\cdot\text{mol}^{-1}$. First, we obtained that the permeation of 20 nm particle depends on both the PEGDA/PEG composition and the pressure applied during filtration. For hydrogel prepared with pure PEGDA and PEGDA with high content of PEG (above the critical overlap concentration), we found that the polystyrene nanoparticles of 20 nm do not permeate through the hydrogels even under the highest applied pressure of 800 mBar. Their concentration calculated in the recovered permeate was zero. However, the most permeable hydrogel prepared with the critical overlap concentration of PEG-300 000 $\text{g}\cdot\text{mol}^{-1}$ allowed the passage of 20 nm particles but not the permeation of the largest particles with 100 nm and 1 μm in diameter.

These results suggest that the permeation of water and particle is controlled by the nanometric defects created by trapped PEG chains in the PEGDA walls between the micron size cavities.

Perspectives

Further progress in this domain could be investigated in order to complete the filtration and structural studies of our PEGDA/PEG hydrogel system.

Concerning the hydrogel structure, further studies can be performed to complement the one we conducted on the PEGDA/PEG hydrogel system. For example, small angle X-ray (SAXS) and neutron scattering (SANS) measurements are well-suited techniques to characterize the nanostructure heterogeneity in polymer hydrogels. In our case, due to the similar structure of PEGDA and PEG, the use of SANS measurement is more suitable as the scattering contrast can be easily enhanced by using a deuterated PEG. Consequently, this technique will probe only the PEGDA structure and therefore determine the direct effect of PEG addition on the PEGDA matrix structure.

Furthermore, by using functionalized PEG and PEGDA chains with two different fluorescent dyes, we can perform confocal microscopy to determine how the PEG chains are organized in

the PEGDA matrix as a function of their concentration. Our first preliminary test was performed with composite hydrogel membrane prepared with PEGDA and Rhodamine-labeled PEG-300 000 g.mol⁻¹ chains. The results showed a homogeneous distribution of the fluorescence signal of Rhodamine-labeled PEG in the hydrogel membrane. In order to successfully study the PEGDA/PEG hydrogel structure, we could consider labeling the PEGDA chains with another fluorescent dye to differentiate between PEGDA and PEG rich-zones.

For filtration studies, it would be interesting to compare the filtration of rigid polystyrene particles to soft ones (such as capsules) through these deformable hydrogel membranes. Capsules can be formed by the layer-by-layer method which consists of the adsorption of oppositely charged polyelectrolytes on colloidal particles surfaces with subsequent removal of the templates core. We could expect that large capsules (with a diameter above 20 nm) can be deformed under the effect of applied pressure to pass through the nanometric cavities of the hydrogel membrane. Furthermore, we can investigate the additional dependence of the capsule composition, shape or shell thickness on their passage through the PEGDA/PEG hydrogel membranes.

In the future, the development of this composite PEGDA/PEG hydrogel membrane with tunable properties could provide numerous new perspectives. For example, it would be interesting to investigate their permeability properties at the microfluidic scale. In particular, the integration of PEGDA/PEG hydrogel membrane within microfluidic channels will be a promising material for various applications, including drug delivery. By performing a tangential filtration through the microfluidic device, we may be able to track the passage of capsules or particles through the hydrogel network. Consequently, we will be able to control and program the release of the drug that can be initiated under different stimuli, such as temperature, pH or pressure.

The good filtration and structural properties, simple synthetic process, and biocompatibility of the PEGDA/PEG hydrogel membrane provide it promising application prospects in the fields of dye separation, biomolecule filtration as well as drug delivery systems.

Supporting Information of Chapter 2

Large and non-linear permeability amplification with polymeric additives in hydrogel membranes

Swelling and water content

In order to determine the water content in PEGDA and PEGDA/PEG hydrogels, the weight of sample membranes of 1 mm of thickness and 45 mm of diameter is measured right after preparation (W_0) and then after placed in an oven at 80°C for several hours (W_d). The water percentage of the hydrogels is expressed by the (Equation S2.1):

$$W = \frac{W_0 - W_d}{W_0} \quad (\text{S2.1})$$

We note that we measure the water content right after polymerization and 24 hours later after immersion in water at room temperature.

Disks were weighed and placed in water at room temperature and then taken out of the solution at time intervals, blotted for removal of the surface water and weighed. The swelling of the network can be expressed by the weight swelling ratio Q in (Equation S2.2):

$$Q = \frac{W_s}{W_0} \quad (\text{S2.2})$$

where W_s is the weight of the swollen hydrogel.

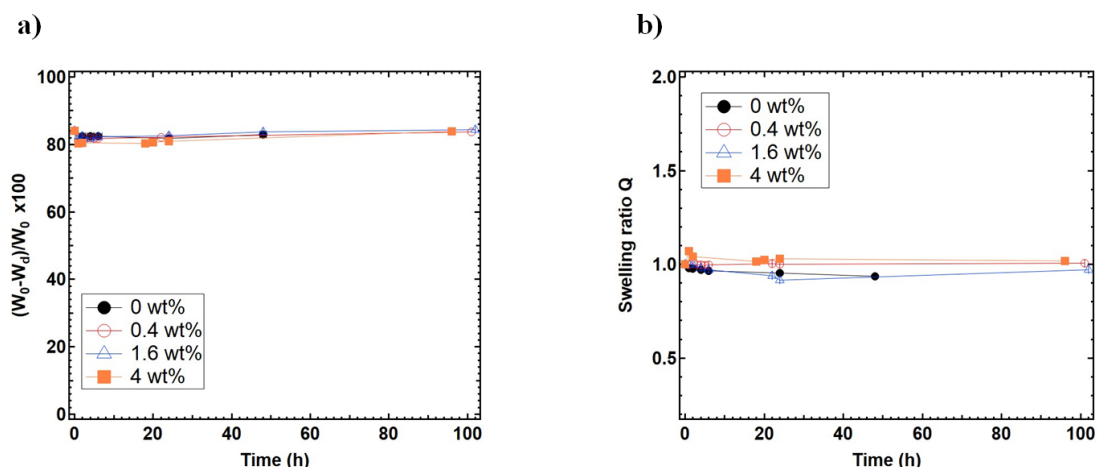


Figure S2.1. a) Water content and b) Swelling behavior of PEGDA hydrogels membranes prepared with 16 wt% of PEGDA and various PEG-300 000 g.mol^{-1} content in the prepolymerization mixture.

The increasing addition of PEG-300 000 g.mol⁻¹ content in prepolymerization mixture does not affect the water content and the swelling behavior of the prepared membrane.

As shown in Figure S2.1 a, the value of 82 wt% of water content is recovered in the different hydrogels membrane prepared with 0 wt%; 0.4 wt%; 1.6 wt% and 4 wt% of PEG-300 000 g.mol⁻¹, after 1 hour of drying at 80°C. This content remains constant even after days of drying. The swelling behavior of the prepared membrane is represented in Figure S2.1 b. The results show that conventional and PEG-modified PEGDA membranes hydrogel systems have a swelling ratio close to 1. This means that gels prepared by 16 wt% of PEGDA with or without the addition of PEG-300 000 g.mol⁻¹ are in their equilibrium state.

In summary, water content and swelling ratio values of cross-linked membranes are never dependent on the content of free PEG chains in the prepolymerization solution.

Compression experiments

The high strain imposed on the hydrogel membrane (e.g ~ 30 %), may lead to the expulsion of water from the hydrogel membrane containing a large content of PEG-300 000 g.mol⁻¹ chains. For example, the video S2.2 a) shows that as soon as the stress is increased (loading phase), the PEGDA/PEG-1.6 wt% gel diameter starts to increase and water is expelled. During the unloading phase, we observe that the hydrogel recovers its initial shape and reabsorbs again the water that was expelled. Whereas, for PEGDA/PEG-0 wt% hydrogel, the second video S2.2 b) shows an increasing of the gel diameter but without the expulsion of water during the compression test. This behavior can be explained by the formation of large pores in the PEGDA/PEG hydrogel membrane.

Videos are available: <https://pubs.acs.org/doi/abs/10.1021/acs.macromol.2c01462>

Rheological experiments

Rheological experiments are done using an ARG-2 rheometer TA, in order to obtain the critical overlap concentration C^* of PEG $\overline{M}_w=300\,000$ g.mol⁻¹ chains.

As shown in Figure S2.2, as expected the viscosity increases when the PEG concentration increases. At some point, there is a transition between the diluted and the semi-diluted regime, represented by the variation of the slope of the line from 0.96 to 3.2, respectively. At this stage, there is a contact between the PEG coils due to the decrease of the distance between them. The associated concentration is called critical overlap concentration C^* being determined at 1.6 wt% of PEG.

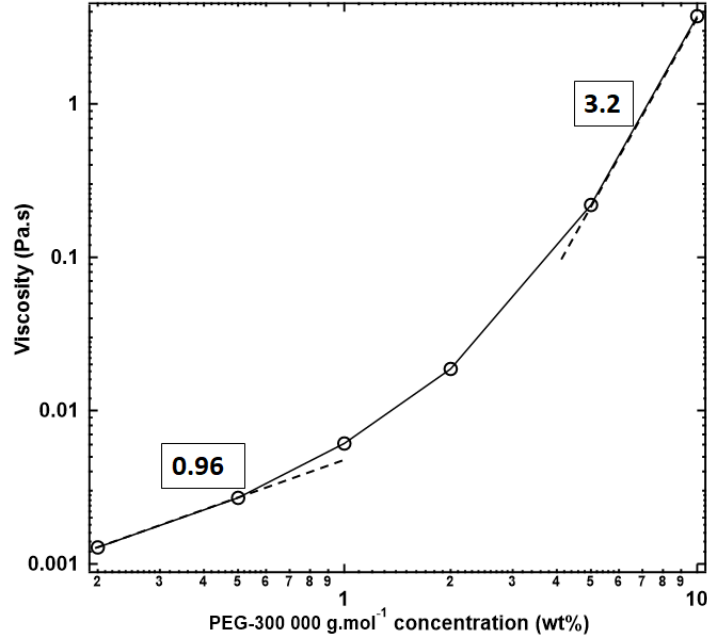


Figure S2.2. The variation of the viscosity as a function of various PEG-300 000 g.mol⁻¹ concentration.

Model of pore compression

Let us take a composite material made of an incompressible elastic solid matrix (PEGDA) of volume V_0 and Young's modulus E_0 , and a set of N_p identical liquid pores (or inclusions) of size d_p , or volume $V_p \sim d_p^3$. The ensemble has an effective Young's modulus $E(\varphi)$, where the volume fraction of liquid (or of pores) φ is given by (Equation S2.3):

$$\varphi = \frac{N_p \cdot V_p}{V} \quad (\text{S2.3})$$

where V is the total volume and given by (Equation S2.4):

$$V = V_0 + N_p \cdot V_p \quad (\text{S2.4})$$

We also introduce an effective Poisson's ratio $\nu < 0.5$. When this matrix full of liquid pores is compressed isotropically with a pressure P , it is the effective compression/bulk modulus B , and not the effective Young's modulus E which it is necessary to take into account. The elastic relation in this case is given by (Equation S2.5):

$$P = B \cdot \frac{dV}{V} \quad (\text{S2.5})$$

where dV is the variation of the total volume.

The two modules are linked by the law reads in (Equation S2.6):

$$B = \frac{E}{3(1-2\nu)} \quad (\text{S2.6})$$

However, since V_0 is constant due to the presumed incompressibility of the matrix, the variation of the total volume dV is given by (Equation S2.7):

$$dV = N_p \cdot dV_p \quad (\text{S2.7})$$

Thus, (Equation S2.5) can be rearranged in (Equation S2.8):

$$P = B \cdot N_p \cdot \frac{dV_p}{V} = B \cdot \varphi \cdot \frac{dV_p}{V_p} = 3 \cdot B \cdot \varphi \cdot \frac{dd_p}{d_p} = \frac{\varphi \cdot E}{(1-2\nu)} \frac{dd_p}{d_p} \quad (\text{S2.8})$$

Finally, one needs to have an expression for $E(\varphi)$. In a work by Style *et al.*¹ for example, a model for identical spherical inclusions is provided. In their work, we see that for fractions that are not too low, the product $\varphi \cdot E(\varphi)$ is of the order of E_0 , whatever the elastocapillary ratio $\gamma/(E_0 \cdot d_p)$, with γ the solid-liquid surface tension. Hence, modeling liquid pores as these inclusions, one gets in fine as a reasonable approximation, in equation (S2.9):

$$P \sim \frac{E_0}{(1-2\nu)} \frac{dd_p}{d_p} \quad (\text{S2.9})$$

References

1. Style, R. W.; Boltyanskiy, R.; Allen, B.; Jensen, K. E.; Foote, H. P.; Wettlaufer, J. S.; Dufresne, E. R., Stiffening solids with liquid inclusions. *Nat. Phys.* **2015**, *11* (1), 82-87, DOI 10.1038/nphys3181.

Supporting Information of Chapter 3

Sieving and clogging in PEG-PEGDA hydrogel membranes

Characterization of latex particles

The characteristic of carboxylate-modified polystyrene particles of different size are represented in Table S3.1. The absorption wavelength, the zeta potential and the pH of the solution with a concentration of $2 \times 10^{-4} \text{ g.mL}^{-1}$ does not depend on the particles size.

The size distributions of different latex particles in water is represented in Figure S3.1. The presence of one pic for each sample signify the monodisperse latex particles with a diameter d of 20, 100 and 1000 nm as represented in Figure S3.1 a, b and c, respectively.

Type of particles	Absorption wavelength (nm)	Size (nm)	Zeta potential (mV)	pH of feed solution
a) Latex NP	580	20	-43,4	7,7
b) Latex NP	580	100	-43,4	7,7
c) Latex MP	580	1000	-43,4	7,7

Table S3.1. Absorption wavelength, size, zeta potential and pH of feed solutions of latex particles with $C=2 \times 10^{-4} \text{ g.mL}^{-1}$.

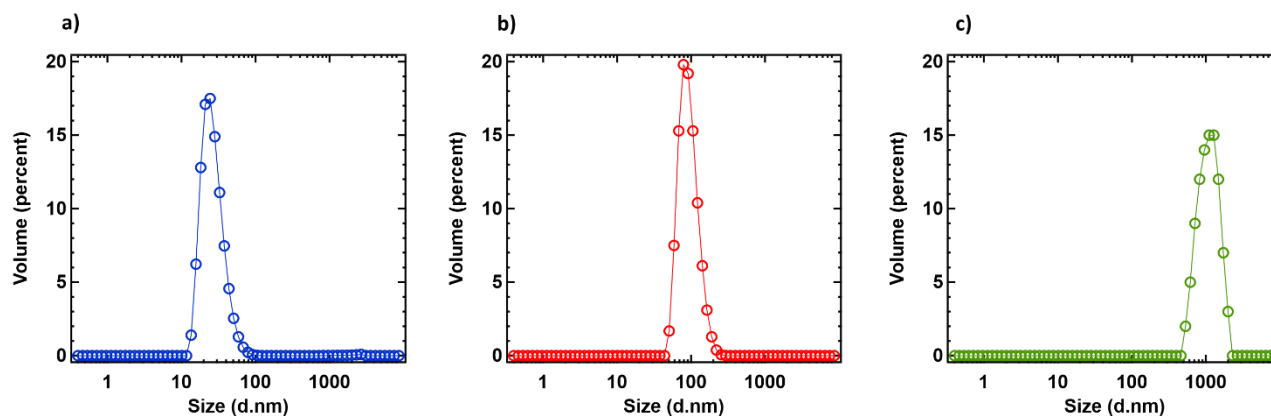


Figure S3.1 .DLS size distributions of different latex particles with a concentration of $2 \times 10^{-4} \text{ g.mL}^{-1}$ in water.

CryoSEM image

We perform cryoSEM experiments of the 1.6 wt% PEG hydrogels after the filtration of the 1 μ m particles to observe the location of the particles in the cavities. As represented Figure S3.2, there is no microparticles present in the cross-section of the hydrogel membrane.

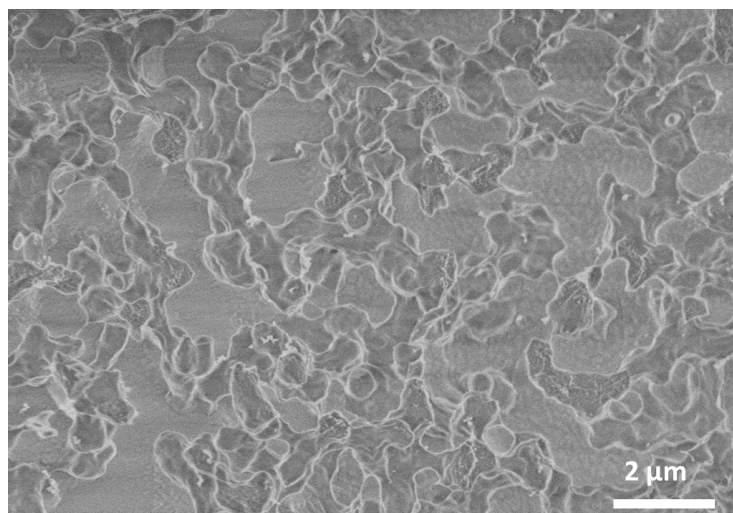


Figure S3.2. CryoSEM image of the cross-section of a PEGDA/1.6 wt% PEG hydrogel membrane after filtration experiments of microparticles of 1 μ m (MP-1 μ m).

Supporting Information of Chapter 4

Effect of PEG content and molar mass on the morphological structure and water permeability properties of PEGDA/PEG composite hydrogel membranes

Chemical composition of hydrogels

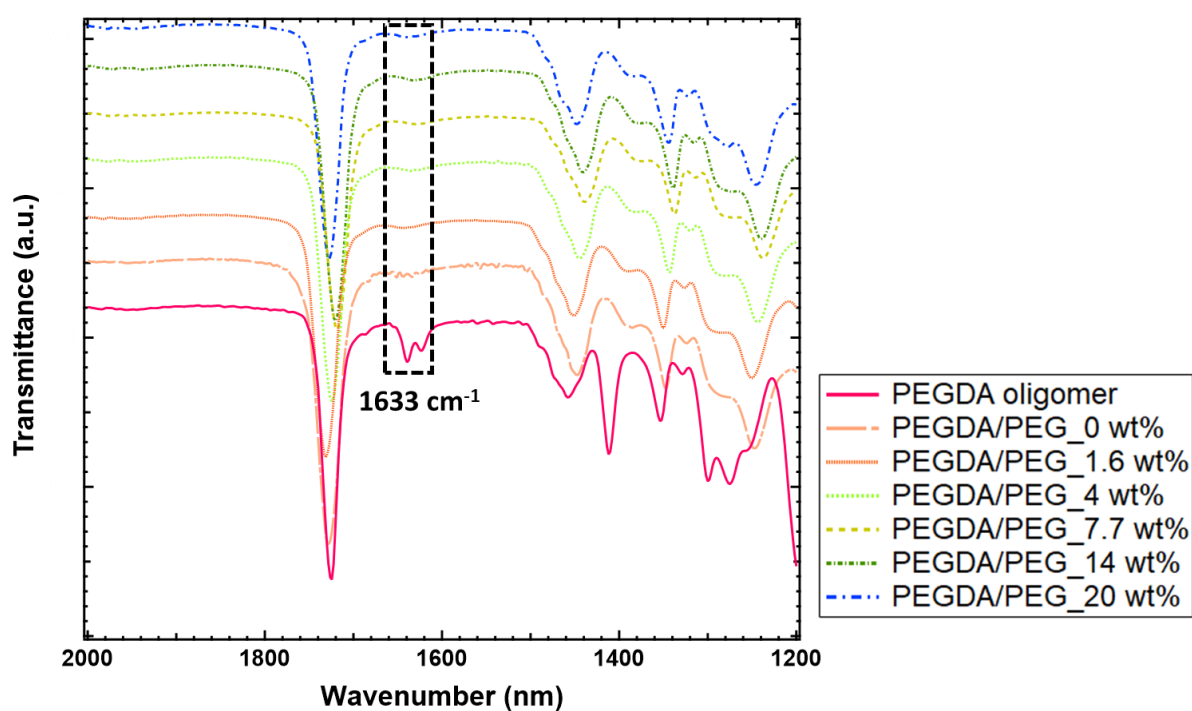


Figure S4.1. FTIR spectra of dried PEGDA hydrogels membranes prepared with 16 wt% of PEGDA and various PEG-3000 g.mol⁻¹ contents in prepolymerization mixture compared to the spectrum of the as-received PEGDA oligomer.

Rheological experiments

Rheological experiments are performed using an ARG-2 rheometer TA, in order to obtain the critical overlap concentration C^* of PEG chains with different molar masses.

As shown in Figure S4.2, as expected the viscosity increases when the PEG concentration increases. For the PEG of different molar masses, we notice a variation of the slope of the line from 1.5 to 3.4 for PEG-3000 $\text{g}\cdot\text{mol}^{-1}$, from 0.68 to 2.7 for PEG-35 000 $\text{g}\cdot\text{mol}^{-1}$ and from 0.9 to 3 and above, for the very high PEG molar masses (i.e. 300 000 and 600 000 $\text{g}\cdot\text{mol}^{-1}$). This variation is a sign of the transition between the diluted and the semi-diluted regime. At this stage, there is a contact between the PEG coils due to the decrease of the distance between them. The associated concentration is called critical overlap concentration C^* being determined at about 35 wt%, 4 wt%, 1.6 wt% and 1 wt% for PEG-3000, 35 000, 300 000 and 600 000 $\text{g}\cdot\text{mol}^{-1}$, respectively.

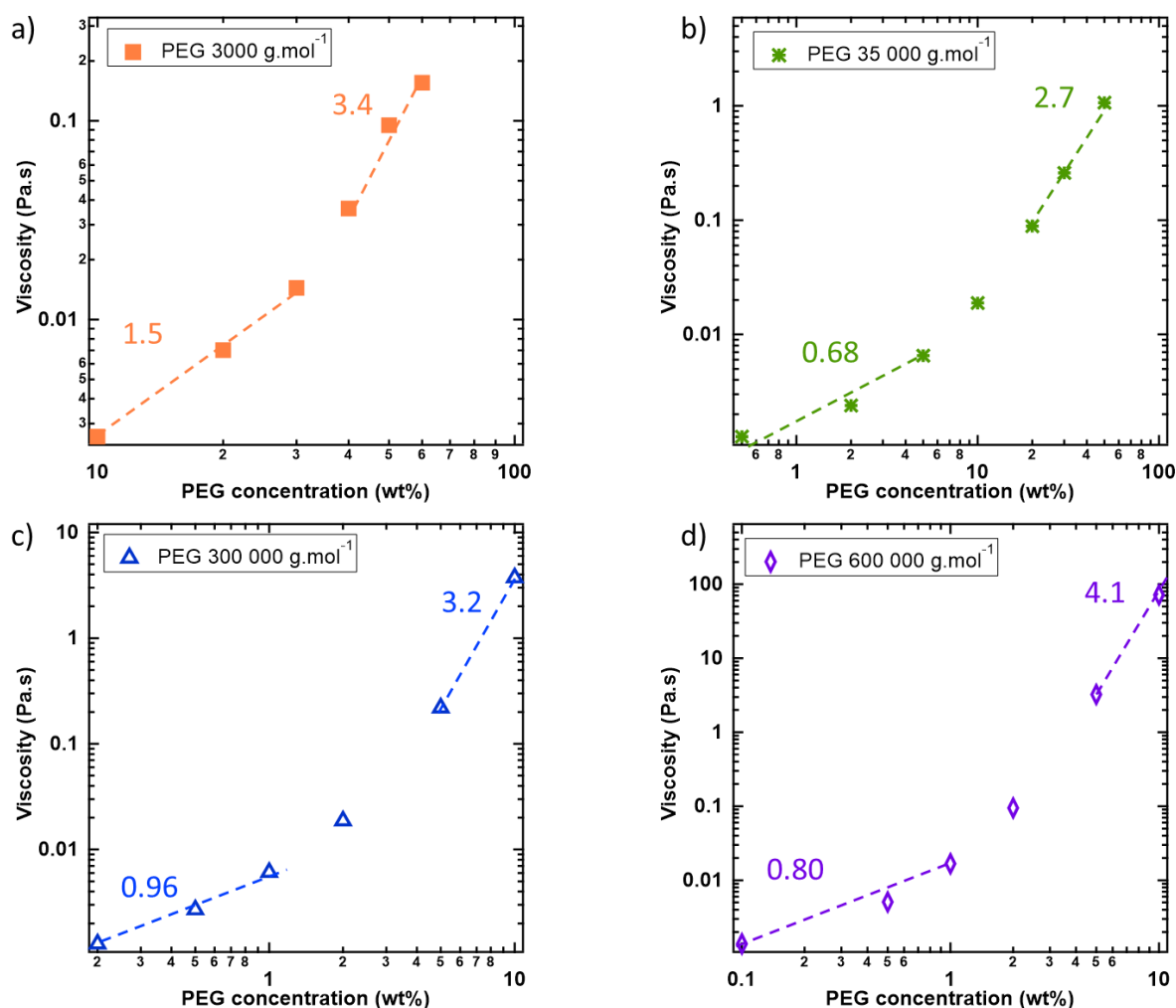


Figure S4.2. The variation of the viscosity as a function of various a) PEG-600, b) PEG-35 000, c) PEG-300 000 and d) PEG-600 000 $\text{g}\cdot\text{mol}^{-1}$.

Polymerization of PEGMA

This images has been taken by Sixtine de Chateauneuf-Randon.

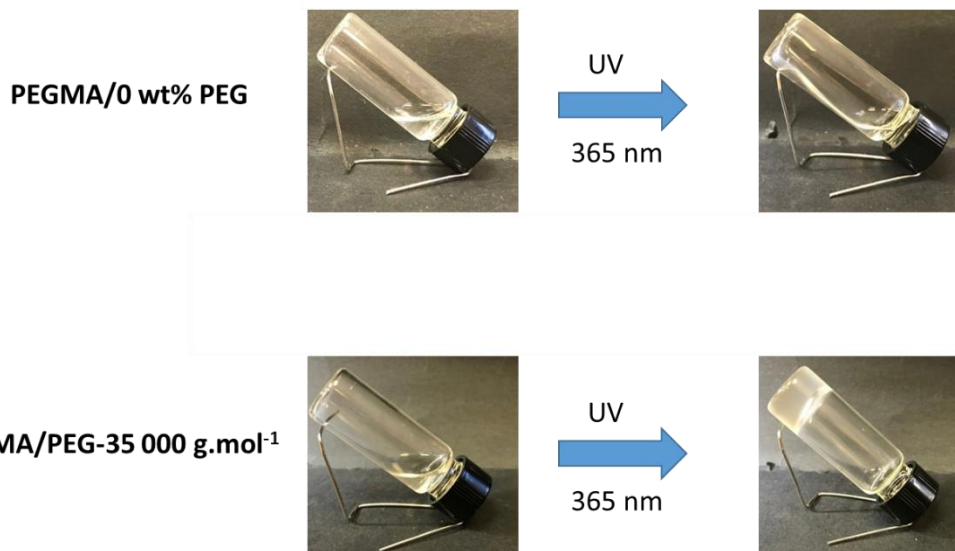


Figure S4.3. Radical polymerization reaction of poly (ethylene glycol) monomethacrylate PEGMA without and with PEG chains.

CryoSEM and AFM images

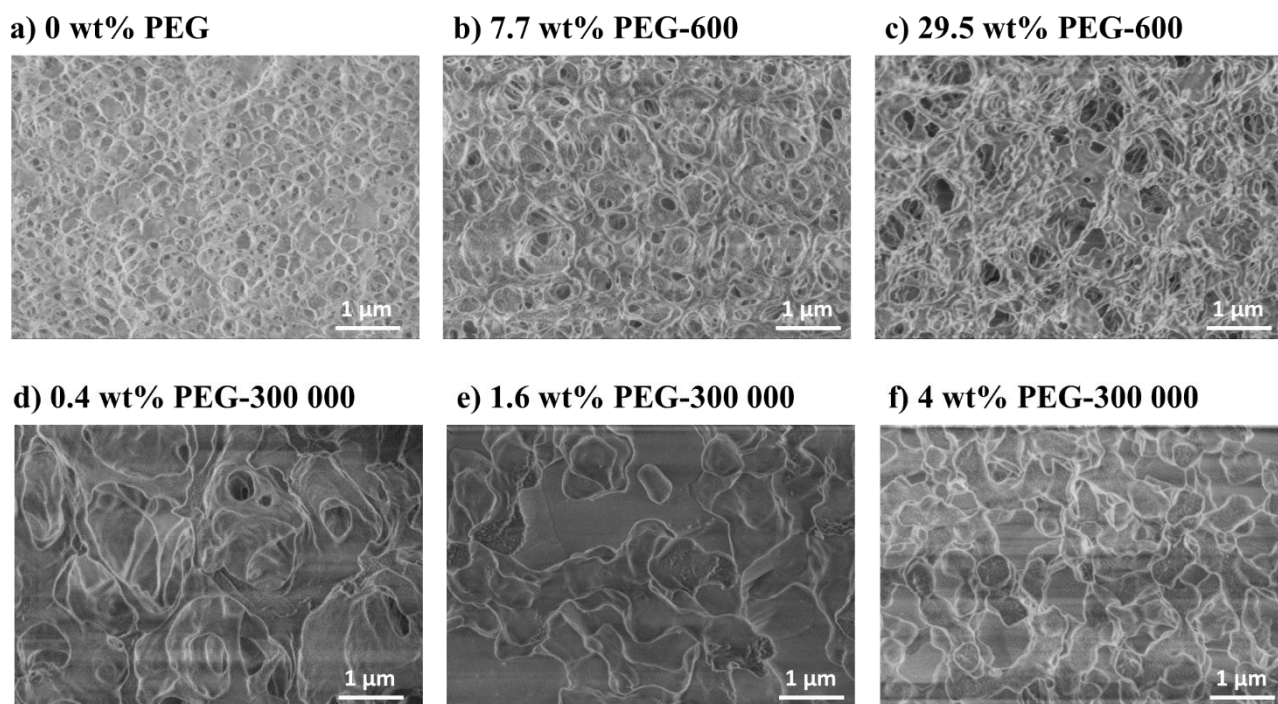


Figure S4.4. CryoSEM images of hydrogel membranes prepared with PEGDA and various content of PEG-600 g.mol^{-1} a) 0; b) 7.7 and c) 29.5 wt% and PEG-300 000 g.mol^{-1} d) 0.4; e) 1.6 and f) 4 wt%.

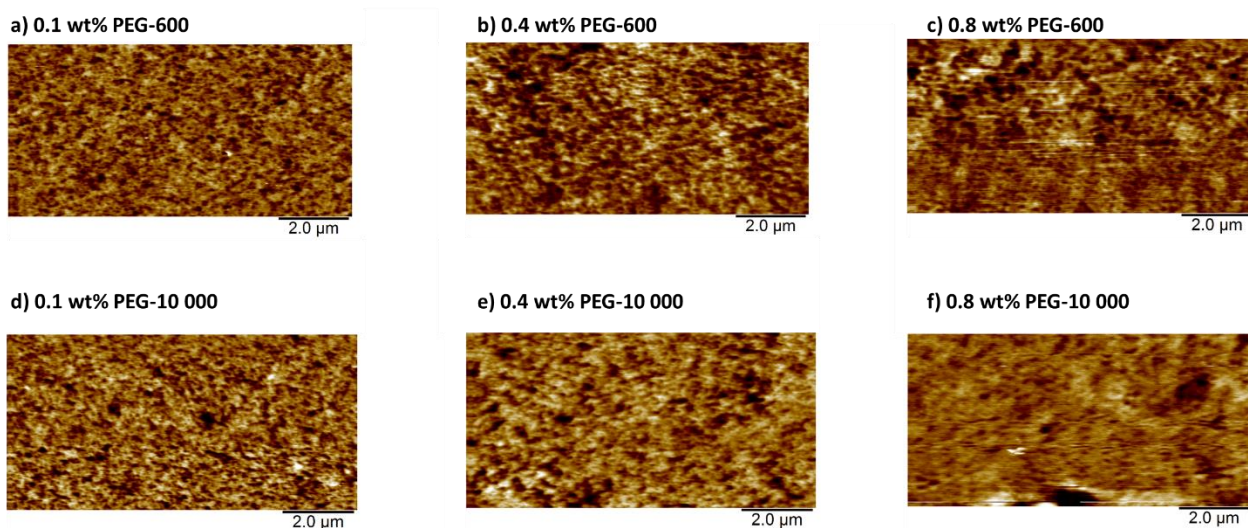


Figure S4.5. Surface AFM images of PEGDA hydrogels membranes prepared with 16 wt % of PEGDA and various content of PEG-600 (a, b and c) and PEG-10 000 g.mol^{-1} (d, e and f). The average Z-scale is $\pm 50 \text{ nm}$.

Influence of PEGs concentration and molar mass on water intrinsic permeability at high applied pressure

In order to study the effect of high applied pressure on the water permeability of PEGDA/PEG hydrogel membranes, we have measured the water flux for different pressure ranging from 2000 to 80000 Pa for hydrogels prepared with various PEG contents and molar masses. The results are presented in Figure S4.6.

Similarly for PEGDA/PEG-300 000 g.mol⁻¹ membranes shown in Chapter 2, we observe a non-linear variation of the water flux J as function of the applied pressure for PEGDA with PEG-600, PEG-3000, PEG-35 000 and PEG-600 000 g.mol⁻¹. Depending on PEG contents and molar masses, water flux reaches a plateau at different pressure. It is about 400 and 600 mbar for PEGDA with 7.7 and 29.5 wt% of PEG-600 g.mol⁻¹, respectively (see Figure S4.6 a). However, this plateau is reached earlier (~ 200 mbar) for PEGDA with 14 and 17 wt% of PEG-3000 g.mol⁻¹ (Figure S4.6 b), as well as for PEGDA with 3.2 to 7.7 wt% of PEG-35 000 g.mol⁻¹ (Figure S4.6 c). Surprisingly, for PEG with high PEG-3000 content (e.g. 20 and 22.5 wt%), the water flux does not present a plateau at high pressure, but it decreases as the applied pressure increases. This new behavior is also observed with a high content of PEG-35 000 g.mol⁻¹ (e.g. 14 and 20 wt%) as represented in (Figure S4.6 c). Consequently, we suppose that the decreasing

of the water flux at high applied pressure for some high content of PEG, or the forming of a plateau is probably due to a compression of the hydrogel and the closure of some pores during filtration experiments.

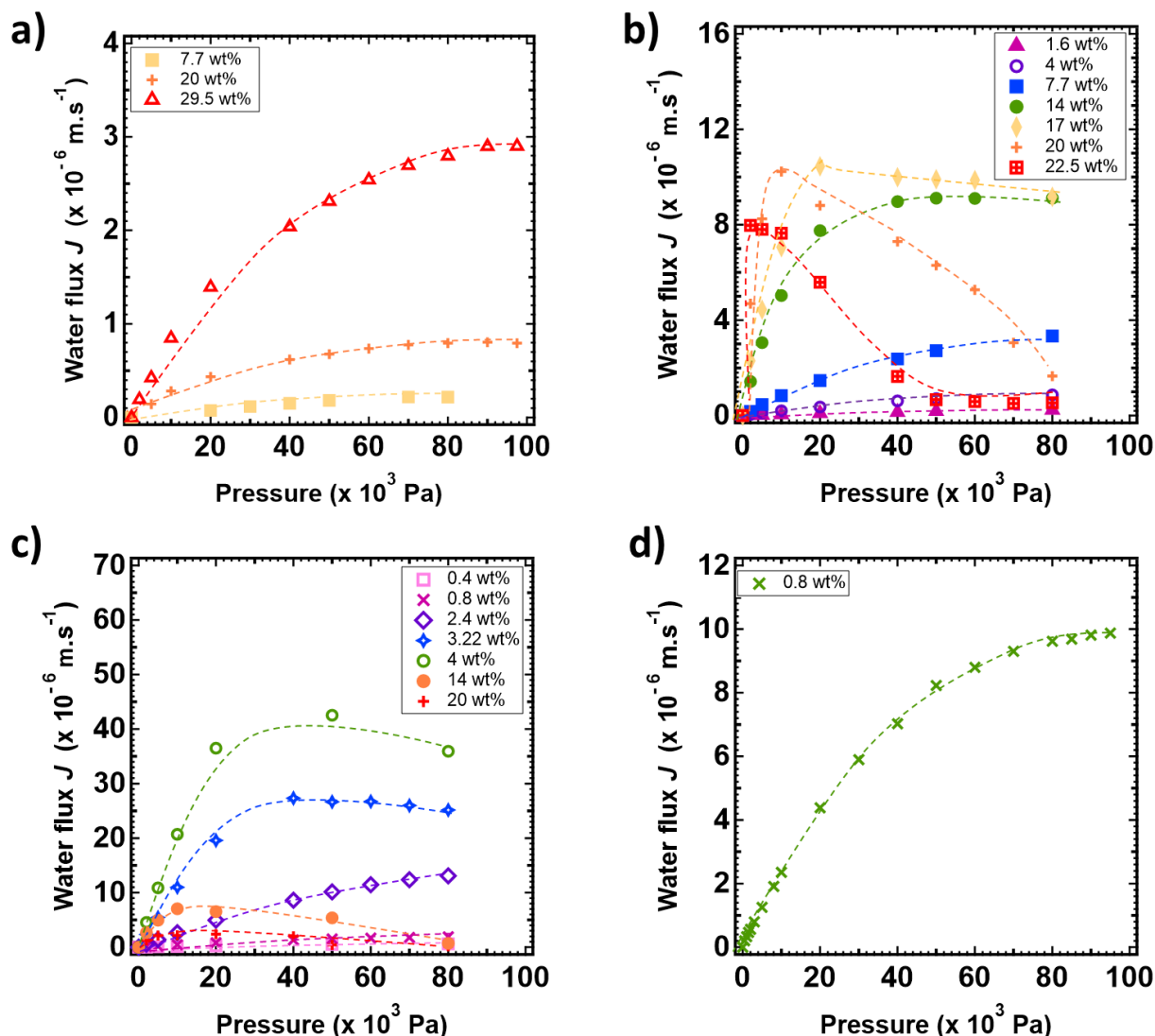


Figure S4.6. Variation of water flux versus applied pressure for PEGDA hydrogel membranes prepared with various content of a) PEG-600, b) PEG-3000, c) PEG-35 000 and d) PEG-600 000 $g.mol^{-1}$.

To further characterize the deformation of PEGDA/PEG membranes samples, we performed the compression experiments for PEGDA/PEG hydrogel membranes prepared with various PEG contents and molar masses, using Instron 5565 machine.

Figure S4.7 presents the variation of the stress as a function of the strain in the linear regime (0-4%) at a deformation rate of 0.01 mm.s^{-1} , for deformations between 0 and 4% and stresses below 0.05 MPa, which are relevant to the filtration experiments where pressures below 1 Bar

(i.e. 0.1 MPa) are applied for hydrogel prepared with PEGDA and various content of PEG 600, 3000, 10 000, 35 000 and 600 000 g.mol⁻¹.

The effective Young's modulus of each gel was calculated from the slope of the stress–strain curve using the Hooke's law $E = \sigma/\epsilon$ in the range of >1-4 % in strain, in the loading phase. For all samples, E was calculated from adjusting the stress-strain data at strain >1-4%, while some curve variability was observed at the very low strains (0-1%) because of parallelism issues. The variation of the effective Young's modulus value as a function of PEG content is represented later. For PEGDA membranes prepared without PEG (0 wt%), the effective Young's modulus value, calculated from the slope of the stress-strain curve (see Figure S4.7 a) at low strain (>1-4%), is 1 MPa, which is of the same order of magnitude as the values reported in the literature. The addition of free PEG chains with different molar mass seems to have the same trend. Increasing the PEG content in the prepolymerization solution decreases the effective Young's modulus of the PEGDA/PEG hydrogel membranes.

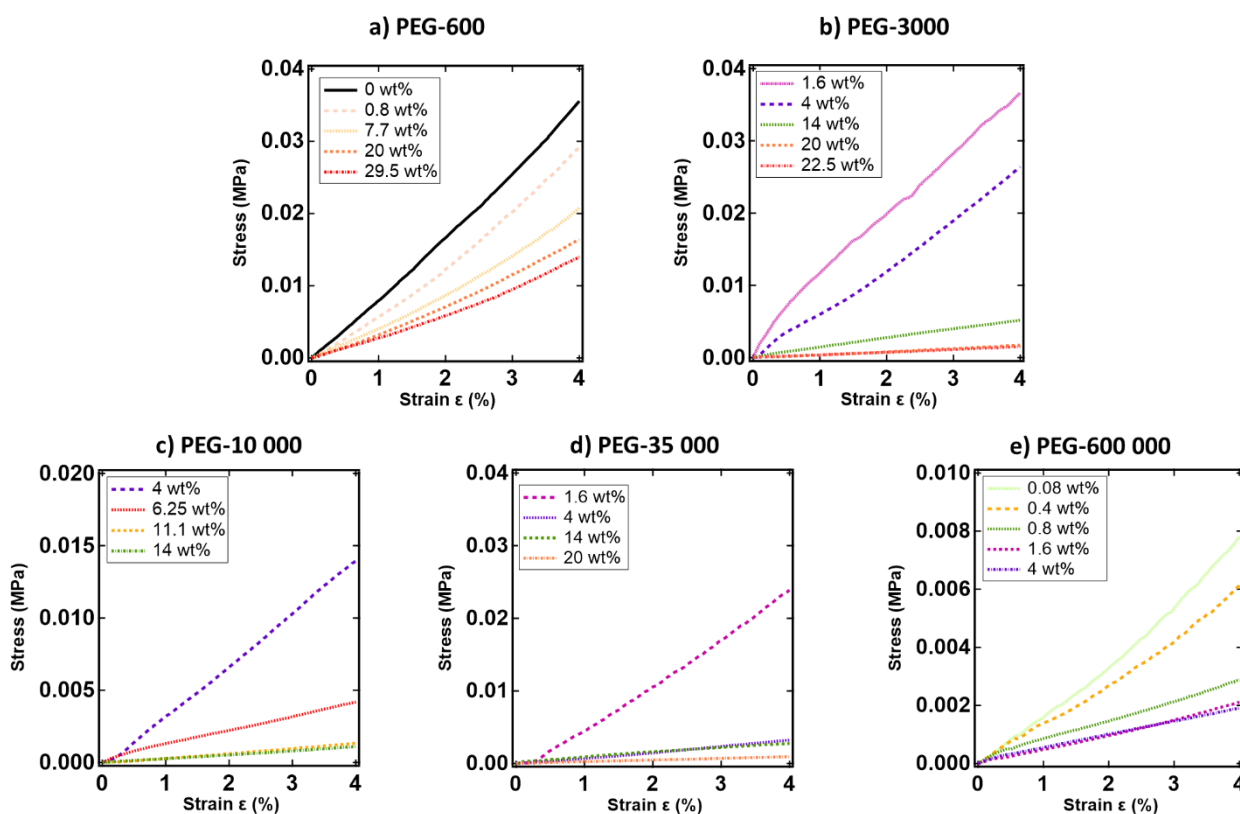


Figure S4.7. Stress versus strain for PEGDA hydrogel membranes prepared with 16 wt% of PEGDA and various contents of a) PEG-600, b) PEG-3000, c) PEG-10 000, d) PEG-35 000 and e) PEG-600 000 g.mol⁻¹.

The values of effective Young's modulus calculated for low strain as a function of the PEG content are represented in Figure S4.8.

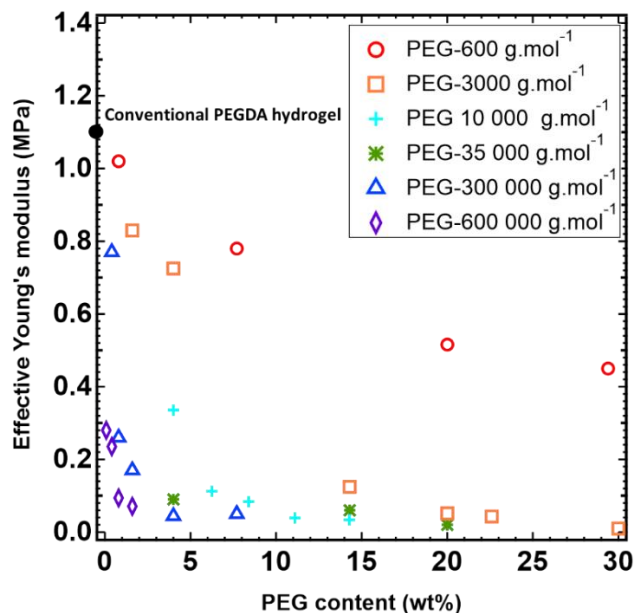


Figure S4.8. Variation of the effective Young's modulus as a function of the content of PEG of different molar mass.

As mentioned before, the addition of PEG content to the PEGDA matrix results in decreasing the effective Young's modulus. As shown in Figure S4.8, the effective Young's modulus for PEGDA prepared with low and high PEG molar mass present the same dependence. For example, for the lowest molar mass (e.g. 600 g.mol^{-1}), it decreases monotonically from 0.78 to 0.45 MPa when the PEG content increases from 7.7 to 29.5 wt%. As well it decreases from 0.28 to 0.07 MPa when the content of highest molar mass of PEG-600 000 g.mol^{-1} increases from 0.08 to 1.6 wt%. In addition, for the same PEG content, the effective Young's modulus decrease as the PEG molar mass increases.

Thus, the PEGDA/PEG hydrogels were significantly softer with increasing molar mass and content of PEG chains. This behavior is likely derives from two effects: either to the large volume fraction of non-cross-linked PEG domains present in the hydrogel membranes, or this is the result of the introduction of PEG chains in the PEGDA network. This PEG integration (particularly for large PEG chains) features a molar mass between cross-links considerably larger than in pure-PEGDA matrix, which should lead to a pronounced softening of the hydrogels membranes. As we have shown before that the PEG chains are not rinsed out of the

hydrogel, but its covalently grafted to the PEGDA network, the latter hypothesis seems more convincing.